

Systematic revision of *Stegodera* Martens, 1876 (Gastropoda, Stylommatophora, Camaenidae), with description of a new genus

Zhe-Yu Chen^{1,2}, Zhi-Tong Lyu³, Min Wu²

1 College of food science and engineering, Wuhan Polytechnic University, Wuhan 430023, China **2** School of Life Sciences, Nanjing University, Nanjing 210023, China **3** The Museum of Biology, School of Life Sciences, Sun Yat-sen University, Guangzhou 510275, China

Corresponding author: Min Wu (minwu1969@aliyun.com)

Academic editor: Frank Köhler | Received 7 May 2021 | Accepted 8 August 2021 | Published 1 September 2021

<http://zoobank.org/650D7F4C-990E-4CBF-88E3-F0CD38EEC377>

Citation: Chen Z-Y, Lyu Z-T, Wu M (2021) Systematic revision of *Stegodera* Martens, 1876 (Gastropoda, Stylommatophora, Camaenidae), with description of a new genus. ZooKeys 1059: 1–21. <https://doi.org/10.3897/zookeys.1059.68385>

Abstract

The monotypic genus *Stegodera* Martens, 1876 is systematically revised based on anatomical and morphological examination of freshly collected specimens. A new species from southern Hunan, which resembles *Stegodera angusticollis*, is confirmed to represent a new genus evidenced by comparative shell morphology and anatomy as well as by molecular phylogenetic analyses. The new genus might be more closely related to *Stegodera* and *Nesiohelix* Kuroda & Emura, but differs anatomically from the latter two genera by the absence of a dart apparatus.

Keywords

16S rRNA, Bradybaeninae, Camaeninae, China, *COI*, new genus, new species

Introduction

Stegodera Martens, 1876 is a monotypic camaenid genus endemic to southern Hubei and northern Jiangxi, China (Zilch 1960; Richardson 1983). Since the original description (Martens 1875a), only a few additional specimens of this species have been reported (Heude 1882; Chen and Gao 1987; Qian et al. 2008; Qian and Zhou 2014). The typical shell character states of *Stegodera* are “shell sinistral, disk-shaped, with low spire and

open, deep umbilicus; solid, opaque, brown. Inner whorls slowly increasing, regular; latter half of the last whorl distorted, straightened, covering the preceding whorl above. Aperture very oblique, crescentic, toothless; peristome reflexed; throat very much contracted” (Pilsbry 1895), while the anatomy of this genus kept unknown. Recently, we received several fresh specimens of *Stegodera angusticollis* (Martens, 1875) from southeastern Hubei. In another recent field investigation in southern Hunan, Dr Lu Qiu found two land snail specimens belonging to a species, which is conchologically similar to *Stegodera angusticollis*, but has been found to differ from it in anatomical characteristics.

Materials and methods

A piece of foot tissue was cut from the living animal and preserved in 99.7% ethanol for molecular analysis. Then the animal was relaxed by drowning in water before being transferred to 70% ethanol for fixation, which was replaced with ethanol of the same concentration after three days. Photographs of the shell and reproductive system were taken using a Canon camera with Macro lens, and then modified in Adobe Photoshop CC 2018. The shells were measured with digital vernier calipers to the nearest 0.1 mm. Measurement abbreviations:

$S_{D_{maj}}$ shell major diameter;
 $S_{D_{min}}$ shell minor diameter;
 S_H Shell height.

Whorls were counted as described by Kerney and Cameron (1979). Directions used in descriptions: proximal, towards the genital atrium; distal, away from the genital atrium.

Molecular phylogenetics

Muscle tissue was obtained from eleven species in this study (Table 1), including *Stegodera angusticollis* and the single paratype of *Pseudostegodera qiului* gen. et sp. nov. Genomic DNA was extracted by using Tiangen DNA Extraction Kit (for SYS samples. Abbreviations see below) and TIANamp Marine Animals DNA Kit (for HBUMM samples). Two mitochondrial genes, partial 16S ribosomal RNA gene (16S) and partial cytochrome *C* oxidase 1 gene (CO1), were amplified. Primers used for 16S were 16SA/16SB (Palumbi et al. 1991), and for CO1 were LCO1490/HCO2198 (Folmer et al. 1994). PCR amplifications were performed in a 20 μ l (for SYS samples) / 50 μ l (for HBUMM samples) reaction volume with the cycling conditions of an initial denaturing step at 94° C for 2 min, 35 cycles of denaturing at 94° C for 30 s, annealing at 58° C (for 16S)/ 50° C (for CO1) for 30 s and extending at 72° C for 30 s, and final extending step of 72° C for 10 min. PCR amplicons were inspected on a 1% agarose gel for quality and fragment size, then were purified, and sequenced on an automated sequencer.

For phylogenetic analysis, sequences from seven camaenid species and one out-group species were obtained from GenBank and incorporated into our dataset

Table 1. Vouchers and the GenBank accession numbers of the species for phylogenetic study (*, from NCBI).

Species	Subfamily	16S/CO1	Museum voucher	Voucher inf.
<i>Pseudostegoderia qiului</i> gen. et sp. nov.	Camaeninae	MW810083/ MW810790	SYS m001017	Paratype of the species; see text
<i>Stegoderia angusticollis</i>	Camaeninae	MW810079/ MW810793	SYS m001016	See text
<i>Amphidromus inversus</i>	Camaeninae	AB112400*/ FJ472655*	/	/
<i>Camaena cicatricosa</i>	Camaeninae	KU586474*/ KU061276*	/	/
<i>Camaena poyuensis</i>	Camaeninae	KU586468*/ KU061273*	/	/
<i>Satsuma guandi</i>	Camaeninae	MW804648/ MW810791 MW804647/ MW810792	HBUMM08239a1 HBUMM08239a2	Guangdong, Shaoguan, coll. Di Yu
<i>Exiligada gregoriana</i>	Camaeninae	JX393672*/ JX393761*	/	/
<i>Falsipleuroxia overlanderensis</i>	Camaeninae	KU519178*/ KU519261*	/	/
<i>Tatemelon musgum</i>	Camaeninae	KU519194*/ KU519277*	/	/
<i>Sinumelon vagente</i>	Camaeninae	KP965282*/ KP965358*	/	/
<i>Acusta ravidia</i>	Bradybaeninae	MW800197/ MW810782	HBUMM06616a	Sichuan, Jiuzhaigou, coll. Min Wu
<i>Bradybaena qixiaensis</i>	Bradybaeninae	MW810081/ MW810783	HBUMM06900–1/ HBUMM06900–2	Jiangsu, Nanjing, coll. Min Wu
<i>Cathaica fasciola</i>	Bradybaeninae	MW800200/ MW810784	HBUMM06477–1/ HBUMM06477–2	Jiangsu, Zhenjiang, coll. Min Wu
<i>Coccolypta liui</i>	Bradybaeninae	MK680922*/ MK680001*	/	/
<i>Coccolypta pinchoniana</i>	Bradybaeninae	MK680923*/ MK680002*	/	/
<i>Dolicheulota formosensis</i>	Bradybaeninae	KR338956*/ KR338956*	/	/
<i>Euhadra dixonii</i>	Bradybaeninae	AF098711*/ AB916773*	/	/
<i>Laeocathaica polytyla</i>	Bradybaeninae	MW810082/ MW810787	HBUMM06726a1	Sichuan, Jiuzhaigou, coll. Min Wu
<i>Laeocathaica distinguenda</i>	Bradybaeninae	MW810084/ MW810785 MW810085/ MW810786	HBUMM06491a1 HBUMM06491a2	Gansu, Wenxian, coll. Min Wu
<i>Nesiobelix moreletiana</i>	Bradybaeninae	MW810080/ MW810788	HBUMM06796	Zhejiang, Hangzhou, coll. Min Wu
<i>Pseudobuliminus piligerus</i>	Bradybaeninae	MW800362/ MW810789	HBUMM06527a1	Gansu, Wenxian, Coll. Min Wu
<i>Cornu aspersum</i> (out-group)	Helicidae	KU586459*/ KU586502*	/	/

(Table 1). *Cornu aspersum* is used as the out-group of the studied Camaenidae, following the previous studies (Wang, Xiao et al. 2014; Wang, Yang et al. 2014; Huang et al. 2015) considering that the branch including Helicidae is a close group of Bradybaenidae + Camaenidae (Asian and Australasian) + Polygyridae (Wade et al. 2007; Razkin et al. 2015). DNA sequences of the two genes were aligned respectively by the Clustal W algorithm with default parameters (Thompson et al. 1997) in MEGA 7.0.26 (Kumar et al. 2015). The substitution saturation assessment for CO1 genes was done using DAMBE 7.0 (Xia 2018) employing the methods introduced by Xia et al. (2003) and Xia and Lemey (2009). The poorly aligned positions and divergent regions of the alignment of 16S were eliminated using Gblocks 0.91b (Castresana 2000), a concatenated matrix of 20 (including outgroup, Table 1)×703 bp was used for the subsequent analyses. Model selection was performed by “Models” in MEGA 7.0.26 (Kumar et al. 2015). The data set was analyzed using Bayesian Inference (BI) in MrBayes 3.2.4 (Ronquist et al. 2012) and the Maximum Likelihood analysis in raxmlGUI 2.0 beta (Edler et al. 2019) (Fig. 1). In Bayesian Inference analysis, three independent runs were conducted, each of which was performed for 10,000,000 generations and sampled every 1000 generations with the first 25% samples discarded as burn-in. Convergence of the Markov Chain Monte Carlo simulations was assessed using Tracer v1.7 (Rambaut et al. 2018), verifying that all ESS values exceeded 200. In addition, we repeated these analyses for a dataset containing a larger number of species (Table 1) (Fig. 1B).

We used Mesquite v. 3.61 (Maddison and Maddison 2019) to reconstruct the evolutionary history of five reproductive characters, which are usually emphasized in camaenid taxonomy, and mapped these characters on the Bayesian phylogeny under Maximum Likelihood-based criterion.

Depository abbreviations

HBUMM	Mollusk collection of Museum of Hebei University, Baoding, China;
IZCAS	Institute of Zoology, Chinese Academy of Sciences (Beijing, China);
MYNU	Mianyang Normal University (Mianyang, China);
OYKC	Private collection of Kai-Chen Ouyang (Kunming, China);
QL	Private collection of Lu Qiu (Luzhou, China);
SMF	Senckenberg Forschungsinstitut und Naturmuseum (Frankfurt am Main, Germany);
SYS	Sun Yat-sen University (Guangzhou, China);
ZMB	Museum für Naturkunde (Berlin, Germany).

Anatomical abbreviations

AS	accessory sac;
At	atrium;
BC	bursa copulatrix;
BCD	bursa copulatrix duct;
DS	dart sac;
DSC	dart sac chamber;
Ep	epiphallus;
Fl	flagellum;
FO	free oviduct;
MG	mucous glands;
MGP	papilla distally leading to mucous glands on inner wall of accessory sac;
P	penis;
PC	penial caecum;
PR	penial retractor muscle;
PS	penis sheath;
Va	vagina; V
VD	vas deferens.

Results

Phylogeny

The substitution saturation assessment for CO1 sequences suggested that the first and second codon positions were relatively conserved but that the third codon po-

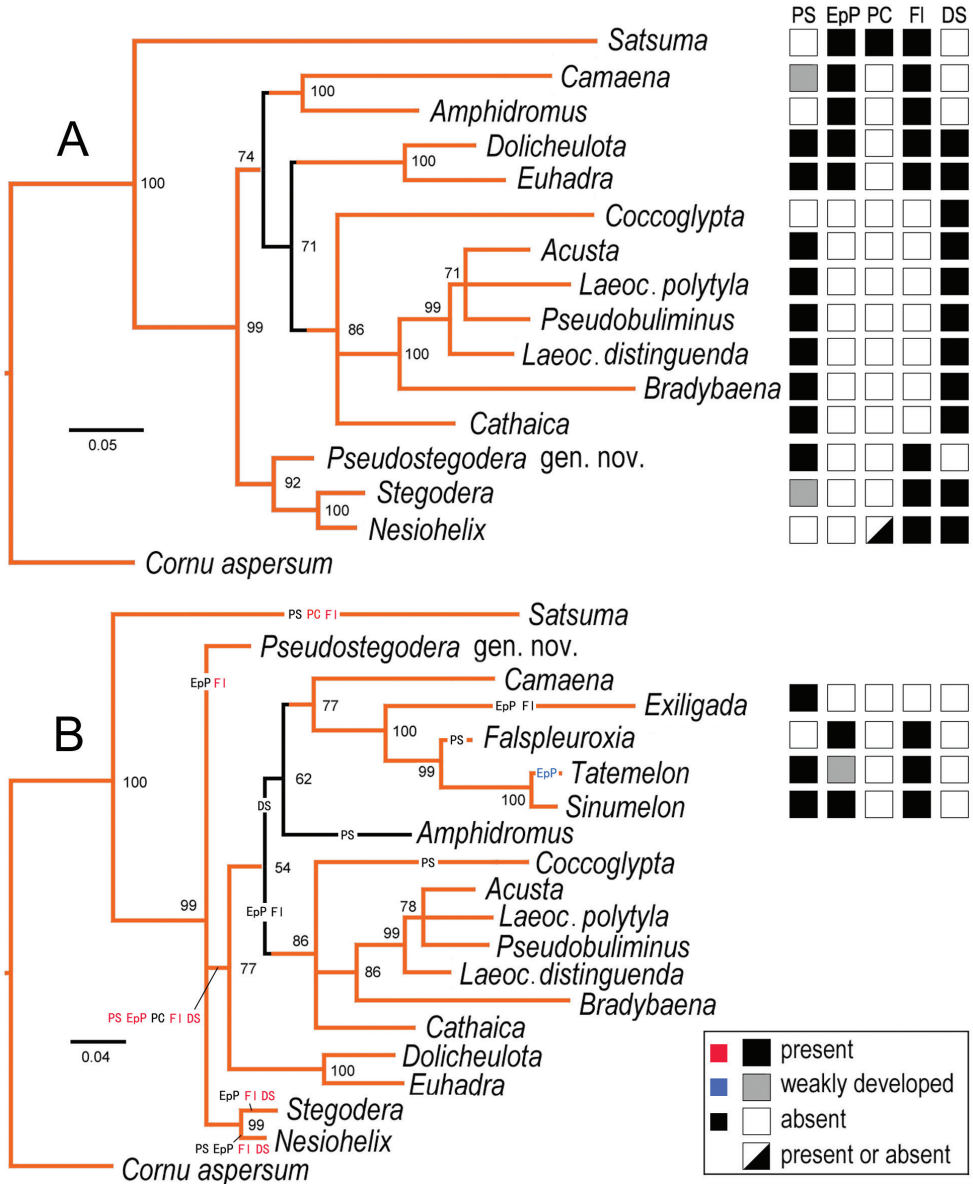


Figure 1. Bayesian Inferences of camaenids (representatives of genera in Table 1) based on partial mitochondrial 16S and CO1 sequences. Numbers near nodes indicate Bayesian posterior probabilities. The squares on the right of each taxon name indicate its character states. Abbreviations: PS: penial sheath; EpP: epiphallallic papilla; PC: penial caecum; FI: flagellum; DS: dart sac apparatus **A** phylogram without Australian camaenids **B** the results of ancestral states (tagged on branch in red, blue, or black) reconstruction mapping on the phylogram with some Australian camaenid genera added. Orange part: the topologies supported by the results respectively by using both Bayesian Inference and Maximum Likelihood methods. Character states are from Schileyko (2003) and Wu (2019). Scale bars for substitutions per site.

sitions revealed sequence saturation and are therefore not suitable for phylogenetic inference (for both symmetrical and asymmetrical trees, $Iss > Iss.c$, $ps < 0.001$). Our final molecular dataset contained nineteen sequences of partial 16S and CO1 genes. After eliminating poorly aligned positions and divergent regions of the alignment of 16S using Gblocks 0.91b (Castresana 2000), a concatenated matrix of 20 (including outgroup, Table 1)×703 bp was used for the subsequent analyses. The models “T92 + G” and “GTR + G + I” were chosen as the best nucleotide substitution models for 16S (lnL = -1877.8, BIC = 4100.7) and CO1 (lnL = -1399.1, BIC = 3216.9), respectively. The model of the combined dataset is “TN93 + G + I” (lnL=-3387.6, BIC = 7192.6).

The phylograms produced by both Maximum Likelihood Inference and Bayesian Inference based on partial 16S + partial CO1 sequences are topologically identical in major branches (Fig. 1). All trees reveal a primary division (posterior probability PP = 1) between penial caecum-bearing *Satsuma* A. Adams, 1868 (Camaeninae) and the remaining studied groups, a mixture of so-called camaenine and bradybaenine genera that usually have no penial caecum. The monophyly of Bradybaeninae is not supported because neither *Nesiohelix* Kuroda & Emura, 1943 nor *Dolicheulota* Pilsbry, 1901, and *Euhadra* Pilsbry, 1890, all well-known bradybaenine genera, are not included in the clade where most bradybaenine genera stay. The monophyly of Camaeninae, which is morphologically characterized by the absence of dart sac apparatus is also not supported when considering that *Satsuma* is situated most basally on the phylograms and meanwhile *Camaena* Albers, 1850 and its sister group *Amphidromus* Albers, 1850 are deeply nested in the clade that comprises most bradybaenine genera. *Stegoderma* E. Martens, 1876 is found to be the sister group of *Nesiohelix* with strong nodal support (PP = 1). In one phylogram (Fig. 1A), *Pseudostegoderma* gen. nov. is a sister group of clade *Stegoderma* + *Nesiohelix* and in the other, it is in an unresolved trichotomy with these two taxa.

As suggested by the analyses of character evolution, the ancestral character states among most studied camaenids, except *Satsuma*, *Pseudostegoderma* gen. nov., *Stegoderma*, and *Nesiohelix*, are: penial sheath, epiphallic papilla, flagellum and dart sac apparatus present, penial caecum absent (Fig. 1B). The penial sheath has been lost in all the studied taxa at least for five times. The epiphallic papilla has been lost at least for four times but regained once in *Tatemelon*. Amongst the ingroup, the dart sac was acquired for three times but lost in *Camaena*, *Amphidromus* and the Australian camaenids. The flagellum has been lost twice, once in *Exiligada* Iredale, 1939, and once in the clade including *Coccolglypta* Pilsbry, 1895, *Acusta* Martens, 1860, *Laeocathaica* Moellendorff, 1899, *Pseudobuliminus* Gredler, 1887, *Bradybaena* Beck, 1837, and *Cathaica* Moellendorff, 1884, which are all bradybaenine genera mainly distributed in the mainland of China.

Systematics

Family Camaenidae Pilsbry, 1895

Stegoderma Martens, 1876

盖螺属

Helix (*Stegodera*) Martens in Pfeiffer 1876: 150; Schmacker and Boettger 1894: 173.
Stegodera. – Pilsbry 1905: 64, Yen 1939: 126; Zilch 1960: 610; Schileyko 2003: 1512.
Steganodera Kobelt, 1879: 236 (incorrect subsequent spelling or unjustified emendation); Schileyko 2003: 1512 (syn pro *Stegodera* Martens, 1876).
Plectopylis (*Stegodera*). – Pilsbry 1894: 147.
Planispira (*Stegodera*). – Thiele 1931: 681.

Type species. *Helix angusticollis* Martens, 1875, by original designation.

Diagnosis. Shell sinistral. Apical whorls with dense fine ribs that gradually becoming granules. The last $\frac{1}{4}$ body whorl compressed, apically covering the contacted penultimate whorl. Peristome expanded and slightly reflexed. Head wart absent. Each side of mantle edge with a leaf-shaped appendage. Penis sheath weakly present. Penis externally simple. Epiphallic papilla absent. Flagellum present. Dart sac apparatus present. Accessory sac well developed. Mucous glands with numerous gland tubes. Membranous sac surrounding terminal genitalia absent. Poly-layered structure in dart sac and/or accessory sac absent.

Remarks. This genus was considered as a subgenus of *Helix* Linnaeus, 1758 or *Plectopylis* Benson, 1860 for some time (Martens 1876; Schmacker and Boettger 1894; Pilsbry 1894). Pilsbry (1905) formally established its independent status. *Stegodera* and *Traumatophora* Ancey, 1887 were considered to be closely related, and *Traumatophora* was once treated as a subgenus of *Stegodera* (Pilsbry 1905; Gude 1920). Pilsbry (1905) believed that the two shallow grooves in the throat area of *Stegodera* are likely to be homologous to the dentition in *Traumatophora*.

In light of the genital system, *Stegodera* shares with *Nesiohelix* the most important character states like the presences of flagellum, numerous tubes of mucous glands and the papilla distally leading to mucous glands on the inner wall of the accessory sac, and the absences of the epiphallic papilla, poly-layered structure in dart sac apparatus and membranous sac surrounding terminal genitalia (Wu 2019). The close relationship between them in genitalia is supported by the phylogenetic result of this work (Fig. 1A, B).

***Stegodera angusticollis* (Martens, 1875)**

狭缘盖螺

Figures 1, 2, 3A, 4A–D, 5A–C, 6A, B, 8A–C

Helix angusticollis Martens, 1875a: 2. Martens 1875b: 185; Pfeiffer 1875: 449, 1876: 149, pl. 134, figs 7–10; Gredler 1882: 175; Heude 1882: 36, pl. 15, fig. 8; Möllendorff 1884: 387.

Helix (*Stegodera*) *angusticollis*. – Martens, 1876 (in Pfeiffer 1870–1876): 149–150; Pilsbry 1890: 7, pl. 1, figs 15–17.

Plectopylis (*Stegodera*) *angusticollis*. – Pilsbry 1894: 147.

Planispira (Stegodera) angusticollis. – Thiele 1931: 681.

Stegodera angusticollis. – Gude 1902: 4; Kobelt 1905: 78; Pilsbry 1905: 64, 66, pl. 2, figs 1–3; Gude 1920: 60; Yen 1939: 126, pl. 13, fig. 9; Zilch 1960: fig. 2138; Richardson 1983: 291; Schileyko 2003: 1512, fig. 1948; Chen and Gao 1987: 107, fig. 137; Qian et al. 2008: 289, fig. 169; Qian and Zhou 2014: 120, figure in text.

Museum material examined. •ZMB. Moll. 31044, syntype, Poyangsee, China, slg. v. Richthofen; ZMB. •ZMB. Moll. 3710/1 China, slg. Paetel; •SMF27113/3, China: Prov. Hupei, slg. O. v. Moellendorff; •SMF27114/2, China: Wü-chang-fú, slg. K. Hashagen (ex. Schmacker); •SMF42579/3, China: Húbei (Hupei), slg. Ehrmann; •IZ-CAS TM108733/1, Kieou-Kiang; •IZCAS TM158903-158920/18, Ou-tchang h[ien], ex. Musée Heude; •IZCAS TM159272-159397/126, Kieou-Kiang, ex. Musée Heude.

New material examined. •One shell of HBUMM08435 (dissected), Guanyin Cave [观音洞], Taizi Town [太子镇], Yangxin County [阳新县], Huangshi City [黄石市], Hubei Province, China, 30°0'3.816"N, 115°11'24.428"E, 140 m a.s.l., 2020-X-15, leg. Xiao-Long Wang & Zi-Hao Shen ($S_{D_{maj}}$ = 26.7 mm, $S_{D_{min}}$ = 21.3 mm, S_H = 11.3 mm). •Three shells of OYKC, one shell of QL, Lushui Lake [陆水湖], Chibi City [赤壁市], Xianning City [咸宁市], Hubei Province, China, 29°40'12"N, 113°58'35"E, 2020-X-03, leg. Di Yu & Kai-Chen Ouyang.

Type locality. Poyang-See (= Poyang Lake [鄱阳湖], Jiangxi).

Measurements of new material. $S_{D_{maj}}$ = 26.7–30.6 mm, $S_{D_{min}}$ = 21.3–23.7 mm, S_H = 11.3–12.2 mm (n = 6).

Diagnosis. Body whorl completely covering partial penultimate whorl. Penial sheath weakly present. Epiphallic papilla absent. Dart sac apparatus and flagellum present. Mucous glands with numerous tubes.

Redescription. Shell (Fig. 3A). Sinistral, large, solid, rather flat, five whorls, in chestnut and darker near aperture. Suture impressed. Protoconch $1\frac{1}{4}$ whorls. After $\sim 3\frac{1}{2}$ whorls, growth lines broken into regularly arranged tubercles. Body whorl compressed from the last $\frac{1}{4}$ to the last $\frac{1}{8}$ whorls, completely covering corresponding part of penultimate whorl including the suture. After the last $\frac{1}{8}$ whorls, body whorl becoming as broad as normal again. On the above compressed region, one shorter ventral depression and one longer apical depression present. Aperture semilunar, slightly descending. Peristome chestnut, thickened, expanded, and slightly reflexed. Umbilicus moderately broad; approximately $\frac{1}{5}$ of shell major diameter. Protoconch visible through umbilicus.

General anatomy (Fig. 4A–D). Head wart absent. On internal body wall of head region between ommatophore insertions with tiny pits rather than glands (Fig. 4C). Each side of mantle edge with a leaf-shaped appendage (Fig. 4A, B). Body reddish brown, central dorsa with light longitudinal stripes. Sole dirty white. Jaw arcuate; with 12 more or less projecting ribs (Fig. 4D).

Genitalia (Figs 5A–C, 6A, B). Penis sheath present but thin and very short. Penis medially slightly thickened, moderately long, ~ 8.8 mm, externally simple. Inside penis with several thin longitudinal pilasters. Epiphallus slightly longer than penis. A

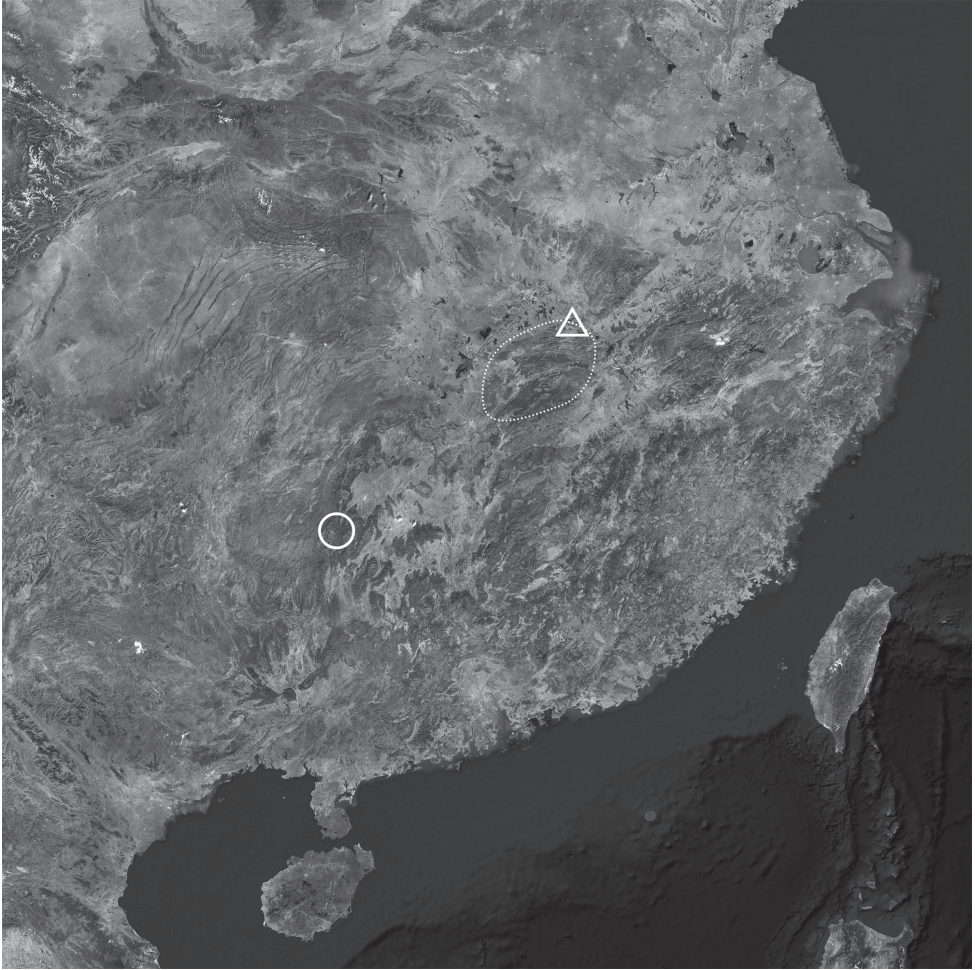


Figure 2. Distribution of *Stegoderia* and *Pseudostegoderia qiului* gen. et sp. nov. Triangle: new locality of *Stegoderia angusticollis* (Martens, 1875); dashed range: area of *Stegoderia angusticollis*; circle: type locality of *Pseudostegoderia qiului* gen. et sp. nov.

very thin membranous sac wrapping distal half of penis with distal end connecting basal penial retractor muscle (Fig. 6B). Flagellum cylindrical, tapering. Vas deferens thin throughout. Dart sac apparatus distally inserting on vagina. Dart sac small. Dart not observed. Membranous sac surrounding terminal genitalia absent. Accessory sac relatively large. Tubes of mucous glands more than twenty, neatly inserting in a single row on distal and same side of dart sac on accessory sac (Figs 5C, 6B). From proximal to distal accessory sac, mucous gland tubes increased gradually in length (Figs 5C, 6B). Papilla distally leading to mucous glands on inner wall of accessory sac integrated into one long thick spongy pilaster on the side of mucous gland tube insertion (Fig. 6A). Bursa copulatrix ball-shaped.

Ecology. This species was observed under litter layer, on nearby rocks and crevices.

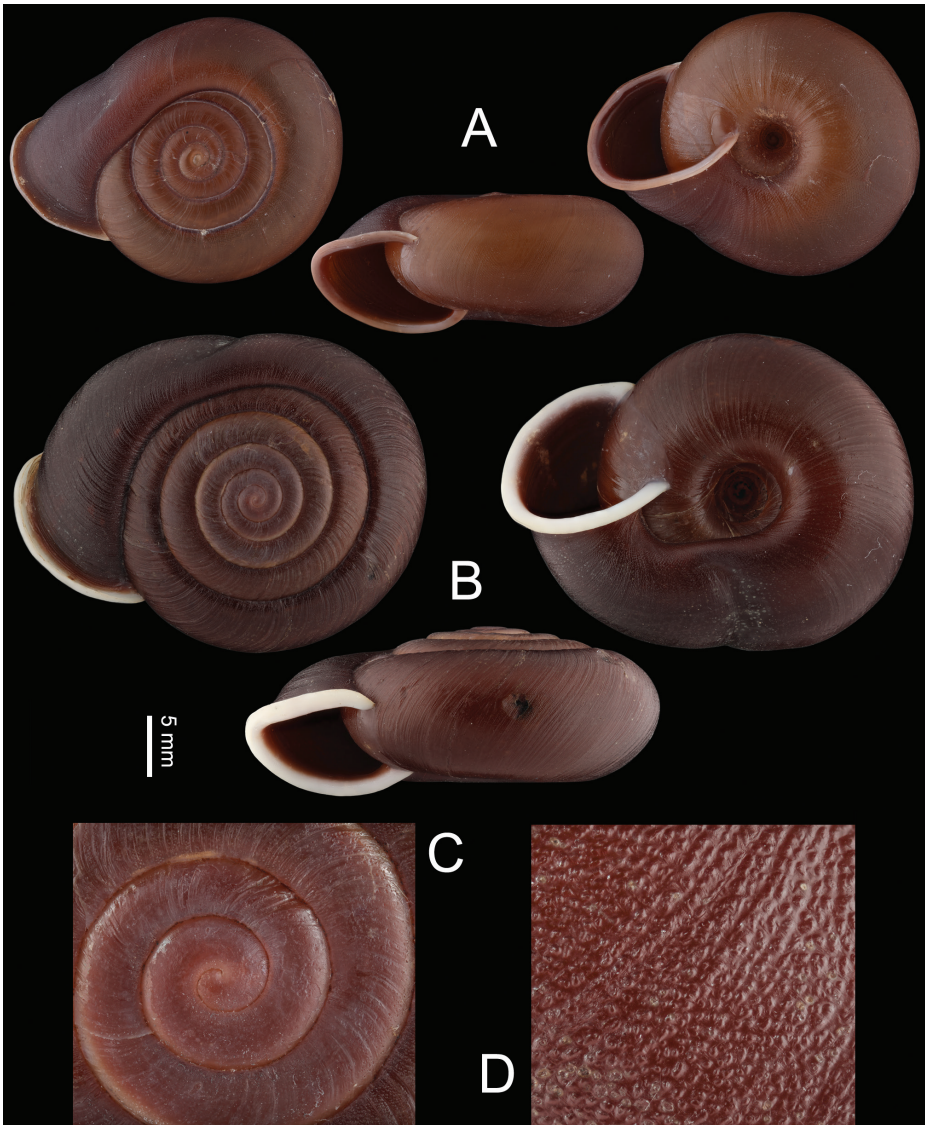


Figure 3. Shells **A** *Stegodera angusticollis* Martens, 1876, HBUMM08435 **B–D** *Pseudostegodera qiului* gen. et sp. nov., holotype IZCAS TM206978 **C** p rotoconch, magnified **D** shell surface, magnified. Scale bar: 5 mm (**A, B**).

Distribution. Central China: Hubei, Jiangxi (Fig. 2).

Remarks. The peristome of *Stegodera angusticollis* is in chestnut in fresh specimens, but in most museum specimens this color gets faint to white. In *Stegodera angusticollis*, the compressed part of body whorl usually completely cover the penultimate whorl, while in *Pseudostegodera qiului* gen. et sp. nov. the corresponding part

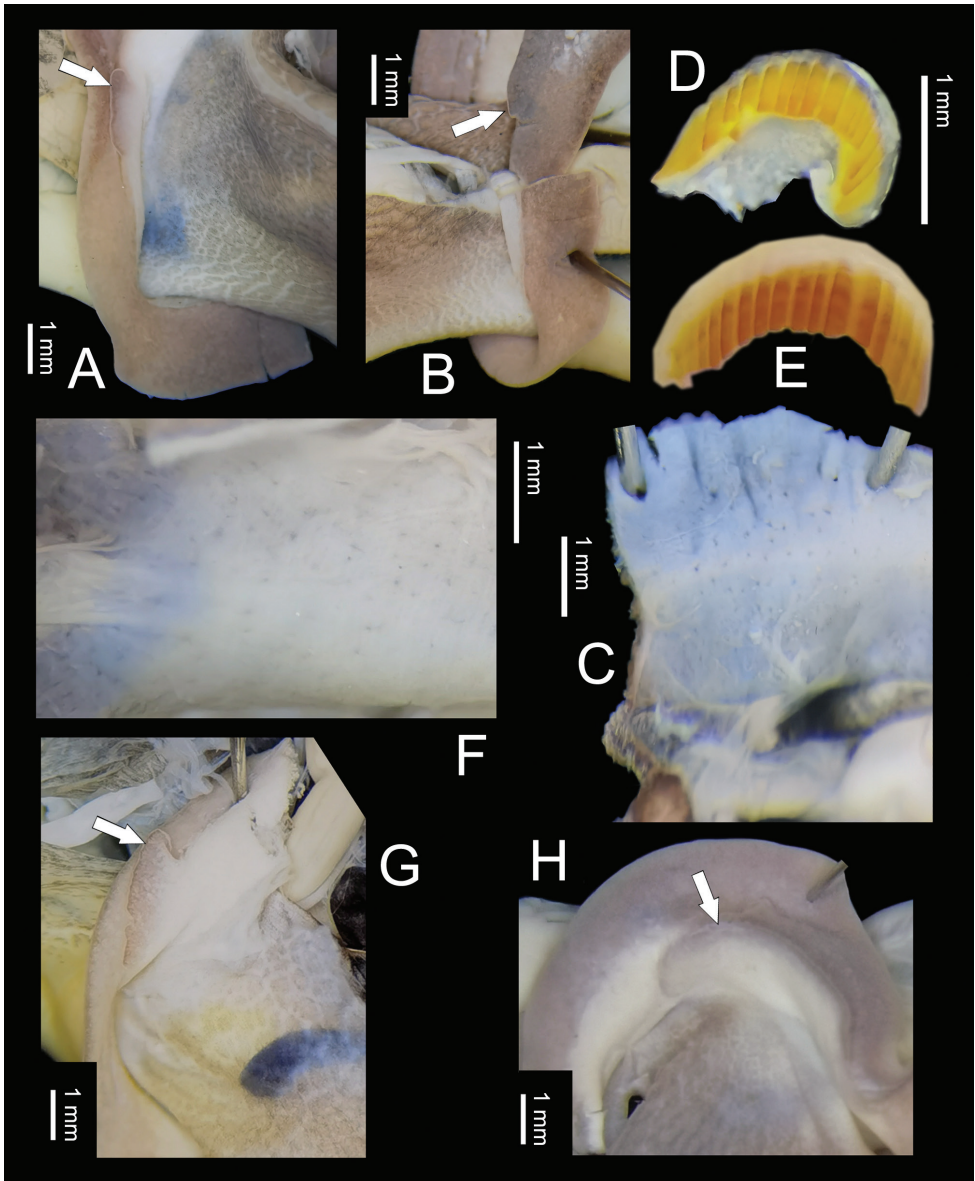


Figure 4. General anatomy **A–D** *Stegodera angusticollis* (Martens, 1875), HBUMM08435 **A** lobe (arrowed) on the left side of mantle edge **B** lobe (arrowed) on the right side of mantle edge **C** internal surface of head region **D** jaw **E–H** *Pseudostegodera qiului* gen. et sp. nov., holotype IZCAS TM206978 **E** jaw **F** internal surface of head region **G** lobe (arrowed) on the left side of mantle edge **H** lobe (arrowed) on the right side of mantle edge.

is not so compressed and the compressed part of body whorl can hardly cover the penultimate whorl.

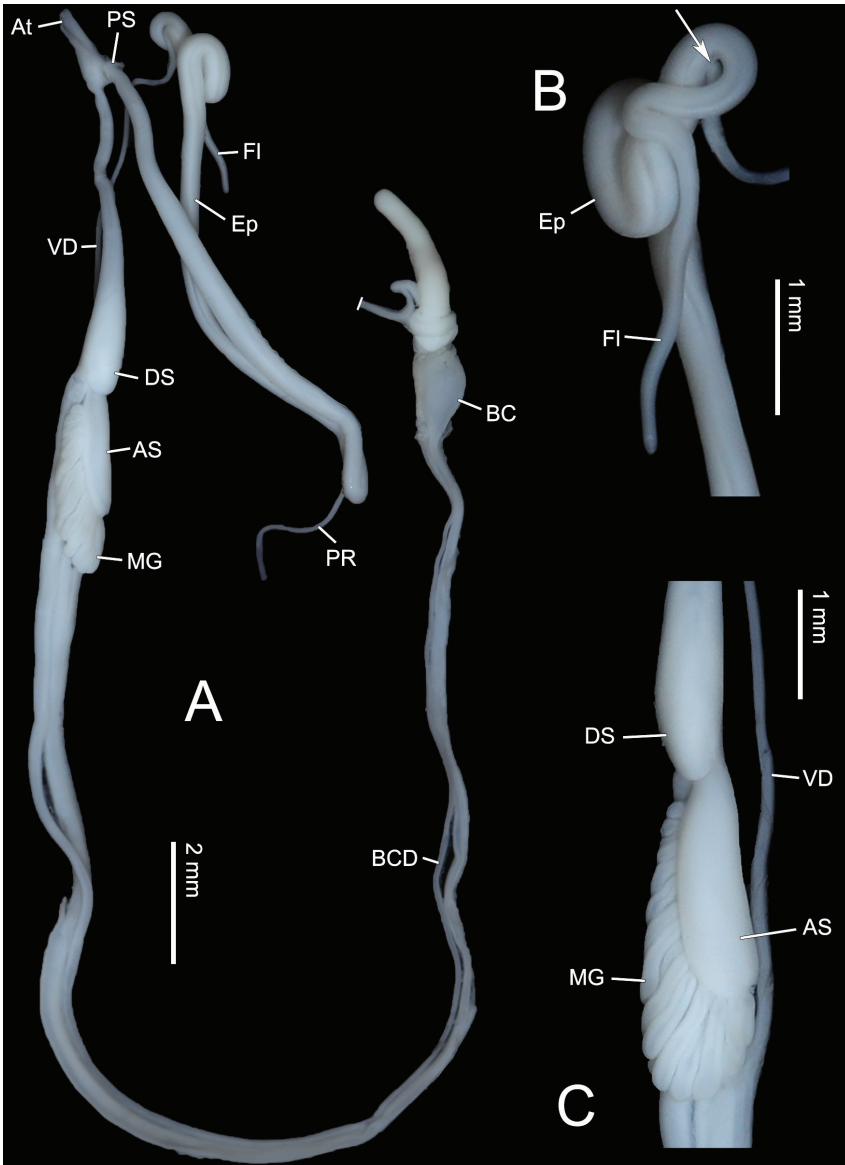


Figure 5. Genitalia of *Stegoderma angusticollis* (Martens, 1875), HBUMM08435 **A** general view **B** male part, showing the vas deferens connecting epiphallus (arrowed) **C** female part, showing the dart sac, accessory sac, and mucous glands.

Some authors (Chen and Gao 1987; Qian et al. 2008; Qian and Zhou 2014) recorded this species in Jiangsu, Zhejiang and Anhui, but voucher specimens from these provinces were neither recorded therein nor being found in the mollusk collection deposited in IZCAS where some of them once worked. Therefore, the accuracy of these records needs to be further confirmed.

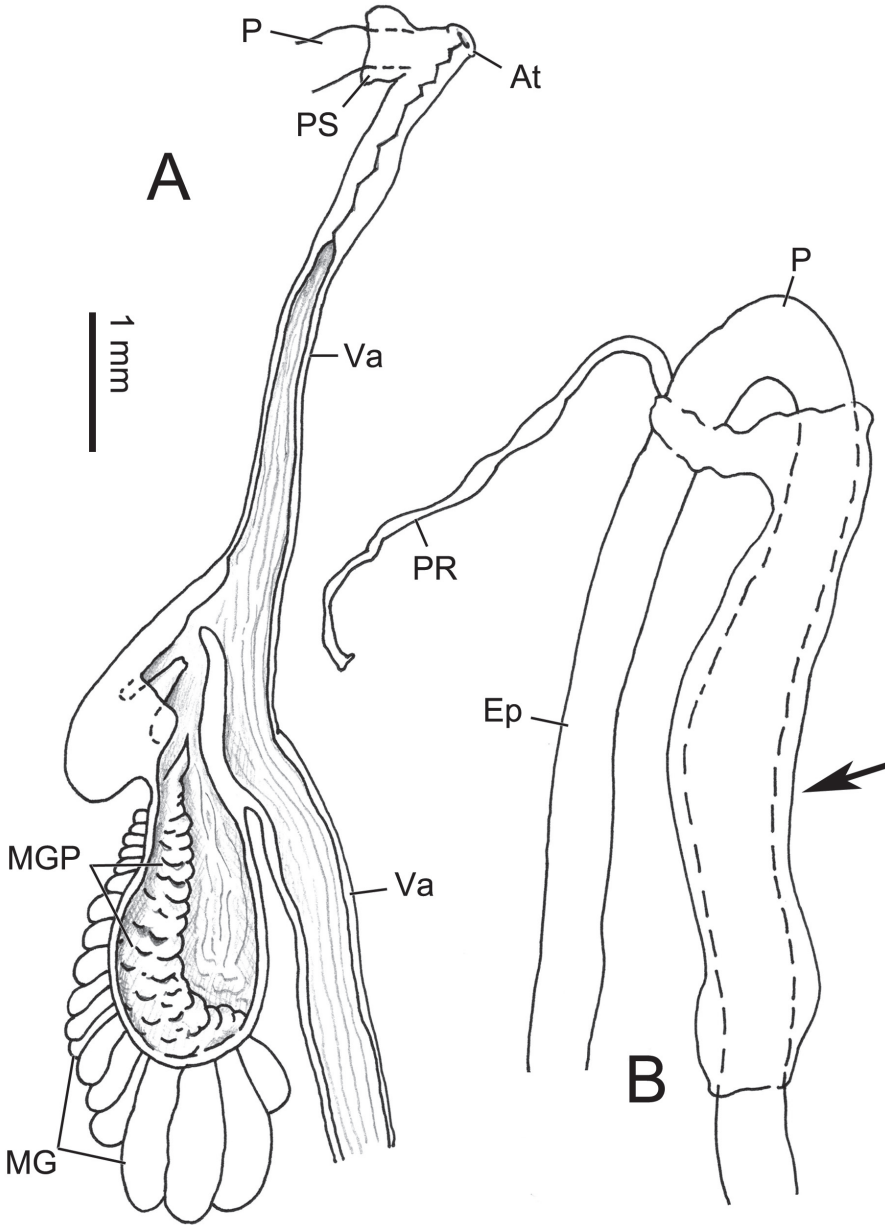


Figure 6. Genitalia of *Stegodera angusticollis* (Martens, 1875), HBUMM08435 **A** exposed dart sac apparatus **B** magnified partial penis and partial epiphallus. Arrow showing a very thin membranous sac wrapping distal half of penis with distal end connecting basal penial retractor muscle.

***Pseudostegodera* Wu & Chen, gen. nov.**

拟盖螺属

<http://zoobank.org/F0A6D222-8DB2-4B57-8910-17CAAE2B7FFA>

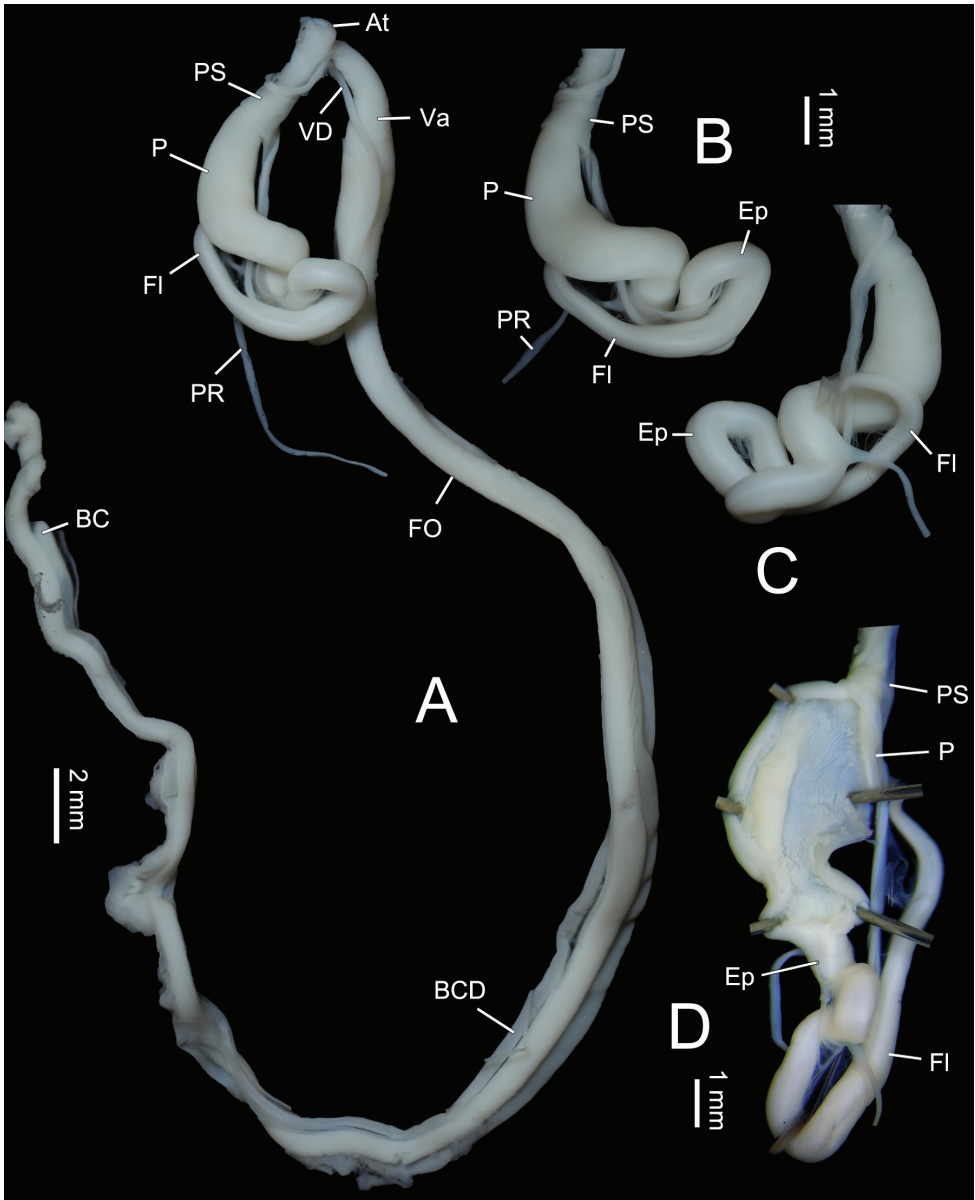


Figure 7. Genitalia of *Pseudostegodera qiului* gen. et sp. nov., holotype IZCAS TM206978 **A** general view **B, C** male part, two sides **D** exposed penis.

Type species. *Pseudostegodera qiului* gen. et sp. nov.

Diagnosis. Shell sinistral. Apical whorls with dense fine ribs gradually becoming granules. The last $\frac{1}{8}$ to $\frac{1}{4}$ body whorl compressed, only partly covering penultimate whorl. Umbilicus broad. Head wart absent. Each side of mantle edge with a leaf-shaped appendage. Penis sheath present. Penis externally simple. Epiphallic papilla absent. Flagellum present. Dart sac apparatus absent.

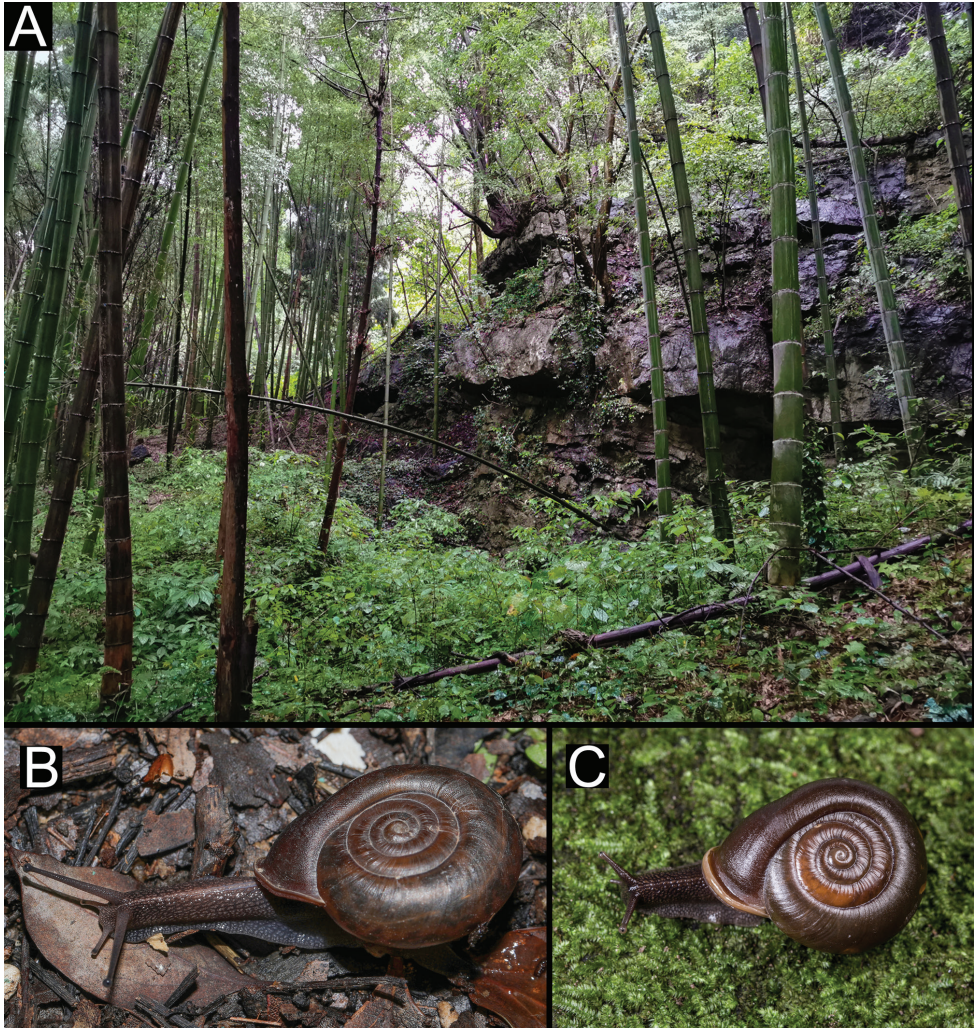


Figure 8. Habitat and living specimens of *Stegoderia angusticollis* (Martens, 1875) **A** habitat (photograph Kai-Chen Ouyang) **B** the living specimen of HBUMM08435 **C** a living specimen from Chibi City (photograph Lu Qiu).

Remarks. Conchologically the new genus can be distinguished from *Stegoderia* by the detached body whorl and penultimate whorl. The new genus is supported to be the closest relative of a clade containing *Stegoderia* + *Nesiohelix* as based on the Maximum Likelihood/Baysian Inference phylogeny shown in Fig. 1A. However, when the Australian camaenids were included in the analysis, the relationships between the new genus, *Stegoderia* + *Nesiohelix*, and all remaining taxa except *Satsuma* remained unresolved (Fig. 1B). The new genus is conchologically similar to *Stegoderia*, however, it differs in certain reproductive characters (see above). We consider that the genital anatomy is more informative than shell features in helicoid systematics (e.g., Criscione and Köhler 2013). In addition, the loss of the dart sac apparatus in

Bradybaeninae and/or Camaeninae is not a frequent event during the evolution of Camaenidae (Fig. 1B). Based on these two considerations, we consider it is reasonable to distinguish this new camaenid taxon as a monotypic genus represented by the new species described below.

***Pseudostegodera qiului* Chen, sp. nov.**

邱氏拟盖螺

<http://zoobank.org/E95104CE-D502-4E48-A256-F0727253745C>

(Figs 1, 2, 3B–D, 4E–H, 7A–D, 9A–C)

Type material. •**Holotype**, IZCAS TM206978, Zihuaping [紫花坪], core area of Shunhuang Mountain National Nature Reserve [舜皇山国家级自然保护区核心区], Huanglong Town [黄龙镇], Xinning County [新宁县], Shaoyang City [邵阳市], Hunan, China, 26°23'31"N, 110°0'25"E, 945 m a.s.l., 2020-VIII-23, leg. Lu Qiu. •**Paratype**, MYNU/1, same data as holotype.

Measurements. $S_{D_{maj}} = 31.0 - 34.0$ mm, $S_{D_{min}} = 25.0 - 26.4$ mm, $S_H = 12.0 - 13.7$ mm ($n = 2$).

Diagnosis. Body whorl incompletely covering partial penultimate whorl. Dart sac apparatus absent. Flagellum present.

Description. Shell (Fig. 3B–D). Sinistral, large, depressed, thick and solid, dark reddish-brown. Shell with $5\frac{1}{2}$ convex whorls. Suture impressed. Protoconch $1\frac{1}{4}$ – $1\frac{1}{2}$ whorls, with regularly arranged fine axial striae that may be invisible by weathering or erosion. Growth lines clear, broken into microscopic tubercles of irregular shape. The last $\frac{1}{8}$ to $\frac{1}{4}$ body whorl compressed, partly covering penultimate whorl. At $\frac{1}{4}$ whorl from the aperture, a spiral depression above periphery and a weak depression near umbilicus making a narrowing on body whorl. Whorl after the narrowing reverting to normal broadness. Aperture semilunar, slightly descending. Peristome white, strongly thickened, expanded, and slightly reflexed. Umbilicus broad, approximately $\frac{1}{3}$ of shell major diameter. Protoconch visible through umbilicus.

General anatomy (Fig. 4E–H). Eversible head wart absent. On internal body wall of head region between ommatophorous insertions with tiny pits rather than glands (Fig. 4F). Each side of mantle edge with a leaf-shaped appendage (Fig. 4G, H). Body reddish brown, central dorsa with light longitudinal stripes. Sole dirty white. Jaw arcuate, with ~ 14 more or less projecting ribs (Fig. 4E).

Genitalia (Fig. 7A–D). Penis sheath short but well developed. Penis somewhat swollen on proximal half, externally simple. In the middle of penis, internally with a single strong longitudinal pilaster almost as thick as epiphallus, ~ 2 mm long (Fig. 7D). Epiphallic papilla absent (Fig. 7D). Flagellum cylindrical, tapering. Vas deferens thin throughout, approximately as long as penis. Dart sac apparatus absent. Bursa copulatrix duct thickened basally. Bursa copulatrix duct longer than 50 mm. Bursa copulatrix rod-shaped.

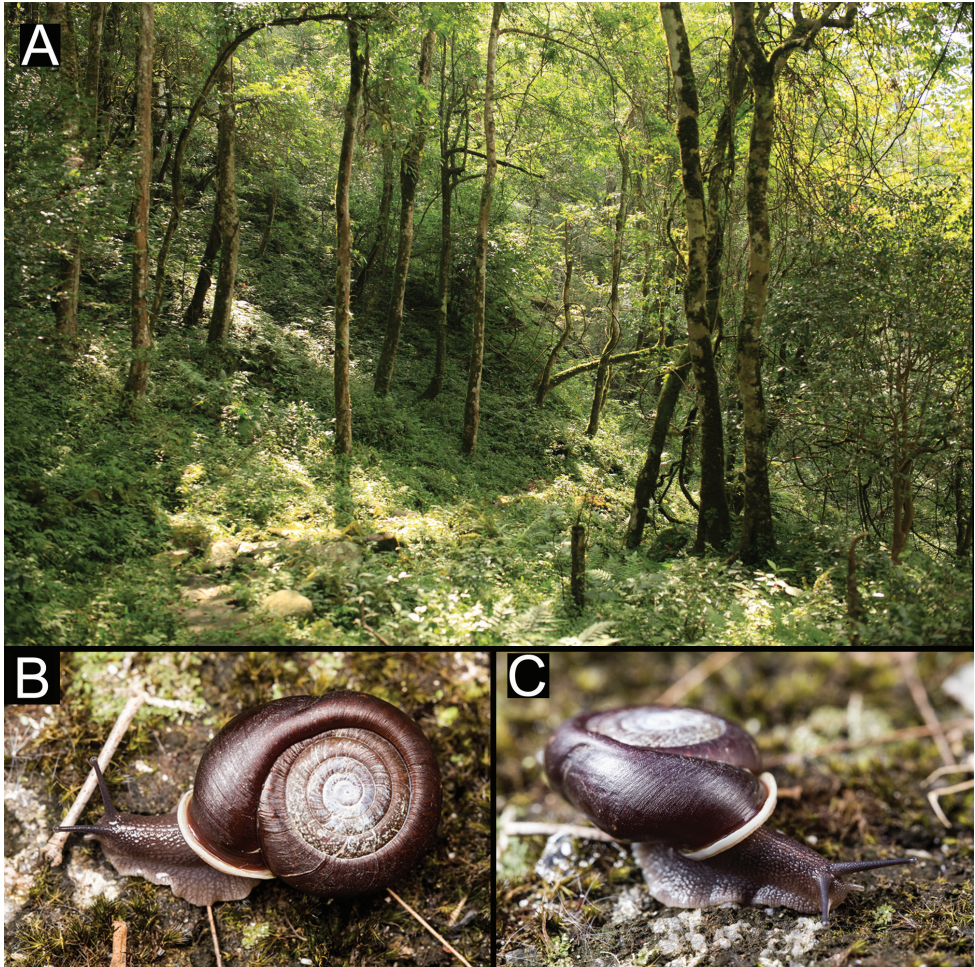


Figure 9. Habitat and living specimens of *Pseudostegodera qiului* gen. et sp. nov. **A** habitat **B, C** a living specimen. Photographs Lu Qiu.

Etymology. This new species is named after Dr Lu Qiu [邱鹭], who provided the specimens and field data.

Ecology. This species was found under rotten wood.

Distribution. Only known from the type locality (Fig. 2).

Remarks. See under the genus.

Discussion

The comparison of the phylograms (Fig. 1) suggests the phylogeny obtained in this paper is more or less robust when the Australian camaenids, which form a monophyly together with the Asian camaenids (as suggested by Scott 1996), are considered. The phy-

logenetic position of *Satsuma* agrees with that suggested by many authors (Chiba 1999: fig. 3; Wade et al. 2007: fig. 2). As indicated by some authors, *Satsuma* is the sister group of the common ancestor of Bradybaeninae and Camaeninae (Fig. 1; Wade et al. 2007: fig. 2), rather than a typical camaenine (sensu Azuma 1995) or bradybaenine (sensu Schileyko 2004). The monophyly made by *Stegodera*, *Nesiohelix* and the new genus is the sister group of all the remaining bradybaenines and camaenines involved in this study. It suggests that neither the Camaeninae including *Satsuma* (sensu Azuma 1995) nor the Bradybaeninae including *Nesiohelix* (sensu nearly all the authors) are monophyletic.

The current work also confirms that so-called important characters of genital system, including penial sheath, epiphallic papilla, penial caecum, flagellum, and dart sac apparatus, have homoplasiously evolved more than once in the studied terminal taxa and their ancestral nodes (Fig. 1B). In other words, widespread homoplasious changes in morphology (Hirano et al. 2014; Fig. 1) including dart sac apparatus based on which Bradybaeninae and Camaeninae are distinguished, rendering the basis of the establishment of Bradybaeninae particularly feeble, explaining that no agreement on the subdivision within Camaenidae was reached to date (Nordsieck 2002; Schileyko 2003, 2004; Wade et al. 2006, 2007; Gittenberger et al. 2012; Bouchet et al. 2017).

Acknowledgements

We are grateful to Sigrid Hof (SMF), Kaibaryer Meng (IZCAS), Christine Zorn and Le-Jia Zhang (ZMB) for searching and imaging the specimens of *Stegodera angusticollis* in their respective collections. Kai-Chen Ouyang (Kunming, China), Di Yu (Wuhan, China), Lu Qiu (MYNU, China), and Zi-Hao Shen (Wuhan, China) are appreciated for providing specimens and field data. We appreciate T. A. Pearce, F. Köhler, and an anonymous reviewer for their very helpful comments.

This work is supported by the National Natural Science Foundation of China (NSFC 31872196) and Guangdong Academy of Science (GDAS) Special Project of Science and Technology Development (No. 2020GDASYL-20200102021).

References

- Azuma M (1995) Colored Illustrations of the Land Snails of Japan. Hoikusha Publishing, 343 pp.
- Bouchet O, Rocroi JP, Hausdorf B, Kaim A, Kano Y, Nützel A, Parkhaev P, Schrödl M, Strong EE (2017) Revised classification, nomenclator and typification of gastropod and monoplacophoran families. *Malacologia* 61(1–2): 1–526. <https://doi.org/10.4002/040.061.0201>
- Castresana J (2000) Selection of conserved blocks from multiple alignments for their use in phylogenetic analysis. *Molecular Biology and Evolution* 17: 540–552. <https://doi.org/10.1093/oxfordjournals.molbev.a026334>

- Chen DN, Gao JX (1987) Economic Fauna of China (Terrestrial Molluscs). Science Press, Beijing, 186 pp. [in Chinese]
- Chiba S (1999) Accelerated evolution of land snails *Mandarina* in the oceanic Bonin Islands: Evidence from mitochondrial DNA Sequences. *Evolution* 53(2): 461–471. <https://doi.org/10.1111/j.1558-5646.1999.tb03781.x>
- Criscione F, Köhler F (2013) Six new species of *Australocosmica* Köhler, 2011 from the Kimberley Islands, Western Australia (Mollusca: Pulmonata: Camaenidae). *Zootaxa* 3608(2): 101–115. <https://doi.org/10.11646/zootaxa.3608.2.1>
- Edler D, Klein J, Antonelli A, Silvestro D (2019) raxmlGUI 2.0 beta: a graphical interface and toolkit for phylogenetic analyses using RAxML. *bioRxiv*. <https://doi.org/10.1101/800912>
- Folmer O, Black M, Hoeh W, Lutz R, Vrijenhoek R (1994) DNA primers for amplification of mitochondrial cytochrome *c* oxidase subunit I from diverse metazoan invertebrates. *Molecular Marine Biology and Biotechnology* 3(5): 294–299.
- Gittenberger E, Hamann TD, Asami T (2012) Chiral speciation in terrestrial pulmonate snails. *PLoS ONE* 7(4): e34005. <https://doi.org/10.1371/journal.pone.0034005>
- Gredler V (1882) Uebersicht der Binnenschnecken von China. *Malakozoologische Blätter, Neue Folge* 5: 165–187.
- Gude GK (1902) A classified list of the helicoid land shells of Asia. *Proceedings of the Malacological Society of London* 9(1): 1–11.
- Gude GK (1920) The armature of land Mollusca. *Proceedings of the Malacological Society of London* 14(1): 52–73.
- Heude PM (1882) Notes sur les mollusques terrestres de la vallée du Fleuve Bleu. *Mémoires concernant l'histoire naturelle de l'Empire chinois* 1: 1–84. <https://doi.org/10.5962/bhl.title.50365>
- Hirano T, Kameda Y, Kimura K, Chiba S (2014) Substantial incongruence among the morphology, taxonomy, and molecular phylogeny of the land snails *Aegista*, *Landouria*, *Trishop-lita*, and *Pseudobuliminus* (Pulmonata: Bradybaenidae) occurring in East Asia. *Molecular Phylogenetics and Evolution* 70: 171–181. <https://doi.org/10.1016/j.ympev.2013.09.020>
- Huang CW, Lin SM, Wu WL (2015) Mitochondrial genome sequences of landsnails *Aegista diversifamilia* and *Dolicheulota formosensis* (Gastropoda: Pulmonata: Stylommatophora). *Mitochondrial DNA, Early Online*: 1–3. <https://doi.org/10.3109/19401736.2015.1053070>
- Kerney MP, Cameron RAD (1979) *A Field Guide to the Land Snails of Britain and North-West Europe*. Collins, London, 288 pp. [24 pls.]
- Kobelt W (1879) *Illustriertes Conchylienbuch*, vol. 2. Bauer & Raspe, Nürnberg, 177–264. [pls 61–80]
- Kobelt W (1905 [1904–1906]) *Die Raublungenschnecken (Agnatha). Erste Abtheilung: Streptaxidae und Daudebardiidae*. In: Kobelt W (Ed.) *Systematisches Conchylien-Cabinet von Martini und Chemnitz*. Neu herausgegeben und vervollständigt. Ersten Bandes, zwölfte Abtheilung (B). Erste Hälfte. (1) 12b. Bauer & Raspe, Nürnberg, 1–96. [pls 42–59]
- Kumar S, Stecher G, Tamura K (2015) MEGA7: Molecular evolutionary genetics analysis version 7.0 for bigger datasets. *Molecular Biology and Evolution* 33: 1870–1874. <https://doi.org/10.1093/molbev/msw054>
- Maddison WP, Maddison DR (2019) *Mesquite: a modular system for evolutionary analysis*. Version 3.61. <http://www.mesquiteproject.org>

- Martens E von (1875a) Ostasiatische Land- und Süßwasserconchylien. Sitzungs-Berichte der Gesellschaft Naturforschender Freunde, Berlin 1875: 2–4.
- Martens E von (1875b) Binnen-Mollusken aus dem mittlern China. Malakozologische Blätter 22: 185–188.
- Möllendorff OF (1884) Materialien zur Fauna von China. Jahrbücher der Deutschen Malakozologischen Gesellschaft 11: 307–391.
- Palumbi S, Martin A, Romano S, McMillan WO, Stice L, Grabowski G (1991) The simple fool's guide to PCR. Department of Zoology, University of Hawaii, Honolulu.
- Pfeiffer L (1875 [1875–1876]) Monographia Heliceorum viventium. Sistens descriptiones systematicas et criticas omnium huius familiae fenerum et specierum hodie cognitarum. Volumen septimum (3): 321–480. F.A. Brockhaus, Lipsiae.
- Pfeiffer L (1870–1876) Novitates Conchologicae. Series prima. Mollusca extramarina. Descriptions et figures de coquilles extramarines nouvelles ou peu connues. Tome IV, 1–8, pls 109–111 [1870], 9–40, pls 112–117 [1871], 41–88, pls 118–125 [1872], 89–112, pls 126–130 [1874], 113–144, pls 131–134 [1875], 145–171, pls 135–137.
- Pilsbry HA (1890) [1890–1891] Manual of conchology, Structural and systematic, with illustrations of the species, Second series, Volume 6 (Helicidae, Vol. IV). Academy of Natural Science Philadelphia, PA, 366 pp. [pp.1–192 (1890)].
- Pilsbry HA (1895) [1893–1895] Manual of conchology, Structural and systematic, with illustrations of the species, Second series, Volume 9 (Helicidae, Vol. 7. Guide to the Study of Helices). Academy of Natural Science Philadelphia, PA, 253 pp. [pp. 161–336 (1895)]
- Pilsbry HA (1905) Notes on *Moellendorffia* and *Stegodera*. The Nautilus 19: 63–67.
- Qian ZX, Zhou WC [Ed.] (2014) Illustrated Handbook of Common Terrestrial Mollusks in China. Zhejiang People's Fine Arts Publishing House, Hangzhou, 228 pp. [in Chinese]
- Qian ZX (ed.) (2008) Farmland Molluscs from Zhejiang. Hangzhou Publishing House, Hangzhou, 425 pp. [in Chinese]
- Rambaut A, Drummond AJ, Xie D, Baele G, Suchard MA (2018) Posterior summarisation in Bayesian phylogenetics using Tracer 1.7. Systematic Biology 67: 901–904. <https://doi.org/10.1093/sysbio/syy032>
- Razkin O, Gómezmoliner BJ, Prieto CE, Martínezortí A, Arrébola JR, Muñoz B, Chueca LJ, Madeira MJ (2015) Molecular phylogeny of the western Palaearctic Helicoidea (Gastropoda, Stylommatophora). Molecular Phylogenetics and Evolution 83: 99–117. <https://doi.org/10.1016/j.ympev.2014.11.014>
- Richardson CL (1983) Bradybaenidae: Catalog of species. Tryonia 12: 1–253.
- Ronquist F, Teslenko M, Van Der Mark P, Ayres DL, Darling A, Höhna S, Larget B, Liu L, Suchard MA, Huelsenbeck JP (2012) MrBayes 3.2: efficient Bayesian phylogenetic inference and model choice across a large model space. Systematic Biology 61(3): 539–542. <https://doi.org/10.1093/sysbio/sys029>
- Shileyko AA (2003) Treatise on recent terrestrial pulmonate molluscs, Part 11. Trigonochlamydidae, Papillodermidae, Vitrinidae, Limacidae, Bielziidae, Agriolimacidae, Boettgeriidae, Camaenidae. Ruthenica, Supplement 2(11): 1467–1626. [figs 1896–2098]
- Shileyko AA (2004) Treatise on recent terrestrial pulmonate molluscs, Part 12. Bradybaenidae, Xanthonychidae, Epiphragmophoridae, Helminthoglyptidae, Elonidae, Sphincterochilidae, Cochlicellidae. Ruthenica, Supplement 2(12): 1627–1763. [figs 2099–2259]

- Schmacker B, Boettger O (1894) Description of some Chinese land-shells. Proceedings of the Malacological Society 1: 169–174. <https://doi.org/10.1093/oxfordjournals.mollus.a064109>
- Scott B (1996) Phylogenetic relationships of the Camaenidae (Pulmonata: Stylommatophora: Helicoidea). Journal of Molluscan Studies 62(1): 65–73. <https://doi.org/10.1093/mollus/62.1.65>
- Thiele J (1931) Handbuch der systematischen Weichtierkunde. Vol. 1, Teil 2: 377–778. Gustav Fischer, Jena.
- Thompson JD, Gibson TJ, Plewniak F, Jeanmougin F, Higgins DG (1997) The CLUSTAL_X windows interface: flexible strategies for multiple sequence alignment aided by quality analysis tools. Nucleic Acids Research 25(24): 4876–4882. <https://doi.org/10.1093/nar/25.24.4876>
- Wade CM, Hudelot C, Davison A, Naggs F, Mordan PB (2007) Molecular phylogeny of the helicoid land snails (Pulmonata: Stylommatophora: Helicoidea), with special emphasis on the Camaenidae. Journal of Molluscan Studies 73: 411–415. <https://doi.org/10.1093/mollus/eym030>
- Wade CM, Mordan PB, Naggs F (2006) Evolutionary relationships among the Pulmonate land snails and slugs (Pulmonata, Stylommatophora). Biological Journal of the Linnean Society 87: 593–610. <https://doi.org/10.1111/j.1095-8312.2006.00596.x>
- Wang P, Xiao Q, Zhou WC, Hwang CC (2014) Revision of three camaenid and one bradybaenid species (Gastropoda, Stylommatophora) from China based on morphological and molecular data, with description of a new bradybaenid subspecies from Inner Mongolia, China. ZooKeys 372: 1–16. <https://doi.org/10.3897/zookeys.372.6581>
- Wang P, Yang HF, Zhou WC, Hwang CC, Zhang WH, Qian ZX (2014) The mitochondrial genome of the land snail *Camaena cicatricosa* (Müller, 1774) (Stylommatophora, Camaenidae): the first complete sequence in the family Camaenidae. ZooKeys 451: 33–48. <https://doi.org/10.3897/zookeys.451.8537>
- Wu M (2019) A taxonomic note on the helicoid land snail genus *Traumatophora* (Eupulmonata, Camaenidae). ZooKeys 835: 139–152. <https://doi.org/10.3897/zookeys.835.32697>
- Xia X (2018) DAMBE7: New and improved tools for data analysis in molecular biology and evolution. Molecular Biology and Evolution 35: 1550–1552. <https://doi.org/10.1093/molbev/msy073>
- Xia X, Lemey P (2009) Assessing substitution saturation with DAMBE. In: Lemey P, Salemi M, Vandamme A-M (Eds) The Phylogenetic Handbook: A Practical Approach to DNA and Protein Phylogeny. 2nd edn. Cambridge University Press, 615–630. <https://doi.org/10.1017/CBO9780511819049.022>
- Xia X, Xie Z, Salemi M, Chen L, Wang Y (2003) An index of substitution saturation and its application. Molecular Phylogenetics and Evolution 26: 1–7. [https://doi.org/10.1016/S1055-7903\(02\)00326-3](https://doi.org/10.1016/S1055-7903(02)00326-3)
- Yen TC (1939) Die chinesischen Land- und Süßwasser-Gastropoden des Natur-Museums Senckenberg. Abhandlungen der Senckenbergischen Naturforschenden Gesellschaft 444: 1–234. [16 pls.]
- Zilch A (1960 [1959–1960]) Teil 2, Euthyneura. In: Wenz W (Ed.) Gastropoda, Handbuch der Paläozoologie (ed. Schindewolf OH), Band 6, Gastropoda. Berlin: Gebrüder Borntraeger, 835 pp. [(4): 601–835 (1960)] [Abb. 2112–2515, I–XII]

The termite genus *Glyptotermes* (Isoptera, Kalotermitidae) from Paraguay

Rudolf H. Scheffrahn¹

¹ University of Florida, Fort Lauderdale Research & Education Center, 3205 College Avenue, Davie, Florida 33314 USA

Corresponding author: Rudolf H. Scheffrahn (rhsc@ufl.edu)

Academic editor: Eliana Canello | Received 22 June 2021 | Accepted 1 August 2021 | Published 1 September 2021

<http://zoobank.org/EA7AA738-00D8-4437-BA70-940A5060DD89>

Citation: Scheffrahn RH (2021) The termite genus *Glyptotermes* (Isoptera, Kalotermitidae) from Paraguay. ZooKeys 1059: 23–33. <https://doi.org/10.3897/zookeys.1059.70500>

Abstract

A 2012 termite expedition yielded the first species of *Glyptotermes* known from Paraguay, *G. hickmani* sp. nov. and *G. canellae* (Müller, 1873), the latter previously known from Argentina and Brazil. Both are described based on the soldier and imago castes.

Keywords

Glyptotermes canellae, *Glyptotermes hickmani* sp. nov., humid Chaco, imago, soldier, redescription

Introduction

Glyptotermes Froggatt, with 127 species worldwide, is the most speciose genus in the termite family Kalotermitidae (Krishna et al. 2013). Now with 27 New World species (all Neotropical), *Glyptotermes* is the second most speciose kalotermitid genus after *Cryptotermes* Banks. Scheffrahn (2019a) reported the current New World range of *Glyptotermes* and provided the first records of this genus from Bolivia, Colombia, Ecuador, French Guiana, Guatemala, Honduras, Paraguay, Peru, and much of the Lesser Antilles. The paucity of *Glyptotermes* records from throughout much of the Caribbean

Basin and South America has been shown to be caused by a field sampling bias toward non-kalotermitids (Scheffrahn et al. 2018).

Glyptotermes species have a rather high wood moisture requirement and, therefore, are not found in arid parts of the Neotropics and are likewise, not economically important. Although the imago morphology is quite conserved, the head capsules of *Glyptotermes* soldiers are variously adorned with protuberances and rugosities, and robust mandibles that facilitate their identification. I herein describe *Glyptotermes hickmani* sp. nov. from three localities in the humid Chaco of Paraguay and redescribe *G. canellae* (Müller, 1873) from the same region.

Material and methods

The distribution map (Fig. 1) was prepared using ArcMap 10.3 software (ESRI, Redlands, CA). Microphotographs (Figs 2–5) were taken as multi-layer montages using a Leica M205C stereomicroscope controlled by Leica Application Suite version 3 software. Preserved specimens were taken from 85% ethanol and suspended in a pool of Purell Hand Sanitizer to position the specimens on a transparent Petri dish background. Additional images of *Glyptotermes* are available at Scheffrahn (2019b).

Taxonomy

Glyptotermes hickmani sp. nov.

<http://zoobank.org/99B790A9-DF50-49E9-9A75-F0D67FB8F3FA>

Figs 2, 3, 6; Tables 1, 2

Diagnosis. Among the ten South American *Glyptotermes* species for which the soldier is known, the *G. hickmani* sp. nov. soldier is closest in head width to *G. guianensis* (Emerson, 1925), but in lateral view, *G. guianensis* has angular frontal horns compared to the rounded frontal horns of *G. hickmani*. The frontal horns of the *G. hickmani* soldier are diagnostic.

Type locality. Paraguay, Nueva Colombia.

Material examined. **Holotype** soldier: Paraguay, Nueva Colombia (-25.1747, -57.2876), elev. 115 m, 5JUN2012, R. Scheffrahn et al. (R. Scheffrahn, J. Chase, R. Hickman, J. Křeček, J. Mangold, A. Mullins), University of Florida Termite Collection (UFTC), Davie Florida, no. PA1265. **Paratypes.** Five additional soldiers, one queen, pseudergates/nymphs, same colony sample as holotype. One additional colony from type locality (same data), four soldiers, one king, one queen, and pseudergates/nymphs (PA1264). Paraguay, Cerra Cora (-22.6788, -55.9950), elev. 293 m, 29MAY2012, R. Scheffrahn et al., UFTC no. PA326 containing two soldiers and pseudergates/nymphs. Paraguay, 58 km W of Pedro Juan Caballero (-22.5600, -56.3006), elev. 328 m, 29MAY2012, R. Scheffrahn et al., UFTC no. PA446 containing one soldier and 12 pseudergates/nymphs.

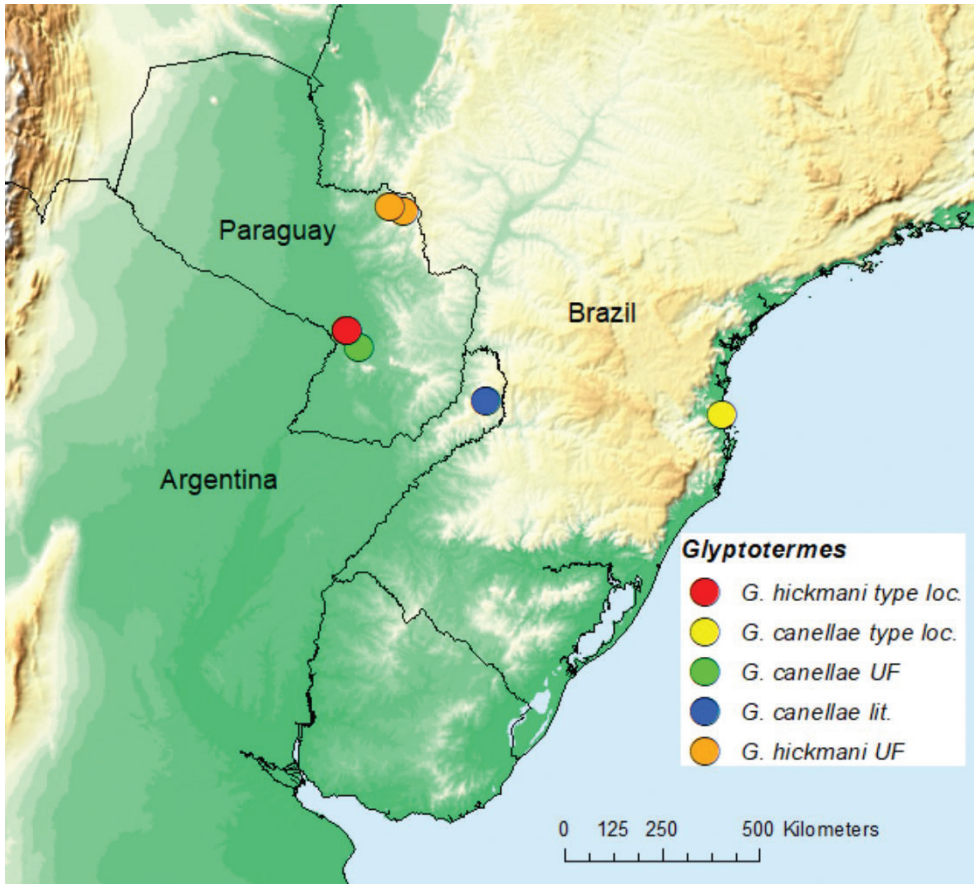


Figure 1. Distribution of *Glyptotermes hickmani* sp. nov. and *G. canellae* (Müller) in Paraguay and literature localities of *G. canellae* in Argentina and Brazil.

Description. Dealated Imago (Fig. 2, Table 1). Head and pronotum castaneous brown (almost black in live habitus, Fig. 6A). Postclypeus hyaline; labrum light orange-brown. Fore wing scales concolorous with pronotum. Femora slightly lighter than pronotum; tibiae concolorous with labrum. In lateral view, vertex of head with 20–24 scattered setae of medium length. In dorsal view, pronotum with about 20 setae of variable length along each lateral margin; in lateral view, with setae in line with anterior and posterior margins; a few in middle. Eyes small, dark gray, occupying less than one-third the distance between vertex and genal margins; ellipsoid with rectate margin at antennal socket. Ocelli small, orange, elliptical; separated from eye by their narrow width. Antennae article formula $2 < 3 > 4 = 5$. Pronotum wider than long, about as wide as head capsule without eyes; anterior and posterior margins with slight concavity, sides slightly convex. Arolia present.

Soldier (Fig. 3, Table 2). Head, in lateral view, grading from light orange at the cervical margin to dark brown at frontal horns (darker in live habitus, Fig. 6B).

Table 1. Measurements (mm) of *Glyptotermes hickmani* sp. nov. and *G. canellae* (Müller) imagos.

Characters	<i>G. hickmani</i>		<i>G. canellae</i>	
	(n = 4)		(n = 12)	
	mean	range	mean	range
Length of head to tip of labrum	1.38	1.35–1.44	1.36	1.30–1.40
Length of head to side base of mandibles	0.64	0.54–0.79	0.64	0.58–0.79
Width of head	1.15	1.11–1.19	1.18	1.14–1.19
Diameter of eye	0.26	0.25–0.30	0.27	0.25–0.28
Eye from lower margin	0.27	0.23–0.33	0.18	0.16–0.25
Length of ocellus	0.1	0.09–0.11	0.1	0.09–0.11
Median length of pronotum	0.62	0.58–0.65	0.57	0.53–0.60
Maximum length of pronotum	0.71	0.70–0.74	0.7	0.65–0.77
Width of pronotum	1.19	1.09–1.26	1.06	1.00–1.11
Length of hind tibia	0.91	0.86–0.96	0.87	0.79–0.91
Length of fore wing from suture			6.57	6.24–6.80
Width of fore wing			1.83	1.68–1.93

Mandibles concolorous with frons. Head capsule nearly cuboid; about as wide as high; with distinct narrowing near anterior fourth. Pronotum more than twice as wide as long, widest near front third; anterior margin weakly concave, posterior margin barely concave in middle. In dorsal and ventral views, setae on head and pronotum medium to long; about 4–5 short setae on basal hump of mandibles. In lateral view, setae less numerous except for setae on postmentum. Mandibles robust, form about two-thirds of total head length; curve apically near anterior half, humps at basal fourth evenly rounded beyond outer blades. Dentition as in Fig. 3. Frons bilobed; lobes rounded in lateral view; frontal furrow between lobes extends to postclypeus. Angle formed by vertex and frons about 75°; lateral view of frons punctuated by large, knob-like, frontal horns. Eye spots very faint. In ventral view, posterior margin of postmentum slightly wider than middle. Genal horns rounded from above, project slightly beyond narrowest point of head capsule. Antenna with 11–12 articles; formula $2 > 3 < 4 < 5$. Femora swollen.

Distribution. See Fig. 1.

Etymology. Named after Robert B. (Bob) Hickman, a friend and able termite collector, who joined us on the Paraguay expedition.

Glyptotermes canellae (Müller, 1873)

Figs 4–6; Tables 1–2

Müller, 1873, 334: *Calotermes canellae*; imago described. Brazil.

Silvestri, 1901, 3: *Calotermes lobicephalus*; soldier described with single measurement. Argentina.

Silvestri, 1903, 36–37: *Calotermes lobicephalus*; soldier described with seven measurements and figured with simple line drawings. Argentina.

Holmgren, 1911, 56: *Calotermes lobicephalus* synonymized with *C. canellae*; imago, soldier figured with photographs.



Figure 2. Dorsal (top) and lateral views of the *Glyptotermes hickmani* sp. nov. female dealate.

See Krishna et al. (2013: 429) for complete synopsis and literature review.

Diagnosis. Among mainland South American *Glyptotermes*, the soldier of *G. canellae* is the second largest after *G. hospitalis* (Emerson, 1925) from Guyana. The projecting genal horns of the *G. canellae* soldier are diagnostic.

Type locality. Brazil: Santa Catarina: Itajaí.

Material examined. Paraguay, S. Piribebuy (-25.5368, -57.0244), elev. 229, 27 May 2012, R. Scheffrahn et al., UFTC no. PA89 containing 2 soldiers, 12 alates,

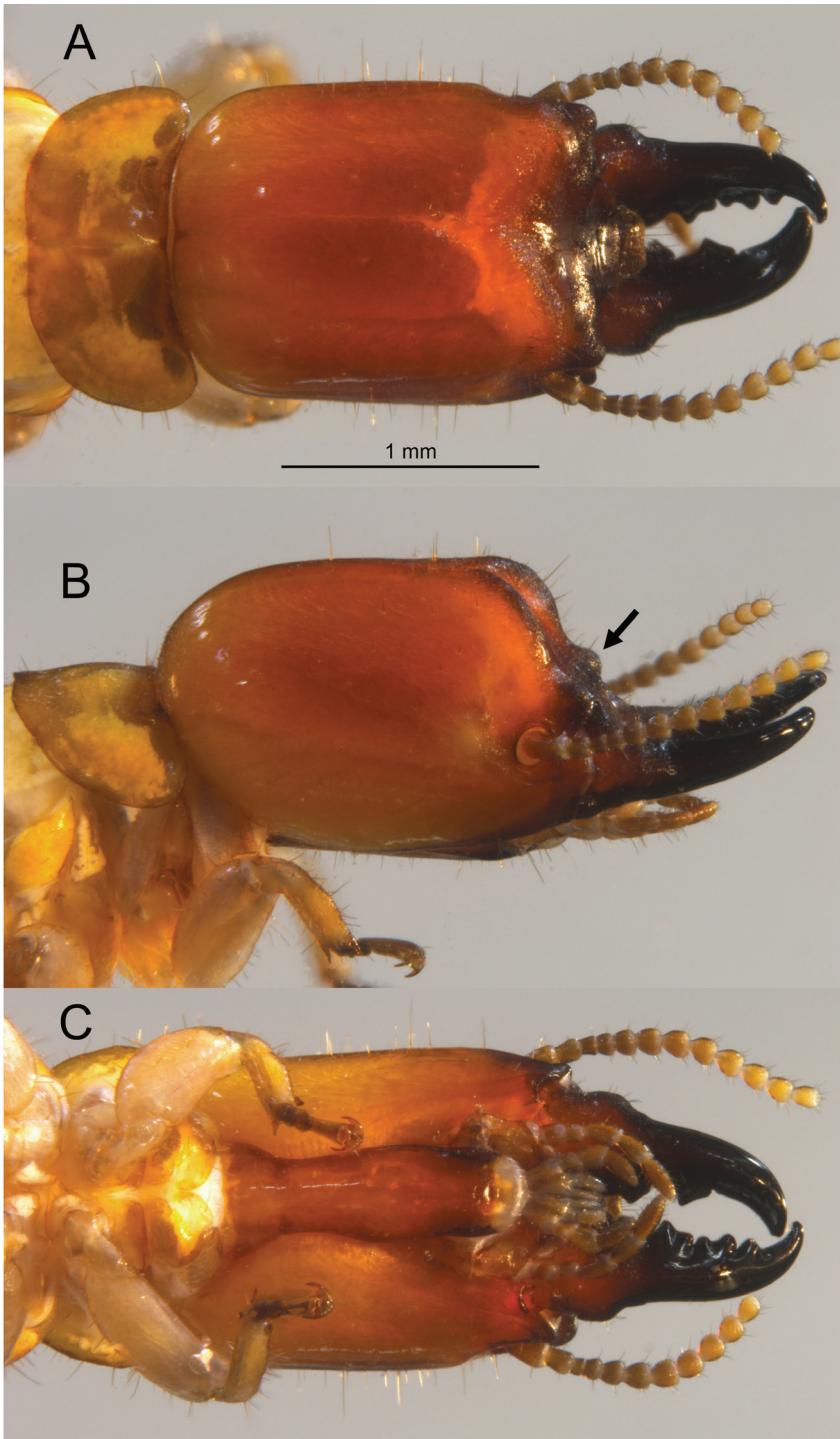


Figure 3. Dorsal (top) (B), lateral/oblique, and ventral views of the *Glyptotermes hickmani* sp. nov. soldier head capsule and pronotum. Arrow = frontal horn.

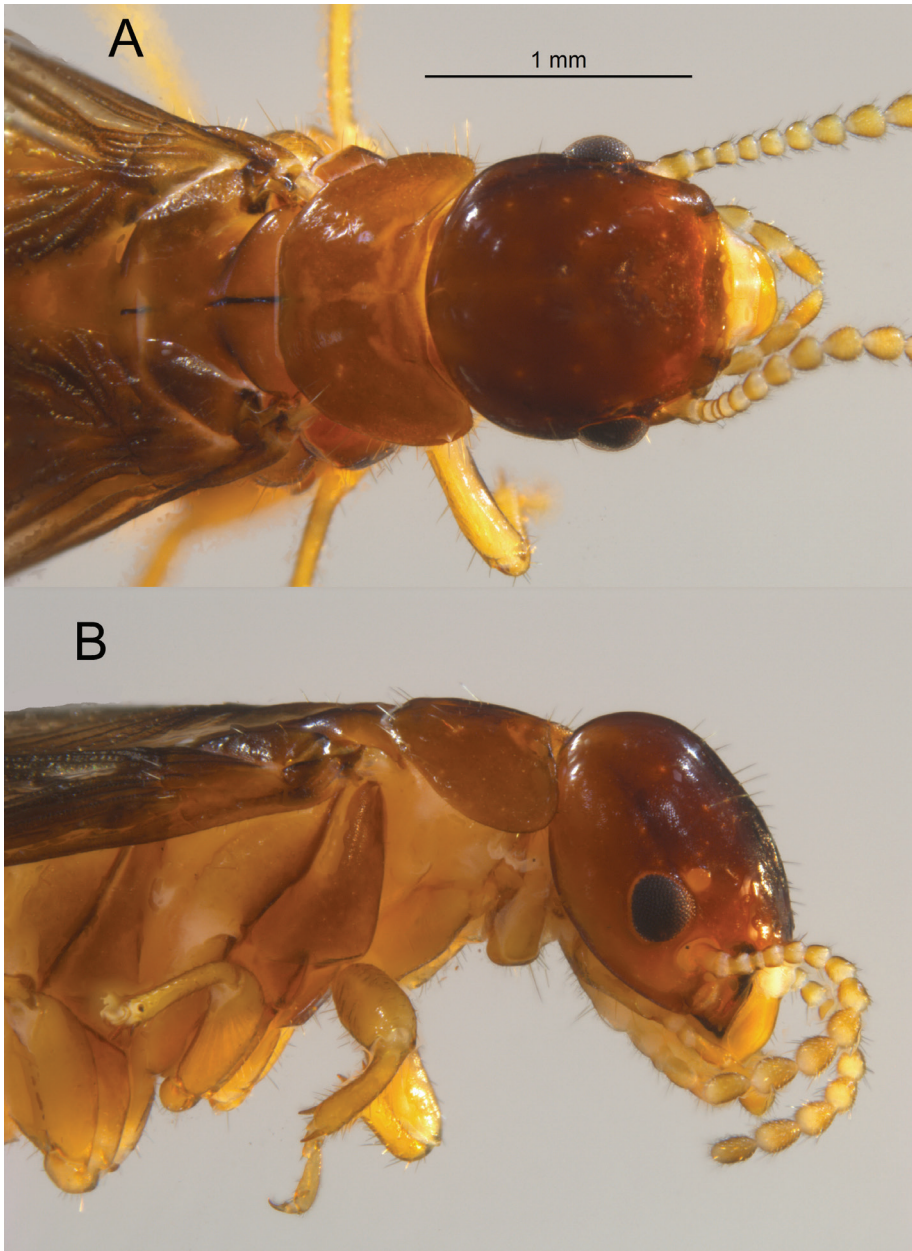


Figure 4. Dorsal (top) and lateral views of the *Glyptotermes canellae* (Müller) female alate.

and many pseudergates. The types were not examined, but the soldier measurements in Silvestri (1903: 36) and photographs in Holmgren (1911; pl. 4, figs 14, 15) of *C. lobicephalus* are of excellent quality. The measurements agree with those in Table 2 and the photographs show the characteristically deeply bilobed frons

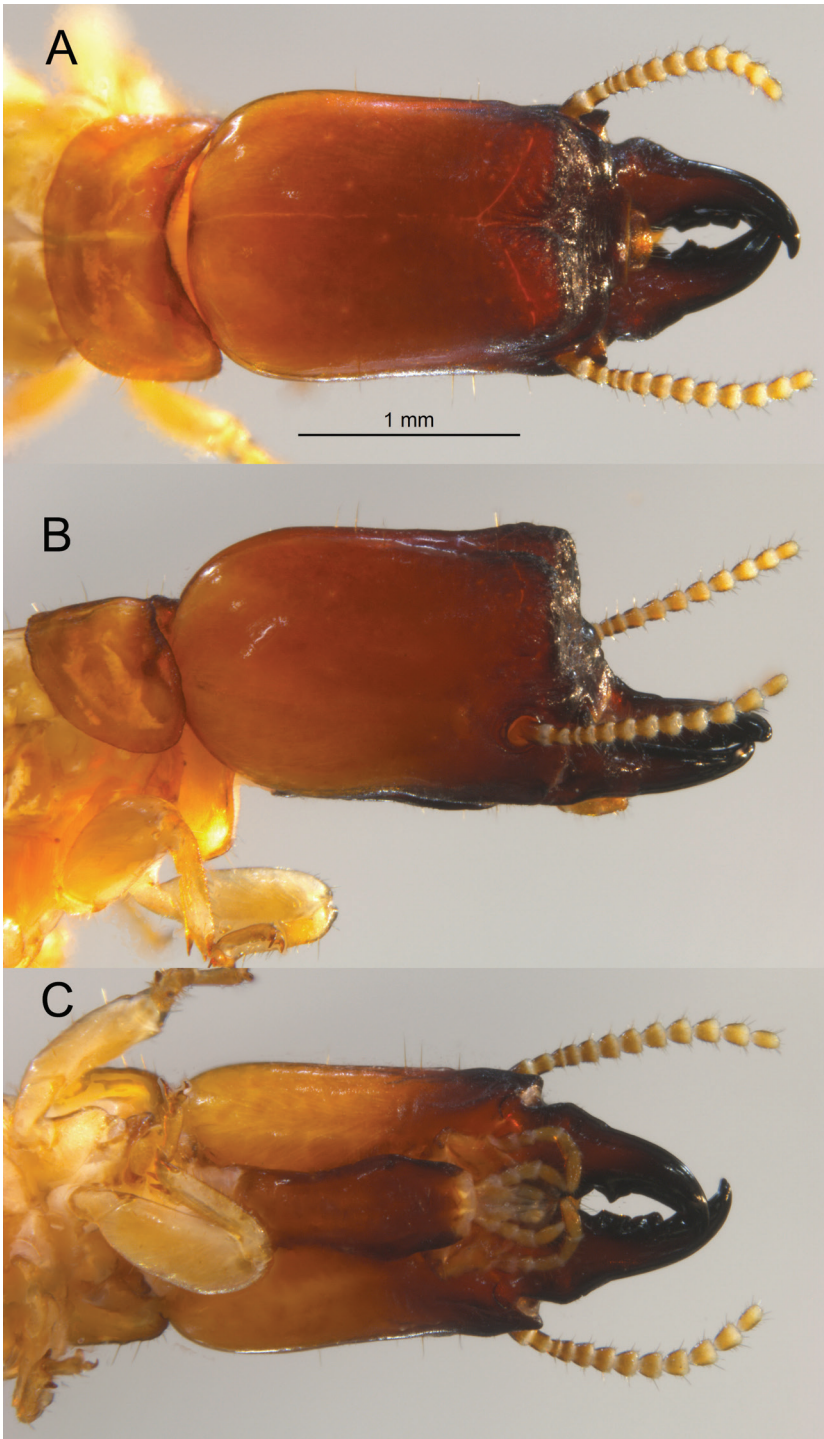


Figure 5. Dorsal (top), lateral/oblique, and ventral views of the *Glyptotermes canellae* (Müller) soldier head capsule and pronotum.

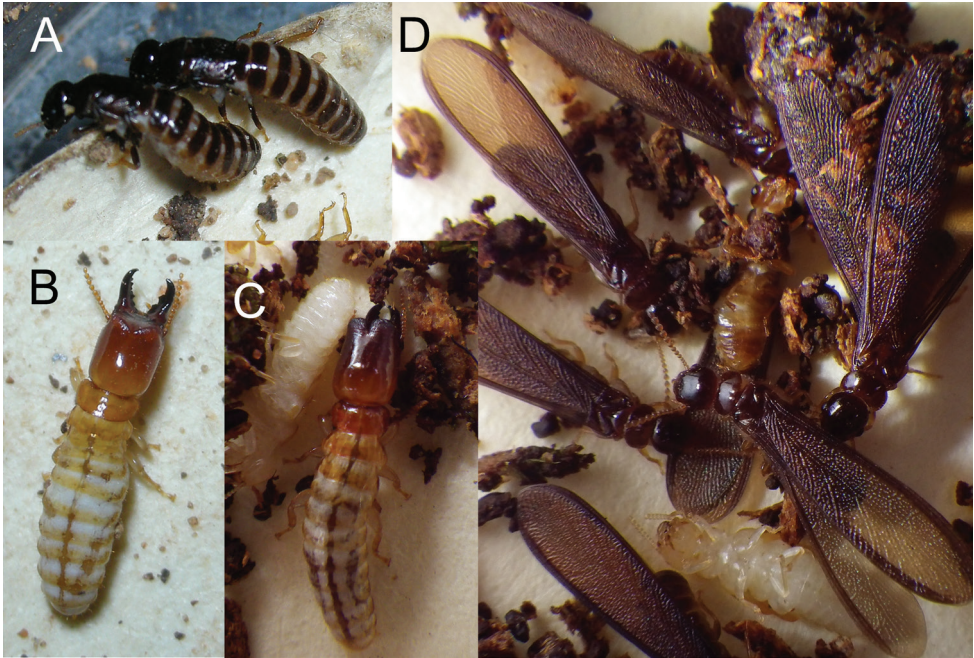


Figure 6. Live habitus of *Glyptotermes hickmani* sp. nov. imagos **A** and soldier **B** and *G. canellae* (Müller) soldier **C** and imagos **D**.

and its steep angle from the vertex (Figs 5, 6C) that are unique for *Glyptotermes* soldiers of this region.

Redescription. Winged Imago (Fig. 4, Table 1). Head medium brown, pronotum light brown (castaneus in live habitus, Fig. 6D). Postclypeus hyaline; labrum light orange-brown. Fore wing scales concolorous with pronotum. Femora and tibiae concolorous with labrum. In lateral view, vertex of head with about 12 scattered setae of medium length. In dorsal view, pronotum with about 8–10 setae of various lengths along lateral margins; in lateral view, about 4–6 setae in line, each with anterior and posterior margins; a few in middle. Eyes medium small, dark gray, occupying about one-third the distance midway between vertex and genal margin; ellipsoid with rectate margin at antennal socket. Ocelli orange, nearly circular; one fifth their diameter from eye. Arolia present.

Soldier (Fig. 5, Table 2). Head, in lateral view, grading from light orange at the cervical margin to dark brown at frons (darker in live habitus, Fig. 6C). Mandibles concolorous with frons. Head capsule much longer than wide; about as wide as high; in dorsal view, posterior wider than width at genal horns. Frontal horns absent. Pronotum more than twice as wide as long, widest near front third; anterior and posterior margins evenly curved, nearly parallel. In all views, setae sparse and uneven in length; no setae on basal hump of mandibles. Mandibles robust, form about one third of total head length; curve apically near anterior half, humps at

Table 2. Measurements (mm) of *Glyptotermes hickmani* sp. nov. and *G. canellae* (Müller) soldiers.

Characters	<i>G. hickmani</i>		<i>G. canellae</i>	
	(n = 9)		(n = 2)	
	mean	range	mean	range
Length of head to side base of mandibles	1.44	1.09–1.70	1.84	1.81–1.88
Width of head	1.22	1.00–1.32	1.37	1.32–1.42
Height of head	1.11	0.95–1.18	1.19	1.19–1.19
Length of left mandible	1.04	0.88–1.14	1.20	1.18–1.23
Maximum width of postmentum	0.38	0.35–0.40	0.51	0.49–0.53
Minimum width of postmentum	0.29	0.26–0.33	0.37	0.35–0.39
Length of postmentum	1.12	0.89–1.25	1.12	1.12–1.12
Median length of pronotum	0.54	0.40–0.61	0.59	0.58–0.60
Maximum length of pronotum	0.65	0.51–0.74	0.73	0.72–0.74
Width of pronotum	1.19	0.91–1.32	1.26	1.23–1.30
Length of hind tibia	0.72	0.61–0.79	0.88	0.88–0.88

basal fourth angular beyond outer blades. Dentition as in Fig. 5. Frons bilobed, lobes and frons rugose. Frontal furrow between lobes extends to middle of frons. Angle formed by vertex and frons about 90°; lateral view of frons with very small elevations near base; insufficient to constitute horns. Eye spots very faint. In ventral view, posterior margin of postmentum narrower than middle. Genal horns acute, visible from above, span narrowest part of head capsule. Antenna with 12 articles; formula 2 > 3 < 4 < 5. Femora swollen.

Distribution. Argentine record of *G. canellae* from Torales et al. (1997) (Fig. 1).

Discussion

Until now, no *Glyptotermes* species were known from Paraguay, while the following Paraguayan kalotermitids are reported: *Cryptotermes chacoensis* (Roisin, 2003), *Neotermes fulvescens* (Silvestri, 1901), *Rugitermes rugosus* (Hagen, 1858) in Scheffrahn (2019b), and *Tauritermes triceromegas* (Silvestri, 1901) in Scheffrahn and Vasconcellos (2020). The distributional range of *G. hickmani* is 340 km within the humid Chaco [tropical monsoon biome per Koppen-Geiger; Kottek et al. (2006)] of Paraguay (Fig. 1). The range of *G. canellae* has been extended by 340 km within this same biome. Many species of South American *Glyptotermes* remain to be described (Scheffrahn 2019b). Our 2012 expedition to Paraguay also yielded a new *Neotermes* species, a new *Rugitermes* species, and many other new termite taxa.

Acknowledgements

I am grateful to The Terminix International Company Limited Partnership and the BASF Corporation for funding the expedition to Paraguay.

References

- Holmgren N (1911) Termitenstudien. 2. Systematik der Termiten. Die Familien Mastotermitidae, Protermitidae und Mesotermitidae. Kungliga Svenska Vetenskaps-Akademiens Handlingar 46: 1–86.
- Kottek M, Grieser J, Beck C, Rudolf B, Rubel F (2006) World map of the Köppen-Geiger climate classification updated. Meteorologische Zeitschrift 15: 259–263. <https://doi.org/10.1127/0941-2948/2006/0130>
- Krishna K, Grimaldi DA, Krishna V, Engel MS (2013) Treatise on the Isoptera of the world: Volume 2 Basal Families. Bulletin of the American Museum of Natural History 377: 200–623. <https://doi.org/10.1206/377.2>
- Müller F (1873) Beiträge zur Kenntniss der Termiten. Jenaische Zeitschrift für Medizin und Naturwissenschaft 7: 333–358, 451–463.
- Roisin Y (2003) *Cryptotermes chacoensis*, a new species from native South American inland habitats (Isoptera: Kalotermitidae). Sociobiology 42: 319–327.
- Scheffrahn RH, Chase JA, Mangold JR, Hochmair HH (2018) Relative occurrence of the family Kalotermitidae (Isoptera) under different termite sampling methods. Sociobiology 65: 88–100. <https://doi.org/10.13102/sociobiology.v65i1.2097>
- Scheffrahn RH (2019a) Expanded New World distributions of genera in the termite family Kalotermitidae. Sociobiology 66: 136–153. <https://doi.org/10.13102/sociobiology.v66i1.3492>
- Scheffrahn RH. (2019b) UF Termite database. University of Florida termite collection. <https://www.termitediversity.org/> [Accessed on: 2020-25-10]
- Scheffrahn RH, Vasconcellos A (2020) *Tauritermes bandeirai*: A new drywood termite (Isoptera, Kalotermitidae) from the Caatinga and Atlantic Forest of Brazil. ZooKeys 954: 75–84. <https://doi.org/10.3897/zookeys.954.52335>
- Silvestri F (1901) Nota preliminare sui Termitidi sud-americani. Bollettino dei Musei di Zoologia ed Anatomia Comparata della Reale Università di Torino 16(389): 1–8. <https://doi.org/10.5962/bhl.part.26628>
- Silvestri F (1903) Contribuzione alla conoscenza dei termiti e termitofili dell'America meridionale. Redia 1: 1–234. <https://doi.org/10.5962/bhl.title.137413>
- Torales G, Laffont ER, Arbino MO, Godoy MC (1997) Primera lista faunística de los Isópteros de la Argentina. Revista de la Sociedad Entomológica Argentina 56: 47–53.

A new species of Music frog (*Anura*, *Ranidae*, *Nidirana*) from Mt Daming, Guangxi, China

Zhi-Tong Lyu^{1*}, Zhong Huang^{2*}, Xiao-Wen Liao², Li Lin³,
Yong Huang⁴, Ying-Yong Wang¹, Yun-Ming Mo²

1 State Key Laboratory of Biocontrol/ The Museum of Biology, School of Life Sciences, Sun Yat-sen University, Guangzhou 510275, China **2** Natural History Museum of Guangxi, Nanning 530012, China **3** Guangxi Daming Mountain National Nature Reserve Administration, Nanning 530114, China **4** Guangxi University of Chinese Medicine, Nanning 530200, China

Corresponding authors: Yun-Ming Mo (moyunming@163.com), Ying-Yong Wang (wangyy@mail.sysu.edu.cn)

Academic editor: Anthony Herrel | Received 3 May 2021 | Accepted 30 July 2021 | Published 1 September 2021

<http://zoobank.org/207DB0D1-B593-4ACD-BF5A-A386AD89399E>

Citation: Lyu Z-T, Huang Z, Liao X-W, Lin L, Huang Y, Wang Y-Y, Mo Y-M (2021) A new species of Music frog (*Anura*, *Ranidae*, *Nidirana*) from Mt Daming, Guangxi, China. ZooKeys 1059: 35–56. <https://doi.org/10.3897/zookeys.1059.68140>

Abstract

Nidirana guangxiensis **sp. nov.**, a new music frog species, is proposed, based on a series of specimens collected from Mt Daming, Guangxi, southern China. The new species is close to *N. yeae*, *N. daunchina*, *N. yaoica*, and *N. chapaensis* from southwestern and south-central China and northern Indochina, while the relationships among these species remain unresolved. *Nidirana guangxiensis* sp. nov. can be distinguished from all known congeners by the genetic divergences in the mitochondrial 16S and COI genes, the behavior of nest construction, the advertisement call containing 6–11 rapidly repeated regular notes, and a combination of morphological characteristics. Furthermore, the *Nidirana* populations recorded in Guangxi are clarified in this work, providing valuable new information on the knowledge of the genus *Nidirana*.

Keywords

Bioacoustics, geography, mitochondrial DNA, morphology, nest construction

* These authors contributed equally as the first authors

Introduction

The music frog genus *Nidirana* Dubois, 1992 was originally proposed as a subgenus of *Rana* Linnaeus, 1758. Later, *Nidirana* was controversially recognized as a full genus or a synonym of *Babina* Thompson, 1912 (Chen et al. 2005; Frost et al. 2006). Recently, comprehensive morphological, molecular, bioacoustic, and biogeographical evidence has resurrected *Nidirana* as a distinct genus (Lyu et al. 2017). The frogs of this genus usually inhabit the natural or artificial swamps, ponds, and paddy fields in the hilly regions of subtropical eastern and southeastern Asia, with some species having nest construction behavior when courting (Fei et al. 2009; Lyu et al. 2017). The known diversity of *Nidirana* increased dramatically from seven to 15 species since 2017 (Lyu et al. 2017, 2019, 2020a). Most of the newly described species were previously misidentified as other congeners, due to their conservative phenotypes (Lyu et al. 2019, 2020a, 2020b). For instance, Lyu et al. (2020b) revised multiple populations historically recorded as *Nidirana adenopleura* (Boulenger, 1909) from China. They suggested that only the populations from Taiwan, Jiangxi, Fujian, and southern Zhejiang are the true *N. adenopleura*, and nominated some other populations as three new species: *N. guangdongensis* Lyu, Wan & Wang, 2020, *N. mangveni* Lyu, Qi & Wang, 2020, and *N. xiangica* Lyu & Wang, 2020. Lyu et al.'s (2020b) work did not clarify all historic records of *N. adenopleura*, and the taxonomic status for the records not involved in their study remains unresolved.

The *Nidirana* populations in Guangxi Zhuang Autonomous Region, southern China, were previously recorded as *N. adenopleura* (Liu and Hu 1962; Zhang and Wen 2000; Fei et al. 2009; Mo et al. 2014). Fei et al. (2009) suspected this identification was not correct, but still tentatively followed it and suggested additional study. Recently, the population from Mt Dayao, eastern Guangxi, has been revealed as a new species, *N. yaoica* Lyu, Mo, Wan, Li, Pang & Wang, 2019, and the population from Mt Dupangling, northeastern Guangxi was assigned to *N. xiangica* (Lyu et al. 2019, 2020b). During our recent surveys in Guangxi, we collected a series of *Nidirana* specimens from Mt Daming (MDM), central Guangxi, and Mt Jiuwan (MJW), northern Guangxi (Fig. 1). After comprehensive analyses, the specimens from MJW are identified as *N. leishanensis* Li, Wei, Xu, Cui, Fei, Jiang, Liu & Wang, 2019, while the specimens from MDM are herein proposed as a new species.

Materials and methods

Phylogenetic analysis

Nine muscular samples of the unnamed species from Guangxi were used for molecular analysis, encompassing five samples from MDM and four from MJW. All samples were obtained from euthanized specimens and then preserved in 95% ethanol and stored at -40°C . In addition, 33 sequences from all known *Nidirana* species and two sequences from the outgroup, *Babina holsti* (Boulenger, 1892) and

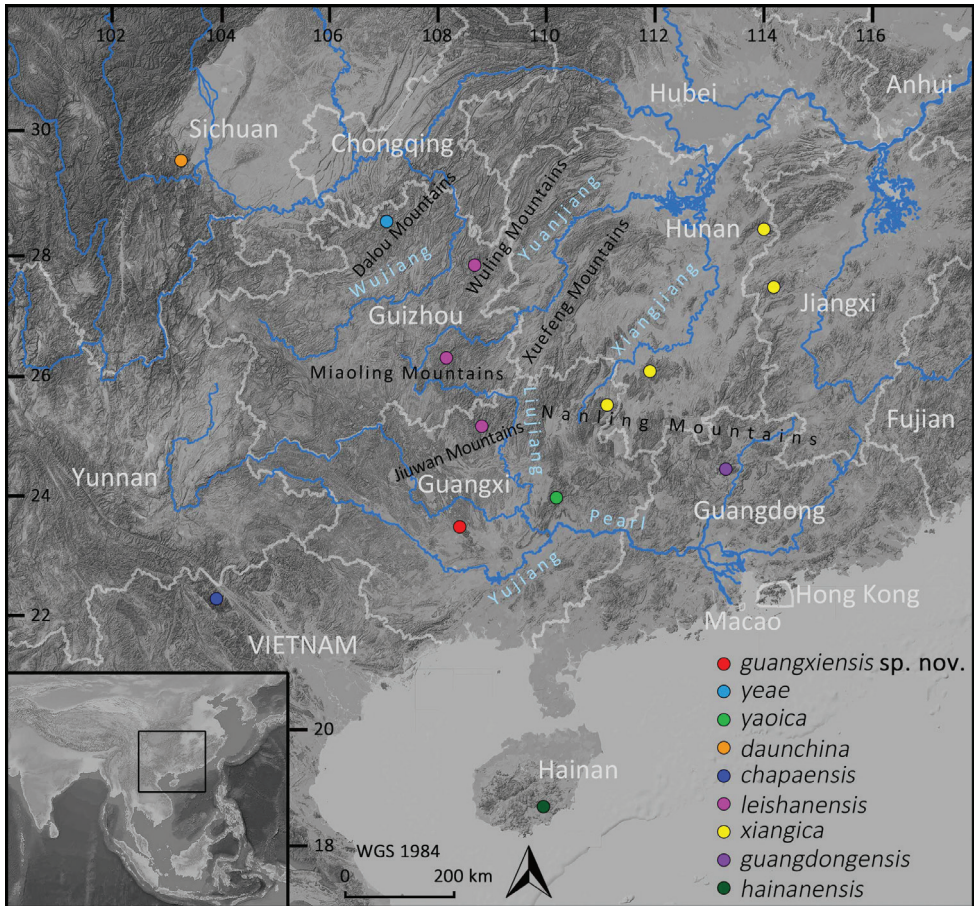


Figure 1. Map showing the collected localities for the *Nidirana* samples of Clade C (see Fig. 2) used in this study.

B. subaspera (Barbour, 1908) (following Lyu et al. 2017), were obtained from GenBank and incorporated into our dataset. Detailed information on these materials is shown in Table 1 and Figure 1.

Two mitochondrial genes, namely partial 16S ribosomal RNA gene (16S) and partial cytochrome c oxidase I gene (COI), were used for phylogenetic analysis. DNA extraction, PCR amplification, and sequencing conducted on the newly collected samples followed Lyu et al. (2019). Two gene segments, 1042 base pairs (bp) of 16S and 639 bp of COI, were concatenated seriatim into a 1681-bp matrix. The final alignment was partitioned by gene and COI was further partitioned by codon position. The partitions were tested in jmodeltest v. 2.1.2, resulting in the best-fitting nucleotide substitution models as GTR+I+G. Sequenced data were analyzed using maximum likelihood (ML) in RaxmlGUI v. 1.3 (Silvestro and Michalak 2012). The bootstrap consensus tree inferred from 1000 replicates was used to represent the evolutionary history of the taxa analyzed.

Table 1. Localities, voucher information, and GenBank numbers for all samples used in this study.

ID	Species	Locality	Voucher number	16S	COI
1	<i>Nidirana guangxiensis</i> sp. nov.	China: Guangxi: Mt Daming*	NHMG 202007001	MZ677222	MZ678729
2	<i>Nidirana guangxiensis</i> sp. nov.	China: Guangxi: Mt Daming*	NHMG 202007002	MZ677223	MZ678730
3	<i>Nidirana guangxiensis</i> sp. nov.	China: Guangxi: Mt Daming*	NHMG 202007003	MZ677224	MZ678731
4	<i>Nidirana guangxiensis</i> sp. nov.	China: Guangxi: Mt Daming*	NHMG 202007004	MZ677225	MZ678732
5	<i>Nidirana guangxiensis</i> sp. nov.	China: Guangxi: Mt Daming*	NHMG 202007005	MZ677226	MZ678733
6	<i>Nidirana yaocica</i>	China: Guangxi: Mt Dayao*	SYS a007020	MK882276	MK895041
7	<i>Nidirana yaocica</i>	China: Guangxi: Mt Dayao*	SYS a007021	MK882277	MK895042
8	<i>Nidirana yaocica</i>	China: Guangxi: Mt Dayao*	SYS a007022	MK882278	MK895043
9	<i>Nidirana leishanensis</i>	China: Guangxi: Mt Jiawan	NHMG 202007021	MZ677227	MZ678734
10	<i>Nidirana leishanensis</i>	China: Guangxi: Mt Jiawan	NHMG 202007022	MZ677228	MZ678735
11	<i>Nidirana leishanensis</i>	China: Guangxi: Mt Jiawan	NHMG 202007023	MZ677229	MZ678736
12	<i>Nidirana leishanensis</i>	China: Guangxi: Mt Jiawan	NHMG 202007025	MZ677230	MZ678737
13	<i>Nidirana leishanensis</i>	China: Guizhou: Mt Leigong*	SYS a007908	MN946453	MN945209
14	<i>Nidirana leishanensis</i>	China: Guizhou: Mt Fanjing	SYS a007195	MN946454	MN945210
15	<i>Nidirana xiangica</i>	China: Guangxi: Mt Dupangling	SYS a006568	MN946442	MN945198
16	<i>Nidirana xiangica</i>	China: Hunan: Mt Dawei*	SYS a006492	MN946434	MN945190
17	<i>Nidirana xiangica</i>	China: Hunan: Mt Yangming	SYS a007273	MN946440	MN945196
18	<i>Nidirana xiangica</i>	China: Jiangxi: Mt Wugong	SYS a002590	MN946441	MN945197
19	<i>Nidirana yeae</i>	China: Guizhou: Tongzi County	CIB TZ20190608004	MN295227	MN295233
20	<i>Nidirana yeae</i>	China: Guizhou: Tongzi County	CIB TZ20190608005	MN295228	MN295234
21	<i>Nidirana yeae</i>	China: Guizhou: Tongzi County	CIB TZ20160714016	MN295231	MN295237
22	<i>Nidirana adenopleura</i>	China: Taiwan: Taichung City	SYS a007358	MN946445	MN945201
23	<i>Nidirana adenopleura</i>	China: Taiwan: Taichung City	SYS a007359	MN946446	MN945202
24	<i>Nidirana chapaensis</i>	Vietnam: Lao Cai: Sapa*	MNHN 2000.4850	KR827711	KR087625
25	<i>Nidirana chapaensis</i>	Vietnam: Lao Cai: Sapa*	MNHN 1999.5871	KR827710	/
26	<i>Nidirana daunchina</i>	China: Sichuan: Mt Emei*	SYS a004594	MF807822	MF807861
27	<i>Nidirana daunchina</i>	China: Sichuan: Mt Emei*	SYS a004595	MF807823	MF807862
28	<i>Nidirana guangdongensis</i>	China: Guangdong: Yingde City*	SYS a005767	MN946406	MN945162
29	<i>Nidirana guangdongensis</i>	China: Guangdong: Yingde City*	SYS a005768	MN946407	MN945163
30	<i>Nidirana hainanensis</i>	China: Hainan: Mt Diaoluo*	SYS a007669	MN946451	MN945207
31	<i>Nidirana hainanensis</i>	China: Hainan: Mt Diaoluo*	SYS a007670	MN946452	MN945208
32	<i>Nidirana lini</i>	China: Yunnan: Jiangcheng County*	SYS a003967	MF807818	MF807857
33	<i>Nidirana lini</i>	China: Yunnan: Jiangcheng County*	SYS a003968	MF807819	MF807858
34	<i>Nidirana mangveni</i>	China: Zhejiang: Mt Dapan*	SYS a006310	MN946424	MN945180
35	<i>Nidirana mangveni</i>	China: Zhejiang: Mt Dapan*	SYS a006311	MN946425	MN945181
36	<i>Nidirana nankunensis</i>	China: Guangdong: Mt Nankun*	SYS a005718	MF807839	MF807878
37	<i>Nidirana nankunensis</i>	China: Guangdong: Mt Nankun*	SYS a005719	MF807840	MF807879
38	<i>Nidirana occidentalis</i>	China: Yunnan: Mt Gaoligong*	SYS a003775	MF807816	MF807855
39	<i>Nidirana occidentalis</i>	China: Yunnan: Mt Gaoligong*	SYS a003776	MF807817	MF807856
40	<i>Nidirana okinavana</i>	Japan: Okinawa: Iriomote Island*	Not given	NC022872	NC022872
41	<i>Nidirana pleuraden</i>	China: Yunnan: Kunming City*	SYS a007858	MT935683	MT932858
42	<i>Nidirana pleuraden</i>	China: Yunnan: Wenshan City	SYS a007717	MT935671	MT932850
43	<i>Babina holsti</i>	Japan: Okinawa*	Not given	NC022870	NC022870
44	<i>Babina subaspera</i>	Japan: Kagoshima: Amami Island*	Not given	NC022871	NC022871

* Type locality.

Morphological examination

Seventeen male and two female unnamed specimens collected from MDM were examined and measured, collection information is given in the taxonomic proposal. All specimens were fixed in 10% buffered formalin, transferred to 70% ethanol, and deposited in the Natural History Museum of Guangxi (NHMG) and the Museum of Biology, Sun Yat-sen University (SYS), China.

Morphological descriptions follow the consistent definition by Lyu et al. (2017, 2019, 2020a, 2020b). External measurements of specimens were made with digital

calipers (Neiko 01407A stainless steel 6-inch digital calipers) to the nearest 0.1 mm. These measurements are as follows:

SVL	snout-vent length (from tip of snout to posterior margin of vent);
HDL	head length (from tip of snout to the articulation of the jaw);
HDW	head width (head width at the commissure of the jaws);
SNT	snout length (from tip of snout to the anterior corner of the eye);
IND	internasal distance (distance between nares);
IOD	interorbital distance (minimum distance between upper eyelids);
ED	eye diameter (from the anterior corner of the eye to posterior corner of the eye);
TD	tympanum diameter (horizontal diameter of tympanum);
TED	tympanum-eye distance (from anterior edge of tympanum to posterior corner of the eye);
HND	hand length (from the proximal border of the outer palmar tubercle to the tip of digit III);
RAD	radio-ulna length (from the flexed elbow to the proximal border of the outer palmar tubercle);
FTL	foot length (from distal end of shank to the tip of digit IV);
TIB	tibial length (from the outer surface of the flexed knee to the heel).

Sex and age were determined by examining the gonads. Webbing formula follows Savage (1975).

Comparison characters of all known congeners were obtained from 129 museum specimens of 12 known congeners listed in the Appendix 1 and from the literature (Boettger 1895; Boulenger 1904, 1909; Schmidt 1925; Chang and Hsu 1932; Bourret 1937; Kuramoto 1985; Chou 1999; Fei et al. 2007, 2009; Matsui 2007; Chuaynkern et al. 2010; Lyu et al. 2017, 2019, 2020a, 2020b; Li et al. 2019; Wei et al. 2020).

Particularly, since the new *Nidirana* species from MDM is geographically and phylogenetically close to *N. yaoica*, and phylogenetically close to *N. yae* Wei, Li, Liu, Cheng, Xu & Wang, 2020, enhanced morphometric data of these three species were used for statistical analyses in R v. 4.0.0. Due to the limited number of females collected, only male specimens were used. Data of the MDM specimens were newly measured in this work; meanwhile data of *N. yaoica* and *N. yae* were obtained from the literature (Lyu et al. 2019; Wei et al. 2020). All measurements were ln-transformed to normalize and reduce the variance. The *t*-test was conducted with statistically similar variances ($p > 0.05$ in the Levene's test) using car R package. Boxplots were visualized with the "ggplot2" R packages. For *t*-test and boxplots, measurements were scaled to remove allometric effects of body size in morphological analysis, using the following equation: $X_a = X_{ln} - \beta \cdot (SVL_{ln} - SVL_m)$, where X_a = adjusted value; X_{ln} = ln-transformed measurements; β = unstandardized regression coefficient for each species; SVL_{ln} = ln-transformed SVL; and SVL_m = overall average SVL_{ln} of all samples. Principal component analysis (PCA) was performed to reduce the dimensionality of variation in the data to find whether morphological variation form the basis of detectable group structure, using the "prcomp" function and "ggplot2" package.

Bioacoustic analysis

Advertisement calls of the *Nidirana* population from MDM were recorded in the field at the air temperature of 18 °C by a Sony PCM D100 digital sound recorder on 20 April 2021. The recorded individuals were observed to ensure as the correct species but were not captured for conservation reasons. The sound files in wave format were sampled at 44.1 kHz with 24 bits in depth. Praat v. 6.0.27 (Boersma 2001) was used to obtain the oscillogram, sonogram, and power spectrum (window length = 0.005 s). Raven Pro v. 1.5 (Cornell Lab of Ornithology 2003–2014) was used to quantify the acoustic properties (window size = 256 points, fast Fourier transform, Hanning window with no overlap). The call duration (the time between onset of the first note and offset of the last note in a call) and call PF (peak frequency; the frequency at which max power occurs within the call) were measured for each call, and the note duration (the time between onset and offset of a note) and note interval (the time between adjacent notes in a call) were measured for each note.

Results

Phylogeny

The result of ML analysis was given in Figure 2, in which the supportive nodes with the bootstrap supports (BS) > 90 were shown. This mitochondrial result is consistent with the phylogenetic relationship from previous studies (e.g. Lyu et al. 2020a), with two species groups and four clades revealed. The *Nidirana* populations from MDM (ID 1–5) and MJW (ID 9–12) are both inserted in the Clade C (clade names following Lyu et al. 2017) of the *N. adenopleura* group, which are distant from the true *N. adenopleura* in Clade D in phylogeny. Within Clade C, the *Nidirana* population from MJW (ID 9–12) is clustered with samples of *N. leishanensis* from Mt Leigong and Mt Fanjing, Guizhou, with strong supports (BS = 100) and small divergences, which indicates the MJW population should be clarified as *N. leishanensis*. The *Nidirana* population from MDM (ID 1–5) forms an independent lineage with strong supports (BS = 100) and almost no divergence, which is close to but diverse from the lineages of *N. yae*, *N. daunchina* (Chang, 1933), *N. yaoica*, and *N. chapaensis* (Bourret, 1937). The relationship among these five lineages remains unresolved, even though the MDM population seems closer to *N. yae* with medium support (BS = 92).

Morphology

Detailed comparisons among all *Nidirana* species are listed in Table 2, which shows the distinct differences of the *Nidirana* specimens from MDM (detailed comparisons presented in the Taxonomic proposal below). The results of *t*-test and boxplots of morphometrics (Table 3; Fig. 3) show that the *Nidirana* specimens from MDM are

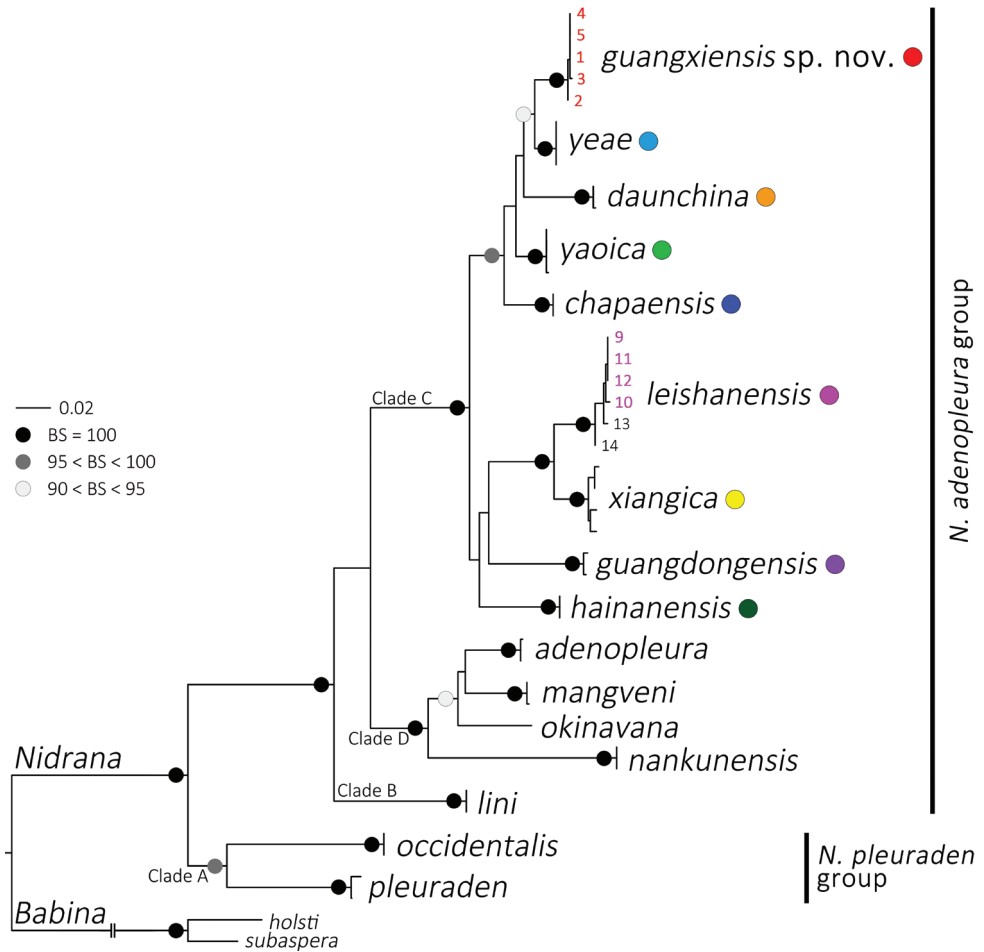


Figure 2. Phylogeny of *Nidirana* based on maximum likelihood. Number at the terminal of the branches corresponds to the ID number in Table 1.

significantly different from *N. yeae* from northern Guizhou, especially in the characteristics of HDL, HDW, IND, TD, RAD, FTL, and TIB, and different from *N. yaoica* from eastern Guangxi in the characteristics of HDL, HDW, SNT, ED, TD, and RAD. In the PCA analyses (Fig. 4), the extracted components PC1, PC2, PC3, and PC4 eigenvectors account for 46.4%, 17.5%, 11.7%, and 8.3% of the variance, respectively, or 83.9% cumulatively. As illustrated in the scatter plots of PC1 and PC2, samples of each species cluster together and do not overlap with each other.

Bioacoustics

The advertisement calls of three male individuals of the *Nidirana* population from MDM are recorded, and the call spectrograms are shown in Figure 5. The advertisement

Table 2. Diagnostic characters separating *Nidriana guangxiensis* sp. nov. from all congeners.

Species	SVL of males (mm)	SVL of females (mm)	Fingers tips	Lateroventral groove on fingers	Relative length of fingers	Toes tips	Lateroventral groove on toes	Tibio-tarsal articulation	Subgular vocal sacs	Nuptial pad	Spinules on dorsal skin	Nest construction	Tadpole labial tooth row formula	Calling	References
<i>N. guangxiensis</i>	40.2–47.6	49.9–51.0	Dilated	Present on fingers III and IV	II < I < IV < III	Dilated	Present	Nostril	Present	One on finger I	Absent	Present	I: 1+1/1+1:II	6–11 rapidly repeated regular notes	This study
<i>N. yeae</i>	41.2–43.5	44.7	Dilated	Absent	II < IV < I < III	Dilated	Present	Eye	Present	One on finger I	Absent	? (Probably absent)	I: 1+1/1+1:II	2–6 notes containing a specific first note	Wei et al. (2020)
<i>N. yaotia</i>	42.1–45.6	?	Dilated	Present	II < IV < IV < III	Dilated	Present	Nostril	Present	One on finger I	Absent	? (Probably present)	? I: 1+1/1+1:II or I: 1+1/2+2:1	1–3 fast-repeated regular notes	Lyu et al. (2019)
<i>N. danchina</i>	40.6–51.0	44.0–53.0	Dilated	Absent or rarely present	II < I < IV < III	Dilated	Present	Nostril	Present	One on finger I	Absent	Present	I: 1+1/1+1:II or I: 1+1/2+2:1	2–5 notes containing a specific first note	Liu (1950); Lyu et al. (2017)
<i>N. shapensis</i>	35.5–42.5	41.0–51.8	Dilated	Present except finger I	II < I = IV < III	Dilated	Present	Nostril	Present	Two on finger I	Absent or few above vent	Present	I: 1+2/1+1:II	3 notes	Chuaynkern et al. (2010)
<i>N. adenopleura</i>	43.1–57.6	47.6–60.7	Dilated	Present except finger I	II < I < IV < III	Dilated	Present	Snout tip or eye-snout	Present	One on finger I	Entire or posterior	Absent	I: 1+1/1+1:II or I: 0+0/1+1:1	2–5 regular notes	Lyu et al. (2017, 2020b)
<i>N. guangdongensis</i>	50.0–58.4	55.3–59.3	Dilated	Present except finger I	II < I < IV < III	Dilated	Present	Nostril	Present	One on finger I	Entire	Absent	?	2–4 regular notes	Lyu et al. (2020b)
<i>N. hainanensis</i>	32.8–44.4	?	Dilated	Present	II < I < IV < III	Dilated	Present	Nostril	Present	Absent	Absent	Present	?	2–4 fast-repeated double notes	Fei et al. (2009, 2012)
<i>N. leishanensis</i>	49.5–56.4	43.7–55.3	Dilated	Present	II < IV < I < III	Dilated	Present	Eye-snout	Present	Two on fingers I and II	Absent	Absent	I: 1+2/1+1:II	1 single note	Li et al. (2019)
<i>N. lini</i>	44.1–63.1	57.7–68.6	Dilated	Present except finger I	II < I < IV < III	Dilated	Present	Beyond snout	Present	One on finger I	Posterior	Absent	I: 1+1/1+1:II	5–7 notes containing a specific first note	Chou (1999); Lyu et al. (2017)
<i>N. mangreni</i>	53.6–59.7	59.7–65.1	Dilated	Present on fingers III and IV	I < II < IV < III	Dilated	Present	Anterior corner of eye	Present	One on finger I	Entire or posterior	Absent	?	2–7 regular notes	Lyu et al. (2020b)
<i>N. nankanensis</i>	33.3–37.1	37.8–39.5	Dilated	Present except finger I	II < I < IV < III	Dilated	Present	Nostril	Present	One on finger I	Absent or few above vent	Present	I: 1+1/1+1:II	13–15 notes containing a specific first note	Lyu et al. (2017)
<i>N. occidentalis</i>	44.5–53.0	55.6–61.3	Not dilated	Absent	II < I < IV < III	Not dilated	Absent	Eye	Present	One on finger I	Posterior	Absent	?	3–5 regular notes	Lyu et al. (2020a)
<i>N. okinawana</i>	35.5–42.8	44.6–48.8	Dilated	Present except finger I	II < I < IV < III	Dilated	Present	Eye center-near nostril	Absent	Poorly one on finger I	Absent	Present	I: 1+1/1+1:II	10–25 fast-repeated notes	Chuaynkern et al. (2010); Lyu et al. (2017)
<i>N. pleuraden</i>	46.2–52.3	46.9–61.7	Not dilated	Absent	II < I < IV < III	Not dilated	Absent	Nostril	Present	One on finger I	Posterior	Absent	I: 1+1/1+1: II	1–4 regular notes	Lyu et al. (2017, 2020a)
<i>N. xiangica</i>	56.3–62.3	53.5–62.6	Dilated	Present	II < I < IV < III	Dilated	Present	Eye-snout	Present	One on finger I	Entire	Absent	?	2–3 notes containing a specific first note	Lyu et al. (2020b)

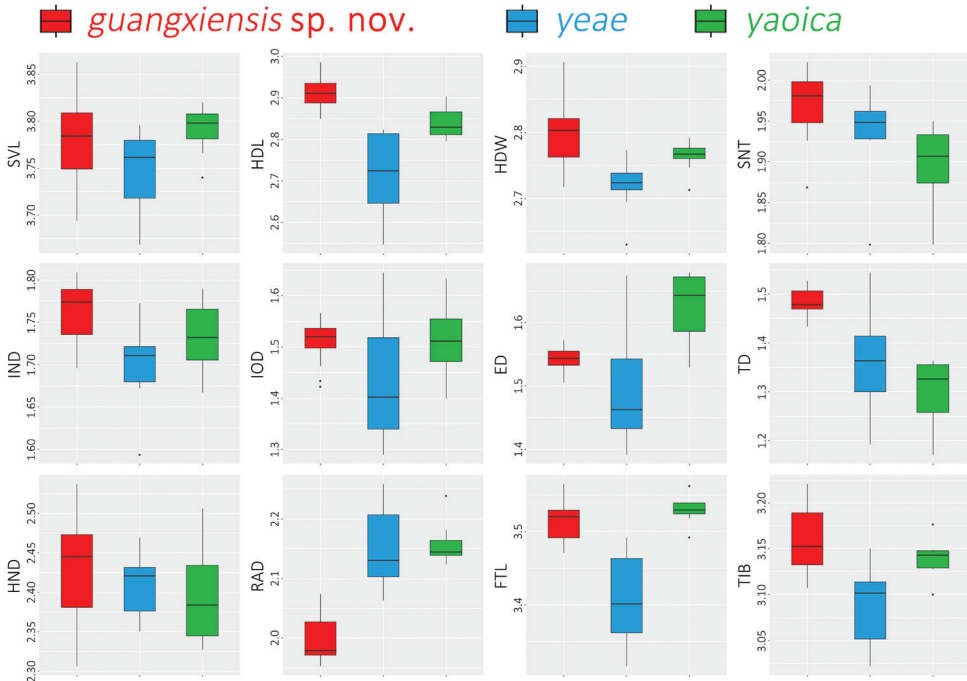


Figure 3. Boxplots of morphometrics based on the morphometric measurements, distinguishing *Nidirana guangxiensis* sp. nov., *N. yeae*, and *N. yaoica*.

Table 3. Morphometric comparisons based on the *t*-test of the morphometric measurements of males *Nidirana guangxiensis* sp. nov. ($N = 17$), *N. yeae* ($N = 9$), and *N. yaoica* ($N = 8$). * *p*-values < 0.05, ** *p*-values < 0.01, *** *p*-values < 0.001.

	<i>guangxiensis</i>	<i>yeae</i>	<i>yaoica</i>	<i>guangxiensis vs yeae</i>	<i>guangxiensis vs yaoica</i>
SVL	40.2–47.6(43.8 ± 2.2)	39.2–44.5(42.4 ± 1.8)	42.1–45.6(44.3 ± 1.2)	0.1226	0.4136
HDL	17.1–19.9(18.5 ± 0.7)	12.8–16.8(15.0 ± 1.5)	16.3–18.6(17.3 ± 0.8)	0.0002 ***	0.0011 **
HDW	15.3–18.4(16.5 ± 0.8)	13.1–16.2(15.0 ± 0.8)	15.0–16.7(16.0 ± 0.6)	0.0002 ***	0.0232 *
SNT	6.4–7.8(7.2 ± 0.4)	5.7–7.3(6.8 ± 0.5)	6.2–7.2(6.7 ± 0.4)	0.1068	0.0031 **
IND	5.4–6.3(5.8 ± 0.2)	4.7–5.9(5.4 ± 0.3)	5.4–6.0(5.7 ± 0.2)	0.0040 **	0.1105
IOD	4.1–5.0(4.6 ± 0.2)	3.5–5.2(4.2 ± 0.6)	4.1–5.1(4.6 ± 0.3)	0.1730	0.8934
ED	4.5–4.9(4.7 ± 0.1)	4.0–5.2(4.5 ± 0.4)	4.6–5.4(5.1 ± 0.3)	0.1964	0.0068**
TD	4.2–4.7(4.4 ± 0.1)	3.3–4.7(3.9 ± 0.4)	3.2–3.9(3.7 ± 0.3)	0.0101*	0.0001***
HND	10.0–12.8(11.4 ± 0.8)	10.1–11.9(11.0 ± 0.5)	10.3–12.4(11.1 ± 0.8)	0.3092	0.2468
RAD	7.1–8.1(7.4 ± 0.3)	7.7–9.6(8.6 ± 0.7)	8.4–9.4(8.7 ± 0.3)	0.0001***	0.0000 ***
FTL	32.0–37.0(33.7 ± 1.3)	26.9–32.2(29.8 ± 1.9)	33.1–35.7(34.4 ± 0.8)	0.0006***	0.1439
TIB	21.9–25.2(23.7 ± 1.1)	19.6–22.8(21.5 ± 1.0)	22.6–23.9(23.3 ± 0.4)	0.0003***	0.0653

calls of the *Nidirana* population in MDM have the duration of 1.012–1.917 s (1.461 ± 0.29 , $N = 20$), with the PF of 1894.9 Hz generally, and consisted of 6–11 (8.4 ± 1.4 , $N = 20$) rapidly repeated notes. All notes are identical and regular, with the duration of 56–101 ms (77.4 ± 6.7 , $N = 168$) and the interval between them lasts for 70–183 ms (110.4 ± 21.36 , $N = 147$). The advertisement calls of the *Nidirana*

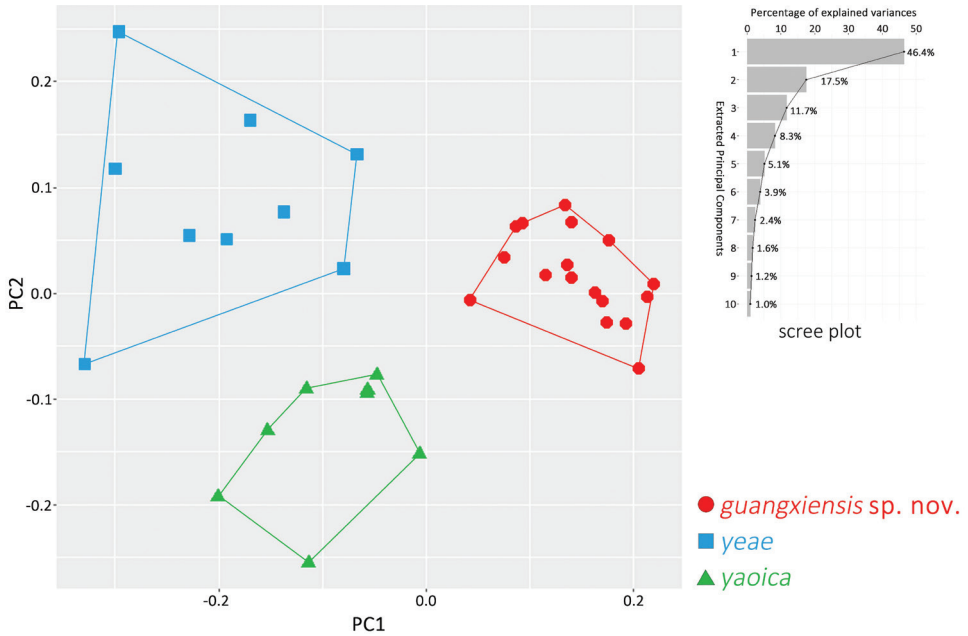


Figure 4. Scatter plot of PC1 and PC2 of principal component analysis based on the morphometric measurements, distinguishing *Nidirana guangxiensis* sp. nov., *N. yeae*, and *N. yaoica*.

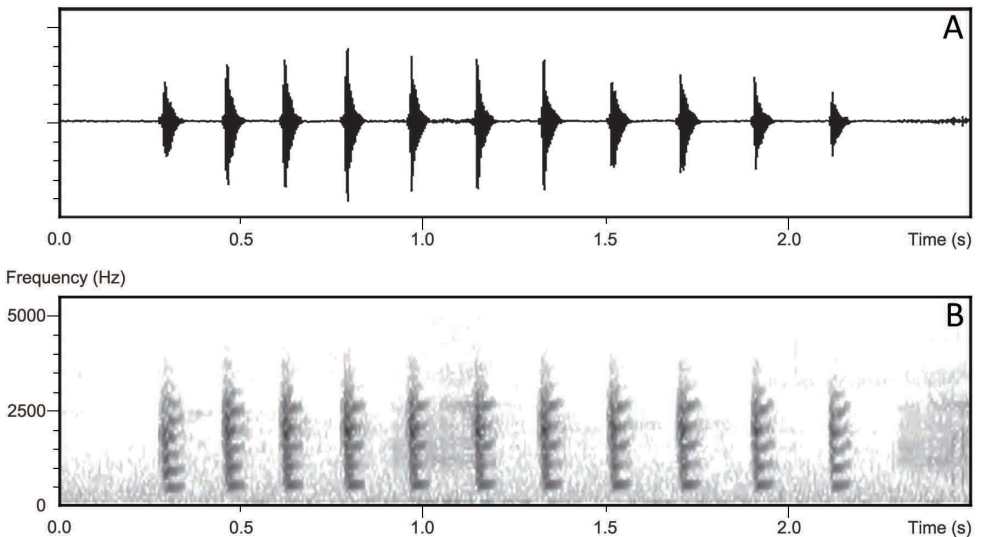


Figure 5. Advertisement call spectrograms of *Nidirana guangxiensis* sp. nov. **A** waveform **B** sonogram.

population in MDM are different from the congeners by (1) all notes in a call are identical and regular [vs containing a significantly different first note in *N. yeae*, *N. daunchina*, *N. lini* (Chou, 1999), *N. nankunensis* Lyu, Zeng, Wang, Lin, Liu & Wang,

2017, and *N. xiangica*; containing 2–4 fast-repeated double-notes in *N. hainanensis* (Fei, Ye & Jiang, 2007)]; (2) containing 6–11 notes in a call [vs containing less than 6 notes in *N. leishanensis*, *N. chapaensis*, *N. yaoica*, *N. adenopleura*, *N. guangdongensis*, *N. occidentalis* Lyu, Yang & Wang, 2020, and *N. pleuraden* (Boulenger, 1904)].

Taxonomic proposal

Based on the molecular, morphological, and bioacoustic differences, the population from MDM, Guangxi represents an unnamed species of genus *Nidirana* which is described here.

Nidirana guangxiensis Mo, Lyu, Huang, Liao & Wang, sp. nov.

<http://zoobank.org/4E5C27A2-D398-4758-A181-BB49D1D5EF42>

Chresonymy.

Hylarana (Hylarana) adenopleura – Zhang and Wen 2000 (Mt. Daming, Guangxi)

Nidirana adenopleura – Mo et al. 2014 (Wuming and Shanglin, Guangxi)

Holotype. NHMG 202007003 (Figs 6, 7A, B), adult male, collected by Zhong Huang and Xiao-Wen Liao on 7 July 2020 from Mt Daming (23.5156°N, 108.4370°E; ca 1260 m a.s.l.), Wuming District, Nanning City, Guangxi Zhuang Autonomous Region, China.

Paratypes. Eighteen specimens. Female NHMG 202007001 (Fig. 7C), and males NHMG 202007002 (Fig. 7D), NHMG 202007004–005, 202007007–015, 202007019–020, collected at the same time with the holotype. Female SYS a008811/NHMG 202008003 and males SYS a008812–8813/NHMG 202008004–005, collected by Yun-Ming Mo, Zhong Huang, and Xiao-Wen Liao on 18 August 2020 from the same locality with the holotype.

Etymology. The specific name *guangxiensis* refers to the type locality of the new species in Guangxi Zhuang Autonomous Region. The Zhuang language, one of the official languages of Guangxi Zhuang Autonomous Region, is based on the dialect of Wuming, from where the new species was collected.

Common name. “Guangxi Music Frog” in English and “广西琴蛙 (guǎng xī qín wā)” in Chinese.

Diagnosis. *Nidirana guangxiensis* sp. nov. is placed in the genus *Nidirana* based on the morphological characteristics of the absence of the thumb-like structure on finger I, presence of well-developed dorsolateral folds, and the presence of supra-brachial glands in breeding males (Lyu et al. 2017). It is further assigned to the *N. adenopleura* group by the presence of lateroventral grooves on all toes (Dubois 1992; Lyu et al. 2019).

Nidirana guangxiensis sp. nov. is distinguished from its congeners by the following combination of the morphological characteristics: (1) body medium sized, with SVL 40.2–47.6 mm (43.8 ± 2.2 , $N = 17$) in adult males and 49.9–51.0 mm ($N = 2$) in

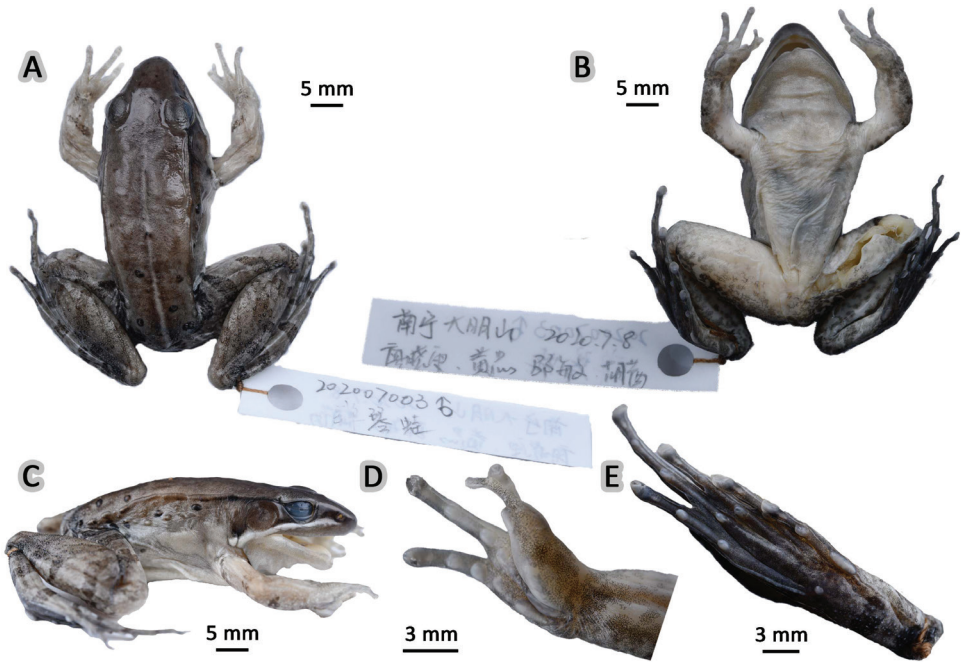


Figure 6. Morphological features of the adult male holotype NHMG 202007003 of *Nidirana guangxiensis* sp. nov. in preservative **A** dorsal view **B** ventral view **C** lateral view **D** right hand **E** right foot. Photos by Shuo Qi.

adult females; (2) disks of digits dilated, pointed; (3) lateroventral grooves present on fingers III and IV, and each toe; (4) relative finger length $II < I < IV < III$; (5) lateral fringes wide on inner sides of fingers II, III and IV but absent on finger I; (6) webbing formula on toes I $2-2\frac{2}{3}$ II $2-3$ III $2\frac{1}{2}-3\frac{2}{3}$ IV $3\frac{2}{3}-2\frac{1}{2}$ V; (7) tibio-tarsal articulation reaching at the nostril; (8) dorsal skin rough with dense granules, several tubercles on the posterior part, flanks, and dorsal hindlimbs, without spinules on the skin; (9) distinct supernumerary tubercles below the base of fingers III and IV, palmar tubercles prominent and distinct; (10) a pair of subgular vocal sacs present; (11) a single nuptial pad on the first finger, nuptial spinules invisible; (12) suprabrachial gland large; (13) nest construction behavior present; (14) calling consisting of 6–11 rapidly repeated regular notes.

Comparison. *Nidirana guangxiensis* sp. nov. can be significantly distinguished from all other recognized congeners by the combination of the following characteristics: (1) body medium-sized, SVL 40.2–47.6 mm ($N = 17$) in adult males and 49.9–51.0 mm ($N = 2$) in adult females [vs SVL < 38 mm in adult male *N. nankunensis*; SVL > 50 mm in adult male *N. guangdongensis*, *N. mangveni*, and *N. xiangica*; SVL < 45 mm in adult female *N. yae* and *N. nankunensis*; SVL > 53 mm in adult female *N. guangdongensis*, *N. lini*, *N. mangveni*, *N. occidentalis*, and *N. xiangica*]; (2) relative fingers length $II < I < IV < III$ [vs $II < IV < I < III$ in *N. yae* and *N. leishanensis*; $II < I$



Figure 7. Variation and colorations of *Nidirana guangxiensis* sp. nov. in life **A, B** male holotype NHMG 202007003 **C** female paratype NHMG 202007001 **D** male paratype NHMG 202007002 **E, F** uncaptured female and male individuals in the wild. Photos by Zhong Huang, Zhi-Tong Lyu, and Yun-Ming Mo.

= IV < III in *N. chapaensis*; I < II < IV < III in *N. mangveni*]; (3) lateroventral grooves present on fingers III and IV [vs absent on all fingers in *N. yae*, *N. occidentalis*, and *N. pleuraden*; present on all fingers in *N. yaoica*, *N. hainanensis*, *N. leishanensis*, and *N. xiangica*; present on all fingers except finger I in *N. chapaensis*, *N. adenopleura*, *N. guangdongensis*, *N. lini*, *N. nankunensis*, and *N. okinavana* (Boettger, 1895)]; (4) lateroventral grooves present on all toes [vs absent on all toes in *N. occidentalis* and *N. pleuraden*]; (5) tibio-tarsal articulation reaches the nostril [vs beyond the snout tip in *N. lini*; at the eye in *N. yae* and *N. occidentalis*]; (6) a single nuptial pad present on

finger I [vs nuptial pad absent in *N. hainanensis*; nuptial pad divided into two parts on finger I in *N. chapaensis*; two nuptial pads respectively on fingers I and II in *N. leishanensis*]; (7) a pair of subgular vocal sacs present in males [vs absent in *N. okinavana*]; (8) spinules on posterior dorsal skin absent [vs present in *N. adenopleura*, *N. lini*, *N. mangveni*, *N. occidentalis*, *N. pleuraden*, and *N. xiangica*].

Particularly, *Nidirana guangxiensis* sp. nov. is relatively close in phylogeny to *N. yae* from northern Guizhou, but it can be distinguished by: the relative fingers length $II < I < IV < III$ [vs $II < IV < I < III$ in *N. yae*]; lateroventral grooves present on fingers III and IV [vs absent on all fingers]; tibio-tarsal articulation reaches the nostril [vs at the eye]; lateral fringes wide on inner sides of fingers II, III and IV but absent on finger I [vs present only on fingers III and IV]; webbing formula on toes I 2–2 $\frac{2}{3}$ II 2–3 III 2 $\frac{1}{2}$ –3 $\frac{2}{3}$ IV 3 $\frac{2}{3}$ –2 $\frac{1}{2}$ V [vs I 2–2 II 1 $\frac{2}{3}$ –3 $\frac{1}{2}$ III 2 $\frac{1}{2}$ –3 $\frac{2}{3}$ IV 3 $\frac{2}{3}$ –2 V]; in males, head larger, HDL/SVL 0.42 ± 0.02 [vs 0.35 ± 0.03], HDW/SVL 0.38 ± 0.02 [vs 0.35 ± 0.01], radio-ulna length shorter, RAD/SVL 0.17 ± 0.01 [vs 0.20 ± 0.01], and foot length longer, FTL/SVL 0.78 ± 0.03 [vs 0.70 ± 0.05].

Description of holotype. NHMG 202007003 (Figs 6, 7A, B), adult male. Body medium-sized, SVL 43.8 mm; head relatively long and wide (HDL/SVL 0.42, HDW/SVL 0.36), longer than wide (HDW/HDL 0.86), flat above; snout rounded in dorsal and lateral views, slightly protruding beyond lower jaw, longer than horizontal diameter of eye (SNT/ED 1.57); canthus rostralis distinct, slightly curved inwards on the nostril; loreal region concave; nostril round, closer to the snout than to the eye; a longitudinal swollen mandibular ridge extending from below nostril through lower edges of eye and tympanum to above insertion of arm, where the ridge is intermittent, forming a maxillary gland and shoulder gland; supratympanic fold absent; interorbital space flat, narrower than internasal distance (IND/IOD 1.31), pineal ocellus invisible; pupil elliptical, horizontal; tympanum distinct, round, relatively large, TD/ED 0.98; vomerine ridge present, bearing small teeth; tongue cordiform, margin of the tongue notched; a pair of subgular vocal sacs present.

Forelimbs moderately robust, lower arm 0.17 of SVL and hand 0.27 of SVL; fingers thin, relative finger lengths $II < I < IV < III$; tip of each finger slightly dilated, forming rounded disks; lateroventral grooves on fingers III and IV, not meeting at the tip of disks; fingers free of webbing; lateral fringes present and distinct on inner and outer sides of fingers II, III and IV, but absent on finger I; subarticular tubercles prominent and rounded; supernumerary tubercles present below the base of fingers III and IV; palmar tubercles three, elliptic, large, prominent and distinct; a single nuptial pad on the dorsal surface of finger I, nuptial spinules invisible.

Hindlimbs robust, tibia 0.53 of SVL, and foot 0.76 of SVL; heels overlapping when hindlimbs flexed at right angles to axis of body; tibio-tarsal articulation reaching at the nostril when hindlimb is stretched along the side of the body; toes relatively long and thin, relative lengths $I < II < V < III < IV$; tip of each toe slightly dilated with remarkable elongated ventral callous pad, forming long and pointed disk; lateroventral grooves well developed on each toe, not meeting at the tip of disks; webbing moderate,

formula: I $1\frac{1}{3}$ –2 II $1\frac{1}{3}$ – $2\frac{1}{3}$ III $1\frac{2}{3}$ –3 IV $3\frac{1}{3}$ – $1\frac{1}{3}$ V; lateral fringes present on inner and outer sides of each toe, forming distinct dermal flap on the lateral edges of toes I and V; subarticular tubercles rounded, prominent; inner metatarsal tubercle elliptic, length triple width; outer metatarsal tubercle indistinct, small and rounded; tarsal folds present and tarsal tubercle absent.

Dorsal skin rough with dense granules, several tubercles on the posterior part, flanks, and dorsal hindlimbs, not bearing spinules on the skin; developed dorsolateral fold from posterior margin of upper eyelid to above groin but intermittent posteriorly; a large and smooth suprabrachial gland behind base of forelimb, prominent; weak longitudinal ridges on upper arms and slightly extending to lower arm; the dorsal surfaces of thigh and tibia relatively rough with tubercles, forming several longitudinal ridges. Ventral surface of throat, body, and limbs smooth; large flattened tubercles densely arranged on the rear of thigh and around vent.

Color of holotype. In life (Fig. 7A, B), dorsal surface of head and body brown; a longitudinal light brown mid-dorsal stripe faintly beginning from interorbital area, extending posteriorly to vent and become more distinct; several black spots on posterior dorsum of body; dorsolateral fold brown; upper flank brown with small black spots; lower flank light brown; suprabrachial gland yellowish brown. Dorsal forelimbs brown; dorsal hindlimbs brown, two olive crossbars on the thigh, three on the tibia, and three on the tarsus; irregular olive marks on dorsal toes. Loreal and temporal regions dark brown, tympanum pink; upper $\frac{1}{3}$ iris brownish white and lower $\frac{2}{3}$ iris reddish brown; maxillary gland and shoulder gland creamy white. Lips, throat, ventral surface of body and limbs creamy white; rear thigh tinged with pink and pale grey patches; ventral hand and foot pale white.

In preservative (Fig. 6), dorsal surface becomes dark brown with the mid-dorsal stripe and black spots more distinct; flank surface and the suprabrachial gland become pale; crossbars and marks on limbs dark brown; loreal and temporal regions dark brown; maxillary gland and shoulder gland more distinct; ventral surface pale grey; rear thigh and ventral foot become dark grey.

Variations. Measurements of type series are given in Table 4. All specimens were similar in morphology. Females are significantly larger than males, with relatively smoother skin and fewer tubercles on dorsum and flanks. The colorations vary from pale brown to reddish brown in individuals (Fig. 7C–F). The patterns of mid-dorsal stripes are also variable but always present.

Male secondary sexual characteristics. A pair of subgular vocal sacs, a pair of slit-like openings at posterior of jaw; a single light brown nuptial pad on the dorsal surface of finger I, nuptial spinules invisible; suprabrachial gland present.

Tadpole. Body length 19.1 mm and tail length 43.1 mm in the 37th stage tadpole SYS a008814 (Fig. 8); body oval, flattened above; snout rounded in dorsal aspect and profile; eyes lateral; labial tooth row formula: 1:1+1/1+1:2; spiracle on left side of body, directed dorsoposteriorly; tail depth larger than body depth; dorsal fin arising just before origin of tail, maximum depth near mid-length, tapering gradually to narrow pointed tip.

Table 4. Measurements (in mm) of the type series of *Nidirana guangxiensis* sp. nov., * for the holotype, M for male, and F for female.

	NHMG 202007002	NHMG 202007003*	NHMG 202007004	NHMG 202007005	NHMG 202007007	NHMG 202007008	NHMG 202007009	NHMG 202007010	NHMG 202007011	NHMG 202007012
Sex	M	M	M	M	M	M	M	M	M	M
SVL	45.4	43.8	44.0	47.6	44.5	41.7	44.0	44.1	47.5	42.6
HDL	18.2	18.4	17.8	19.6	18.4	17.4	19.9	19.1	19.6	17.1
HDW	15.5	15.9	15.7	17.0	16.6	16.4	18.4	17.0	17.5	15.3
SNT	7.4	7.4	6.9	7.6	7.1	6.7	7.6	7.3	7.8	6.4
IND	6.0	6.0	5.7	5.9	5.6	5.7	6.0	6.1	6.3	5.4
IOD	4.6	4.6	4.8	5.0	4.7	4.1	4.5	4.6	4.8	4.1
ED	4.6	4.7	4.6	4.8	4.8	4.6	4.7	4.7	4.9	4.6
TD	4.4	4.6	4.2	4.6	4.4	4.3	4.4	4.3	4.7	4.3
HND	11.6	11.9	11.3	12.8	11.8	10.5	11.6	11.6	12.4	10.6
RAD	7.5	7.2	7.8	7.8	7.2	7.1	7.2	7.2	8.1	7.2
FTL	33.2	33.4	32.6	37.0	33.2	33.2	34.0	35.6	34.7	33.7
TIB	23.7	23.4	23.4	25.2	24.8	22.2	22.5	25.2	25.2	23.1
	NHMG 202007013	NHMG 202007014	NHMG 202007015	NHMG 202007019	NHMG 202007020	SYS a008812 /NHMG 202008004	SYS a008813 /NHMG 202008005	NHMG 202007001	SYS a008811 /NHMG 202008003	
Sex	M	M	M	M	M	M	M	F	F	
SVL	40.2	43.2	41.5	42.5	40.3	45.1	46.5	49.9	51.0	
HDL	18.0	18.3	18.0	18.5	18.6	18.5	18.5	20.3	20.4	
HDW	15.8	16.2	16.2	16.7	17.0	16.1	17.1	18.7	18.8	
SNT	6.7	7.3	7.2	7.3	7.0	7.4	7.5	7.9	7.8	
IND	5.6	5.9	5.9	5.9	5.9	5.7	5.8	6.0	6.1	
IOD	4.4	4.3	4.4	4.6	4.6	4.6	4.6	4.7	5.0	
ED	4.5	4.7	4.6	4.7	4.7	4.8	4.6	5.1	5.2	
TD	4.3	4.5	4.3	4.5	4.4	4.6	4.3	4.2	4.2	
HND	10.3	10.0	11.6	11.7	12.2	11.0	11.2	12.1	12.1	
RAD	7.1	7.2	7.3	7.2	7.8	7.1	7.7	8.6	8.8	
FTL	32.0	32.7	33.7	33.8	32.4	32.8	35.1	37.5	39.5	
TIB	21.9	24.3	23.6	24.7	23.2	23.0	23.7	27.1	26.7	

Distribution and ecology. Currently, *Nidirana guangxiensis* sp. nov. is known only from the type locality, Mt Daming, which is located between Wuming District and Shanglin County, Nanning, Guangxi (Fig. 1). This species of frog can only be found in the alpine swamp and neighboring brushwood on the peak of Mt Daming. The estimated extent of occurrence is less than 500 km², and the estimated area of occupancy is less than 50 km². The swamp was surrounded by subtropical evergreen broadleaf forests (Fig. 9A). Sympatric frog species observed in the swamp are *Duttaphrynus melanostictus* (Schneider, 1799), *Gracixalus jinxiuensis* (Hu, 1978), *Kurixalus odontotarsus* (Ye & Fei, 1993), and *Polypedates mutus* (Smith, 1940).

Nidirana guangxiensis sp. nov. was observed to have nest construction behavior. The nest is in the form of a mud burrow ca 25–30 mm in diameter and near the roots of plants. The top of the nest is open and may fill with water during the rainy season (Fig. 9B). From April to August, males call from dusk to midnight in the nest. In late April, tadpoles at the 26th–42nd stages can be observed, with the majority at the 33rd–37th stages.



Figure 8. Tadpole SYS a008814 of *Nidirana guangxiensis* sp. nov. Photos by Shuo Qi.

Discussion

With this work, the historically recorded populations of *Nidirana adenopleura* from Guangxi, are all reassigned to other recently described species, namely *N. yaoica* from Mt Dayao in the east, *N. xiangica* from Mt Dupangling in the northeast, *N. leishanensis* from Mt Jiuwan in the north, and *Nidirana guangxiensis* sp. nov. from Mt Daming, central Guangxi (Fig. 1). Among them, *Nidirana guangxiensis* sp. nov. is phylogenetically close to *N. yaoica*, while *N. xiangica* and *N. leishanensis* are sister species (Fig. 2). The complex rivers and mountainous systems in Guangxi may play as important barriers to the speciation of these species pairs.

As indicated by the etymology of the generic epithet (Dubois 1992), some species of *Nidirana* were observed with the behavior of nest construction (*Nidirana guangxiensis* sp. nov., *N. okinavana*, *N. nankunensis*, *N. hainanensis*, *N. chapaensis*, and *N. daunchina*). According to our field observations, these nest-constructing species usually live in natural swamps and ponds with muddy bottoms (Fei et al. 2009, 2012; Lyu et al. 2017; this work). Such habitats obtain seasonal rainfall and unpredictable water accumulation, which implies that constructing a nest would be helpful for the growth of the eggs and tadpoles. In contrast, the congeners without such behavior (*N. adenopleura*, *N. guangdongensis*, *N. leishanensis*, *N. lini*, *N. mangveni*,



Figure 9. **A** habitat of *Nidirana guangxiensis* sp. nov. in the type locality in Mt Daming **B** a male calling in a nest and two nests filled with half of water. Photos by Yun-Ming Mo and Shuo Qi.

N. occidentalis, *N. pleuraden*, and *N. xiangica*) usually inhabit natural or artificial ponds and paddies with perennial water, which allows them to directly oviposit into the water (Fei et al. 2009, 2012; Lyu et al. 2020a, 2020b). Additionally, the nest construction behaviors of two other congeners are still unknown (*N. yaoica* and *N. yae*; Table 2), but to roughly illustrate and compare the reported ecological data which is correlated to such courtship behavior, *N. yaoica* living in seasonal swamps (Lyu et al. 2019) is likely to construct nests, and *N. yae* inhabiting paddy field with tadpoles observed at the water surface (Wei et al. 2020) may not possess such behavior. Regarded as important for breeding, this behavior was used for the species-group

divisions (Fei et al. 2009; Chuaynkern et al. 2010). Nevertheless, Lyu et al. (2019) revised the species groups based on phylogenetic results and found that the behavior of nest construction seems to evolve independently in different clades. As an infrequent habit in the family Ranidae, the evolution of nest construction behavior in *Nidirana* species would be a topic worth studying and requires more ethological and ecological work and the application of genomic data.

Based on the phylogenetic relationships, Lyu et al. (2017) partitioned the genus *Nidirana* into four robustly supported clades (Fig. 2). Clade A corresponds to the *N. pleuraden* group with two recognized species (Lyu et al. 2019, 2020a), while the other clades belong to the *N. adenopleura* group (Lyu et al. 2019). Clade B is monotypic and includes only *N. lini*, clade D is comprised of four species, and clade C includes nine species which are more than half the members of the genus. By bringing the phylogenetic analyses from this work and previous studies (Lyu et al. 2019, 2020a, b), the interspecies relationships within clade C are unclear due to the relatively lower supported values in mitochondrial genes. Species of clade C are mostly distributed in the hilly regions throughout southwestern and south-central China and northern Indochina (Fig. 1), at the edge of the Indo-Burma biodiversity hotspot. In view of the extensiveness of these hilly areas and the unclear relationship within this clade, *Nidirana* diversity in these areas seems still underestimated, which suggests that further surveys are required.

Acknowledgements

We thank Wei-Liang Xie, Zhao-Chi Zeng, Shuo Qi, Jian Wang, Pi-Ning Zhou, Min Shao, and Xi Hu for their help in the field and lab. We thank Yinpeng Zhang and Robin Moser from Michigan State University for polishing the language. This work was supported by National Animal Collection Resource Center, China, and Guangxi Natural Science Foundation (grant no. 2017GXNSFDA198001).

References

- Boersma P (2001) Praat, a system for doing phonetics by computer. *Glott International* 5: 341–345.
- Boettger O (1895) Neue Frösche und Schlangen von den Liukiu-Inseln. *Zoologischer Anzeiger* 18: 66–270.
- Boulenger GA (1904) Descriptions of new frogs and snakes from Yunnan. *Annals and Magazine of Natural History (Series 7)* 13: 130–135. <https://doi.org/10.1080/00222930408562447>
- Boulenger GA (1909) Descriptions of four new frogs and a new snake discovered by Mr. H. Sauter in Formosa. *Annals and Magazine of Natural History (Series 8)* 4: 492–495. <https://doi.org/10.1080/00222930908692704>

- Bourret R (1937) Notes herpétologiques sur l'Indochine française. XIV. Les batraciens de la collection du Laboratoire des Sciences Naturelles de l'Université. Descriptions de quinze espèces ou variétés nouvelles. Annexe au Bulletin Général de l'Instruction Publique, Hanoi.
- Chang MLY, Hsu HF (1932) Study of some amphibians from Szechuan. Contributions from the Biological Laboratory of the Science Society of China, Zoological Series 8: 137–181.
- Chen L, Murphy RW, Lathrop A, Ngo A, Orlov NL, Ho CT, Somorjai IL (2005) Taxonomic chaos in Asian ranid frogs: an initial phylogenetic resolution. *The Herpetological Journal* 15: 231–243.
- Chou WH (1999) A new frog of the genus *Rana* (Anura: Ranidae) from China. *Herpetologica* 55: 389–400.
- Chuaynkern Y, Ohler A, Inthara C, Duengkae P, Makchai S, Salangsingha N (2010) A revision of species in the subgenus *Nidirana* Dubois, 1992, with special attention to the identity of specimens allocated to *Rana adenopleura* Boulenger, 1909, and *Rana chapaensis* (Bourret, 1937) (Amphibia: Anura: Ranidae) from Thailand and Laos. *Raffles Bulletin of Zoology* 58: 291–310.
- Dubois, A (1992) Notes sur la classification des Ranidae (Amphibiens anoures). *Bulletin Mensuel de la Société Linnéenne de Lyon* 61: 305–352. <https://doi.org/10.3406/linly.1992.11011>
- Fei L, Ye CY, Jiang JP (2007) A new species of Ranidae, *Hylarana* (*Nidirana*) *hainanensis*, from China (Amphibia: Anura). *Herpetologica Sinica* 11: 1–4.
- Fei L, Hu SQ, Ye CY, Huang YZ (2009) *Fauna Sinica. Amphibia Vol. 3 Anura*. Science Press, Beijing.
- Frost DR, Grant T, Faivovich J, Bain RH, Haas A, Haddad CF, De Sa RO, Channing A, Wilkinson M, Donnellan SC, Raxworthy CJ, Campbell JA, Blotto BL, Moler P, Drewes RC, Nussbaum RA, Lynch JD, Green DM, Wheeler WC (2006) The amphibian tree of life. *Bulletin of the American Museum of natural History* 297: 1–291. [https://doi.org/10.1206/0003-0090\(2006\)297\[0001:TATOL\]2.0.CO;2](https://doi.org/10.1206/0003-0090(2006)297[0001:TATOL]2.0.CO;2)
- Kuramoto M (1985) A new frog (genus *Rana*) from the Yaeyama Group of the Ryukyu Islands. *Herpetologica* 41: 150–158.
- Li S, Wei G, Xu N, Cui J, Fei L, Jiang J, Liu J, Wang B (2019) A new species of the Asian music frog genus *Nidirana* (Amphibia, Anura, Ranidae) from Southwestern China. *PeerJ* 7: e7157. <https://doi.org/10.7717/peerj.7157>
- Liu CC, Hu SQ (1962) A herpetological report of Kwangsi. *Acta Zoologica Sinica* 14: 73–104.
- Lyu ZT, Chen Y, Yang JH, Zeng ZC, Wang J, Zhao J, Wan H, Pang H, Wang YY (2020a) A new species of *Nidirana* from the *N. pleuraden* group (Anura, Ranidae) from western Yunnan, China. *Zootaxa* 4861: 43–62. <https://doi.org/10.11646/zootaxa.4861.1.3>
- Lyu ZT, Dai KY, Li Y, Wan H, Liu ZY, Qi S, Lin SM, Wang J, Li YL, Zeng YJ, Li PP, Pang H, Wang YY (2020b) Comprehensive approaches reveal three cryptic species of genus *Nidirana* (Anura, Ranidae) from China. *ZooKeys* 914: 127–159. <https://doi.org/10.3897/zookeys.914.36604>
- Lyu ZT, Mo YM, Wan H, Li YL, Pang H, Wang Y Y (2019) Description of a new species of music frogs (Anura, Ranidae, *Nidirana*) from Mt Dayao, southern China. *ZooKeys* 858: 109–126. <https://doi.org/10.3897/zookeys.858.34363>

- Lyu ZT, Zeng ZC, Wang J, Lin CY, Liu ZY, Wang YY (2017) Resurrection of genus *Nidirana* (Anura: Ranidae) and synonymizing *N. caldwelli* with *N. adenopleura*, with description of a new species from China. *Amphibia-Reptilia* 38: 483–502. <https://doi.org/10.1163/15685381-00003130>
- Matsui M (2007) Unmasking *Rana okinavana* Boettger, 1895 from the Ryukyus, Japan (Amphibia: Anura: Ranidae). *Zoological Science* 24: 199–204. <https://doi.org/10.2108/zsj.24.199>
- Mo YM, Wei ZY, Chen WC (2014) Colored Atlas of Guangxi Amphibians. Guangxi Science and Technology Publishing House.
- Savage JM (1975) Systematics and distribution of the Mexican and Central American stream frogs related to *Eleutherodactylus rugulosus*. *Copeia* 2: 254–306. <https://doi.org/10.2307/1442883>
- Schmidt KP (1925) New Chinese amphibians and reptiles. *American Museum Novitates* 175: 1–3.
- Silvestro D, Michalak I (2012) RaxmlGUI: a graphical front-end for RAXML. *Organisms Diversity and Evolution* 12: 335–337. <https://doi.org/10.1007/s13127-011-0056-0>
- Wei G, Li SZ, Liu J, Cheng YL, Xu N, Wang B (2020) A new species of the music frog *Nidirana* (Anura, Ranidae) from Guizhou Province, China. *ZooKeys* 904: 63–87. <https://doi.org/10.3897/zookeys.904.39161>
- Zhang YX, Wen YT (2020) Amphibians in Guangxi. Guangxi Normal University Press, Guilin, China.

Appendix I

Specimens examined

- Nidirana adenopleura* (37): **China: Taiwan:** Taichung City: SYS a007358–7365; **Fujian:** Yanping District: SYS a005911–5916; Mt Wuyi: SYS a005939–5943; Jianguoshi Nature Reserve: SYS a004112, 4132; Mt Yashu: SYS a005890–5891, 5901–5902; **Jiangxi:** Tongboshan Nature Reserve: SYS a001663–1665, 1667, 1698; Yangjifeng Nature Reserve: SYS a0000317, 0334; Jinggangshan Nature Reserve: SYS a004025–4027; **Zhejiang:** Jingning County: Dongkeng Town: SYS a002725–2726.
- Nidirana daunchina* (5): **China: Sichuan:** Mt Emei: SYS a004594–4595 (topotypes); Hejiang County: Zihuai Town: SYS a004930–4932.
- Nidirana guangdongensis* (8): **China: Guangdong:** Shimentai Nature Reserve: SYS a005765–5767, 5995, 5997–5998, 6879, 7688 (holotype and paratypes series).
- Nidirana hainanensis* (4): **China: Hainan:** Mt Diaoluo: SYS a003741, 7669–7671 (topotypes).
- Nidirana leishanensis* (13): **China: Guizhou:** Mt Leigong: SYS a007908 (topotypes); Mt Fanjing: SYS a007195–7196; **Guangxi:** Mt Jiuwan: NHMG 202007021–023, 025–029, 042–043.

- Nidirana lini* (4): **China: Yunnan:** Jiangcheng County: Hongjiang Town: SYS a003967–3970 (topotypes).
- Nidirana mangveni* (9): **China: Zhejiang:** Mt Dapan: SYS a006310–6314; Mt. Longmen: SYS a006413–6414, 6416; Hangzhou City: SYNU 12050569 (holotype and paratypes series).
- Nidirana nankunensis* (12): **China: Guangdong:** Mt Nankun: SYS a003615, 3617–3620, 4019, 4905–4907, 5717–5719 (holotype and paratypes series).
- Nidirana occidentalis* (8): **China: Yunnan:** Mt. Gaoligong: SYS a003775–3778; Shuangjiang County: SYS a007829–7832 (holotype and paratypes series).
- Nidirana pleuraden* (16): **China: Yunnan:** Kunming City: SYS a007585 (juvenile individual, topotype); Wenshan City: SYS a007717–7723, 7730; Xiping County: SYS a007767, 7769–7770; Shiping County: SYS a007786–7789.
- Nidirana xiangica* (10): **China: Hunan:** Mt Dawei: SYS a006491–6493; Mt. Yangming: SYS a007269–7273; **Jiangxi:** Mt Wugong: SYS a002590–2591 (holotype and paratypes series).
- Nidirana yaoica* (13): **China: Guangxi:** Mt Dayao: SYS a007009, 7011–7014, 7020–7022, NHMG 1503043–047 (holotype and paratypes series).

Two new genera and three new species of cavernicolous trechines from the western Wuling Mountains, China (Coleoptera, Carabidae, Trechinae)

Mingyi Tian¹, Sunbin Huang², Xinyang Jia¹, Yi Zhao¹

1 Department of Entomology, College of Plant Protection, South China Agricultural University, 483 Wushan Road, Guangzhou, 510642, China **2** Mécanismes adaptatifs et évolution (MECADEV), UMR 7179 CNRS–MNHN, Muséum national d'Histoire naturelle, CP50, 57 Rue Cuvier, 75005 Paris, France

Corresponding author: Mingyi Tian (mytian@scau.edu.cn)

Academic editor: Achille Casale | Received 15 June 2021 | Accepted 16 August 2021 | Published 3 September 2021

<http://zoobank.org/D5A7EE06-08C1-4E4B-9FC4-442CDE55A576>

Citation: Tian M, Huang S, Jia X, Zhao Y (2021) Two new genera and three new species of cavernicolous trechines from the western Wuling Mountains, China (Coleoptera, Carabidae, Trechinae). ZooKeys 1059: 57–78. <https://doi.org/10.3897/zookeys.1059.70009>

Abstract

Two new genera and three new species of cave-adapted ground beetles belonging to the tribe Trechini are established and described: *Wulongius qilinger* **gen. nov.** and **sp. nov.** from limestone cave Qiankou Dong (Chongqing: Wulong), *Qianotrechus congcong* **sp. nov.** from cave Shigao Dong (Chongqing: Nanchuan), and *Qianlongius zhoui* **gen. nov.** and **sp. nov.** from cave Qianlong Dong (Guizhou: Songtao). *Wulongius qilinger* **sp. nov.** is a small aphaenopsian beetle with a thin and elongated body, while *Qianlongius zhoui* **sp. nov.** is a semi-aphaenopsian with a stout body. Both new genera are not closely related to any genus of Trechini occurring in the South China Karst, and so their systematic positions remain unclear.

Keywords

Aphaenopsian, cave-dwelling, Chongqing, ground beetles, Guizhou, semi-aphaenopsian

Introduction

The scientific discoveries made in recent years have revealed that the Wuling Mountains harbour a very rich fauna of cavernicolous trechine beetles which is composed of over 30 species in 13 genera (Tian et al. 2021). However, our knowledge on cave beetles in these regions is still increasing. In April 2021, we conducted a biological survey in three limestone caves in the eastern part of the Wuling Mountains in Chongqing Shi and Guizhou Province (Fig. 1). The main purpose of our survey was to investigate the cave biodiversity in the Furong Dong cave system, a well-known show cave in Wulong, Chongqing, which is also a World Heritage Site of South China Karst. Thanks to the assistance of several cavers from the Qilinger Cave Exploration Team (Nanning) and Chongqing Cave Exploration Team (Chongqing), we could successfully survey in cave Qiankou Dong, an upper cave of the Furong Dong system in Tianxing Karst, Wulong. In the deepest point of the vertical pit, which is 55 m deep, we came across a single beetle. This strange looking trechine was undoubtedly an aphaenopsian due to its thin body and elongated appendages. Further study in the laboratory showed that it is a representative of an unknown lineage of cave trechine beetles in China. On the way to Wulong, we visited a cave named Shigao Dong in Nanchuan, Chongqing, and collected two trechine individuals. They are members of a new species belonging to the genus *Qianotrechus* Uéno, 2000 and close to *Q. laevis* Uéno, 2000. After the survey in Wulong, we had an opportunity to investigate Qianlong Dong, a beautiful show cave in Songtao Maio Autonomous County, northeastern Guizhou, thanks to the assistance of Mr Wenlong Zhou (Guizhou Institute of Mountainous Region Resources, Guizhou Academy of Sciences, Guiyang), and discovered a new species of semi-aphaenopsian trechine, which is also a representative of an unknown genus. In this paper, we describe three new species of cavernicolous trechine beetles discovered in caves Qiankou Dong (Wulong, Chongqing), Qianlong Dong (Songtao, Guizhou) and Shigao Dong (Nanchuan, Chongqing). We also establish two new genera to place the first and second new species.

Material and methods

All beetles for this study were collected with the naked eyes using an aspirator in dark zones of the caves and kept in vials with 50% ethanol before studying. One exemplar of each species (but three legs removed from the holotype of *Wulongius qilinger* gen. nov. and sp. nov.) were kept into 95% ethanol for DNA sequencing. Dissections and observations were made by using a binocular Leica MZ75 dissecting microscope (Wetzlar, Germany). Dissected genitalia, including the median lobe and parameres of the aedeagus, were glued on small transparent plastic cards and pinned under the specimen from which they were removed. Digital pictures were taken using a Canon EOS 5D Mark III camera (Tokyo, Japan) and then processed by means of Adobe Photoshop CS5 software (Adobe System Incorporated, California, USA). Measurements and terminologies used in the text are as in Tian et al. (2016). All specimens of the type series are deposited in the insect collection of South China Agricultural University, Guangzhou, China (SCAU).

Taxonomy

Wulongius Tian & Huang, gen. nov.

<http://zoobank.org/0274541E-3999-4F57-8016-491DBC9422EA>

武隆盲步甲属

Type species. *Wulongius qilinger* Tian & Huang, sp. nov. (cave Qiankou Dong, Wulong, Chongqing).

Generic characteristics. Medium-sized for cavernicolous trechine beetles, aphaenopsian and depigmented; body thin and elongate, with thin and slender appendages. Head glabrous, pronotum covered with dense and long erected setae; apical portions of elytra covered with very sparse and short hairs; head strongly elongate, much longer than wide (excluding mandibles); widest at about middle, gently narrowed posteriad, neck constriction short; 2 pairs of supra-orbital setiferous pores present; frontal furrows short and incomplete, ending at the level of the head widest portion; vertex strongly convex; mandibles thin, sharply hooked at apices, right mandibular tooth completely reduced; labial suture clear; mentum with 2 setae on each side of median tooth, base of mentum with small basal pits on each side; submentum with a row of 10 setae; palps thin and very elongate, all glabrous but bisetose on inner margin of 2nd labial palpomere; antennae very thin and long, extending over apices of elytra. Propleura visible from above; pronotum cylindrical, distinctly elongated, much longer than wide, lateral margins nearly parallel-sided though slightly divergent medially, presence of only anterior latero-marginal setae (posterior ones lacking), both fore and hind angles widely obtuse. Scutellum present. Elytra elongated ovate, dorsum strongly convex and expanded laterally, partly concealing lateral margin of elytra in middle portion; humeral angle indistinct, lateral margin well bordered and ciliate throughout; striae almost obsolete though traceable; 2 pairs of dorsal setiferous pores present on the 3rd stria, preapical pores present; basal pores located behind scutellum; the humeral group of the marginal umbilicate pores not aggregated, 1st pore inwardly and backwardly shifted to the site of 6th stria and located at level between 2nd and 3rd pores, 5th and 6th pores widely spaced each other.

Remarks. The position of *Wulongius* gen. nov. within Trechini is undetermined. It might be related to the genus *Xiangxius* Tian & X. Huang, 2021, which has been recently described from Tangle Dong cave in western Hunan, in the eastern Wuling Mountains. Both genera are aphaenopsian, with highly specialized morphological characters. They are somewhat similar in thoracic configuration and, in particular, in the elytral chaetotaxy, in which the 1st pore of the marginal umbilicate series is backwardly and inwardly shifted and both 5th and 6th pores are widely spaced. However, there are many different important characters between them including the body shape: (1) elytra are much more convex and expanded laterally in *Wulongius*, concealing median part of the lateral margins, and without protruding humeral angle on each elytron, versus elytra less expanded laterally in *Xiangxius*, whole lateral margin visible from above, and with a distinct protruding humeral angle on each elytron; (2)

pronotum covered with long setae, without posterior latero-marginal setae in *Wulongius*, versus pronotum glabrous, with posterior latero-marginal setae in *Xiangxius*; (3) mentum glabrous in *Wulongius*, but pubescent in *Xiangxius*; (4) labial suture clear in *Wulongius*, whereas mentum fused with submentum in *Xiangxius*; (5) right mandibular tooth edentate in *Wulongius*, while bidentate in *Xiangxius*; (6) submentum with a row of 10 setae in *Wulongius*, instead of 15 or 16 setae in *Xiangxius*; (7) head slender in *Wulongius*, not thickened, with longer antennae extending beyond the apices of elytra, versus head stout, widely convex laterally, and with shorter antennae extending only to apical 2/3 of elytra in *Xiangxius*.

Etymology. “*Wulong*” + “*-ius*”, indicating the homeland of this new genus. Gender masculine.

Generic range. China (Chongqing). Known only from limestone cave Qiankou Dong (Fig. 1).

***Wulongius qilinger* Tian & Huang, sp. nov.**

<http://zoobank.org/FE36775A-E68D-47FB-8309-ED3999B229FB>

七零二武隆盲步甲

Figures 1–5

Type material. *Holotype* female, cave Qiankou Dong, Tongluo, Jiangkou, Wulong, Chongqing, 29.32°N, 107.91°E, 1103 m, 2021-IV-14, leg. “Wu Ya” (a nickmane of Mr Hongying Wu) & Mingyi Tian, in SCAU.

Diagnosis. A medium-sized aphaenopsian trechine species, with a distinctly elongated body and thin appendages, without eyes and pigmentation, elytra remarkably expanded laterally and partially concealing median part of elytral margins.

Description. Length: 6.5 mm, width: 1.6 mm. Habitus as in Figure 2. Body yellow, antennae, palps and tarsi pale; head covered with a few sparse setae, pronotum covered with dense and long setae, elytra smooth and glabrous in most parts, but with short and sparse setae along lateral margins, underside of head with a few setae laterally and ventrally, sparsely setose on ventral thorax and abdominal ventrites medially; moderately shining. Microsculpture reduced on head; striated on pronotum and elytra.

Head much longer than wide, HLm/HW = 2.68, HLI/HW = 1.96; genae not expanded, widest at about middle of head excluding mandibles, gradually narrowed posteriad, neck short and narrow; frons and vertex moderately convex; frontal furrows nearly parallel-sided, shortly divergent apically, ending at about middle of head; anterior and posterior supraorbital pores located at about basal 3/8 and 1/5 of head, respectively; clypeus 4-setose; labrum transverse, frontal margin almost straight, 6-setose; mentum bisetose, tooth rather narrow, bifid at tip, slightly longer than half of the lateral lobes; ligula 10-setose at apex, inner 2 much longer than others; distal palpomeres of maxilla and labium 1.3 times as long as the penultimate palpomeres; suborbital pores much closer to neck constriction than to submentum (Fig. 3A); antennae pubescent from pedicle to 11th antennomeres, scape not pubescent, stouter and shorter

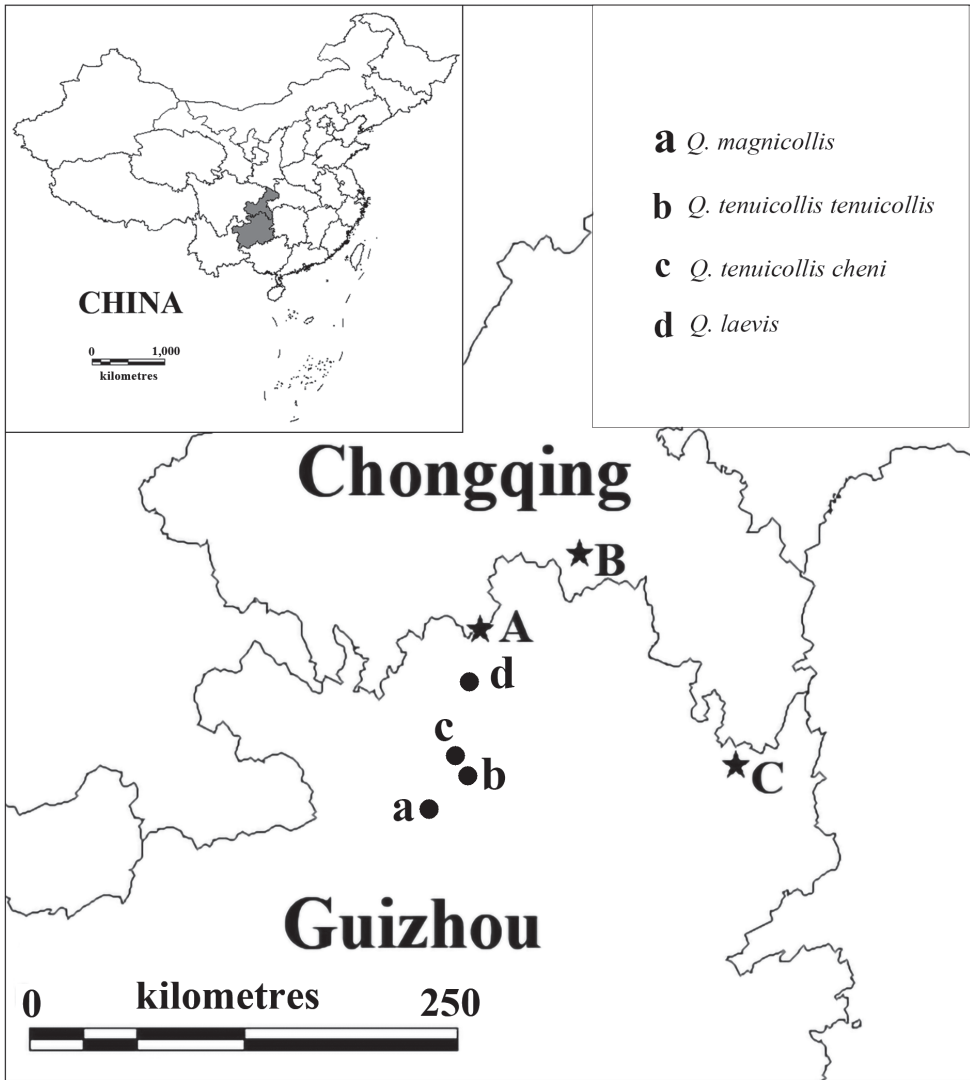


Figure 1. A distribution map showing the localities of the three surveyed caves (stars) and the known species and subspecies of the genus *Qianotrechus* Uéno, 2000 (dots) **A** Shigao Dong **B** Qiankou Dong **C** Qianlong Dong.

than other articles, with several long setae; relative length of each antennomere compared with scape as follows: the 1st (1.0), 2nd (1.4), 3rd (1.9), 4th (2.2), 5th (2.5), 6th (2.3), 7th (2.1), 8th (1.8), 9th (1.8), 10th (1.5) and 11th (2.0).

Prothorax distinctly tumid at sides, propleura slightly wider than pronotum, PrW/PnW = 1.1, visible from above, widest a little before basal 1/3, wider than head, PrW/HW = 1.2; pronotum much longer than wide, PnL/PnW = 1.6, shorter than head excluding mandibles, PL/HL = 0.9; widest at about 3/7 of pronotum from base; lateral margins finely bordered throughout, gently contracted forwards and backwards, slightly



Figure 2. *Wulongius qilinger* gen. nov. and sp. nov., habitus, holotype female.

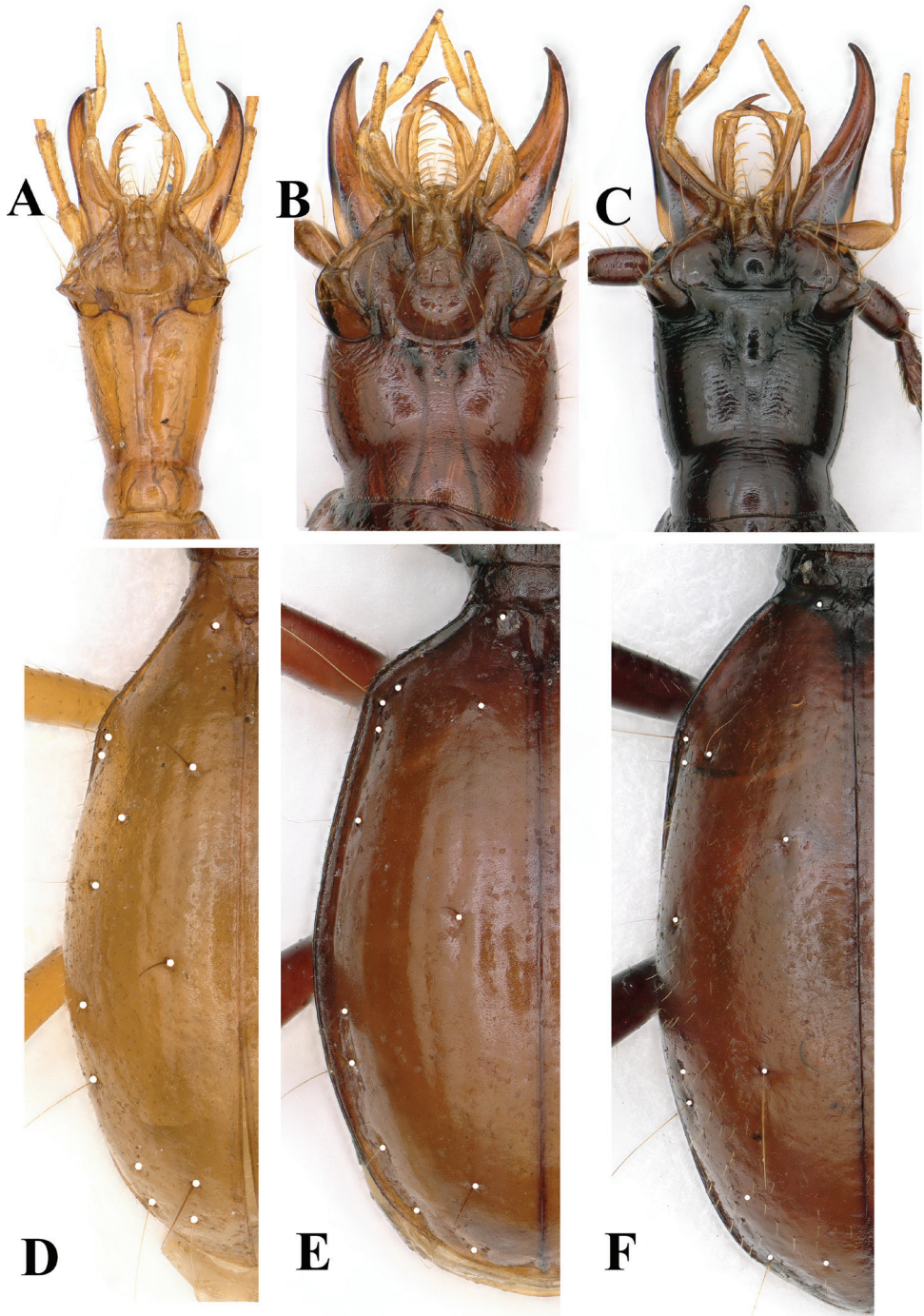


Figure 3. Ventral head (**A–C**) and elytral chaetotaxy (**E, F**) of cave beetles **A, D** *Wulongius qilinger* gen. nov. and sp. nov. **B, E** *Qianotrechus congcongae* sp. nov. **C, F** *Qianlongius zhoui* gen. nov. and sp. nov.).

Qiān Kǒi Dòng (48H-I12-39)
千口洞 Many Entrances Cave
 Tian Xing, Wulong County
 Chongqing, P. R. of China

WGS84 UTM 48R 0783075 3236436
 Altitude 1087m
 Length 114m Depth 53m
 Surveyed to BCRA Grade 5c
 by Hong Meigui CES 2003

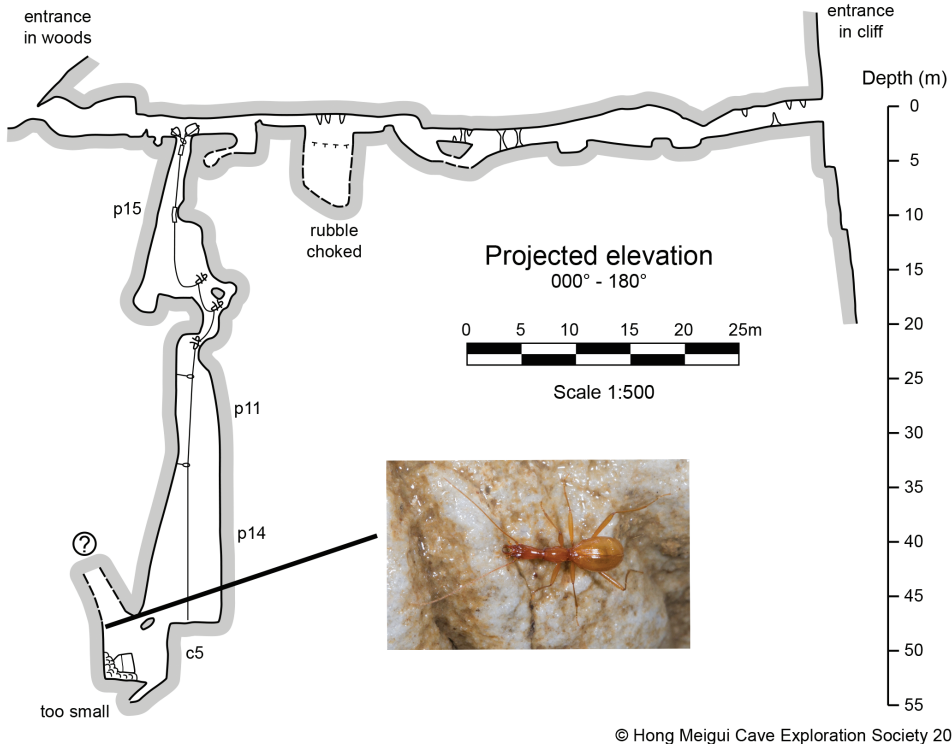


Figure 4. Map of Qiankou Dong, to show where the holotype of *Wulongius qilinger* gen. nov. and sp. nov. was discovered) (courtesy of Prof. Yuanhai Zhang and Hong Meigui Cave Exploration Society).

sinuate before hind angles which are wide and blunt though more or less rectangular; frontal angles rounded off; base straight, front margin slightly arcuate, both unbordered, base slightly wider than front margin; only anterior latero-marginal setae present, at about 2/9 from front margin; disc slightly convex, mid-line well-marked; both fore and basal transversal impressions faint, basal foveae shallow. Scutellum quite large.

Elytra (Fig. 2, 3D) almost as long as fore body including mandibles, much longer than wide, $EL/EW = 1.9$, almost twice as wide as prothorax, $EW/PrW = 2.1$; base unbordered, lateral margins not serrate but ciliate throughout, widest at about middle, humeral angles obtuse, margins invisible from above in middle; apical striole reduced; basal pore present, anterior and posterior dorsal pores on the 3rd stria at basal 2/7 and apical 4/9 of

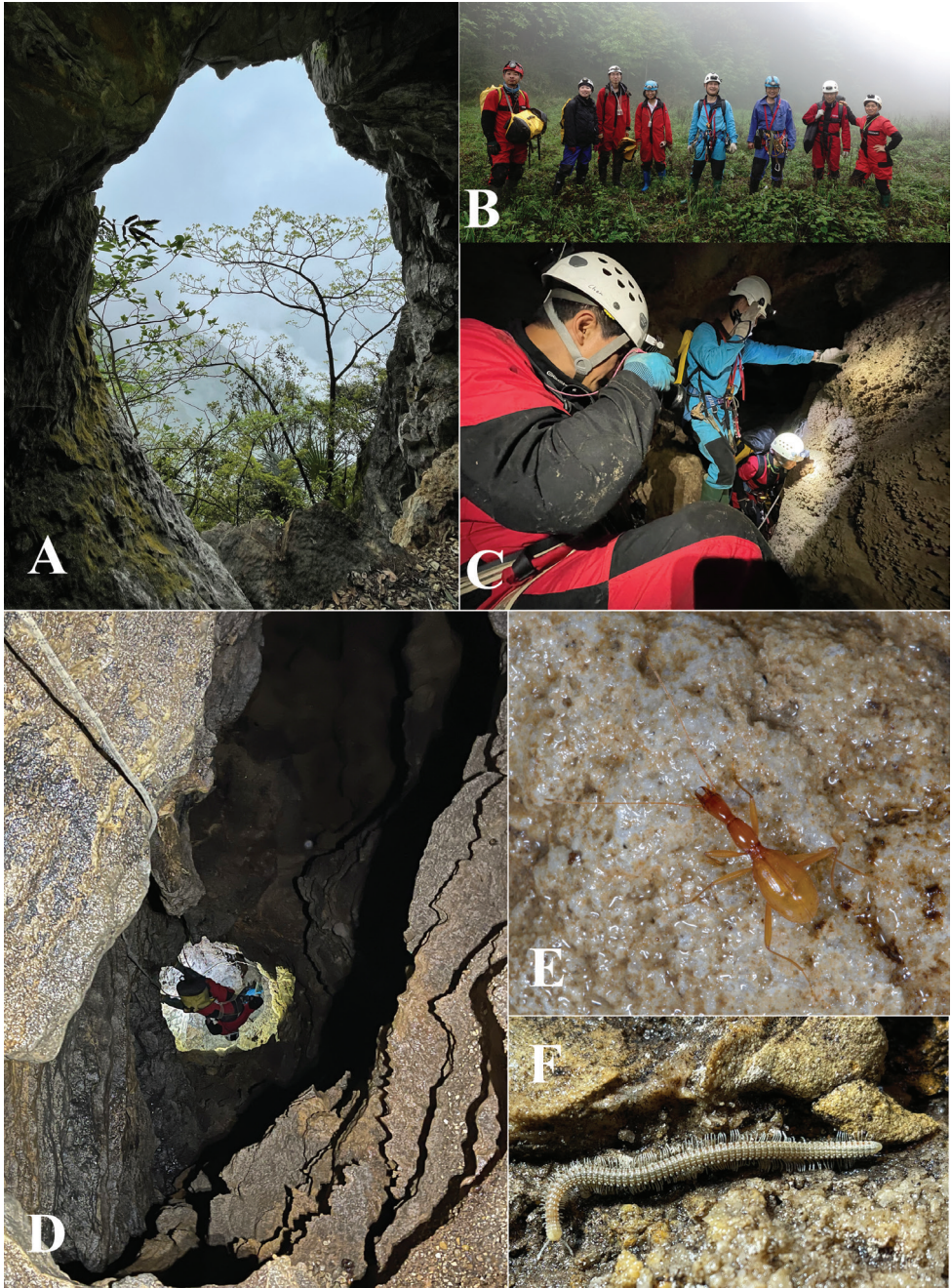


Figure 5. Cave Qiankou Dong **A** entrance in the cliff **B** team photo outside the cave **C** surveying in the cave **D** the vertical pit **E** a running individual of *Wulongius qilinger* gen. nov. and sp. nov. **F** a millipede, *Glyphiulus* sp. (team photo courtesy of Mr Lixin Chen).

elytra, respectively; preapical pores located at apical anastomosis of 3rd and 4th striae; only an apical pore present, subequal to suture and to margin of elytra; the anguloapical pore absent; only 2nd and 3rd pores of marginal umbilicate group close to the marginal gutter, 1st pore closer to 4th than to 2nd; the 7th and 8th pores distant from marginal gutter.

Legs densely pubescent; 1st tarsomere shorter than 2nd–4th combined in fore legs, whereas slightly longer and as long as in middle and hind legs, respectively; tibiae without longitudinal sulci.

Ventrite IV–VI bisetose, VII quadrisetose in female.

Male. unknown.

Etymology. Referring to the Qilinger Cave Exploration Team (Nanning), led by Mr Lixin Chen, a famous TV reporter on cave exploration in China.

Distribution. China (Chongqing). Known only from limestone cave Qiankou Dong (Fig. 1). Qiankou Dong (Figs 4, 5) is located at about 200 m from the beautiful show cave Furong Dong to the northeast and probably was the upper part of the Furong Dong cave system in the past (Yuanhai Zhang pers. comm.). It was well surveyed by the Hong Meigui Cave Exploration Society (U.K.) in 2003. The cave is 114 m long, with two entrances, one in a forest near a farm house and the other in a cliff. There is a 55 m deep vertical pit, although the passage of the cave is more or less horizontal. The single specimen of the new species was discovered by “Wu Ya” (Mr Hongying Wu, an active and well-known caver, who discovered many Tiankengs in China by using Google Earth) and M. Tian. Other cave animals also observed in Qiankou Dong are millipedes (*Oxidus gracilis* (C.L. Koch, 1847), *Eutrichodesmus* sp., *Epanerchodus* sp., and *Glyphiulus* sp.), a cricket (*Tachycines* sp.), an earwig (*Challia fletcheri* Burr, 1904), spiders (*Parasteatoda tepidariorum* (C.L. Koch, 1841) and *Pholcus* sp.), and an ant-loving beetle (*Batrisocenus* sp.).

***Qianotrechus congongae* Tian & Zhao, sp. nov.**

<http://zoobank.org/51137F01-C791-4B90-B94F-64822C00FD2C>

小葱黔穴步甲

Figures 1, 3B, E, 6–8

Type material. Holotype male, cave Shigao Dong, Hexi, Nanchuan, Chongqing, 28.82° N, 107.32° E, 729 m, 2021-IV-13, leg. Yi Zhao, Xinyang Jia and Mingyi Tian, in SCAU.

Diagnosis. A small, stout cave trechine, semi-aphaenopsian, with a brown body, rather short appendages and broadly tumid prothorax.

Description. Length: 5.5–5.8 mm, width: 1.9 mm. Habitus as in Figure 6.

Body brown, palps, antennae and tarsi yellow. Surface and underside smooth and glabrous. Microsculpture: isodiametric meshes on head, transversal meshes or striate on pronotum and elytra.

Head (Figs 3B, 6) moderately elongate, longer than wide excluding mandibles, HLI/HW = 1.4; genae moderately convex, widest near head mid-length; frons and vertex moderately convex; frontal furrows nearly parallel-sided, but slightly and shortly



Figure 6. *Qianotrechus congcongae* sp. nov., habitus, holotype male.

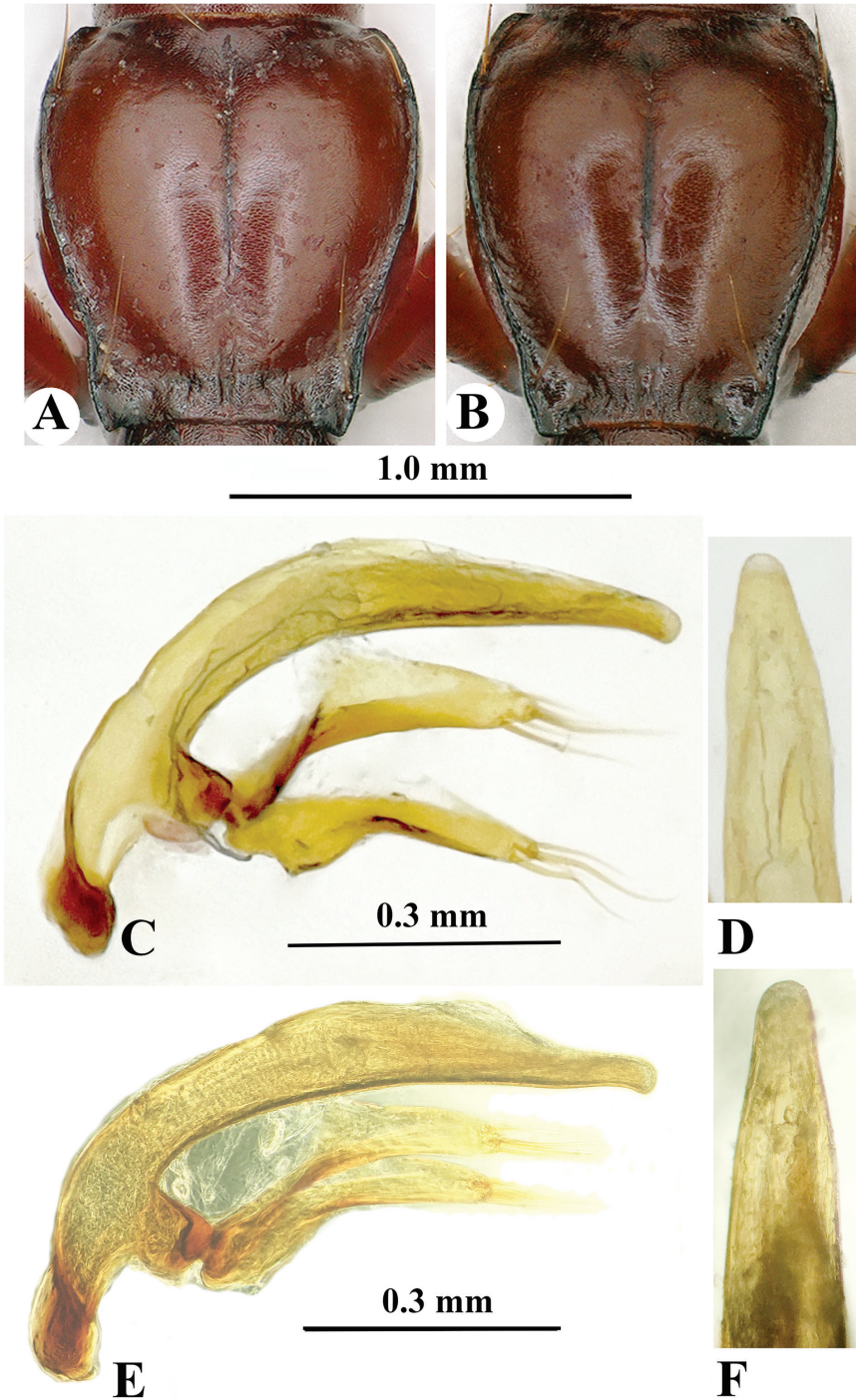


Figure 7. Pronotum and male genitalia of *Qianotrechus* species. **A, C, E** *Q. congcongae* sp. nov. **B, D, F** *Q. laevis* Uéno, 2000 **A, B** pronotum **C, E** median lobe and parameres, lateral view **D, F** apical lobe, dorsal view.

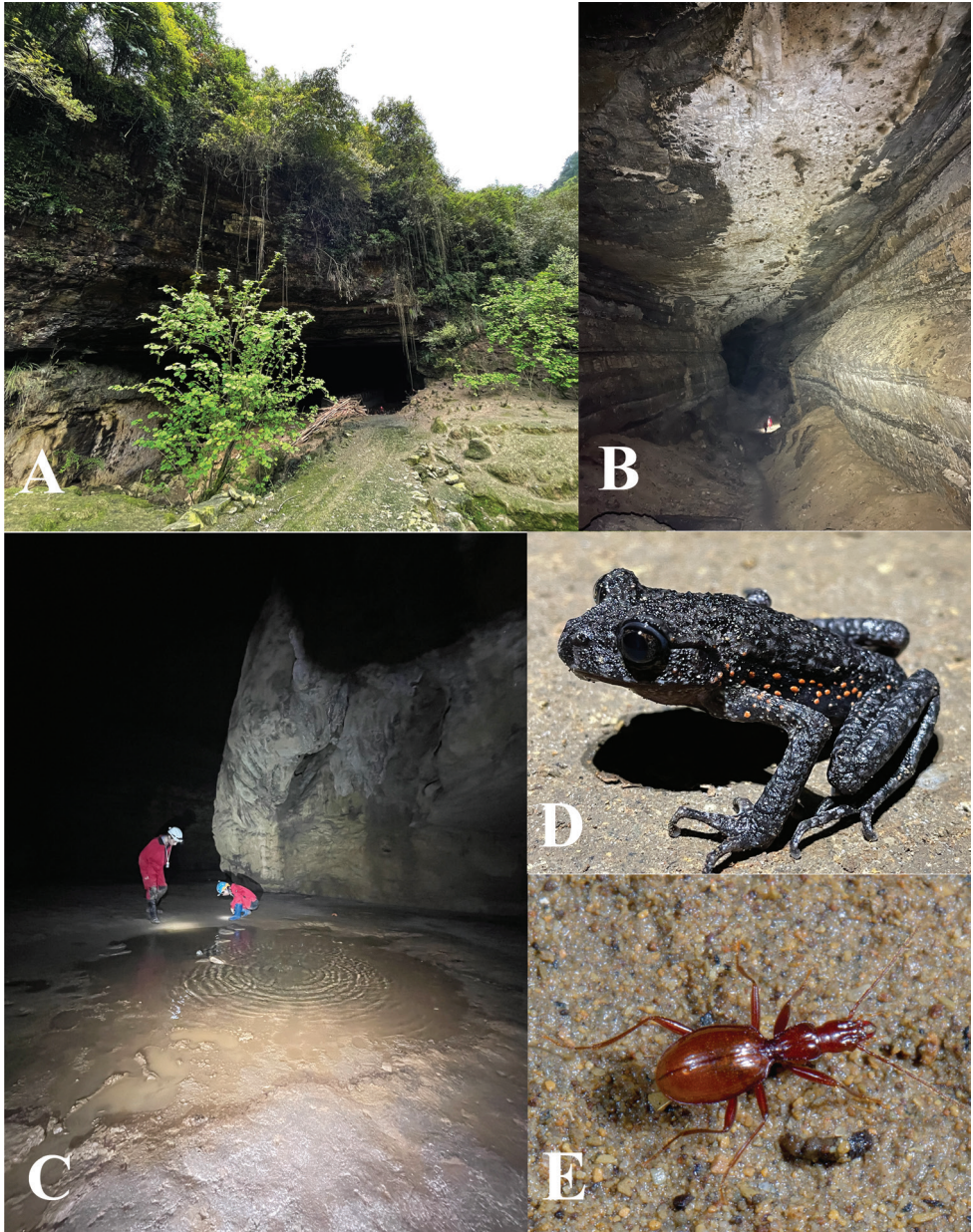


Figure 8. Cave Shigao Dong. **A** entrance **B** the huge passage **C** place where the two beetles were discovered **D** a frog, *Oreolalax rhodostigmatus* Hu & Fei, 1979 **E** a running individual of *Qianotrechus congcongae* sp. nov.

convergent posteriorly, ending at widest point of head; anterior and posterior supraorbital pores present, located at about middle and basal 1/5 of head excluding mandibles; clypeus 4-setose, labrum transverse, faintly bisinuate at the front margin, 6-setose; right mandibular teeth bidentate; mentum completely fused with submentum, 2-se-

tose, tooth short and pointed at apex, much shorter than the lateral lobes; ligula fused with paraglossae, 8-setose at apex; palps thin and slender, the 2nd labial palpomere about 0.9 times as long as 3rd, 3rd maxillary palpomere as long as 4th; suborbital pores close to neck; antennae thin, filiform, extending to about middle of elytra; 3rd antennomere longest, about twice as long as scape; relative length of each antennomere compared with scape in the holotype as follows: 1st (1.0), 2nd (1.1), 3rd (1.9), 4th (1.7), 5th (1.6), 6th (1.4), 7th (1.2), 8th (1.2), 9th (1.0), 10th (1.0) and 11th (1.4).

Prothorax quadrate, as long as wide, widest behind middle; as long as head excluding mandibles, as wide as pronotum (Fig. 7A). Pronotum slightly wider than head, PnW/HW = 1.2, widest at about apical 1/4, lateral margins finely bordered throughout, suddenly narrowed before hind angles; base and front unbordered, the former narrower than the latter; anterior latero-marginal pores located at apical 1/5 and the posterior pores in front of hind angles. Scutellum small.

Elytra (Fig. 6, 3E) stout, longer than wide, EL/EW = 1.6, wider than pronotum, EW/PW = 2.1, and much longer than fore body including mandibles; lateral margins ciliate throughout; disc strongly convex, striae shallow, easily traceable though more or less reduced, intervals flat; anterior and posterior dorsal pores of the 3rd striae at about basal 1/6 and middle of elytra, respectively, preapical pore at about apical 1/7 of elytra, much closer to elytral suture than to apical margin; only an apical pore present, the anguloapical pore absent.

Legs moderately long and densely pubescent; fore and middle tibiae longitudinally grooved externally, whereas simple in hind tibiae; the 1st and 2nd protarsomeres dilated and spurred inwards at apex in male.

Ventrites IV–VI, each with a pair of paramedial setae, ventrite VII bisetose in male. Male genitalia (Fig. 7C, D): median lobe of aedeagus well-sclerotised, long, and elongate, slightly arcuate at median portion, gradually narrowed toward apex which is bluntly obtuse; basal opening large, with a large sagittal aileron; inner sac provided with a thick and long copulatory piece which is about 2/9 as long as aedeagus; in dorsal view, apical lobe longer than wide, gradually narrowed toward apex which is broadly rounded; parameres well developed, shorter than median lobe, each armed with 4 and 5 long setae at apex.

Female. unknown.

Remarks. The genus *Qianotrechus* Uéno, 2000 is comprised of three semi-aphaenosiian trechine species and one subspecies (Fig. 1): *Q. magnicollis* Uéno, 2000, *Q. tenuicollis tenuicollis* Uéno, 2000, and *Q. tenuicollis cheni* Uéno, 2003 from Suiyang County and *Q. laevis* Uéno, 2000 from Zheng'an County, Zunyi Shi, Guizhou Province (Uéno 2000, 2003). Another species, *Q. fani* Uéno, 2003, has been reported from Gulin County, Luzhou Shi, Sichuan Province, but it is not a *Qianotrechus* and so has been transferred into the genus *Uenoaphaenops* Tian & He, 2020 (Tian and He 2020).

Qianotrechus congcongae sp. nov. is closely similar to *Q. laevis* from Zheng'an County of northeastern Guizhou Province (Uéno 2000). The locality of the latter species (Mawan Dong) is about 30 km in a straight line from Shigao Dong in

Nanchuan, Chongqing. However, *Q. congcongae* is different from *Q. laevis* in having a stouter body (more elongated in *Q. laevis*), a broader prothorax with propleura widely visible from above (narrowly visible in *Q. laevis*) (Fig. 7A, B), and the pronotum evidently narrowed near the base, which is distinctly sinuate before posterior latero-marginal setae (only slightly sinuate in *Q. laevis*). In addition, the median lobe of the aedeagus is straight and widened at apex (slightly sinuate and narrowed in *Q. laevis*) (Fig. 7C–F).

Etymology. The name of this beautiful species is in honour of “Xiao Cong”, a nickname of Ms Jia Liu, an outstanding and leading caver in the Chongqing Cave Exploration Team, Chongqing, for her kind assistance in our collecting trips in Chongqing.

Distribution. China (Chongqing). Known only from the limestone cave in Shigao Dong, Nanchuan (Fig. 1). Shigao Dong is located about 0.5 km from Hexi Zhen (Nanchuan) in a straight line to the south. The cave, which is near a small road and just behind a farm house, has a large entrance (Fig. 8A). There is an underground river inside the cave. The main passage is about 100 m from the entrance. At first, we reached as far as 300 m along the right passage of the cave, which is huge, several dozen metres high and wide (Fig. 8B), but without any finding specimens. Later, we came back to the cave and went explored the left passage, where we observed two beetles running on the wet ground near a small pool, about 160 m from the cave’s entrance (Fig. 8C, E). Apart from *Qianotrechus congcongae* sp. nov., three species of millipedes, a dipluran, and a troglophilic frog (*Oreolalax rhodostigmatus* Hu & Fei, 1979) were also observed in this cave (Fig. 8D).

***Qianlongius* Tian & Jia, gen. nov.**

<http://zoobank.org/5A4CC615-25EA-4D8F-95E7-F6A6B6A12305/>

潜龙盲步甲属

Type species. *Qianlongius zhoui* Tian & Jia, sp. nov. (Qianlong Dong cave, Songtao, Guizhou).

Generic characteristics. Large for cavernicolous trechines, semi-aphaenopsian, but more or less pigmented; body stout, appendages moderate long; head and pronotum smooth and glabrous, elytra wholly pubescent; moderately shining. Head subquadrate, distinctly longer than wide excluding mandibles, nearly parallel-sided; frontal furrows sub-parallel-sided, 2 supra-orbital pores present; mandible thin and sharp at apices, right mandible tridentate; labial suture well-marked; mentum bisetose, slightly shallow at base; submentum with a row of 6 setae; palps thin and elongated, the 2nd labial palpomere without additional setae apart from the 2 setae on inner margin; antennae thin and long, extending almost to apices of elytra, scape as long as pedicel. Prothorax slightly tumid at sides and visible from above; prothorax longer than wide, slightly shorter than head excluding mandibles, widest at about basal 1/3; pronotum subquadrate, evidently longer than wide, wider than head, slightly narrower than prothorax; 2 pairs of latero-

marginal setae present, both front and hind angles broadly obtuse. Elytra stout, but longer than fore body including mandibles, slightly expanded at sides, widest a little before middle, strongly convex, partly concealed marginal gutter in middle; humeral angles widely rounded, lateral margins smooth, not ciliate, apices almost rounded; elytral striae obliterated though still traceable; 2 dorsal pores present on the 3rd stria, the preapical dorsal pores present; apical striole invisible; humeral group (the 1st–4th pores) of marginal umbilicate series not aggregated, 2nd, 3rd and 8th pores close to the marginal gutter, 1st pore inwardly and backwardly shifted, 4th pore widely isolated; median group (the 5th and 6th pores) backwardly shifted, close from each other. Protarsomeres not modified in male; the 1st tarsomere much shorter than 2nd to 4th tarsomeres combined in fore legs, whereas as long in middle and hind legs. Ventricle VII with 2 pairs of apical setae in male. Male genitalia short and thick, moderately sclerotized.

Remarks. The position of this new genus within the tribe Trechini remains unclear. However, *Qianlongius* gen. nov. is, on the first sight, more or less similar in body shape and colouration to *Guizhaphaenopsodes* Tian & X. Huang, 2020 (from Tangle Dong cave in Jishou, western Hunan), but these genera belong to different lineages on account of the following differences in important characteristics. First of all, *Qianlongius* is more aphaenopsian than *Guizhaphaenopsodes* due to its thinner body with a more elongated head, distinctly reduced frontal furrows, propleura tumid and visible from above, and thinner antennae reaching the elytral apices. Second, the right mandibular tooth is tridentate, and mentum and submentum are not fused in *Qianlongius*, versus bidentate right mandibular tooth, and completely fused mentum and submentum in *Guizhaphaenopsodes*. Third, the male protarsi of *Qianlongius* are simple, while the first protarsomere is modified in *Guizhaphaenopsodes*. Fourth, ventrite VII is 4-setose in the male of *Qianlongius*, instead of bisetose in *Guizhaphaenopsodes*. And fifth, the male genitalia are quite large and moderately elongated in *Qianlongius*, while small and very short in *Guizhaphaenopsodes*.

Etymology. Referring to Qianlong Dong cave, locality of the type species *Qianlongius zhoui* sp. nov. Gender masculine.

Generic range. China (Guizhou). Known only from cave Qianlong Dong (Fig. 1).

***Qianlongius zhoui* Tian & Jia, sp. nov.**

<http://zoobank.org/602A3633-B600-4BC4-B6FD-649C01F0CDE0>

周氏潜龙盲步甲

Figures 1, 3C, F, 9–12

Type material. Holotype male, cave Qianlong Dong, Qianlong, Wuluo, Songtao, Tongren, Guizhou Province, 28.16° N, 108.84°E, 908 m, 2021-IV-2, leg. Yi Zhao, Xinyang Jia and Mingyi Tian, in SCAU. Paratype: 1 male, *ibid*.

Diagnosis. A medium-sized, semi-aphaenopsian species, with a rather stout body though both head and pronotum longer than wide, head and pronotum dark brown,



Figure 9. *Qianlongius zhoui* gen. nov. and sp. nov., habitus, holotype male.

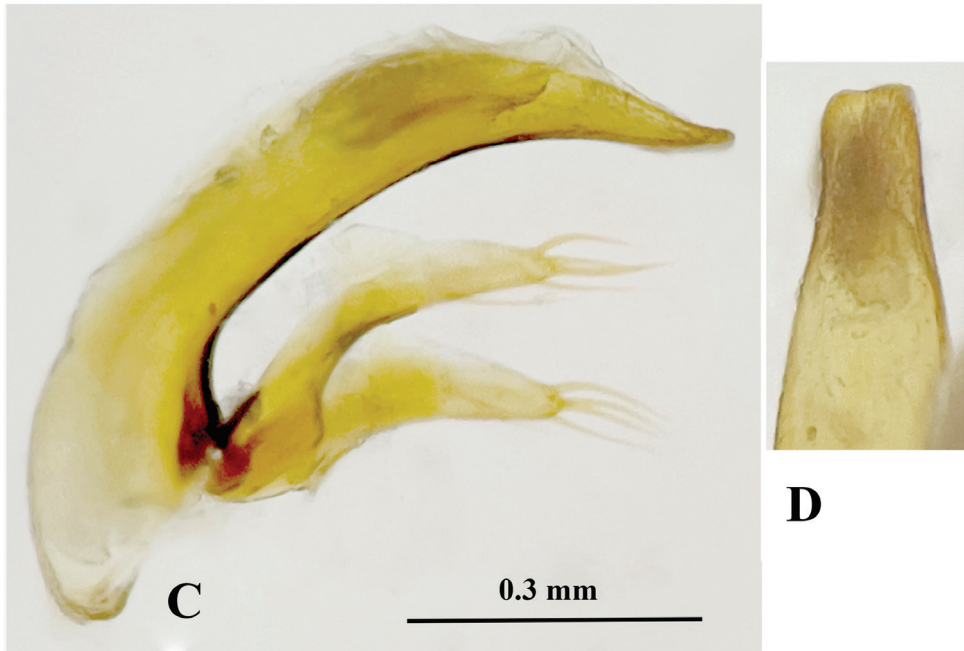


Figure 10. Male genitalia of *Xianlongius zhoui* gen. nov. and sp. nov. **A** median lobe and parameres, lateral view **B** apical lobe, dorsal view.

elytra reddish-brown, fore body including mandibles slightly shorter than elytra, antennae extending to apices of elytra, propleura visible from above.

Description. Length: 6.5–7.0 mm, width: 2.0–2.1 mm. Habitus as in Figure 9. Head, pronotum, undersides of head and thorax, ventrites, femora and tibiae dark brown, elytra, labrum and mandibles reddish-brown, palps, antennae and tarsi yellow. Head smooth, with a few short setae, 1 or 2 on dorsal surface, while 2 on genae; pronotum and elytra with short pubescence, prosternum bisetose; abdominal ventrites wholly pubescent. Microsculpture: isodiametric meshes on neck, transversal striate on frons, vertex, pronotum and elytra.

Head moderately elongate, longer than wide, $HLm/HW = 2.0\text{--}2.4$, $HLL/HW = 1.5\text{--}1.7$; nearly parallel-sided, widest at about middle of head excluding mandibles; frons and vertex convex; frontal furrows wide and incomplete, more or less parallel-sided, but slightly and shortly convergent backwards, ending about middle of head; anterior and posterior supraorbital pores located at about $4/7$ and $1/4$ of head from labrum to neck; clypeus 6-setose, labrum transverse, faintly bisinuate in the front margin, 6-setose; mandibles developed and moderately curved at apices; mentum tooth short but sharp at apex, bifid at tip, slightly shorter than the lateral lobes; ligula fused with paraglossae, 8-setose; palps thin and slender, the 2nd labial palpomere about 1.2 times as long as 3rd; 3rd maxillary palpomere 1.1 times as long as 4th; suborbital pores absent (Fig. 3C); antennae thin, filiform, pubescent from pedicle to 11th antennomeres, 3rd–5th antennomeres the longest, each almost twice as long as scape; relative length of

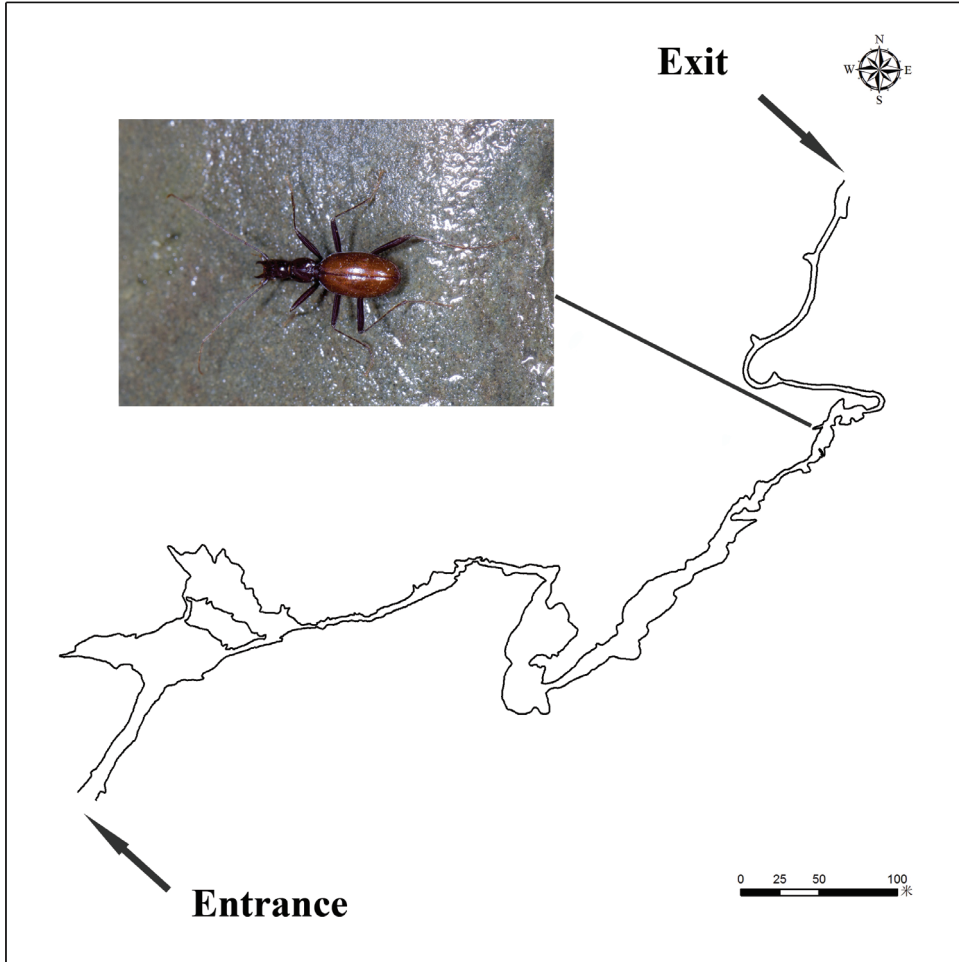


Figure 11. Map of Qianlong Dong, to show where the exemplars of *Qianlongius zhoui* gen. nov. and sp. nov. were discovered (map courtesy of Mr Wenlong Zhou).

each antennomere compared with scape in the holotype as follows: 1st (1.0), 2nd (1.1), 3rd (2.0), 4th (2.1), 5th (2.1), 6th (1.9), 7th (1.8), 8th (1.6), 9th (1.6), 10th (1.4) and 11th (1.6). Prothorax slightly longer than wide, PrL/PrW = 1.1–1.3; Pronotum longer than wide, PnL/PnW = 1.1–1.2; slightly narrower than prothorax, PrW/PnW = 1.0–1.1; wider than head, PnW/HW = 1.2, but shorter than head excluding mandibles, PnL/HLl = 0.9; widest at about apical 3/5, lateral margins gently expanded, narrowly and evenly bordered throughout, shortly reflexed near hind angles which are widely obtuse; base and front unbordered, almost straight, the former slightly narrower than the latter; anterior latero-marginal pores located at apical quarter and the posterior pores a little before hind angles; frontal and basal transverse impressions faint; middle line well marked; disc moderately convex. Scutellum small. Elytra (Fig. 3F) much longer than

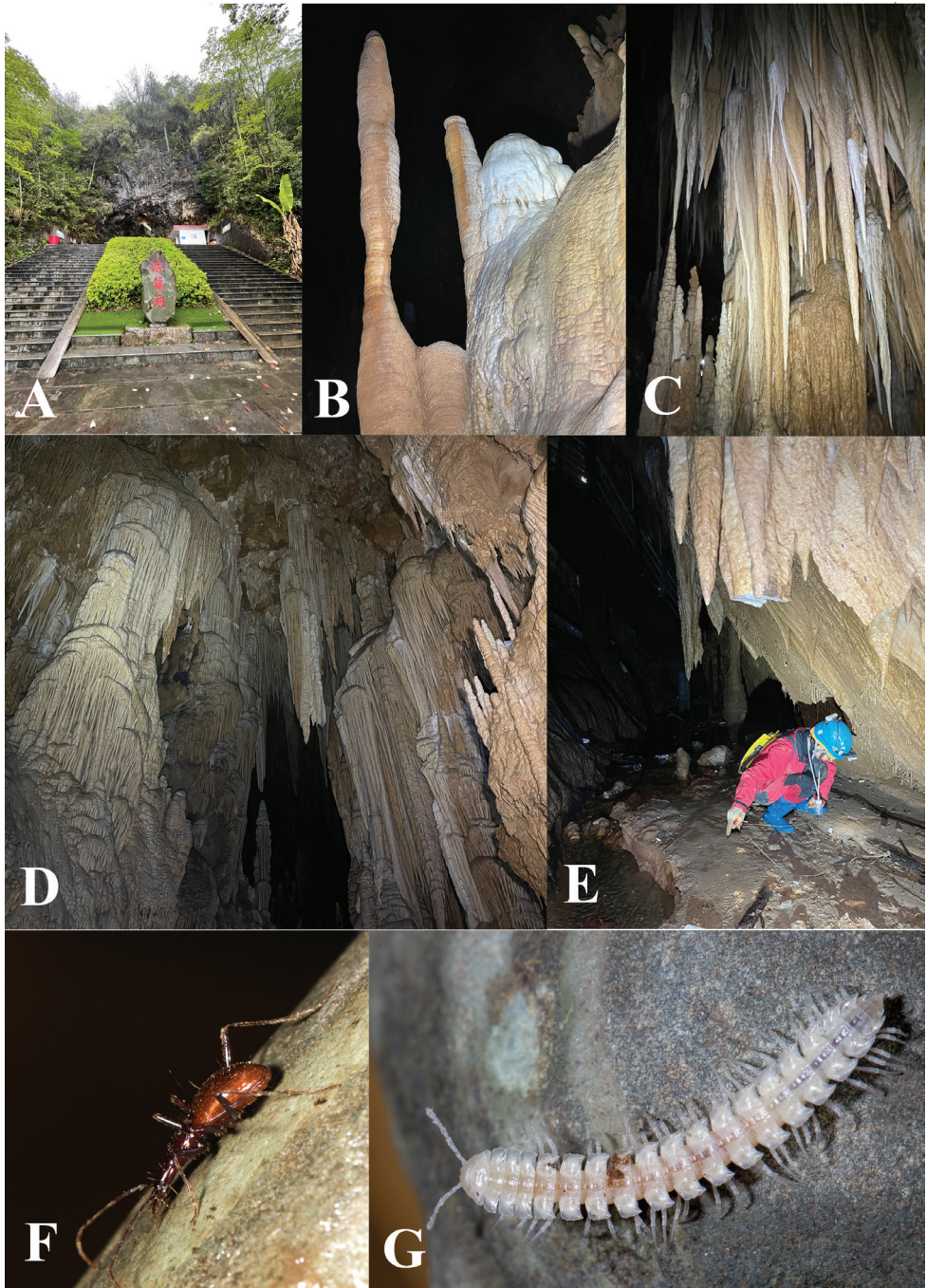


Figure 12. Cave Qianlong Dong **A** entrance **B–D** beautiful speleothems inside the cave **E** the locality of *Qianlongius zhoui* gen. nov. and sp. nov. **F** a running individual of *Q. zhoui* gen. nov. and sp. nov. **G** a millipede, *Epanerchodus* sp.

wide, $EL/EW = 1.9$, wider than pronotum, $EW/PW = 1.8-1.9$, and longer than fore body including mandibles $EL/(HLM+PnL) = 1.1$; unbordered at base; disc strongly convex, intervals flat; basal pore at side of scutellum, located against 3rd stria; anterior and posterior dorsal pores of the 3rd striae at about 1/3 and 2/3 of elytra from base, respectively; preapical pore at about apical 1/9 of elytra, closer to elytral suture than to apical margin; only an apical pore present; pore 7 distant from elytral marginal gutter.

Legs moderately long and densely pubescent; fore tibiae longitudinally grooved externally, whereas middle and hind tibiae simple.

Ventrites IV–VI each with a pair of paramedial setae. Ventrite VII with 2 setae in male.

Male genitalia (Fig. 10): median lobe of aedeagus rather short but stout, slightly arcuate at median portion, gradually narrowed toward apex, which is more or less reflexed; basal opening large, without a sagittal aileron; inner sac provided with a thick and long copulatory piece which is about 2/9 as long as aedeagus; in dorsal view, apical lobe longer than wide, apical margin broad, but emarginate at middle; parameres well developed and elongated, but much shorter than median lobe, each armed with 4 long setae at apex and another seta at subapex.

Female. unknown.

Etymology. In honour of Mr Wenlong Zhou, an active speleologist (Guizhou Institute of Mountainous Region Resources, Guiyang) to thank him for supporting our survey in Qianlong Dong.

Distribution. China (Hunan). Known only from limestone cave Qianlong Dong (Fig. 1).

Qianlong Dong is a show cave located at Qianlong village, Wuluo Zhen, Songtao Miao Autonomous County, northeastern Guizhou. This beautiful cave is 1481 m long and with many wonderful speleothems (Barbary et al. 2011) (Fig. 11, 12B–D). Some parts inside the cave have natural conditions, although almost the entire cave has been developed for touristic purposes. Both specimens of this new species were discovered in the innermost part of the cave along the creek, not far from the artificial exit tunnel; one beetle was running on the ground and the other was found under a stone (Fig. 12E, F). Other cave animals observed in Qianlong Dong were: a millipede (*Epanerchodus* sp.; Fig. 12G), springtails, crickets, and a harvestman.

Acknowledgements

First of all, we thank Prof. Yuanhai Zhang (Institute of Karst Geology, Chinese Academy of Geological Sciences, Guilin) and Ms Lin Duo (Head of the Administrative Committee of Wulong World Natural Heritage, Wulong) for their kind invitation to survey in Wulong. Our deep appreciations also extend to Mr Lixin Chen, “Wu Ya”, “Ye Gong”, “Ye Po”, and “La Pi” (Qilinger Cave Exploration Team, Nanning) and Ms Jia Liu (Chongqing Cave Exploration Team) for their assistance during our survey in Wulong, to Mr Tongwang Yang (Manager of Qianlong Dong Scenic Spot) for his help dur-

ing the investigation in Qianlong Dong, and Mr Wenlong Zhou (Guizhou Institute of Mountainous Region Resources, Guizhou Academy of Sciences, Guiyang) for providing the cave map of Qianlong Dong and an important literature. For the identification of other cave animals, we thank the following colleagues: Dr Guchun Zhou (Gannan Normal University, Ganzhou) for spiders, Dr Ziwei Yin (Shanghai Normal University, Shanghai) for ant-loving beetles, and Dr Weixin Liu (South China Agricultural University, Guangzhou) for millipedes. In particular, we thank Dr Arnaud Faille (Stuttgart State Museum of Natural History, Stuttgart) and Dr Igor A. Belousov (All-Russian Institute of Plant Protection, Podbelskogo) for their critical comments and suggestions which helped us improve the manuscript. This study was sponsored by a project of the National Foundation of Natural Science of China (grant number 41871039).

References

- Barbary JP, Bottazzi J, Hugon B, Sanson E, Andrieu A, Dodelin C, Li P (2011) Contribution à la connaissance spéléologique du district de Songtao. *Spelunca Memoire* 35. *Voyages en Terre Chinoise* 3: 29–35.
- Tian MY, Huang SB, Wang XH, Tang MR (2016) Contributions to the knowledge of subterranean trechine beetles in southern China's karsts: five new genera (Insecta: Coleoptera: Carabidae: Trechini). *ZooKeys* 564: 121–156. <https://doi.org/10.3897/zookeys.564.6819>
- Tian MY, Huang XL, Li CL (2021) Contribution to the knowledge of subterranean ground beetles from eastern Wuling Mountains, China (Coleoptera: Carabidae: Trechinae). *Zootaxa* 4926(4): 521–534. <https://doi.org/10.11646/zootaxa.4926.4.3>
- Tian MY, He L (2020) A contribution to the knowledge of cavernicolous ground beetles from Sichuan Province, southwestern China (Coleoptera, Carabidae, Trechini, Platynini). *ZooKeys* 1008: 69–91. <https://doi.org/10.3897/zookeys.1008.61040>
- Uéno SI (2000) New cave trechines (Coleoptera, Trechinae) from northeastern Guizhou, South China. *Journal of the Speleological Society of Japan* 25: 1–38.
- Uéno SI (2003) Two new cave trechines of the genus *Qianotrechus* (Coleoptera, Trechinae). *Journal of the Speleological Society of Japan* 28: 1–11.

A new Colombian species of *Liodesus* diving beetles from the Páramo de Sumapaz (Coleoptera, Dytiscidae, Bidessini)

Michael Balke^{1,2}, Yoandri Suarez-Megna³, Rodulfo Ospina-Torres⁴,
Juan Simon Venegas⁴, Carlos Prieto^{5,6}, Lars Hendrich¹

1 SNSB-Zoologische Staatssammlung München, Münchhausenstraße 21, D-81247 Munich, Germany
2 GeoBioCenter, Ludwig Maximilians University, Munich, Germany **3** Departamento de Biología, Universidad de Oriente. Patricio Lumumba s/n, Santiago, Santiago de Cuba, Cuba **4** Departamento de Biología, Universidad Nacional de Colombia, Bogota, Colombia **5** Departamento de Biología, Universidad del Atlántico, Barranquilla, Colombia **6** Corporación Universitaria Autónoma del Cauca, Popayán, Colombia

Corresponding author: Michael Balke (balke.m@snsb.de)

Academic editor: Mariano Michat | Received 14 June 2021 | Accepted 27 July 2021 | Published 8 September 2021

<http://zoobank.org/94DF435F-9686-4B70-A041-1921F6A0F68F>

Citation: Balke M, Suarez-Megna Y, Ospina-Torres R, Venegas JS, Prieto C, Hendrich L (2021) A new Colombian species of *Liodesus* diving beetles from the Páramo de Sumapaz (Coleoptera, Dytiscidae, Bidessini). ZooKeys 1059: 79–87. <https://doi.org/10.3897/zookeys.1059.70134>

Abstract

Liodesus picinus sp. nov. is described from the Páramo de Sumapaz near Bogota D.C. at 3,500 m above sea level. The species can be distinguished from the other Colombian *Liodesus* species by its dark coloration, discontinuous habitus, shiny surface of the pronotum and elytron, presence of a distinct occipital line, distinct basal pronotal striae, short or even faint basal elytral striae, as well as by its distinct geographic distribution and cox1 signature.

Keywords

Colombia, Dytiscidae, *Liodesus*, new species, Páramo, Sumapaz

Introduction

Diving beetles of the genus *Liodesus* Guignot, 1939 belong to the tribe Bidessini and occur in the New World as well as the Afrotropical Region (Biström 1988; Nilsson and Hájek 2021). They are typically smaller than 3 mm and inhabit a variety of mainly

lotic habitats. Andean species reach altitudes of nearly 5,000 m, where they are the most abundant aquatic beetles (Balke et al. 2020a, 2020b).

However, diving beetles from the high altitudes of the Puna and Páramo regions remain poorly studied. Since 2019, as the result of a research and training cooperation between our institutions, 10 new species were described from these regions of Peru (Balke et al. 2019, 2020b) and Colombia (Megna et al. 2019; Balke et al. 2021). It became apparent that many more new species of *Liodesus* remain to be discovered in the vast Andean highland ecosystems, most of them likely endemic to one or a few Páramo or Puna areas, respectively. To address this in a combined evidence pipeline, we suggested a DNA sequence-based platform for the study of these insects (Balke et al. 2020a, 2020b) using the Barcode of Life Data System (BOLD) of the Canadian Centre for DNA Barcoding and the 5' mitochondrial *cox1* gene fragment (<http://www.boldsystems.org>) (Ratnasingham and Hebert 2007).

It is well understood that one genetic marker alone cannot be the omnipotent tool for taxonomy, in particular markers such as *cox1*, which are not involved in speciation *per se* (Kwong et al. 2012). Rather, such DNA sequence data have the purpose of guiding the sorting of specimens to operational units and then flank taxonomic decision-making process. This approach has been utilized successfully to study very diverse beetle taxa (Tänzler et al. 2012; Riedel et al. 2013a, 2013b), including our own previous work on *Liodesus*. The approach can technically be scaled up massively using next generation sequencing technology, which is already also reducing analytical costs (Wang et al. 2018). This does, however, and that is important to note, not replace taxonomic expertise and the evaluation of morphological structures (Riedel et al. 2013a). Here, we report the discovery of another new species of *Liodesus* from Páramo de Sumapaz (Fig. 3A), the world's largest Páramo system, near Bogota, Colombia. Interestingly, while we sampled more than 100 specimens of *Liodesus bogotensis* Guignot, 1953, we only found three females of the new species.

Materials and methods

Acronyms

- LIAUN** Laboratorio de Insectos Acuáticos, Departamento de Biología, Universidad Nacional de Colombia, Bogota, Colombia;
- ZSM** SNSB-Zoologische Staatssammlung, München, Germany; temporarily stored for further morphological work.

Morphological descriptions and photography

The description of morphological characters follows our previous work on *Liodesus* beetles (e.g. Balke et al. 2020b).

Images were taken with a Canon EOS R camera. We used a Mitutoyo 10× ELWD Plan Apo objective, attached to a Carl Zeiss Jena Sonnar 3.5/135 MC as focus lens. Illumination was with three LED segments SN-1 from Stonemaster (<https://www.stonemaster-onlineshop.de>). Image stacks were generated using the Stackmaster macro rail (Stonemaster), and images were then assembled with the computer software Helicon Focus v. 4.77TM on an iMac with a Radeon Pro 5500 XT GPU.

DNA analysis

The DNA sequencing and data analysis laboratory protocol follows standard Canadian Centre for DNA Barcoding (CCDB) barcoding procedures (<https://ccdb.ca/>). We delivered tissue samples to CCDB, which were processed, and the barcode data uploaded to BOLD systems. We used a simple approach to calculate a neighbour-joining tree (p -distances) in Geneious software v. 11.0.4 in order to learn if newly added entries could be assigned to existing species groups or not. This approach has been proven helpful and strongly guiding the morphological descriptive process, not the least by enabling us to unambiguously identify the new species presented here in the absence of male specimens.

Results

Liodesus picinus sp. nov.

<http://zoobank.org/AD2344A0-BD40-47BB-B99D-6B20430DC8A1>

Figures 1, 2G, 3

Type locality. Sumapaz National Park, Bogota, Colombia.

Holotype. “Colombia, ♀; Bogota D.C., PN Sumapaz; 3,500 m; 13.xi.2018; 4.290°N; 74.207°W; Ospina, Venegas, Balke and Megna (COL_MB_2018_04) Voucher MB8416” (LIAUN).

Paratypes. 2 ♀♀, same data but voucher numbers MB8414, 8415 (ZSM).

Description of holotype. Habitus with distinct discontinuity between pronotum and elytra (Fig. 1A), pronotum widest before base (Fig. 1A, B). Total length of beetle 2.0 mm; length without head 1.8 mm; maximum width 0.9 mm.

Color. Very dark brown to blackish dorsally and ventrally, base of meso- and metatibia contrastingly of lighter color (Fig. 1A, B).

Surface sculpture. Head with few setiferous punctures in front of a distinct occipital line, distinct microreticulation present except on middle of head between the eyes (Fig. 1B); posteriorly of occipital line with distinct microreticulation and few punctures. Pronotum and elytron shiny, with moderately dense and coarse setiferous punctation; pronotum with few wrinkles laterally (Fig. 1B).

Structures. Head with distinct occipital line, with rounded clypeus. Antenna stout. Pronotum with distinct lateral bead and distinct, long and deep basal striae



Figure 1. *Liodesus picinus* sp. nov. **A** dorsal habitus **B** dorsal head, pronotum, and base of elytra. Scale bar: 2 mm.

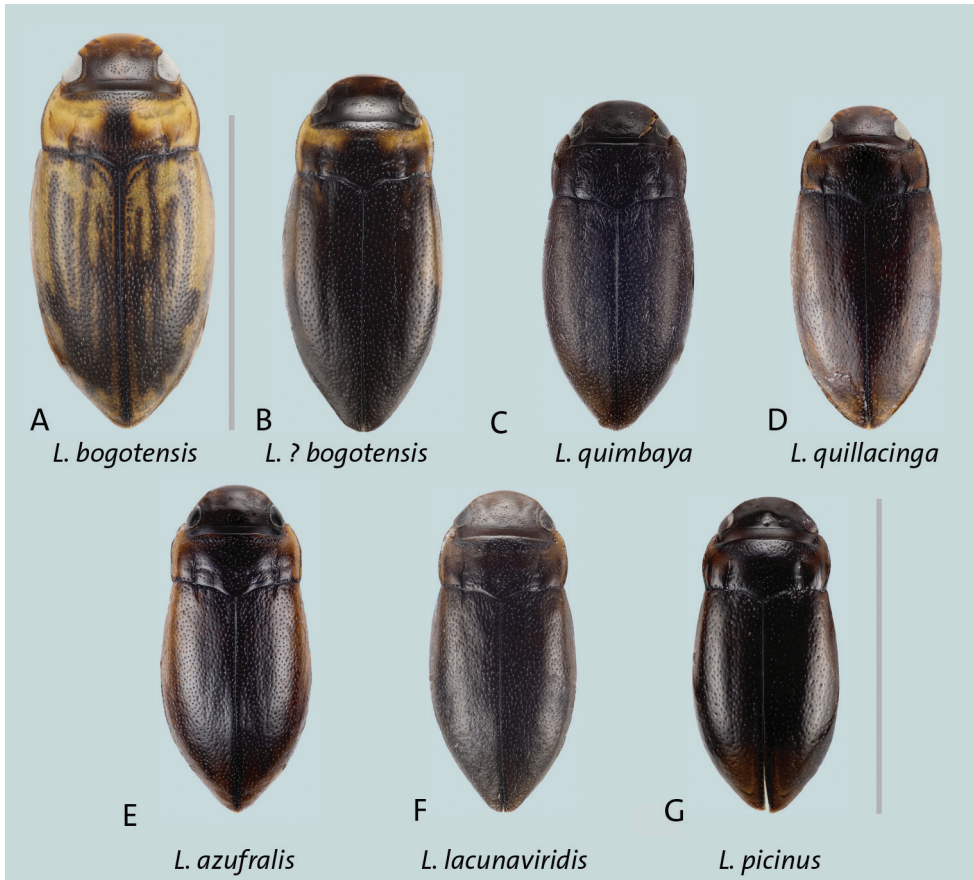


Figure 2. *Liodesus* spp. Dorsal habitus without appendages **A** *L. bogotensis* **B** *L. bogotensis* darker form from Sumapaz **C** *L. quimbaya* **D** *L. quillacinga* **E** *L. azufralis* **F** *L. lacunaviridis* **G** *L. picinus* sp. nov. Scale bars: 2 mm.

(Fig. 1A, B). Elytron with short basal striae, without sutural line and without basal epi-pleural transverse carina. Metathoracic wings not examined in holotype (in paratype: short, about half the length of elytron).

Variation. One paratype is slightly larger, TL 2.1 mm. In one paratype, the elytral basal striae are not very obvious.

Male. Unknown.

Etymology. *Picinus*, black, highlighting the dark coloration of the species.

Comparative notes. The species is well characterized by its small size (2.0–2.1 mm total length, shorter than most other Colombian Páramo species (Megna et al. 2019; Balke et al. 2021) except *L. lacunaviridis* (Balke et al. 2021)); dark coloration, discontinuous habitus, shiny surface of pronotum and elytrae, presence of distinct occipital line, distinct basal pronotal striae with short or even faint basal elytral striae.



Figure 3. Habitat of *Liodessus picinus* sp. nov. **A** Sumapaz National Park, general setting **B–D** collecting site with collecting tools.

We assembled sequences of the Colombian species, trimming the sequence ends to avoid missing characters. We obtained a 611 base pair reference alignment to observe sequence variation. *Liodessus picinus* sp. nov. differs by approx. 9–11% (5' *cox1*) from each of the other Colombian species and therefore forms a well-delineated clade with distinct mitochondrial *cox1* signature.

Distinguishing characters of the other Colombian Páramo species from the new species are:

Liodessus azufralis Megna et al., 2019: lighter coloration, brown to dark brown (Fig. 2E);

L. bogotensis: brighter coloration (Fig. 2A, B); *L. lacunaviridis* Balke et al., 2021 and *L. quimbaya* Megna et al., 2019: female with dull surface of pronotum and elytron due to presence of fine microreticulation (e.g. Fig. 2C, F); *L. quillacinga* Megna et al., 2019: long, distinct basal elytral stria (Fig. 2D).

Distribution. Only known from the type locality.

Habitat. Shallow and exposed peatland puddles, collected with strainer out of mats of vegetation including mosses (most likely *Sphagnum* sp.), *Ranunculus* sp. and *Azolla* sp. (Fig. 3B–D). The species is syntopic with *L. bogotensis*.

Checklist of the High Andean species of *Liodessus* Guignot, 1953

1. *Liodessus acollensis* Guignot, 1955: Peru
2. *Liodessus alpinus* Balke, Megna, Zenteno, Figueroa & Hendrich, 2020b: Peru
3. *Liodessus altoperuensis* Balke, Megna, Zenteno, Figueroa & Hendrich, 2020a: Peru
4. *Liodessus andinus* Guignot, 1957: Bolivia
5. *Liodessus azufralis* Megna, Hendrich & Balke, 2019: Colombia
6. *Liodessus bogotensis* Guignot, 1953: Colombia
7. *Liodessus caxamarca* Balke, Megna, Zenteno, Figueroa & Hendrich, 2020a: Peru
8. *Liodessus hauthi* Balke, Megna, Zenteno, Figueroa & Hendrich, 2020b: Peru
9. *Liodessus lacunaviridis* Balke, Ospina-Torres, Megna & Hendrich, 2020a: Colombia
10. *Liodessus picinus* sp. nov.: Colombia
- 11a. *Liodessus quillacinga quillacinga* Megna, Hendrich & Balke, 2019: Colombia
- 11b. *Liodessus quillacinga cochaensis* Megna, Hendrich & Balke, 2019: Colombia
- 11c. *Liodessus quillacinga cumbalis* Megna, Hendrich & Balke, 2019: Colombia
12. *Liodessus quimbaya* Megna, Hendrich & Balke, 2019: Colombia
13. *Liodessus rhigos* Balke, Megna, Zenteno, Figueroa & Hendrich, 2020b: Peru
14. *Liodessus thespesios* Balke, Megna, Zenteno, Figueroa & Hendrich, 2020b: Peru

Acknowledgements

This work was made possible by a grant from the Alexander von Humboldt foundation under the Research Group Linkage Programme, Evolution of the high Andean insect fauna project. We are grateful for the generous support from the SNSB-Innovative

scheme, funded by the Bayerisches Staatsministerium für Wissenschaft und Kunst (Project: “Geographische Isolation, Endemismus und Artbildungsprozesse bei Insekten in der hochmontanen Páramo Kolumbiens (und darüber hinaus)”). Michael Balke acknowledges support from the EU SYNTHESYS program, projects FR-TAF 6972 and GB-TAF-6776, which supported this research during visits to Natural History Museum in London and Muséum national d’Histoire naturelle in Paris in 2017. We thank the Agencia Nacional de Licencias Ambientales (ANLA) for issuing collecting and export permits. We thank Dr Simon Pflanzelt (Botanischer Garten München-Nymphenburg) for identifying the plant genera depicted in Figure 3C and D.

Consortium of European Taxonomic Facilities (CETAF) data use statement: “Data on genetic material contained in this taxonomic article are published for non-commercial use only. Utilization by third parties for purposes other than non-commercial scientific research may infringe the conditions under which the genetic resources were originally accessed, and should not be undertaken without obtaining consent from the original provider of the genetic material.”

References

- Balke M, Megna YS, Zenteno N, Figueroa L, Hendrich L (2020a) New *Liodes* species from the high Andes of Peru (Coleoptera: Dytiscidae, Bidessini). *Zootaxa* 4852: 151–165. <https://doi.org/10.11646/zootaxa.4852.2.1>
- Balke M, Megna YS, Zenteno N, Figueroa L, Hendrich L (2020b) Two new species of *Liodes* Guignot, 1939 diving beetles from Northern Peru (Coleoptera, Dytiscidae, Hydrophorinae). *Alpine Entomology* 4: 173–178. <https://doi.org/10.3897/alpento.4.55139>
- Balke M, Ospina-Torres R, Suarez-Megna Y, Hendrich L (2021) *Liodes lacunaviridis* sp. n. from the high Andes of Colombia (Coleoptera: Dytiscidae: Hydrophorinae: Bidessini). *Tijdschrift voor Entomologie* 163 (2020): 7–11. <https://doi.org/10.1163/22119434-20192084>
- Balke M, Suarez-Megna Y, Hendrich L, Zenteno N, Figueroa L (2019) New records for the Peruvian high-altitude diving beetle *Rhantus blancasi* Guignot, 1955 (Coleoptera, Dytiscidae, Colymbetinae). *Check List* 15: 941–944. <https://doi.org/10.15560/15.5.941>
- Biström O (1988) Generic review of the Bidessini (Coleoptera, Dytiscidae). Contribution to the study of Dytiscidae 37. *Acta Zoologica Fennica*: 1–41.
- Kwong S, Srivathsan A, Vaidya G, Meier R (2012) Is the COI barcoding gene involved in speciation through intergenomic conflict? *Molecular Phylogenetics and Evolution* 62: 1009–1012. <https://doi.org/10.1016/j.ympev.2011.11.034>
- Megna YS, Hendrich L, García-Hernández AL, Ospina-Torres R, Prieto C, Balke M (2019) Diving beetles of the genus *Liodes* Guignot, 1953 in Colombia, with description of three new species (Coleoptera: Dytiscidae). *Aquatic Insects* 40: 99–122. <https://doi.org/10.1080/01650424.2018.1538521>

- Nilsson A, Hájek J (2021) A world catalogue of the family Dytiscidae, or the diving beetles (Coleoptera, Adephaga). Version 1. I. 2021, 315 pp. http://www.waterbeetles.eu/documents/W_CAT_Dytiscidae_2020.pdf
- Ratnasingham S, Hebert PD (2007) BOLD: the Barcode of Life Data System (<http://www.barcodinglife.org>). *Molecular Ecology Notes* 7: 355–364. <https://doi.org/10.1111/j.1471-8286.2007.01678.x>
- Riedel A, Sagata K, Suhardjono YR, Tänzler R, Balke M (2013a) Integrative taxonomy on the fast track-towards more sustainability in biodiversity research. *Frontiers in Zoology* 10: 1–9. <https://doi.org/10.1186/1742-9994-10-15>
- Riedel A, Sagata K, Surbakti S, Tänzler R, Balke M (2013b) One hundred and one new species of *Trigonopterus* weevils from New Guinea. *ZooKeys*: 1–150. <https://doi.org/10.3897/zookeys.280.3906>
- Tänzler R, Sagata K, Surbakti S, Balke M, Riedel A (2012) DNA barcoding for community ecology-how to tackle a hyperdiverse, mostly undescribed Melanesian fauna. *PLoS ONE* 7: 1–11. <https://doi.org/10.1371/journal.pone.0028832>
- Wang WY, Srivathsan A, Foo M, Yamane SK, Meier R (2018) Sorting specimen-rich invertebrate samples with cost-effective NGS barcodes: Validating a reverse workflow for specimen processing. *Molecular Ecology Resources* 18: 490–501. <https://doi.org/10.1111/1755-0998.12751>

Two new species of *Dugesia* (Platyhelminthes, Tricladida, DugesIIDae) from the tropical monsoon forest in southern China

Lei Wang^{1,3}, Jin-zi Chen¹, Zi-mei Dong¹,
Guang-wen Chen¹, Ronald Sluys², De-zeng Liu¹

1 College of Life Science, Henan Normal University, Xinxiang, 453007 Henan, China **2** Naturalis Biodiversity Center, Leiden, The Netherlands **3** Medical College, Xinxiang University, Xinxiang 453003, China

Corresponding authors: Guang-wen Chen (chengw0183@sina.com); Zi-mei Dong (dzmhxx@163.com)

Academic editor: Tom Artois | Received 8 March 2021 | Accepted 17 June 2021 | Published 8 September 2021

<http://zoobank.org/731F8C31-26B3-4F81-8FE8-3595E360BC58>

Citation: Wang L, Chen J, Dong Z, Chen G, Sluys R, Liu D (2021) Two new species of *Dugesia* (Platyhelminthes, Tricladida, DugesIIDae) from the tropical monsoon forest in southern China. ZooKeys 1059: 89–116. <https://doi.org/10.3897/zookeys.1059.65633>

Abstract

Two new species of the genus *Dugesia* (Platyhelminthes, Tricladida, DugesIIDae) from the tropical monsoon forest in southern China are described on the basis of an integrative taxonomic study involving morphology, karyology, histology, and molecular analyses. The new species *Dugesia circumcisa* Chen & Dong, **sp. nov.** is characterised by asymmetrical openings of the oviducts; right vas deferens opening at anterior portion of the seminal vesicle and the left one opening at mid-lateral portion of the seminal vesicle; two diaphragms in ejaculatory duct, the latter being ventrally displaced and opening at the tip of the penis papilla, which is provided with a nozzle; wide duct connecting male atrium and common atrium; chromosome complement triploid with 24 metacentric chromosomes. The other new species, *Dugesia verrucula* Chen & Dong, **sp. nov.**, is characterised by the large size of the living worm, usually exceeding 3.5 cm in length; asymmetrical openings of the oviducts; subterminal opening of ventrally displaced ejaculatory duct; vasa deferentia symmetrically opening into the postero-lateral portion of the seminal vesicle; well-developed duct between the seminal vesicle and diaphragm; single dorsal bump near the root of the penis papilla; bursal canal with pleated wall and spacious posterior section; unstalked cocoons; chromosome complement diploid with 16 metacentric chromosomes. Inter-specific molecular distances and their positions in the phylogenetic tree reveal that *D. circumcisa* and *D. verrucula* are clearly separated from their congeners.

Keywords

Genetic distance, karyology, molecular phylogeny, monsoon forest, new species, taxonomy

Introduction

Approximately 96 species of the freshwater planarian genus *Dugesia* Girard, 1850 are distributed in a major portion of the Old World and Australia (Sluys and Riutort 2018; Song et al. 2020), with only five species being known from China, viz., *Dugesia japonica* Ichikawa & Kawakatsu, 1964, *D. sinensis* Chen & Wang, 2015, *D. umbonata* Song & Wang, 2020, *D. semiglobosa* Chen & Dong, 2021, and *D. majuscula* Chen & Dong, 2021 (Kawakatsu et al. 1976; Chen et al. 2015; Song et al. 2020; Wang et al. 2021). Only three of these species were recorded from mainland China, since *D. semiglobosa* and *D. majuscula* are known only from Hainan Island. An interesting and equally tropical mainland region is located immediately north of Hainan Island, viz., the Guangxi Province. This part of southern China has a tropical monsoon climate and is occupied by characteristic biota, such as the Wengan Biota and Chengjiang Biota (Yuan and Zhou 1999; Hou et al. 2004). The Guangxi Province is adjacent to the Indo-Chinese peninsula and thus forms a biotic link between Southern China and mainland Southeast Asia. In this paper, we describe for the first time two new species of *Dugesia* from the tropical monsoon forest in this part of China on the basis of morphological, histological, karyological, and molecular data.

Materials and methods

Specimen collection and culturing

On 1 January 2019, the specimens were collected in the Shiwan Dashan Mountain National Natural Reserve in Guangxi Province, where some animals were collected from under stones in a freshwater stream, while others were collected from under stones in a pond under a waterfall (for sampling localities, see Fig. 1). After collection, the worms were transferred to plastic bottles filled with spring water that during transportation to the laboratory were placed in a cooler filled with an ice bag. The planarians were cultured in autoclaved tap water at 16 °C and fed with fresh beef liver once per week. The worms were starved for at least one week before being used for karyotype and histological studies and DNA extraction. Images of their external morphology were obtained by using a digital camera attached to a stereo-microscope.

DNA extraction, amplification, sequencing, and phylogenetic analysis

Total genomic DNA was extracted from specimens by using the QIAamp DNA Mini Tissue Kit (Qiagen, Germany), according to the manufacturer's protocols. The primers BarS and COIR were used for amplification of fragments of the Cytochrome c oxidase subunit I (COI) (Lázaro et al. 2009; Álvarez-Presas et al. 2011). For amplification of internal transcribed spacer-1 (ITS-1), the primers 9F and ITSr were used (Baguña et al. 1999). Premix Ex Taq Hot Start Version (TaKaRa, Otsu Japan) was used for the

polymerase chain reaction (PCR). Amplifications were conducted in a final volume of 30 μ L under the following conditions: 5 min at 94 °C, 35 cycles of 40 s at 94 °C, an annealing step for 30 s, and 1 min at 72 °C, and 5 min at 72 °C as a final extension. The annealing temperatures were 43 °C and 45 °C, respectively, and according to those specified by Stocchino et al. (2017). Purification of PCR products and sequencing were done by GENEWIZ (Tianjin, China). Sequencing reactions were performed with the same primers used to amplify the fragments. All specimens were sequenced for both forward and reverse DNA strands. Chromatograms were visually checked. In both two new species, four specimens were used to extract DNA, from which COI and ITS-1 were amplified.

In order to determine whether the presumed new species are molecularly different from other species of *Dugesia*, we performed a phylogenetic analysis and calculated genetic distances. The ingroup included the two new species, as well as 28 other *Dugesia* species from major portions of the geographic range of the genus. *Schmidtea mediterranea* (Benazzi et al., 1975) was chosen as the outgroup taxon (for GenBank accession numbers, see Table 1).

Nuclear ribosomal markers were aligned online with MAFFT (Online Version 7.247) using the G-INS-i algorithm (Kato and Standley 2013), and were

Table 1. GenBank accession numbers of COI and ITS-1 sequences used for molecular analyses.

Species	GenBank	
	CO I	ITS-1
<i>D. aethiopica</i>	KY498845	KY498785
<i>D. afromontana</i>	KY498846	KY498786
<i>D. ariadnae</i>	KC006972	KC007048
<i>D. arcadia</i>	KC006971	KC007044
<i>D. batuensis</i>	KF907818	KF907815
<i>D. benazzii</i>	FJ646977+FJ646933	FJ646890
<i>D. bengalensis</i>		FJ646897
<i>D. bifida</i>	KY498851	KY498791
<i>D. bijuga</i>	MH119630	
<i>D. circumcisa</i>	MZ147041	MZ146782
<i>D. cretica</i>	KC006976	KC007050
<i>D. deharvengi</i>	KF907820	KF907817
<i>D. elegans</i>	KC006984	KC007063
<i>D. gibberosa</i>	KY498857	KY498803
<i>D. hepta</i>	FJ646988+FJ646943	FJ646902
<i>D. japonica</i>	FJ646990	FJ646904
<i>D. majuscula</i>	MW533425	MW533591
<i>D. naiadis</i>	KF308756	
<i>D. notogaea</i>	FJ646993+FJ646945	FJ646908
<i>D. pustulata</i>	MH119631	
<i>D. ryukyuensis</i>	AF178311	FJ646910
<i>D. semiglobosa</i>	MW525210	MW526992
<i>D. sicula</i>	FJ646994 + FJ646947	DSU84356
<i>D. signoides</i>	KY498849	KY498789
<i>D. sinensis</i>	KP401592	
<i>D. subtentaculata</i>	FJ646995 +FJ646949	DSU84369
<i>D. umbonata</i>	MT176641	MT177211
<i>D. verrucula</i>	MZ147040	MZ146760
<i>S. mediterranea</i>	JF837062	AF047854

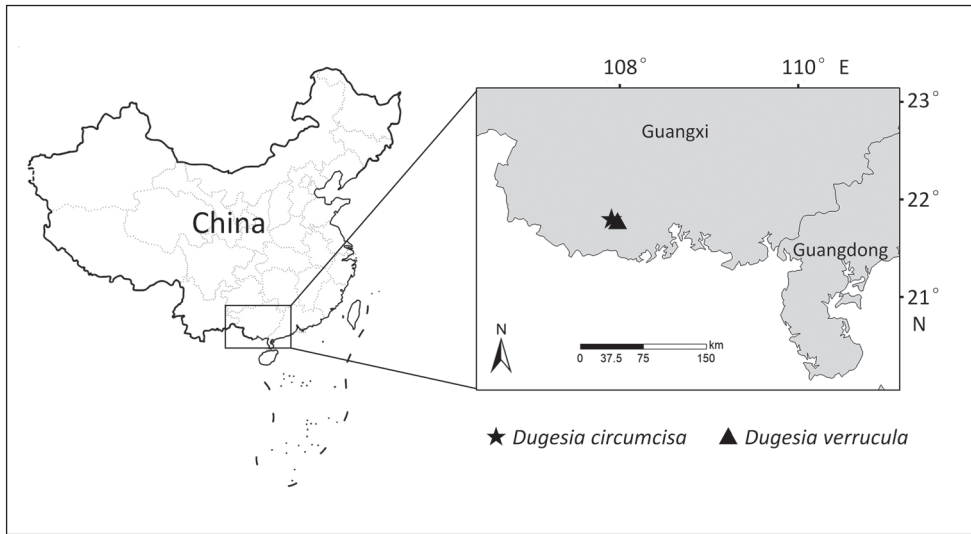


Figure 1. Collection sites of *Dugesia* in Guangxi Province.

checked by using BioEdit 7.2.6.1. For aligning the protein-coding COI sequences, the TranslatorX pipeline was used (<http://translatorx.co.uk>; Abascal et al. 2010). Nucleotide sequences were translated into amino acid sequences, with the help of NCBI's genetic codes table 9, followed by MAFFT (Online Version 7.247), using FFT-NS-2 progressive alignment method, checked by BioEdit 7.2.6.1, and then back-translated to nucleotide sequences. Since automated removal of gap columns and variable regions has been reported to negatively affect the accuracy of the inferred phylogeny (Dessimoz and Gil 2010; Tan et al. 2015), the Gblocks option (Talavera and Castresana 2007) was disabled. The concatenated sequences for the phylogenetic analysis were in the order ITS-1+ COI and consisted of a total of 1578 base pairs (bp), including 5.65% missing data. In the concatenated sequences, missing data were marked as “?”.

Mr Bayes v 3.2 (Ronquist et al. 2012) and RaxML 8.2.10 (Stamatakis 2014) were used to infer phylogenies with the Bayesian Inference (BI) and Maximum-likelihood (ML) method, respectively. BI was run for 3 million generations, while 25% burn-in was used under the GTR+I+G model. For the ML analysis, we performed 10,000 replicates under the GTR+I+G model. BI and ML trees were visualised and edited using Figtree v1.4.3.

The genetic distances of COI and ITS-1 were calculated by MEGA 6.06 (Tamura et al. 2013) with the Kimura 2-parameter substitution model (Lázaro et al. 2009; Solà et al. 2013).

Histology and karyology

Histological sections were prepared as described previously by Dong et al. (2017). In brief, worms were killed and thereafter fixed in Bouin's fluid for 24 h, and,

subsequently, rinsed and stored in 70% ethanol. For histological study, specimens were dehydrated in an ascending series of ethanol solutions, after which they were cleared in xylene and embedded in synthetic paraffin. Serial sections were made at intervals of 6 μm and were stained with haematoxylin-eosin. Photomicrographs were taken with a Leica digital camera attached to a compound microscope. Histological preparations of specimens have been deposited in the Zoological Museum of the College of Life Science of Henan Normal University (ZMHNU), Xinxiang, China, and Naturalis Biodiversity Center, Leiden, The Netherlands (RMNH).

Karyological preparations were obtained by air-drying, following methods described by Dong et al. (2017). In brief, worms were cut transversally into three pieces, which were cultured in distilled water for three days. Regenerative blastemas were treated with a 0.02% colchicine solution at 13 °C for 2.5–3.5 h and then placed in 0.1% KCl hypotonic solution at 16 °C for approximately 2.0–3.5 h. Hereafter, the blastemas were washed with deionised water and then fixed on a slide for ca. 30 s in each of the following solutions: fixative fluid I (glacial acetic acid: absolute alcohol: deionised water in the ratio of 3:3:4), fixative fluid II (glacial acetic acid: absolute alcohol in the ratio of 1:1) and fixative fluid III (glacial acetic acid). Subsequently, the dispersed cells were dried at room temperature for 24 h, and stained with a 0.5% Giemsa solution for 12–15 min. The mitotic metaphase chromosomes were observed and photographed under a compound microscope equipped with a digital camera. Well-spread sets of metaphase plates from five or six randomly selected individuals were used for karyotype analysis; karyotype parameter measurements were carried out as described previously by Chen et al. (2008). Chromosomal nomenclature follows Levan et al. (1964).

Results

Molecular phylogeny and genetic distances

The concatenated sequences included 846 base pairs (bp) for COI and 732 bp for ITS-1. The populations of both *D. circumcisa* and *D. verrucula* showed no variation in either COI or ITS-1.

The phylogenetic trees obtained by BI and ML from the concatenated dataset showed similar topologies and supported nodes (Fig. 2; Suppl. material 1: Fig. S1). The new species *D. circumcisa* and *D. verrucula* occupy separate branches that are clearly differentiated from their congeners. Notably, *D. circumcisa* is part of a clade consisting of two other species, viz., *D. sinensis* and *D. semiglobosa*, while *D. verrucula* belongs to another clade that includes the species *D. majuscula* and *D. japonica*. These two clades form part of a group of Eastern Palearctic/Oriental/Australasian species that in total comprises four clades of which the interrelationships are unresolved, thus forming a polytomy (Fig. 2). This major clade of Eastern Palearctic/Oriental/Australasian species is molecularly well separated from its sister clade, composed of species from the Western Palearctic.

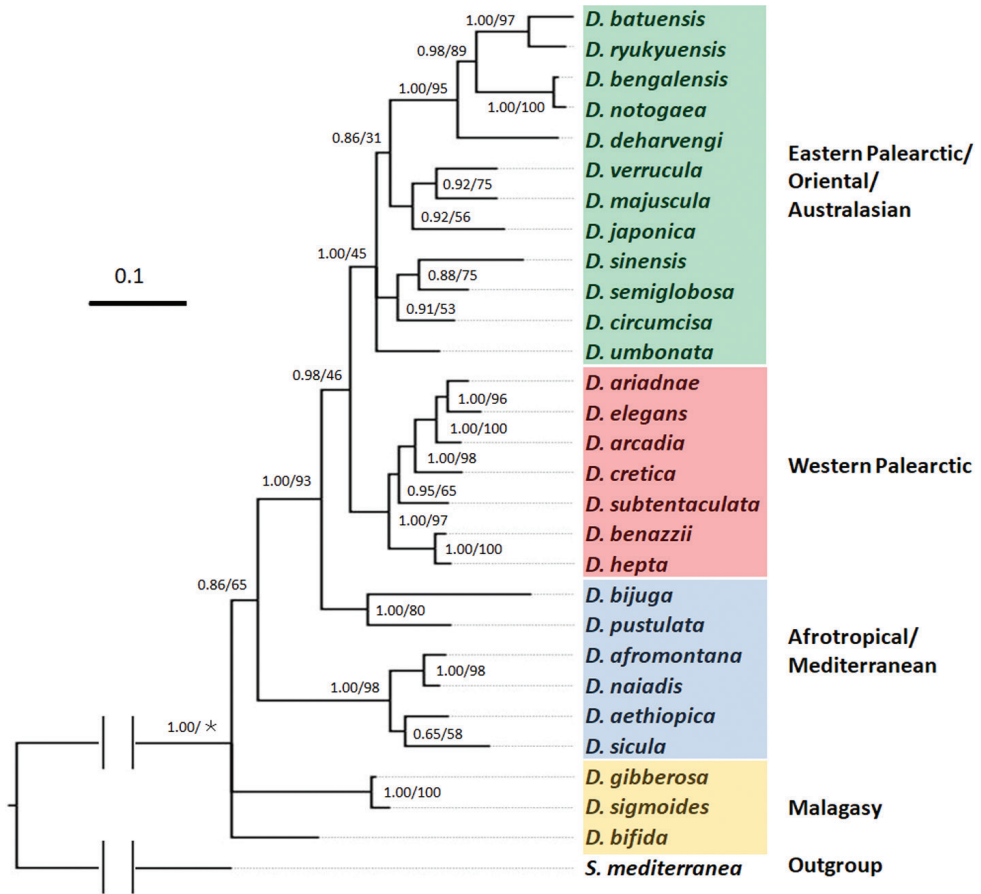


Figure 2. Phylogenetic tree obtained from Bayesian analysis of the concatenated dataset. Numbers at nodes indicate support values (pp/bs). *: Bootstrap value not applicable to the node, because of different topologies of trees obtained by BI and ML methods. Scale bar: substitutions per site.

The separate species status of *D. circumcisa* and *D. verrucula* is supported also by the genetic distances between the species included in our analysis, albeit that COI distances vary greatly among species (Suppl. material 2: Table S1).

The highest distance value between *D. circumcisa* and its congeners is 24.65% (with *D. batuensis* Ball, 1970 and *D. sicula* Lepori, 1948), while the lowest distance value is 11.20% (with *D. umbonata*). With respect to *D. verrucula*, the highest distance value between this species and its congeners is 26.09% (with *D. aethiopica* Stocchino et al., 2002), while the lowest distance value is 15.47% (with *D. umbonata*). Furthermore, there is a 17.15% difference between the two new species.

With respect to ITS-1, *D. circumcisa* and *D. verrucula* show highest distance values with *D. sicula*, which are 18.65% and 17.57%, respectively. Furthermore, their lowest distance values are with *D. majuscula*, which are 4.8% and 2.77%, respectively. For this marker, the molecular distance between the two new species is 4.98% (Suppl. material 3: Table S2).

Systematic account

Order Tricladida Lang, 1884

Suborder Continenticola Carranza, Littlewood, Clough, Ruiz-Trillo, Baguña & Riutort, 1998

Family DugesIIDae Ball, 1974

Genus *Dugesia* Girard, 1850

***Dugesia circumcisa* Chen & Dong, sp. nov.**

<http://zoobank.org/292AFA17-03F6-4153-BC1D-61F0212F207A>

Material examined. Holotype. ZMHNU-YWSZ2, Shiwan Dashan Mountain National Natural Reserve (21°54'34"N, 107°54'52"E), Shangsi County, Guangxi Province, China, alt. 245 m above sea level (a.s.l.), 1 January 2019, coll. G-W Chen, D-Z Dong and co-workers, sagittal sections on 14 slides. **Paratypes.** ZMHNU-YWSZ1, *ibid.*, sagittal sections on 28 slides; RMNH VER. 19974.a, *ibid.*, sagittal sections on 26 slides; ZMHNU-YWSZ5, *ibid.*, horizontal sections on 15 slides; ZMHNU-YWSZ6, *ibid.*, transverse sections on 30 slides; ZMHNU-YWSZ8, *ibid.*, sagittal sections on 19 slides; ZMHNU-YWSZ9, *ibid.*, sagittal sections on 15 slides; RMNH VER. 19974.b, *ibid.*, sagittal sections on 21 slides; ZMHNU-YWSZ11, *ibid.*, transverse sections on 60 slides; ZMHNU-YWSZ12, *ibid.*, horizontal sections on 19 slides.

Diagnosis. *Dugesia circumcisa* is characterised by the presence of the following features: right vas deferens opening at anterior portion of the seminal vesicle, and the left one opening at lateral portion of the vesicle, with the left sperm duct opening dorsally to the right one; two diaphragms in ejaculatory duct, the distal one receiving secretion of penial glands; ejaculatory duct with ventral course through penis papilla and with terminal opening; small nozzle at tip of penis papilla; wide duct connecting male and common atrium; asymmetrical openings of the oviducts into the bursal canal; chromosome complement triploid, with 24 metacentric chromosomes.

Etymology. The specific epithet is derived from the Latin adjective *circumcisis*, 'pruned of excess, sheared on all sides', and alludes to the appearance of the tip of the penis papilla.

Habitat and reproduction. Approximately 20 animals were collected from a freshwater stream on the Shiwan Dashan Mountain (Fig. 3A, B) at an altitude of 245 m a.s.l. (air temperature 8.6 °C, water temperature 12 °C). The Shiwan Dashan Mountain lies in the tropical monsoon forest, which forms a discontinuous system in tropical areas of Asia, Africa, and South America. The most typical tropical monsoon rainforests are distributed in Southeast Asia, with those of mainland China being located mainly near the Tropic of Cancer, thus including parts of the provinces of Hainan, Guangdong, Guangxi, Yunnan, and Tibet. Within this monsoon rainforest of mainland China, Shiwan Dashan Mountain forms its southernmost part. None of the animals was sexually mature at collection. During the first period of 150 days (Janu-

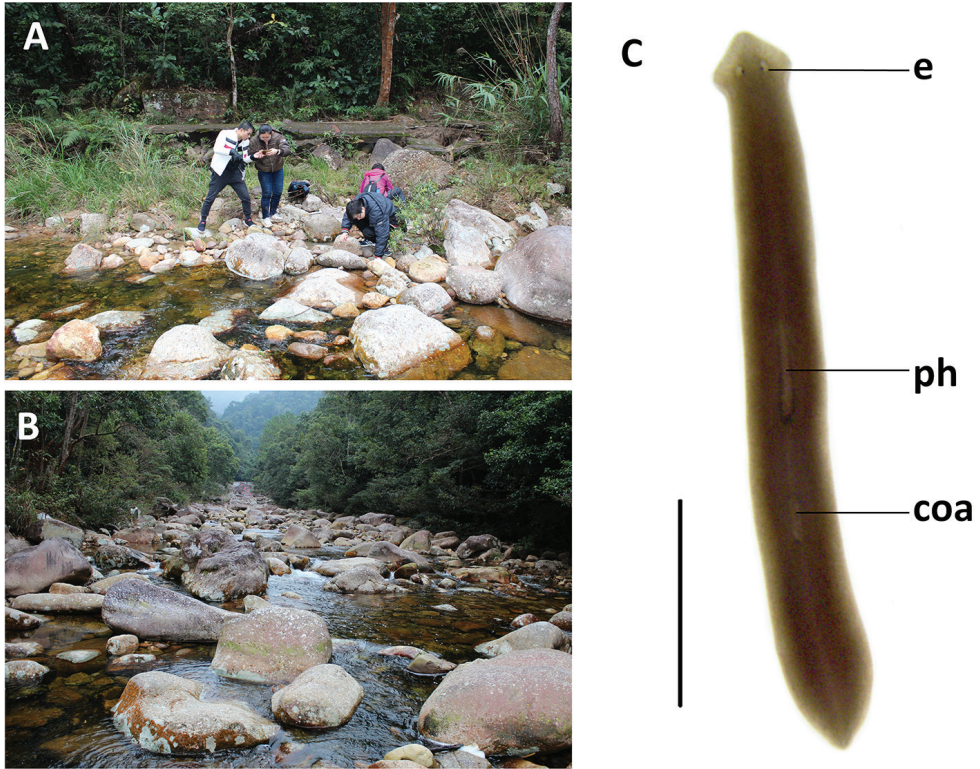


Figure 3. Habitat and external appearance of *Dugesia circumcisa* **A** sampling site **B** habitat **C** sexually mature, live individual. Abbreviations: coa: copulatory apparatus; e: eye; ph: pharynx. Scale bar: 5 mm.

ary to May) in the laboratory culture, the worms only showed asexual reproduction by means of fission. However, during the following days, seven individuals sexualised, while eventually 3/5 of the animals sexualised, although thus far they have not produced any cocoons.

Karyology. Each of the five, randomly selected specimens exhibited triploid chromosome complements. In a total of 100 metaphase plates examined, 86 chromosome complements were triploid with $2n = 3 \times = 24$ chromosomes, with all chromosomes being metacentric (Fig. 4); chromosome complements of the remaining 14 plates could not be determined, due to either lack of well-dispersed chromosomes or over-dispersed sets of chromosomes. Karyotype parameters, including relative length, arm ratio, and centromeric index, are given in Table 2. The first pair of chromosomes is clearly larger than the others, being 2.17 times larger than the shortest chromosome.

Description. In asexual living specimens, body 8–15 mm in length and 0.8–1.5 mm in width, while in sexualised specimens the body measures 15–22 mm in length and 1.5–2.3 mm in width. Head of low triangular shape and provided with two auricles, as well as two eyes located in pigment-free patches (Fig. 3C). Dorsal

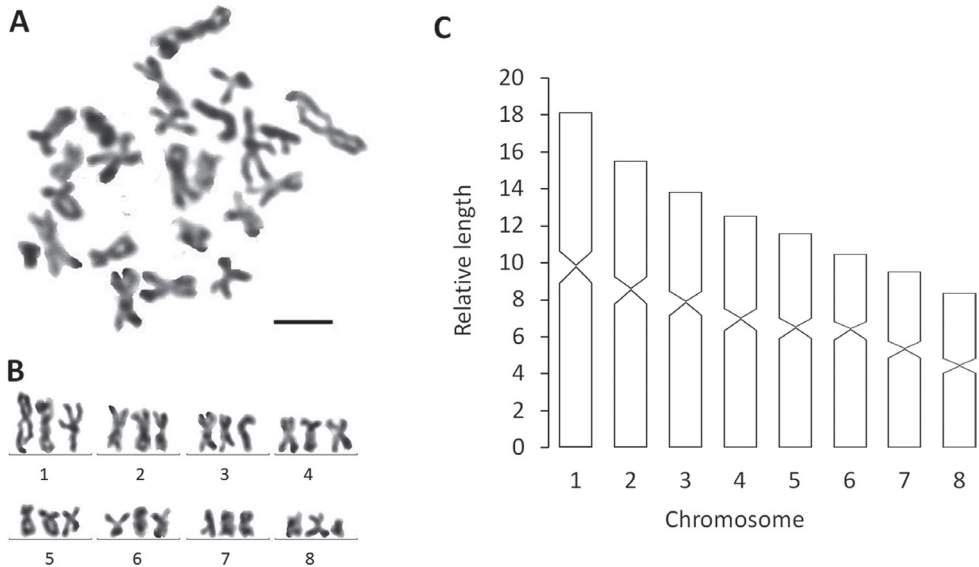


Figure 4. *Dugesia circumcisa* **A** metaphasic plate **B** karyogram **C** idiogram Scale bar: 5 μm .

Table 2. Karyotype parameters (mean values and standard deviations) of *Dugesia circumcisa*; m: metacentric.

Chromosome	Relative length	Arm ratio	Centromeric index	Chromosome type
1	18.15 \pm 0.86	1.18 \pm 0.12	46.13 \pm 2.38	m
2	15.53 \pm 0.95	1.23 \pm 0.13	45.08 \pm 2.44	m
3	13.83 \pm 0.15	1.34 \pm 0.12	43.01 \pm 2.26	m
4	12.53 \pm 0.44	1.25 \pm 0.11	44.64 \pm 2.09	m
5	11.59 \pm 0.52	1.29 \pm 0.09	44.10 \pm 1.67	m
6	10.48 \pm 0.14	1.60 \pm 0.28	39.22 \pm 4.07	m
7	9.55 \pm 0.20	1.28 \pm 0.16	44.19 \pm 2.99	m
8	8.35 \pm 0.43	1.15 \pm 0.12	46.73 \pm 2.39	m

surface dark brown, excepting pale body margin and a fuzzy, pale mid-dorsal stripe; accumulations of pigment follow the outline of the pharyngeal pocket. Ventral surface light brown.

Pharynx situated in the mid-region of the body, measuring ca. 1/5th of the body length (Fig. 3C); mouth opening located at the posterior end of the pharyngeal pocket. Outer pharyngeal musculature composed of a subepidermal layer of longitudinal muscles, followed by a layer of circular muscles (Fig. 5A). Inner pharyngeal musculature composed of a thick subepithelial layer of circular muscles, followed by a thin layer of longitudinal muscles (Fig. 5A).

The ventral ovaries are located at a short distance behind the brain and dorso-medially to the ventral nerve cords. The development of the ovaries differs greatly between specimens. In some animals the ovaries are rather small or even poorly developed (Fig. 5B), while in others the gonads are clearly hyperplastic (Fig. 5C, D). The oviducts arise from the dorsal surface of the ovaries and run dorsally to the

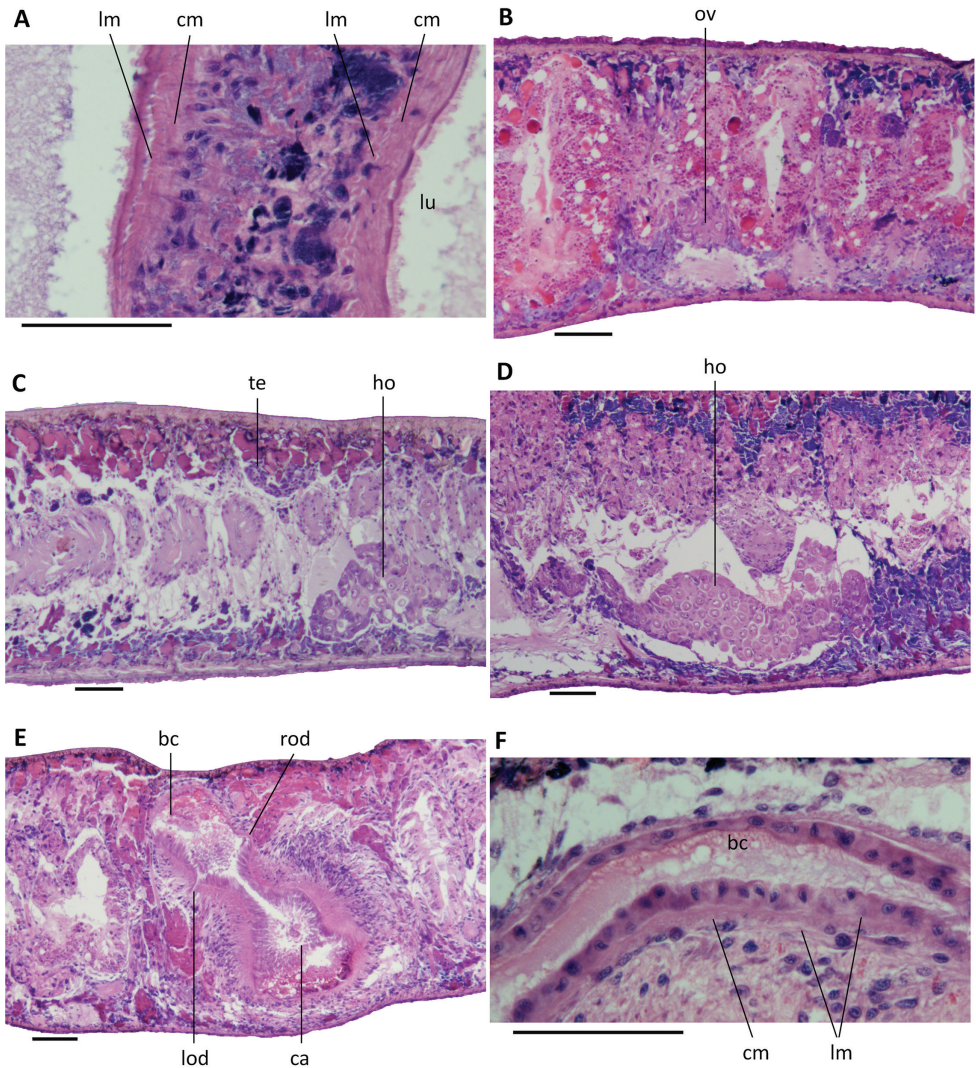


Figure 5. *Dugesia circumcisa* **A** transverse section of pharynx of paratype YWSZ11, showing musculature **B** sagittal section of paratype YWSZ8, showing poorly developed ovary **C** sagittal section of paratype YWSZ9, showing hyperplastic ovaries and poorly developed testes **D** sagittal section of paratype RMNH VER. 19974.a, showing hyperplastic ovaries **E** transverse section of paratype YWSZ11, showing openings of oviducts into bursal canal **F** sagittal section of holotype YWSZ2, showing musculature of bursal canal. Abbreviations: bc: bursal canal; ca: common atrium; cm: circular muscles; ho: hyperplastic ovaries; lm: longitudinal muscles; lod: left oviduct; lu: lumen; ov: ovary; rod: right oviduct; te: testis. Scale bars: 100 μ m.

ventral nerve cords in a caudal direction. At approximately the level of the gonopore, the oviducts curve dorsad to open separately and asymmetrically into the vaginal portion of the bursal canal, with the right oviduct opening dorsally to the left one (Figs 5E, 7, 8).

The large sac-shaped copulatory bursa, which occupies the entire dorso-ventral space, is lined by a vacuolated epithelium with basal nuclei and is almost devoid of any surrounding musculature (Figs 6A, 7, 8). From the postero-dorsal wall of the bursa, the rather narrow bursal canal runs in a caudal direction to the left side of the copulatory apparatus, after which it curves ventrally and opens into the common atrium (Figs 6A, 7, 8). The bursal canal is lined with columnar, nucleated, ciliated cells and surrounded by a thin subepithelial layer of longitudinal muscles, followed by a slightly thicker layer of circular muscle (Fig. 5F). An ectal reinforcement layer of longitudinal muscles runs from the vaginal region to ca. halfway along the bursal canal. Shell glands discharge their erythrophil secretion into the vaginal region of the bursal canal, near the oviducal openings.

The small, dorsally located testes are poorly developed and provided with immature spermatozoa (Fig. 5C). Testicular follicles are arranged on either side of the midline of the body in three or four longitudinal zones, extending from the posterior level of the ovaries to almost the posterior end of the body. Spermatozoa are absent also from the vasa deferentia, which upon reaching the level of the penis bulb curve dorso-medial and asymmetrically penetrate the wall of the penis bulb. The right sperm duct penetrates the antero-lateral wall of the penis bulb and opens into the anterior portion of the seminal vesicle (Figs 6B, D, 7, 8). The left sperm duct penetrates the lateral wall of the penis bulb and opens through the mid-lateral wall of the seminal vesicle (Figs 6C, 7). Furthermore, the left sperm duct opens dorsally to the right one. The sperm ducts are lined with nucleated cells and are surrounded by a layer of circular muscles.

The large and well-developed penis bulb occupies the major part of the dorso-ventral space and is composed of intermingled muscle fibres (Figs 6B–F, 7, 8). The penis bulb is asymmetrical in that a major portion expands dorsally to well beyond the midline of the body or even almost extends to the dorsal epidermis. This dorsal portion houses the oblate seminal vesicle, which is lined with a flat, nucleated epithelium. Via a valve-like diaphragm in its ventral wall, the seminal vesicle communicates with an expansion or vesicle in the proximal portion of the ejaculatory duct, which has a more or less vertical orientation. Subsequently, this expansion communicates via a large, blunt, valve-like diaphragm with a much larger expansion of the ejaculatory duct (Figs 6B, 7, 8), which is lined by a nucleated epithelium. The second diaphragm receives the openings of erythrophil penis glands, in contrast to the proximal, first diaphragm, which does not receive any secretion.

From the point of the large expansion, the ejaculatory duct changes its vertical orientation and starts to run more or less parallel to the body surface or attains an oblique, ventro-caudal orientation, thus basically conforming to the particular orientation of the penis papilla. The narrow section of the ejaculatory duct that runs between the large expansion and the tip of the penis papilla is lined by an infranucleated epithelium and follows a ventral course through the papilla, opening terminally at its tip (Figs 6F–H, 7, 8). In point of fact, the ejaculatory duct opens at a small nozzle located at the otherwise blunt tip of the penis papilla (Figs 6F, G, 7, 8). This nozzle can either be extended (Figs 6G, 8) or be withdrawn to greater or lesser extent (Fig. 6H).

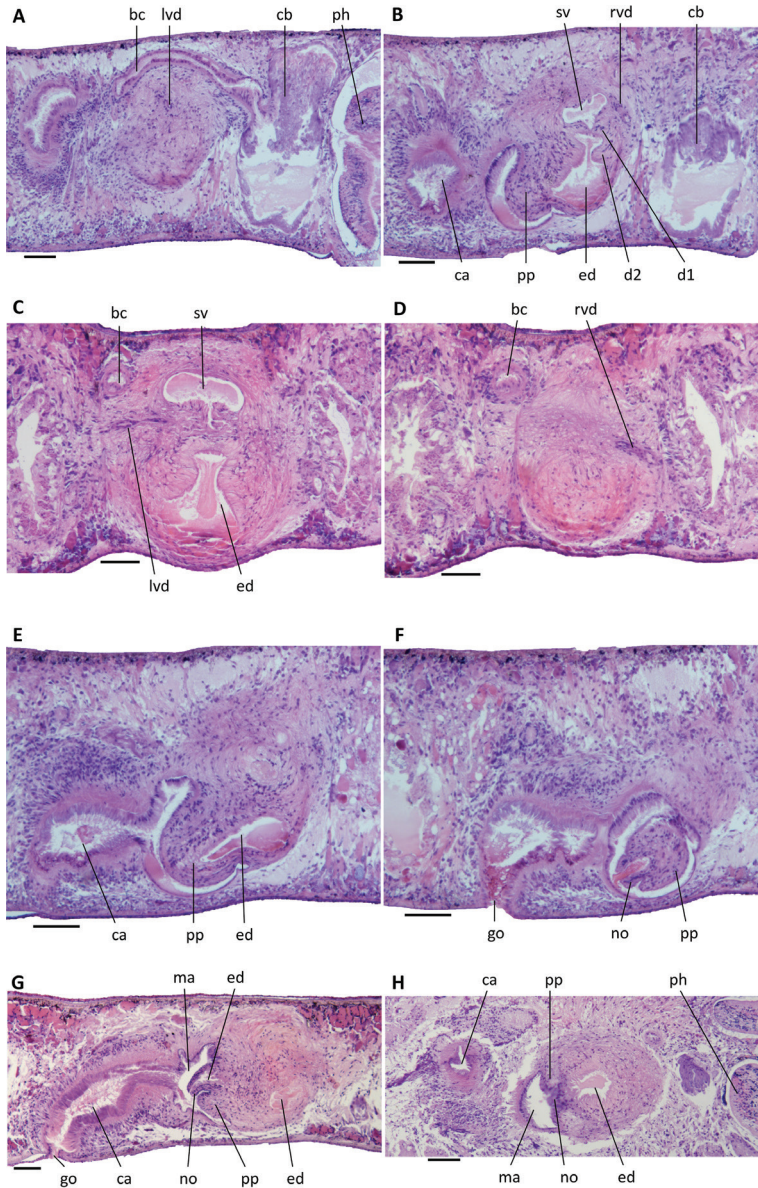


Figure 6. *Dugesia circumcisa* **A** sagittal section of holotype YWSZ2, showing bursal canal and copulatory bursa **B** sagittal section of holotype YWSZ2, showing opening of the right vas deferens into seminal vesicle, and two diaphragms **C** transverse section of paratype YWSZ11, showing left vas deferens, seminal vesicle, and ejaculatory duct **D** transverse section of paratype YWSZ11, showing right vas deferens **E** sagittal section of holotype YWSZ2, showing ejaculatory duct **F** sagittal section of holotype YWSZ2, showing small nozzle at tip of penis papilla **G** sagittal section of paratype YWSZ9, showing small nozzle at tip of penis papilla and the duct connecting male and common atrium **H** horizontal section of paratype YWSZ12, showing small nozzle at tip of penis papilla. Abbreviations: bc: bursal canal; ca: common atrium; cb: copulatory bursa; d: diaphragm; ed: ejaculatory duct; go: gonopore; lvd: left vas deferens; ma: male atrium; no: nozzle; ph: pharynx; pp: penis papilla; rvd: right vas deferens; sv: seminal vesicle. Scale bars: 100 μ m.

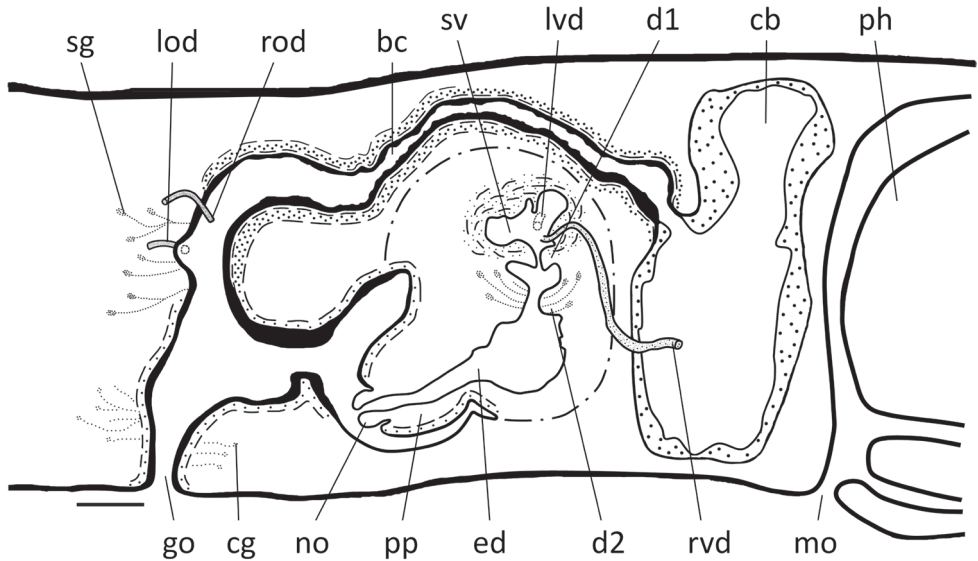


Figure 7. *Dugesia circumcisa* Sagittal reconstruction of the copulatory apparatus of holotype YWSZ2. Abbreviations: bc: bursal canal; cb: copulatory bursa; cg: cement glands; d1: first diaphragm; d2: second diaphragm; ed: ejaculatory duct; go: gonopore; lod: left oviduct; lvd: left vas deferens; mo: mouth; no: nozzle; ph: pharynx; pp: penis papilla; rod: right oviduct; rvd: right vas deferens; sg: shell glands; sv: seminal vesicle. Scale bar: 100 μ m.

The asymmetrical penis papilla is covered by an infranucleated epithelium, which is underlain by a subepithelial layer of circular muscle, followed by a layer of longitudinal muscle fibres. The penis papilla almost completely occupies the small male atrium, the latter communicating with the common atrium via a wide duct (Figs 6G, 7, 8). The common atrium opens to the exterior via a gonoduct, which is lined by a columnar epithelium and receives the openings of abundant cement glands.

Discussion. Generally, there is only one diaphragm present in the ejaculatory duct of species of *Dugesia*, and only a few species exhibit two diaphragms, such as *D. bijuga* Harrath & Sluys, 2019, *D. machadoi* de Beauchamp, 1952, *D. mirabilis* de Vries, 1988, *D. maghrebiana* Stocchino et al., 2009, *D. didiaphragma* de Vries, 1988, and *D. semiglobosa* (De Vries 1988; Stocchino et al. 2009; Harrath et al. 2019; Wang et al. 2020). However, in the three first-mentioned species, the ejaculatory duct runs a central course through the penis papilla, in contrast to the ventral trajectories in *D. semiglobosa*, *D. maghrebiana*, *D. didiaphragma*, and the new species *D. circumcisa*. The copulatory bursa of the latter lacks the complex stratified epithelium, which projects through an opening of the bursa that is present in *D. semiglobosa*, while it also lacks the large seminal vesicle enclosed by a highly muscularised, elongated penis bulb as present in *D. didiaphragma* and the knob-like extension on the penis papilla of *D. maghrebiana*.

In species with two diaphragms, the proximal diaphragm is usually small and basically formed by a non-glandular constriction of the seminal vesicle, while the true diaphragm is a larger structure that receives the secretion of penial glands, as is usual

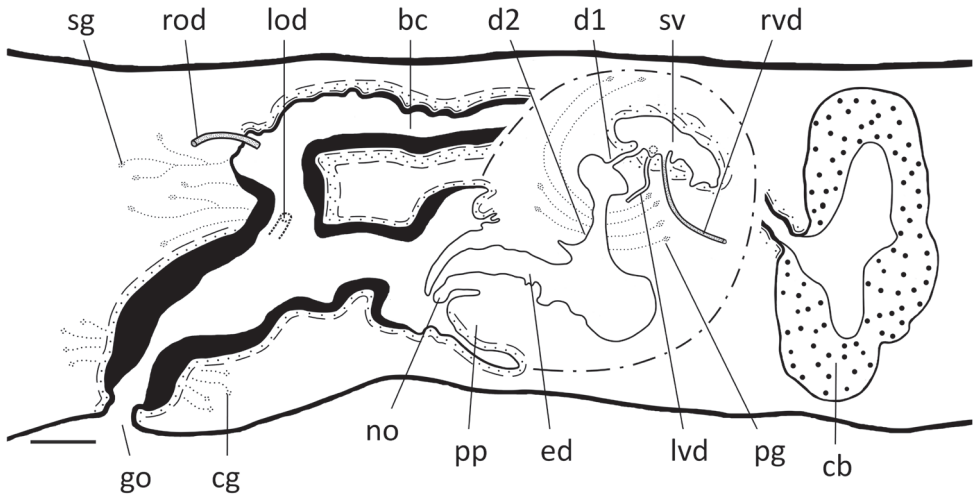


Figure 8. *Dugesia circumcisa* Sagittal reconstruction of the copulatory apparatus of paratype YWSZ9. Abbreviations: bc: bursal canal; cb: copulatory bursa; cg: cement glands; d1: first diaphragm; d2: second diaphragm; ed: ejaculatory duct; go: gonopore; lod: left oviduct; lvd: left vas deferens; no: nozzle; pg: penial glands; pp: penis papilla; rod: right oviduct; rvd: right vas deferens; sg: shell glands; sv: seminal vesicle. Scale bar: 100 μ m.

for the diaphragm in species of *Dugesia*. The situation in *D. circumcisa* is slightly different in that the proximal diaphragm is not small but consists of a well-developed valve.

Generally, in species of *Dugesia* the openings of the left and right sperm ducts into the intrabulbar seminal vesicle are located at ca. the same level. However, in *D. circumcisa* the vasa deferentia open asymmetrically into the seminal vesicle. Such asymmetrical openings have been reported explicitly for *D. bifida* Stocchino & Sluys, 2014, in which the sperm ducts open halfway into the vesicle, with the right duct opening dorsally to the left one. This contrasts with the situation in *D. circumcisa*, in which the right sperm duct opens into the anterior portion of the seminal vesicle and the left duct opens through the mid-lateral wall of the seminal vesicle, with the left sperm duct opening dorsally to the right one.

The characteristic nozzle at the tip of the penis papilla in *D. circumcisa* is paralleled in *D. bakurianica* Porfirjeva, 1958, *D. bijuga*, and perhaps also in *D. sinensis*. From that perspective, it is interesting that *D. bijuga* also possesses two diaphragms (see above). However, other parts of the male copulatory apparatus of *D. circumcisa* are different from that of *D. bijuga* (e.g., glands opening at a major portion of the blunt penis papilla, as well as atrial folds in the latter species). Furthermore, in the phylogenetic tree, *D. circumcisa* is far removed from *D. bijuga* (Fig. 2). *Dugesia circumcisa* differs from *D. sinensis* in the presence of atrial folds in the latter, while it differs from *D. bakurianica* in that this species only has a single diaphragm.

Another characteristic feature of *D. circumcisa* is the rather wide and long duct connecting the male atrium with the common atrium. Generally, in species of *Dugesia* the

male atrium opens more or less directly into the common atrium, without interpolation of a well-defined duct. Apart from *D. circumcisa*, other exceptions to this ground-plan condition can be found in *D. bactriana* de Beauchamp, 1959, *D. bengalensis* Kawakatsu, 1983, *D. bifida*, *D. capensis* Sluys, 2007, and *D. colapha* Dahm, 1967. However, other characters prevent synonymisation of *D. circumcisa* with any of these species, which in the case of *D. bifida* is supported also by completely different positions in the phylogenetic tree (Fig. 2).

***Dugesia verrucula* Chen & Dong, sp. nov.**

<http://zoobank.org/3DC3C5B0-1846-4A5D-9E41-04FD869447A4>

Material examined. Holotype. ZMHNU-ZJYA5, sagittal sections on 27 slides, Shiwan Dashan Mountain National Natural Reserve (21°53'40"N, 107°54'30"E; alt. 520 m a.s.l.), Shangsi County, Guangxi Province, China, 1 January 2019, coll. G-W Chen, D-Z Dong and co-workers. **Paratypes.** ZMHNU-ZJYA1, *ibid.*, sagittal sections on 25 slides; ZMHNU-ZJYA2, *ibid.*, sagittal sections on 36 slides; ZMHNU-ZJYA3, *ibid.*, sagittal sections on 38 slides; RMNH VER. 19975.a, *ibid.*, sagittal sections on 34 slides; ZMHNU-ZJYA6, *ibid.*, horizontal sections on 24 slides; ZMHNU-ZJYA7, *ibid.*, transverse sections on 30 slides; RMNH VER. 19975.b, *ibid.*, sagittal sections on 24 slides; ZMHNU-ZJYA9, *ibid.*, horizontal sections on 19 slides; ZMHNU-ZJYA10, *ibid.*, sagittal sections on 32 slides; ZMHNU-ZJYA11, *ibid.*, sagittal sections on 30 slides.

Diagnosis. *Dugesia verrucula* is characterised by the presence of the following features: large size of the live worm, usually exceeding 3.5 cm in length; asymmetrical openings of the oviducts into the bursal canal; subterminal opening of the ventrally displaced ejaculatory duct; vasa deferentia symmetrically opening into the posterolateral portion of the seminal vesicle; well-developed duct between seminal vesicle and diaphragm; single dorsal bump near root of penis papilla; bursal canal with pleated wall and spacious posterior section; unstalked cocoons; chromosome complement diploid with 16 metacentric chromosomes.

Etymology. The specific epithet is derived from the Latin *verrucula*, small wart, and alludes to the dorsal bump on the penis papilla; the specific epithet is treated as an adjective.

Habitat and reproduction. The average annual temperature of the tropical monsoon rain forest in the Shiwan Dashan Mountain National Natural Reserve ranges between 20 and 25 °C, while in the coldest month (January), the average temperature is ca. 10–13 °C. The worms were collected from a pond under a waterfall on the Shiwan Dashan Mountain, with a water temperature of 8.4 °C, while air temperature was 5.5 °C (Fig. 9A, B). It is noteworthy that the water temperature is lower than the coldest average temperature of the tropical monsoon rain forest and that, thus, the worms live under relatively harsh climatic conditions, as compared to that of the forest itself. At collection, ten specimens were sexually mature. After ca. 30 days of culturing under laboratory conditions, the animals produced unstalked spherical cocoons (approx. 1.5 mm in diameter) that were firmly attached to the glass wall of

the containers. Newly laid cocoons at first were red but turned dark brown after two or three days. After 10–20 days, 8–11 juveniles hatched from each cocoon. Juvenile planarians were light brown, after ca. 2 days, measuring 1.5–2.0 mm in length and 0.18–0.21 mm in width. After approximately 50 days, the animals measured 15–20 mm in length and 1.4–1.8 mm in width and were sexual (Fig. 9C). Fission was not observed in the laboratory culture.

Karyology. Each of the six, randomly selected specimens exhibited diploid chromosome complements. In a total of 100 metaphase plates examined, 85 chromosome complements were diploid with $2n = 2x = 16$ chromosomes, with all chromosomes being metacentric (Fig. 4); chromosome complements of the remaining 15 plates could not be determined, due to either lack of well-dispersed chromosomes or over-dispersed sets of chromosomes. The first pair of chromosomes is clearly larger than others, being 2.21 times larger than the shortest chromosome. Karyotype parameters, including relative length, arm ratio, and centromeric index are given in Table 3, while a chromosomal plate and idiogram are shown in Fig. 10.

Description. The body of live, sexual specimens measures 2.8–3.9 mm in length and 1.8–2.8 mm in width. Low-triangular head provided with two blunt auricles and two eyes, which are located in the centre of the head and placed in pigment-free spots and house numerous retinal cells (Fig. 9C). Dorsal surface brown, excepting the pale body margin and an accumulation of pigment following the outline of the pharynx. Furthermore, there is a dark brown mid-dorsal stripe, extending from the head to the posterior end of the body. The ventral surface is light brown.

Pharynx situated in the mid-region of the body and measuring ca. $1/5^{\text{th}}$ of the body length (Fig. 9C). Mouth opening located at the posterior end of the pharyngeal pocket. Outer pharyngeal musculature composed of a subepidermal layer of longitudinal muscles, followed by a layer of circular muscles; inner pharyngeal musculature composed of a thick subepithelial layer of circular muscles, followed by a layer of longitudinal muscles (Fig. 11A).

Ventral ovaries located at a short distance behind the brain, occupying ca. $1/6^{\text{th}}$ of the dorso-ventral space (Fig. 11B). The oviducts run ventrally in a caudal direction posteriorly to the genital pore, after which they curve dorsally to open separately and asymmetrically

Table 3. Karyotype parameters (mean values and standard deviations) of *Dugesia verrucula*; m: metacentric.

Chromosome	Relative length	Arm ratio	Centromeric index	Chromosome type
1	18.72±0.66	1.31±0.16	43.54±3.00	m
2	15.81±0.56	1.25±0.12	44.75±2.62	m
3	13.88±0.42	1.47±0.27	41.35±3.36	m
4	12.31±0.29	1.34±0.15	43.03±2.63	m
5	11.1±0.33	1.59±0.30	39.89±4.45	m
6	10.22±0.46	1.19±0.09	45.81±1.87	m
7	9.49±0.32	1.48±0.25	41.49±3.28	m
8	8.47±0.53	1.32±0.18	43.36±3.22	m

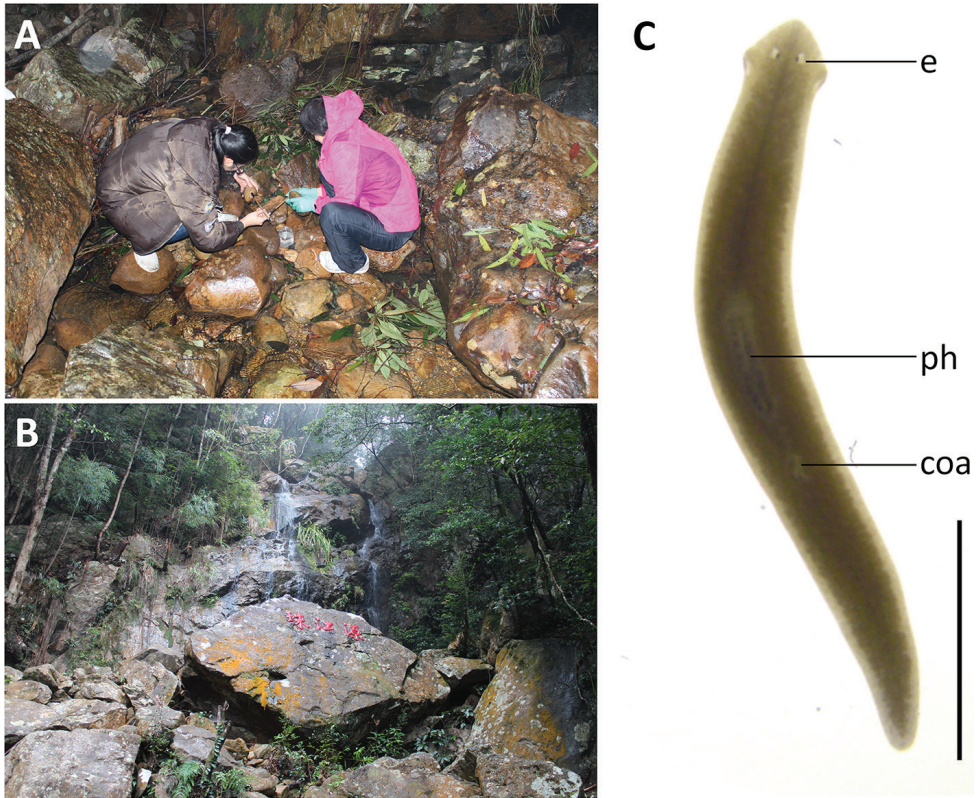


Figure 9. Habitat and external appearance of *Dugesia verrucula* **A** sampling site **B** habitat **C** sexually mature living individual (ca. 50 days old). Abbreviations: coa: copulatory apparatus; e: eye; ph: pharynx. Scale bar: 5 mm.

into the ventral portion of the bursal canal. The right branch opens dorsally to the left one, the latter actually opening into the common atrium (Figs 11C, 13, 14).

The large, sac-shaped copulatory bursa occupies the entire dorso-ventral space, and is lined by a vacuolated epithelium with basal nuclei (Fig. 11E, F). From the dorso-posterior wall of the bursa, the bursal canal runs in a caudal direction to the left side of the copulatory apparatus. The anterior section of the bursal canal is narrow, but dorsally to the male copulatory apparatus the canal expands in dorso-ventral direction and also presents a distinctly folded wall, formed by numerous pleats, particularly in its dorsal wall. In particular the posterior portion of the bursal canal expands to form a spacious chamber that almost imperceptibly grades into the equally spacious common atrium (Figs 11D, 13, 14B). The ventral portion of the latter communicates with the gonoduct (Figs 12D, G, 13, 14B).

The bursal canal is lined with columnar, nucleated, ciliated cells and is surrounded by a thin subepithelial layer of longitudinal muscles, followed by a thicker layer of circular muscle. An ectal reinforcement layer of longitudinal muscles runs from the

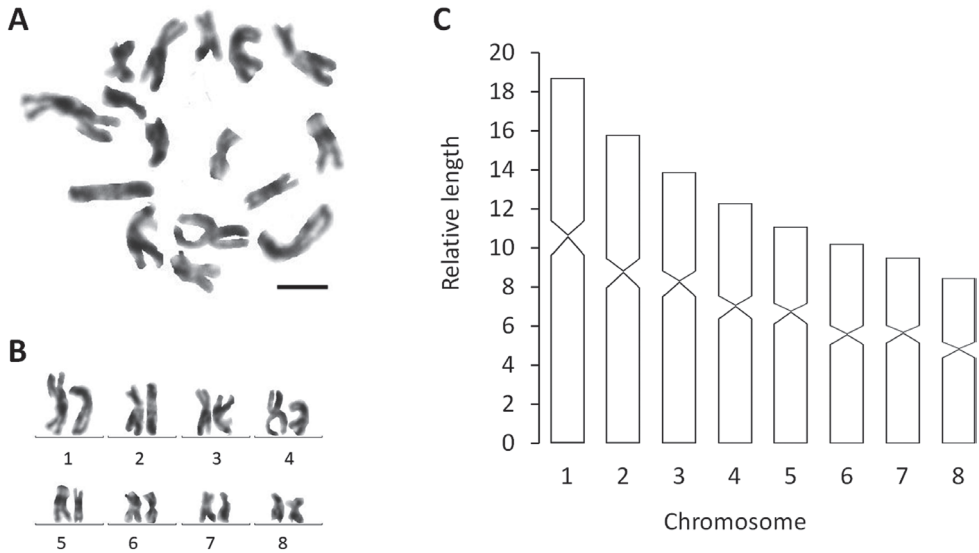


Figure 10. *Dugesia verrucula* **A** metaphasic plate, **B** karyogram **C** idiogram. Scale bar: 5 μ m.

vaginal region to ca. halfway along the bursal canal (Figs 11D, 13, 14B). Shell glands discharge their erythrophil secretion into the vaginal region of the bursal canal, near the oviducal openings.

The well-developed testes are situated dorsally and provided with mature spermatozoa (Fig. 12A). On either side of the midline of the body, testicular follicles are arranged in five or six longitudinal zones and extend from the posterior level of the ovaries to almost the posterior end of the body.

The vasa deferentia expand to form large spermiducal vesicles, filled with sperm (Figs 12C, 13, 14A). At the level of the penis bulb, the sperm ducts curve medio-dorsad and considerably decrease in diameter before penetrating the lateral wall of the penis bulb, and, subsequently, separately and symmetrically open into the ventrolateral or mid-lateral portion of the relatively large, rounded seminal vesicle (Figs 12B, 13, 14A). The latter is lined by a flat, nucleated epithelium and is surrounded by a layer of intermingled muscle fibres.

The ejaculatory duct arises from the antero-dorsal wall of the seminal vesicle and, subsequently, curves downwards towards the ventral root of the penis papilla. Near the ventral root of the papilla the ejaculatory duct is provided with a small diaphragm and changes its more or less vertical orientation by turning towards the tip of the penis papilla, having a subterminal opening at its tip (Figs 12C–H, 13, 14A). The ejaculatory duct is lined by an infranucleated epithelium and is hardly surrounded by any musculature. The diaphragm receives the secretion of erythrophil glands, while the ejaculatory duct also receives the abundant secretion of extrabulbar penis glands (Figs 12E–H, 14A).

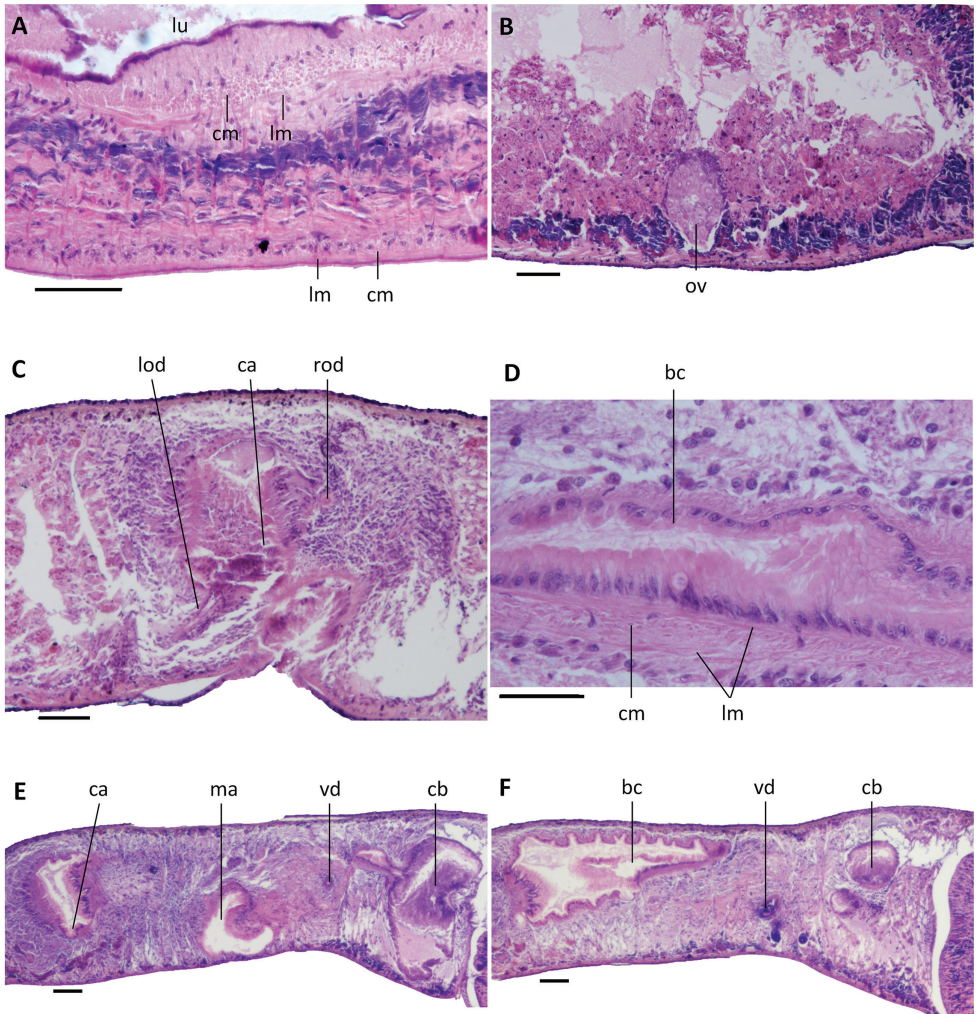


Figure 11. *Dugesia verrucula* **A** sagittal section of paratype RMNH VER. 19975.a, showing the musculature of the pharynx **B** sagittal section paratype RMNH VER. 19975.a, showing an ovary **C** transverse section of paratype ZJYA7, showing asymmetrical openings of the oviducts **D** sagittal section of paratype ZJYA11, showing musculature of bursal canal **E** sagittal section of paratype ZJYA11, showing copulatory bursa **F** sagittal section of paratype ZJYA11, showing wide portion of bursal canal, with its pleated walls. Abbreviations: bc: bursal canal; ca: common atrium; cb: copulatory bursa; cm: circular muscles; lm: longitudinal muscles; lod: left oviduct; lu: lumen; ma: male atrium; ov: ovary; rod: right oviduct; vd: vas deferens. Scale bars: 100 μ m.

Because of the ventrally displaced course of the ejaculatory duct, the penis papilla is asymmetrical, with its dorsal lip being considerably larger than the ventral lip. The conical or sub-cylindrical penis papilla has an oblique, ventro-caudad orientation and is covered by an infranucleated epithelium, which is underlain by a subepithelial layer of circular muscle, followed by a layer of longitudinal muscle

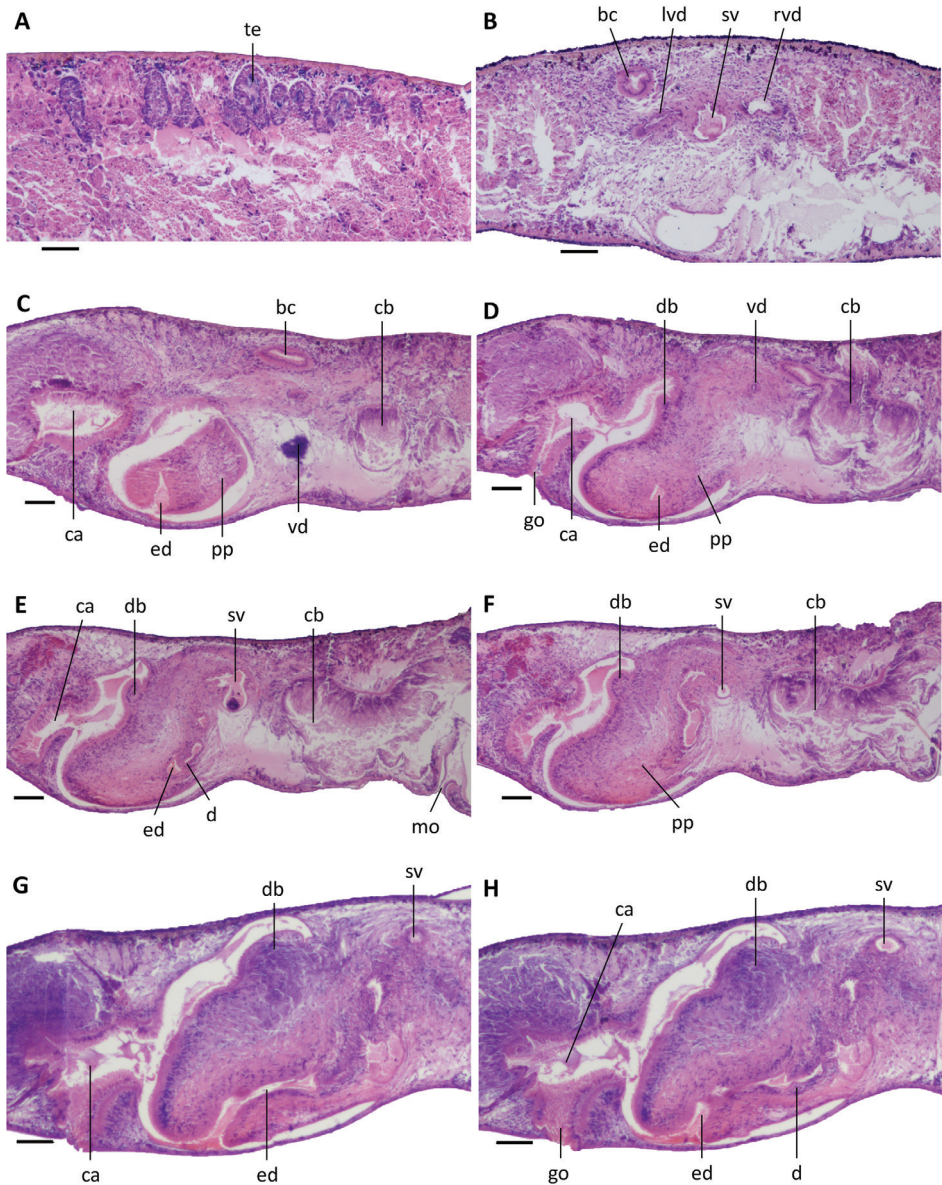


Figure 12. *Dugesia verrucula* **A** sagittal section of holotype ZJYA5, showing the testes **B** transverse section of paratype ZJYA7, showing vasa deferentia and seminal vesicle **C** sagittal section of holotype ZJYA5, showing subterminal opening of ejaculatory duct at tip of penis papilla **D** sagittal section of holotype ZJYA5, showing dorsal bump and copulatory bursa **E** sagittal section of holotype ZJYA5, showing seminal vesicle, diaphragm in the ejaculatory duct, dorsal bump, and copulatory bursa **F** sagittal section of holotype ZJYA5, showing seminal vesicle, dorsal bump, and copulatory bursa **G** sagittal section of paratype ZJYA11, showing subterminal opening of ejaculatory duct and dorsal bump **H** sagittal section of paratype ZJYA11, showing gonopore, ejaculatory duct, and diaphragm. Abbreviations: bc: bursal canal; ca: common atrium; cb: copulatory bursa; d: diaphragm; db: dorsal bump; ed: ejaculatory duct; go: gonopore; lvd: left vas deferens; mo: mouth; pp: penis papilla; rvd: right vas deferens; sv: seminal vesicle; te: testis; vd: vas deferens. Scale bars: 100 μ m.

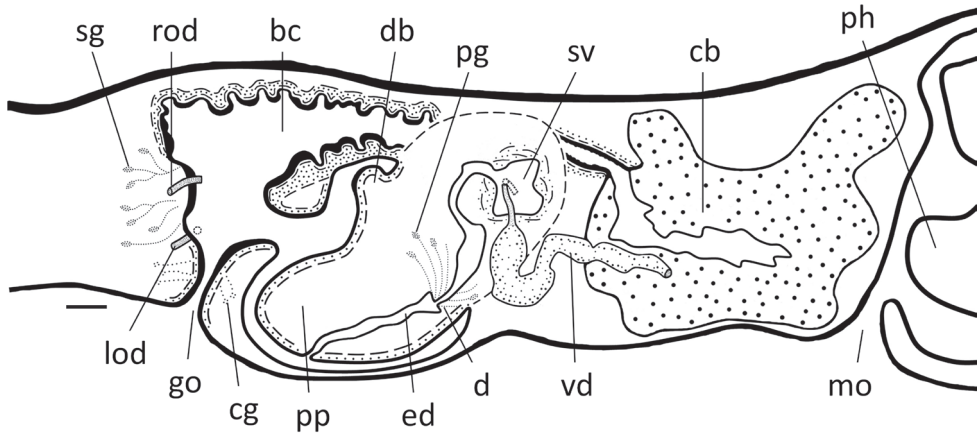


Figure 13. *Dugesia verrucula* Sagittal reconstruction of the copulatory apparatus of holotype ZJYA5. Abbreviations: bc: bursal canal; cb: copulatory bursa; cg: cement glands; d: diaphragm; db: dorsal bump; ed: ejaculatory duct; go: gonopore; lod: left oviduct; mo: mouth; pg: penial glands; ph: pharynx; pp: penis papilla; rod: right oviduct; sg: shell glands; sv: seminal vesicle; vd: vas deferens. Scale bar: 100 μ m.

fibres. Near its dorsal root, the penis papilla is provided with a pronounced bump (Figs 12D–H, 13, 14A).

Discussion. The most characteristic feature of *D. verrucula* is the permanent dorsal bump on its penis papilla, a similar character being known only from *Dugesia gibberosa* Stocchino & Sluys, 2017. However, the latter is provided with two dorsal bumps on its penis papilla instead of one, while its ejaculatory duct opens terminally at the tip of the papilla (Stocchino et al. 2017), in contrast to the subterminal opening in *D. verrucula*.

Apart from the penial bump and the subterminal opening of the ejaculatory duct, other characteristic features of *D. verrucula* are the asymmetrical penis papilla with ventrally displaced ejaculatory duct (character 1, state 1 in Sluys et al. 1998; see also Stocchino et al. 2017), and the presence of a duct between the seminal vesicle and the diaphragm (character 5, state 1 in Sluys et al. 1998). Besides *D. verrucula*, these two character states are also expressed in the following species: *D. andamanensis* (Kaburaki, 1925), *D. austroasiatica* Kawakatsu, 1985, *D. batuensis*, *D. bengalensis*, *D. borneana* Kawakatsu, 1972, *D. burmaensis* (Kaburaki, 1918), *D. deharvengi* Kawakatsu & Mitchell, 1989, *D. gibberosa*, *D. hymanae* (Sivickis, 1928), *D. indonesiana* Kawakatsu, 1973, *D. japonica*, *D. lindbergi* De Beauchamp, 1959, *D. mertonii* (Steinmann, 1914), *D. naiadis* Sluys, 2013, *D. notogaea* Sluys & Kawakatsu, 1998, *D. novaguineana* Kawakatsu, 1976, *D. ryukyuensis* Kawakatsu, 1976, *D. siamana* Kawakatsu, 1980, *D. tamilensis* Kawakatsu, 1980, *D. majuscula*, *D. umbonata* (see Sluys et al. 1998; Sluys et al. 2013; Stocchino et al. 2017; Song et al. 2020; Wang et al. 2021). However, these species all differ from *D. verrucula* in the gross anatomy of the copulatory apparatus or in detailed character states, such as the openings of the oviducts (common oviduct or symmetrical openings, in contrast to the asymmetrical oviducal openings in *D. verrucula*), opening of the ejaculatory duct at the tip of the penis papilla (terminal, in contrast to the subterminal opening in *D. verrucula*),

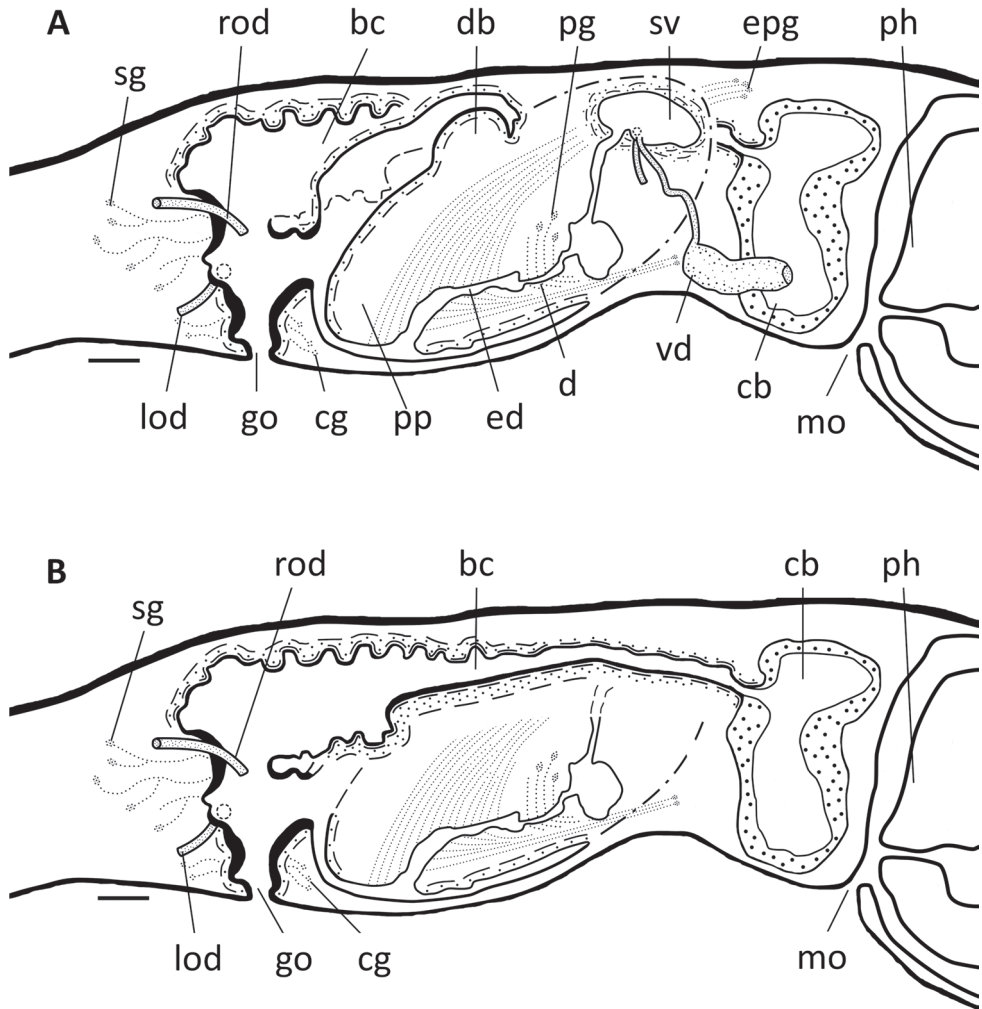


Figure 14. *Dugesia verrucula* Sagittal reconstruction of the copulatory apparatus of paratype ZJYA11 **A** sagittal reconstruction of male copulatory apparatus **B** sagittal reconstruction of female copulatory apparatus. Abbreviations: bc: bursal canal; cb: copulatory bursa; cg: cement glands; d: diaphragm; db: dorsal bump; ed: ejaculatory duct; epg: extrabulbar penial glands; go: gonopore; lod: left oviduct; mo: mouth; pg: penial glands; ph: pharynx; pp: penis papilla; rod: right oviduct; sg: shell glands; sv: seminal vesicle; vd: vas deferens. Scale bar: 100 μm .

or presence of a penial valve (absent in *D. verrucula*). It is noteworthy that the cocoons of *D. verrucula* are unstalked, since usually in species of *Dugesia* the egg capsules are provided with a pedicel (Sluys and Riutort 2018), the only other exception being *D. bifida* from Madagascar (Stocchino et al. 2014). However, in other aspects of their reproduction *D. verrucula* and *D. bifida* are rather different, in that in the latter cocoons were produced by ex-fissiparous, sexualised specimens, which had developed hyperplastic ovaries; the juveniles emerging from these fertile cocoons gave rise to new fissiparous clones. This reproductive strategy differs much from the fully sexual life cycle of *D. verrucula*.

General discussion

Inter-specific genetic distances of both COI and ITS-1 reveal that *D. circumcisa* and *D. verrucula* are well-separated from their congeners. The lowest COI distance values between *D. circumcisa* and *D. verrucula* and other congeners are 11.20% and 15.47%, respectively, while the distance between the two new species is 17.15% (Suppl. material 2: Table S1). With respect to ITS-1, the lowest distance values between *D. circumcisa* and *D. verrucula* and other congeners are 4.8% and 2.77%, respectively, while the distance between the two new species is 4.98% (Suppl. material 3: Table S2). Previous studies showed that the lowest COI distance value between species usually is in the range between 6% and 10% (Lázaro et al. 2009; Solà et al. 2013; Stocchino et al. 2017; Harrath et al. 2019). For ITS-1, the lowest distances reported between species ranged between 1% and 7% (Lázaro et al. 2009; Solà et al. 2013; Stocchino et al. 2017). All of these values are surpassed by the genetic distances determined for both *D. circumcisa* and *D. verrucula*, which thus support the results of the morphological and phylogenetic analyses.

The topology of our phylogenetic tree (Fig. 2) basically agrees with results from previous phylogenetic analyses (Lázaro et al. 2009; Solà et al. 2013; Stocchino et al. 2017; Song et al. 2020). It is noteworthy that although the two new species occur at the same geographic location, they belong to two different clades, together with other species from southern China.

The two new species show a haploid number of $n = 8$ metacentric chromosomes, thus conforming to the situation that in the genus *Dugesia* the basic chromosome number is 7, 8 or 9 (Stocchino et al. 2004). Chromosome portraits similar to the ones of *D. circumcisa* and *D. verrucula* are also present in the following species: many Sardinian populations of *D. benazzii* Lepori, 1951, *D. etrusca labronica* Lepori, 1950, *D. elegans* de Vries, 1984, *D. gonocephala* (Dugès, 1830), *D. japonica*, *D. indonesiana*, *D. majuscula*, *D. sagitta* (Schmidt, 1861), *D. semiglobosa*, *D. salina* (Whitehouse, 1914), and presumably also *D. colapha* Dahm, 1967 (cf. Dahm 1967; Benazzi and Gourbault 1975; Kawakatsu et al. 1976; Ball 1979; De Vries 1984; Deri et al. 1999; Pala et al. 1999; Stocchino 2018; Wang et al. 2020; Bromley-Schnur 2021).

The number of 8–11 juveniles hatching from a single cocoon of *D. verrucula* falls at the higher end of the range as reported for other sexual species of *Dugesia*, such as *D. benazzii* (8–10 hatchlings), *D. etrusca* (8–10), *D. hepta* Pala et al., 1981 (8–10), *D. cretica* (Meixner, 1928) (4–15) (Bromley 1974; Kobayashi et al. 2009; Stocchino and Manconi 2013). However, in some species of *Dugesia*, ex-fissiparous individuals are also able to produce fertile cocoons, for example in *D. sicula* (1 or 2 hatchlings), *D. afromontana* Stocchino & Sluys, 2012 (1 or 2), *D. arabica* Harrath & Sluys, 2013 (1–3), *D. ryukyuensis* (1–5), and *D. aethiopica* (1–6) (Harrath et al. 2013; Stocchino and Manconi 2013 and references therein; Stocchino et al. 2014). The number of young hatching from such capsules produced by ex-fissiparous specimens often is lower than in sexual species.

In contrast, *D. circumcisa* never produced cocoons and only showed asexual reproduction by means of fission, which corresponds with its poorly developed or hyperplastic

ovaries and the triploid chromosome complement. It has been established that in such abnormal ovaries the oocytes are anomalous (Harrath et al. 2014), thus preventing regular oogenesis.

Acknowledgements

This work was supported by the National Natural Science Foundation of China (grant numbers: 32070427, 31570376, 31471965, u1604173), the Major Public Welfare project of Henan Province (grant: 201300311700) and by the Puyang Field Scientific Observation and Research Station for Yellow River Wetland Ecosystem, Henan Province.

References

- Abascal F, Zardoya R, Telford MJ (2010) TranslatorX: Multiple alignment of nucleotide sequences guided by amino acid translations. *Nucleic Acids Research* 38: W7–W13. <https://doi.org/10.1093/nar/gkq291>
- Álvarez-Presas M, Carbayo F, Rozas J, Riutort M (2011) Land planarians (Platyhelminthes) as a model organism for fine-scale phylogeographic studies: understanding patterns of biodiversity in the Brazilian Atlantic Forest hotspot. *Journal Evolutionary Biology* 24: 887–896. <https://doi.org/10.1111/j.1420-9101.2010.02220.x>
- Baguña J, Carranza S, Pala M, Ribera C, Giribet G, Arnedo M, Ribas M, Riutort M (1999) From morphology and karyology to molecules. New methods for taxonomical identification of asexual populations of freshwater planarians. *Italian Journal of Zoology* 66: 207–214. <https://doi.org/10.1080/11250009909356258>
- Ball IR (1979) The karyotypes of two *Dugesia* species from Corfu, Greece (Platyhelminthes, Turbellaria). *Bijdragen tot de Dierkunde* 48: 187–190. <https://doi.org/10.1163/26660644-04802007>
- Benazzi M, Benazzi Lentati G (1970) *Animal Cytogenetics Vol. 1: Platyhelminthes*. Gebrüder Borntraeger, Berlin, Stuttgart, 182 pp.
- Benazzi M, Gourbault N (1975) Cytotaxonomical study of *Dugesia indonesiana* Kawakatsu (Tricladida Paludicola). *Accademia Nazionale dei Lincei, Rendiconti della Classe di Scienze fisiche, matematiche e naturali, ser. 8, 58(2): 237–243*.
- Bromley HJ (1974) Morpho-karyological types of *Dugesia* (Turbellaria, Tricladida) in Israel and their distribution patterns. *Zoologica Scripta* 3: 239–242. <https://doi.org/10.1111/j.1463-6409.1974.tb00820.x>
- Bromley-Schnur HJ (2021) The genus *Phagocata* Leidy (Platyhelminthes, Tricladida) in Israel, a new species of *Phagocata* from Lake Kinneret, and an emended description of *Dugesia salina*. *Zootaxa* 4969: 293–317. <https://doi.org/10.11646/zootaxa.4949.2.4>
- Chen G-W, Wang Y-L, Wang H-K, Fu R-M, Zhang J-F, Liu D-Z (2008) Chromosome and karyotype analysis of *Polycelis wutaishanica* (Turbellaria, Tricladida) from Shanxi province, China. *Acta Zootaxonomica Sinica* 33(3): 449–452.

- Chen Y-H, Chen X-M, Wu C-C, Wang A-T (2015) A new species of the genus *Dugesia* (Tricladida, Dugesiidae) from China. *Zoological Systematics* 40: 237–249. <https://doi.org/10.11865/zs.20150301>
- Dahm AG (1967) A new *Dugesia* “microspecies” from Ghana belonging to the *Dugesia gonocephala* group – Turbellaria Tricladida Paludicola. *Arkiv för Zoologi* 19: 309–321.
- Deri P, Colognato R, Rossi L, Salvetti A, Batistoni R (1999) A karyological study on populations of *Dugesia gonocephala* s.l. (Turbellaria, Tricladida). *Italian Journal of Zoology* 66: 245–253. <https://doi.org/10.1080/11250009909356262>
- Dessimoz C, Gil M (2010) Phylogenetic assessment of alignments reveals neglected tree signal in gaps. *Genome Biology* 11: R37. <https://doi.org/10.1186/gb-2010-11-4-r37>
- De Vries EJ (1984) On the karyology of *Dugesia gonocephala* s.l. (Turbellaria, Tricladida) from Montpellier, France. *Hydrobiologia* 132: 251–256. <https://doi.org/10.1007/BF00046257>
- De Vries EJ (1988) A synopsis of the nominal species of the subgenus *Dugesia* (Platyhelminthes, Tricladida, Paludicola) from Africa and Madagascar. *Zoological Journal of the Linnean Society* 92: 345–382. <https://doi.org/10.1111/j.1096-3642.1988.tb01729.x>
- Dong Z-M, Chen G-W, Zhang H-C, Liu D-Z (2017) A new species of *Polycelis* (Platyhelminthes, Tricladida, Planariidae) from China. *Acta Zoologica Academiae Scientiarum Hungaricae* 63(3): 263–276. <https://doi.org/10.17109/AZH.63.3.263.2017>
- Harrath AH, Semaili A, Mansour L, Ahmed M, Sirotkin AV, Al Omar SY, Arfah M, Al Anazi MS, Alhazza IM, Nyengaard JR, Alwaseel S (2014) Infertility in the hyperplastic ovary of freshwater planarians: the role of programmed cell death. *Cell and Tissue Research* 358: 607–620. <https://doi.org/10.1007/s00441-014-1971-0>
- Harrath AH, Sluys R, Aldahmash W, Al-Razaki A, Alwaseel S (2013) Reproductive strategies, karyology, parasites, and taxonomic status of *Dugesia* populations from Yemen (Platyhelminthes, Tricladida, Dugesiidae). *Zoological Science* 30: 502–508. <https://doi.org/10.2108/zsj.30.502>
- Harrath AH, Sluys R, Mansour L, Folefack GL, Aldahmash W, Alwaseel S, Solà E, Riutort M (2019) Molecular and morphological identification of two new African species of *Dugesia* (Platyhelminthes, Tricladida, Dugesiidae) from Cameroon. *Journal of Natural History* 53: 253–271. <https://doi.org/10.1080/00222933.2019.1577508>
- Hou X-G, Aldridge RJ, Bergström J, Siveter DJ, Siveter DJ, Feng X-H (2004) The Cambrian fossils of Chengjiang, China: The flowering of early animal life. Blackwell Publishing, New Jersey, 284 pp.
- Katoh K, Standley DM (2013) MAFFT multiple sequence alignment software version 7: Improvements in performance and usability. *Molecular Biology and Evolution* 30: 772–780. <https://doi.org/10.1002/9780470999950>
- Kawakatsu M, Oki I, Tamura S, Sugino H (1976) Studies on the morphology, karyology and taxonomy of the Japanese freshwater planarian *Dugesia japonica* Ichikawa et Kawakatsu, with a description of a new subspecies, *Dugesia japonica ryukyensis* subsp. nov. *The Bulletin of Fuji Women's College* 14, ser. II: 81–126.
- Kobayashi K, Arioka S, Hoshi M, Matsumoto M (2009) Production of asexual and sexual offspring in the triploid planarian *Dugesia ryukyensis*. *Integrative Zoology* 4: 265–271. <https://doi.org/10.1111/j.1749-4877.2009.00164.x>

- Lázaro EM, Sluys R, Pala M, Stocchino GA, Baguñà J, Riutort M (2009) Molecular barcoding and phylogeography of sexual and asexual freshwater planarians of the genus *Dugesia* in the Western Mediterranean (Platyhelminthes, Tricladida, Dugesidae). *Molecular Phylogenetics and Evolution* 52: 835–845. <https://doi.org/10.1016/j.ympev.2009.04.022>
- Levan A, Fredga K, Sandberg AA (1964) Nomenclature for centromeric position on chromosomes. *Hereditas* 52: 201–220. <https://doi.org/10.1111/j.1601-5223.1964.tb01953.x>
- Pala M, Casu S, Stocchino G (1999) Karyology and karyotype analysis of diploid freshwater planarian populations of the *Dugesia gonocephala* group (Platyhelminthes, Tricladida) found in Sardinia. *Hydrobiologia* 392: 113–119. <https://doi.org/10.1023/A:1003534507632>
- Ronquist F, Teslenko M, van der Mark P, Ayres DL, Darling A, Höhna S, Larget B, Liu L, Suchard MA, Huelsenbeck JP (2012) MrBayes 3.2: efficient Bayesian phylogenetic inference and model choice across a large model space. *Systematic Biology* 61: 539–542. <https://doi.org/10.1093/sysbio/sys029>
- Sluys R, Kawakatsu M, Winsor L (1998) The genus *Dugesia* in Australia, with its phylogenetic analysis and historical biogeography (Platyhelminthes, Tricladida, Dugesidae). *Zoologica Scripta* 27: 273–289. <https://doi.org/10.1111/j.1463-6409.1998.tb00461.x>
- Sluys R, Riutort M (2018) Planarian diversity and phylogeny. In: Rink JC (Ed.) *Planarian Regeneration: Methods and Protocols*. *Methods in Molecular Biology*, vol. 1774. Humana Press, Springer Science+Business Media, New York, 1–56. https://doi.org/10.1007/978-1-4939-7802-1_1
- Sluys R, Solà E, Gritzalis K, Vila-Farré M, Mateos, E, Riutort M (2013) Integrative delineation of species of Mediterranean freshwater planarians (Platyhelminthes: Dugesidae). *Zoological Journal of the Linnean Society* 169: 523–547. <https://doi.org/10.1111/zoj.12077>
- Solà E, Sluys R, Gritzalis K, Riutort M (2013) Fluvial basin history in the northeastern Mediterranean region underlies dispersal and speciation patterns in the genus *Dugesia* (Platyhelminthes, Tricladida, Dugesidae). *Molecular Phylogenetics and Evolution* 66: 877–888. <https://doi.org/10.1016/j.ympev.2012.11.010>
- Song X-Y, Li W-X, Sluys R, Huang S-X, Wang A-T (2020) A new species of *Dugesia* (Platyhelminthes, Tricladida, Dugesidae) from China, with an account on the histochemical structure of its major nervous system. *Zoosystematics and Evolution* 96(2): 431–447.
- Stamatakis A (2014) RAxML version 8: a tool for phylogenetic analysis and post-analysis of large phylogenies. *Bioinformatics (Oxford, England)* 30: 1312–1313. <https://doi.org/10.3897/zse.96.52484>
- Stocchino GA (2018) 80 years of research on planarians (Platyhelminthes, Tricladida) from Sardinia, Italy: an annotated checklist. *Zootaxa* 4532: 539–552. <https://doi.org/10.11646/zootaxa.4532.4.5>
- Stocchino GA, Manconi R (2013) Overview of life cycles in model species of the genus *Dugesia* (Platyhelminthes Tricladida). *Italian Journal of Zoology* 80(3): 319–328. <https://doi.org/10.1080/11250003.2013.822025>
- Stocchino GA, Manconi R, Corso G, Pala M (2004) Karyology and karyometric analysis of an Afrotropical freshwater planarian (Platyhelminthes, Tricladida). *Italian Journal of Zoology* 71: 89–93. <https://doi.org/10.1080/11250000409356557>

- Stocchino GA, Manconi R, Corso G, Sluys R, Casu S, Pala M (2009) African planarians: Morphology and karyology of *Dugesia maghrebiana* sp. n. (Platyhelminthes, Tricladida) from Tunisia. *Italian Journal of Zoology* 76: 83–91. <https://doi.org/10.1080/11250000802141683>
- Stocchino GA, Sluys R, Manconi R (2014) A new and aberrant species of *Dugesia* (Platyhelminthes, Tricladida) from Madagascar. *ZooKeys* 425: 71–88. <https://doi.org/10.3897/zookeys.425.7811>
- Stocchino GA, Sluys R, Riutort M, Solà E, Manconi R (2017) Freshwater planarian diversity (Platyhelminthes: Tricladida: Dugesiidae) in Madagascar: new species, cryptic species, with a redefinition of character states. *Zoological Journal of the Linnean Society* 181: 727–756. <https://doi.org/10.1093/zoolinnean/zlx017>
- Tamura K, Stecher G, Peterson D, Filipowski A, Kumar S (2013) MEGA6: Molecular Evolutionary Genetics Analysis version 6.0. *Molecular Biology and Evolution* 30: 2725–2729. <https://doi.org/10.1093/molbev/mst197>
- Talavera G, Castresana J (2007) Improvement of phylogenies after removing divergent and ambiguously aligned blocks from protein sequence alignments. *Systematic Biology* 56: 564–577. <https://doi.org/10.1080/10635150701472164>
- Tan G, Muffato M, Ledergerber C, Herrero J, Goldman N, Gil M, Dessimoz C (2015) Current methods for automated filtering of multiple sequence alignments frequently worsen single-gene phylogenetic inference. *Systematic Biology* 64: 778–791. <https://doi.org/10.1093/sysbio/syv033>
- Wang L, Dong Z-M, Chen G-W, Sluys R, Liu D-Z (2021) Integrative descriptions of two new species of *Dugesia* from Hainan Island, China (Platyhelminthes, Tricladida, Dugesiidae). *ZooKeys* 1028: 1–28. <https://doi.org/10.3897/zookeys.1028.60838>
- Yuan X-L, Zhou C-M (1999) A Neoproterozoic Doushantuo microfossils assemblage-Wengan biota at Wengan county of Guizhou in South China. *Jiangsu Geology* 23(4): 202–211. [in Chinese]

Supplementary material I

Figure S1

Authors: Lei Wang, Jin-zi Chen, Zi-mei Dong, Guang-wen Chen, Ronald Sluys, De-zeng Liu

Data type: Phylogenetic tree

Explanation note: Phylogenetic tree obtained from ML analysis of the concatenated dataset. Numbers at nodes indicate support values (bootstrap). Scale bar: substitutions per site.

Copyright notice: This dataset is made available under the Open Database License (<http://opendatacommons.org/licenses/odbl/1.0/>). The Open Database License (ODbL) is a license agreement intended to allow users to freely share, modify, and use this Dataset while maintaining this same freedom for others, provided that the original source and author(s) are credited.

Link: <https://doi.org/10.3897/zookeys.1059.65633.suppl1>

Supplementary material 2

Table S1

Authors: Lei Wang, Jin-zi Chen, Zi-mei Dong, Guang-wen Chen, Ronald Sluys, De-zeng Liu

Data type: Genetic distances

Explanation note: Genetic distances for COI. Highest and lowest distance values between the two new Chinese species and Oriental-Australasian congeners indicated in red and blue, respectively. Purple: distance value between the two new species.

Copyright notice: This dataset is made available under the Open Database License (<http://opendatacommons.org/licenses/odbl/1.0/>). The Open Database License (ODbL) is a license agreement intended to allow users to freely share, modify, and use this Dataset while maintaining this same freedom for others, provided that the original source and author(s) are credited.

Link: <https://doi.org/10.3897/zookeys.1059.65633.suppl2>

Supplementary material 3

Table S2

Authors: Lei Wang, Jin-zi Chen, Zi-mei Dong, Guang-wen Chen, Ronald Sluys, De-zeng Liu

Data type: Genetic distances

Explanation note: Genetic distances for ITS-1. Highest and lowest distance values between the two new Chinese species and Oriental-Australasian congeners indicated in red and blue, respectively. Purple: distance value between the two new species.

Copyright notice: This dataset is made available under the Open Database License (<http://opendatacommons.org/licenses/odbl/1.0/>). The Open Database License (ODbL) is a license agreement intended to allow users to freely share, modify, and use this Dataset while maintaining this same freedom for others, provided that the original source and author(s) are credited.

Link: <https://doi.org/10.3897/zookeys.1059.65633.suppl3>

The *Nazeris* fauna of the Nanling Mountain Range, China (Coleoptera, Staphylinidae, Paederinae)

Xiao-Bin Lin¹, Jia-Yao Hu¹

¹ Department of Biology, College of Life Sciences, Shanghai Normal University, 100 Guilin Road, 1st Educational Building 423-A Room, Shanghai, 200234 China

Corresponding author: Jia-Yao Hu (hujiaoyao@shnu.edu.cn)

Academic editor: Adam Brunke | Received 27 July 2021 | Accepted 14 August 2021 | Published 8 September 2021

<http://zoobank.org/74BFDC46-8DE9-424C-B168-5F03CF818C3C>

Citation: Lin X-B, Hu J-Y (2021) The *Nazeris* fauna of the Nanling Mountain Range, China (Coleoptera, Staphylinidae, Paederinae). ZooKeys 1059: 117–133. <https://doi.org/10.3897/zookeys.1059.72240>

Abstract

Fourteen species of *Nazeris* Fauvel, 1873 are reported for the Nanling Mountain Range, China. Four of them are described as new: *N. xingmini* Lin & Hu, **sp. nov.** (Guangdong, Jiangxi), *N. huaiweni* Lin & Hu, **sp. nov.** (Guangdong), *N. meihuaae* Lin & Hu, **sp. nov.** (Guangdong, Jiangxi) and *N. lichongi* Lin & Hu, **sp. nov.** (Hunan). An identification key to the *Nazeris* species reported for the Nanling Mountains, and a map showing their distribution are provided.

Keywords

Flightless, leaf litter, new species, Oriental Region, rove beetles, taxonomy

Introduction

The speciose paederine genus *Nazeris* Fauvel, 1873 previously included 191 species and one subspecies in China. The genus is distinguished from other paederines particularly by the morphology of the aedeagus, which has a pair of dorso-lateral apophyses (Assing

2009). All the known species of the genus are micropterous and flightless. Therefore, most of them have very narrow distributions.

The Nanling Mountain Range in central and eastern China, extend more than 500 km through Guangxi, Hunan, Guangdong and Jiangxi provinces, with several peaks of more than 1500 m. To the present, fifteen *Nazeris* species have been described from Nanling Mountain Range (Assing 2014, 2016; Hu and Li 2017; Hu et al. 2018a; Hu and Qiao 2019). During recent field trips in the Nanling Mountains, many specimens of *Nazeris* were collected. Among them, four new species were found. In the present paper, we describe the new species and provide illustrations of their major diagnostic features.

Material and methods

The type material is deposited in the Insect Collection of the Shanghai Normal University, Shanghai, China (SNUC). The dissected body parts were mounted in Euparal on plastic slides. The habitus photos were taken using a Canon 7D camera. The photos of the sternites and aedeagi were taken using a Canon G9 camera mounted on an Olympus CX31 microscope. The original map source was obtained from <http://www.simplemapp.net>, an on-line tool for creating maps that can be freely used for publications and presentations.

Measurements

Body length: measured from the anterior margin of the labrum to the apex of the abdomen

Length of forebody: measured from anterior margin of labrum to the posterior margin of the elytra

Eye length: longitudinal length of eye in dorsal view

Postocular length: measured from posterior margin of eye to posterior constriction of head in dorsal view

Head width: width of head across (and including) eyes

Head length: measured from clypeal anterior margin to posterior constriction of head

Pronotum width: maximal width of pronotum

Pronotum length: measured in midline from front margin to posterior margin

Width of elytra: combined width of elytra at posterior margin

Length of elytra: measured from apex of scutellum to posterior margin.

Results

Nazeris alatus Hu & Li, 2017

Fig. 27

Non-type material examined. CHINA: **Guangxi Prov.:** Guilin, Huaping N. R.: 5 ♂♂, 4 ♀♀, nr. Guangfu Peak, 24°33'36.57"N, 109°55'40.81"E, ca 1800 m, 22.iv.2021, sifted,

Yin, Zhang, Pan and Shen leg.; 4 ♂♂, 3 ♀♀, Yunxi Valley, 25°34'00.62"N, 109°56'19.59"E, 1460–1550 m, 23.iv.2021, sifted, Yin, Zhang, Pan and Shen leg. (SNUC).

Comparative notes. *Nazeris alatus* is very similar to *N. yanzhuqii* Hu & Qiao, 2019 in general appearance, but can be separated by the midline of the pronotum with short and narrow impunctate elevation posteriorly (Hu and Li 2017: 337, fig. 15); by the shorter and narrower ventral process of the aedeagus, and by the narrower dorso-lateral apophyses of the aedeagus (Hu and Li 2017: 337, fig. 18).

Distribution and habitat data. The species is known only from Huaping in northeast Guangxi (Fig. 27). The specimens were collected by sifting leaf litter at altitudes of 1700–1800 m.

Nazeris gaoleii Hu, Luo & Li, 2018

Fig. 27

Non-type material examined. CHINA: **Guangdong Prov.:** Shaoguan, Nanling N. R.: 1 ♂, 1 ♀, 24°56'38"N, 112°59'31"E, 1316–1575 m, 29.vi.2020, Xia, Zhang, Yin and Lin leg.; 2 ♀♀, Guangdong Diyifeng, 24°55'29.62"N, 112°59'31.42"E, 1538–1784 m, 28.vi.2020, Xia, Zhang, Yin and Lin leg.; 1 ♂, Xiaohuangshan, 24°53'58"N, 113°01'27"E, 1,425 m, 23.viii.2020, sifted, Zhong Peng leg.; **Hunan Prov.:** Yizhang, Mangshan N. R.: 3 ♂♂, 3 ♀♀, Mengkengshi, 24°55'10"N, 112°58'37"E, 1625 m, 28.viii.2020, sifted, Zhong Peng leg.; 1 ♂, Jiangjunzhai, 24°57'03"N, 112°55'37"E, 1220 m, 27.viii.2020, sifted, Zhong Peng leg. (SNUC).

Comparative notes. *Nazeris gaoleii* is very similar to *N. jiawei* Hu, Liu & Li, 2018b in general appearance and aedeagal characters, but can be separated by the narrower posterior excision of male sternite VIII (Hu et al. 2018a: 179, fig. 21), and much shorter dorso-lateral apophyses of the aedeagus (Hu et al. 2018a: 179, fig. 22).

Distribution and habitat data. The species is known from Nanling in northern Guangdong and Mangshan in southern Hunan (Fig. 27). The specimens were collected by sifting leaf litter at altitudes of 1220–1820 m.

Nazeris huapingensis Hu & Li, 2017

Fig. 27

Non-type material examined. CHINA: **Guangxi Prov.:** Guilin, Huaping N. R.: 6 ♂♂, 9 ♀♀, nr. Guangfu Peak, 24°33'36.57"N, 109°55'40.81"E, ca 1800 m, 22.iv.2021, sifted, Yin, Zhang, Pan and Shen leg.; 8 ♂♂, 11 ♀♀, Yunxi Valley, 25°34'00.62"N, 109°56'19.59"E, 1460–1550 m, 23.iv.2021, sifted, Yin, Zhang, Pan and Shen leg. (SNUC).

Comparative notes. *Nazeris huapingensis* is very similar to *N. obtortus* Assing, 2016 from the same locality in general appearance and separated only by aedeagal characters: the apex of the ventral process in ventral view is much broader; apices of the dorso-lateral apophyses rounder and broader (Hu and Li 2017: 336, fig. 13).

Distribution and habitat data. The species is known only from Huaping in northeast Guangxi (Fig. 27). The specimens were collected by sifting leaf litter at altitudes of 1300–1800 m.

***Nazeris latilobatus* Assing, 2016**

Fig. 27

Non-type material examined. CHINA: **Guangxi:** Xing'an, Mao'ershan N. R.: 1 ♂, 25°52'29.52"N, 110°28'20.01"E, 528 m, 25.viii.2020, Chong Li leg.; 2 ♂♂, 25°30'15.72"N, 110°25'50.87"E, 1900–2040 m, 27.viii.2020, Lu Qiu leg.; 20 ♂♂, 16 ♀♀, Antangping, 25°54'44.07"N, 110°27'37.68"E, 1660 m, 6–7.v.2021, sifted, Yin, Zhang, Pan and Shen leg.; 1 ♂, botanical garden, 25°53'03.83"N, 110°29'13.53"E, 1160 m, 8.v.2021, sifted, Yin, Zhang, Pan and Shen leg. (SNUC).

Comparative notes. *Nazeris latilobatus* is similar to *N. qini* Hu & Li, 2012 from Dayaoshan in external and the male sexual characters, but can be separated by the deeper posterior excision of the male sternite VIII (Assing 2016: 307, fig. 9), and the much broader apex of the aedeagal ventral process (Assing 2016: 307, fig. 11).

Distribution and habitat data. The species is known only from Mao'ershan in northeast Guangxi (Fig. 27). The specimen was collected by sifting leaf litter at altitudes of 450–2040 m.

***Nazeris nanlingensis* Hu, Luo & Li, 2018**

Fig. 27

Non-type material examined. CHINA: **Guangdong Prov.:** Shaoguan, Nanling N. R.: 2 ♂♂, 1 ♀, 24°56'38"N, 112°59'31"E, 1316–1575 m, 29.vi.2020, Xia, Zhang, Yin and Lin leg.; 2 ♂♂, 2 ♀♀, Xiaohuangshan, 24°53'58"N, 113°01'27"E, 1425 m, 23.viii.2020, sifted, Zhong Peng leg.; **Hunan Prov.:** Yizhang County, Mangshan N. R.: 2 ♂♂, 1 ♀, Mengkengshi, 24°55'10"N, 112°58'37"E, 1625 m, 28.viii.2020, sifted, Zhong Peng leg.; 6 ♂♂, 5 ♀♀, Jiangjunzhai, 24°57'03"N, 112°55'37"E, 1220 m, 27.viii.2020, sifted, Zhong Peng leg. (SNUC).

Comparative notes. *Nazeris nanlingensis* is very similar to *N. rubidus* Hu, Luo & Li, 2018a from the same locality in general appearance and aedeagal characters, but can be separated by the smaller forebody size; less dense punctuation of the head and pronotum (Hu et al. 2018a: 177, fig. 14); a wider ventral process and slenderer dorso-lateral apophyses of the aedeagus in ventral view (Hu et al. 2018a: 177, fig. 17).

Distribution and habitat data. The species is known from Nanling in northern Guangdong and Mangshan in southern Hunan (Fig. 27). The specimens were collected by sifting leaf litter at altitudes of 1100–1850 m.

***Nazeris obtortus* Assing, 2016**

Fig. 27

Non-type material examined. CHINA: **Guangxi Prov.:** Guilin, Huaping N. R.: 1 ♂, 3 ♀♀, Hongtan, 25°36'15"N, 109°57'35"E, 820–950 m, 24.iv.2021, sifted, Yin, Zhang, Pan and Shen leg. (SNUC).

Comparative notes. *Nazeris obtortus* is quite similar to *N. huapingensis* and separated only by aedeagal characters: the apex of the ventral process and apices of the dorso-lateral apophyses are much narrower (Assing 2016: 309, fig. 16).

Distribution and habitat data. The species is known only from Huaping in northeast Guangxi (Fig. 27). The specimens were collected by sifting leaf litter at altitudes of 820–1200 m.

***Nazeris rubidus* Hu, Luo & Li, 2018**

Fig. 27

Non-type material examined. CHINA: **Guangdong Prov.:** Shaoguan, Nanling N. R.: 5 ♂♂, 7 ♀♀, 24°56'38"N, 112°59'31"E, 1316–1575 m, 29.vi.2020, Xia, Zhang, Yin and Lin leg.; ♂♂, 43 ♀♀, 24°55'43.67"N, 113°0'58.50"E, 1,020 m, 27.vi.2020, Xia, Zhang, Yin and Lin leg.; 2 ♂♂, 5 ♀♀, Xiaohuangshan, 24°53'58"N, 113°01'27"E, 1425 m, 23.viii.2020, sifted, Zhong Peng leg. (SNUC).

Comparative notes. *Nazeris rubidus* is very similar to *N. huapingensis* in general appearance and aedeagal characters, but can be separated by the following combination of characters: the posterior excision of the male sternite VIII is wider (Hu et al. 2018a: 176, fig. 11); the apex of the ventral process of the aedeagus is widely rounded in ventral view (Hu et al. 2018a: 176, fig. 12); the dorso-lateral apophyses is nearly straight in lateral view (Hu et al. 2018a: 176, fig. 13).

Distribution and habitat data. The species is known from Nanling in northern Guangdong and Mangshan in southern Hunan (Fig. 27). The specimens were collected by sifted leaf litter at altitudes of 700–1820 m.

***Nazeris rugosus* Hu & Qiao, 2019**

Fig. 27

Non-type material examined. CHINA: **Guangxi Prov.:** Xing'an, Mao'ershan N. R.: 1 ♂, 25°51'57.56"N, 110°24'46.19"E, 2100 m, 5.v.2021, bamboo, broad-leaved bush, sifted, Yin, Zhang, Pan and Shen leg.; 1 ♂, Lijiangyuan, 25°53'32.64"N, 110°25'41.68"E, 1990–2030 m, 6.v.2021, sifted, Yin, Zhang, Pan and Shen leg. (SNUC).

Comparative notes. *Nazeris rugosus* is distinguished from all the known species of *Nazeris* from the Nanling Mountains by the microsculpture covering the head, pronotum and abdomen (Hu and Qiao 2019: 436, figs 18–20), and by the distinctive shape of the aedeagus, particularly the apically narrowed ventral process (Hu and Qiao 2019: 436, fig. 23).

Distribution and habitat data. The species is known only from Mao'ershan in northeast Guangxi (Fig. 27). The specimen was collected by sifting leaf litter at altitudes of 1990–2100 m.

***Nazeris yanzhuqii* Hu & Qiao, 2019**

Fig. 27

Non-type material examined. CHINA: **Guangxi Prov.:** Xing'an, Mao'ershan N. R.: 1 ♀, Lijiangyuan, 25°53'32.64"N, 110°25'41.68"E, 1990–2030 m, 6.v.2021, sifted, Yin, Zhang, Pan and Shen leg. (SNUC).

Comparative notes. *Nazeris yanzhuqii* is most similar to *N. alatus* in general appearance and aedeagal characters, but can be separated by the impunctate elevation of the pronotum very narrow or absent (Hu and Qiao 2019: 438, fig. 35), by the longer and wider ventral process of the aedeagus in ventral view, with much smaller basal laminae, and by the wider dorso-lateral apophyses of the aedeagus (Hu and Qiao 2019: 438, fig. 38).

Distribution and habitat data. The species is known only from Mao'ershan in northeast Guangxi (Fig. 27). The specimen was collected by sifting leaf litter at altitudes of 1940–2140 m.

***Nazeris yuyimingi* Hu & Qiao, 2019**

Fig. 27

Non-type material examined. CHINA: **Guangxi Prov.:** Xing'an, Mao'ershan N. R.: 1 ♀, nr. Antangping, 25°54'44.07"N, 110°27'37.68"E, 1660 m, 7.v.2021, sifted, Yin, Zhang, Pan and Shen leg. (SNUC).

Comparative notes. *Nazeris yuyimingi* is similar in general appearance and aedeagal characters to *N. chenyanae* Hu & Li, 2017, but can be separated by the shallowly emarginate male sternite VII (Hu and Qiao 2019: 437, fig. 26), by the narrower ventral process and the wider apex of the dorso-lateral apophyses of the aedeagus in ventral view (Hu and Qiao 2019: 437, fig. 28).

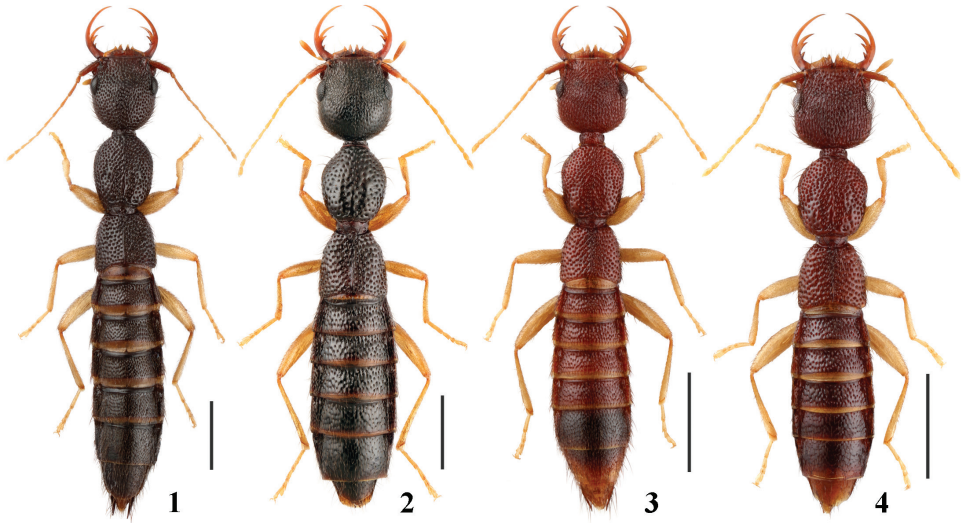
Distribution and habitat data. The species is known only from Mao'ershan in northeast Guangxi (Fig. 27). The specimen was collected by sifting leaf litter at altitudes of 1143–1660 m.

***Nazeris xingmini* Lin & Hu, sp. nov.**

<http://zoobank.org/C2BCCA84-E6E7-430C-BEE6-D7A6FA183751>

Figs 1, 5–9, 27

Type material. **Holotype:** CHINA: ♂: “China: Guangdong Prov., Shixing County, Chebaling N. R., 24°43'22"N, 114°15'22"E, 357 m, 19.viii.2020, Liang Tang leg.”



Figures 1–4. Male habitus of *Nazeris* spp **1** *N. xingmini* **2** *N. huaiweni* **3** *N. meihuaae* **4** *N. lichongi*. Scale bars: 1.0 mm.

(SNUC). **Paratypes:** 1 ♂, same data as holotype; 1 ♂, 2 ♀♀, “China: Jiangxi Prov., Longnan County, Jiulianshan N. R., 24°30'59.23"N, 114°24'52.98"E, alt. 587 m, 16.viii.2020, Liang Tang leg.” (SNUC).

Description. Body length 6.4–7.5 mm; forebody length 3.2–3.4 mm.

Body (Fig. 1) dark brown; legs yellowish brown; antennae dark brown to light brown.

Head (Fig. 5) 1.02–1.12 times as long as wide; punctuation very dense, moderately coarse, non-umbilicate, interstices lacking microsculpture; postocular portion approximately 1.6–2.1 times as long as eye length.

Pronotum (Fig. 5) 1.18–1.22 times as long as wide, 0.95–1.02 times as long and 0.83–0.91 times as broad as head; punctuation non-umbilicate, moderately dense and as coarse as that of head; midline posteriorly with short and very narrow impunctate elevation; interstices lacking microsculpture.

Elytra (Fig. 5) 0.59–0.67 times as long as wide, 0.50–0.57 times as long and 0.96–1.09 times as broad as pronotum; punctuation as dense as, and slightly coarser than that of pronotum; interstices lacking microsculpture.

Abdomen with punctuation dense and rather coarse on tergites III–V, dense and less coarse on tergite VI, moderately dense and fine on tergites VII–VIII; interstices lacking microsculpture.

Male. Sternite VII (Fig. 6) with posterior margin truncate at middle. Sternite VIII (Fig. 7) with wide triangular posterior excision. Aedeagus (Figs 8, 9) well sclerotized; with ventral process narrowed near middle in ventral view, with U-shaped excision at apex in ventral view, with pair of wing-like basal laminae ventrally; dorso-lateral apophyses moderately strong, distinctly curved in ventral view, curved dorsally and slightly widened at apices in lateral view, extending beyond apex of ventral process.

Distribution and habitat data. The species is known from Chebaling in northern Guangdong and Jiulianshan in southern Jiangxi (Fig. 27). The specimens were collected by sifting leaf litter at altitudes of 357–587 m.

Comparative notes. The new species is very similar to *N. inaequalis* Assing, 2014 in general appearance and separated only by the aedeagal characters: the apex of the ventral process is symmetric in ventral view (Fig. 8); dorso-lateral apophyses extending beyond the apex of the ventral process.

Etymology. The species is named in honor of Xing-Min Wang (South China Agricultural University) who helped a lot during our collection in Nanling.

***Nazeris huaiweni* Lin & Hu, sp. nov.**

<http://zoobank.org/2C276CF2-9719-40ED-A290-B50052066D15>

Figs 2, 10–14, 27

Type material. Holotype: CHINA: ♂: “China: Guangdong, Shaoguan, Nanling N. R., 24°56'38"N, 112°59'31"E, 1316–1575 m, 29.vi.2020, Xia, Zhang, Yin and Lin leg.” (SNUC). **Paratypes:** 2 ♀♀, same data, except “Ruyuan, Nanling, nr. Ruyang, Xiaohuangshan, 24°53'44.7"N, 113°1'26.9"E, 1270–1570 m, 2021.v.02, Hu, Lin, Zhou and Li leg.” (SNUC).

Description. Body length 6.2–6.8 mm; forebody length 3.2–3.3 mm.

Body (Fig. 2) dark brown; antennae and legs yellowish brown.

Head (Fig. 10) approximately as long as wide; punctation very dense, moderately coarse, distinctly umbilicate, interstices lacking microsculpture; postocular portion approximately twice as long as eye length.

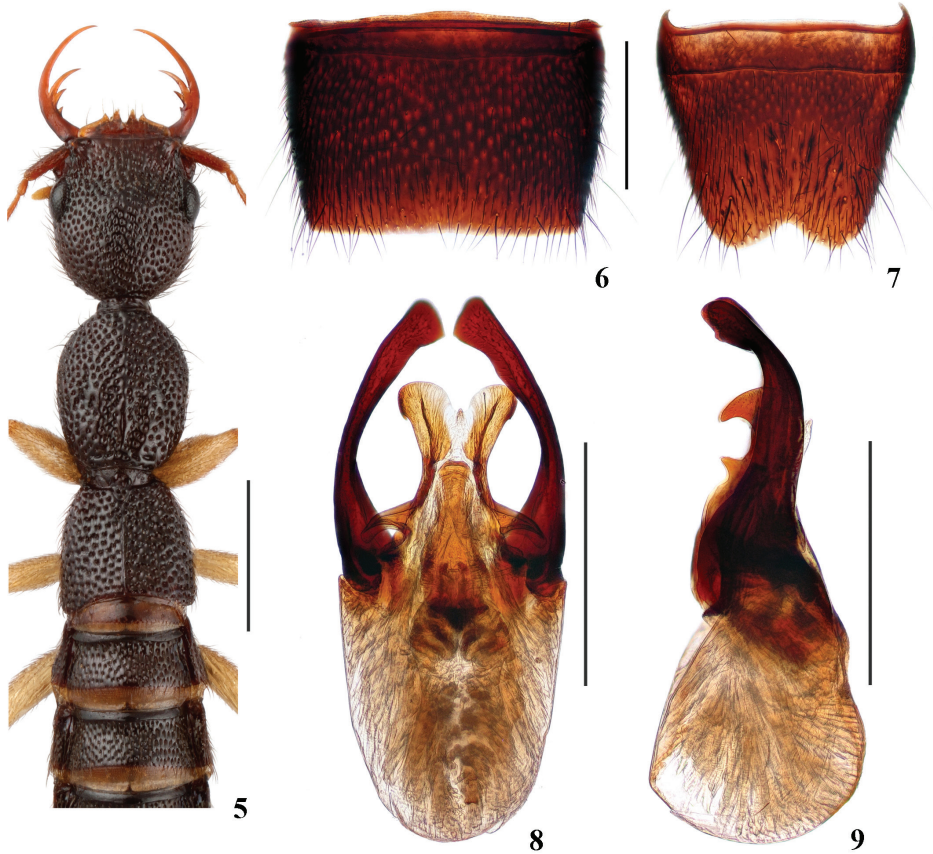
Pronotum (Fig. 10) 1.12–1.21 times as long as wide, 0.93–1.02 times as long and 0.83–0.84 times as broad as head; punctation non-umbilicate, moderately dense and as coarse as that of head; midline posteriorly with short and very narrow impunctate elevation; interstices lacking microsculpture.

Elytra (Fig. 10) 0.67–0.76 times as long as wide, 0.69–0.71 times as long and 1.03–1.12 times as broad as pronotum; punctation slightly denser and coarser than that of pronotum; interstices lacking microsculpture.

Abdomen with punctation dense and rather coarse on tergites III–V, dense and less coarse on tergite VI, moderately dense and fine on tergites VII–VIII; interstices lacking microsculpture.

Male. Sternite VII (Fig. 11) with posterior margin truncate at middle. Sternite VIII (Fig. 12) with triangular posterior excision. Aedeagus (Figs 13, 14) with ventral process gradually narrowed in apical half, with acute apex in ventral view or lateral view, with pair of wing-like basal laminae ventrally; dorso-lateral apophyses moderately slender, slightly widened near middle and apices in ventral view, not reaching apex of ventral process.

Distribution and habitat data. The species is known only from Nanling in northern Guangdong (Fig. 27). The specimens were collected by sifted leaf litter at altitudes of 1270–1575 m.



Figures 5–9. *Nazeris xingmini* **5** forebody **6** male sternite VII **7** male sternite VIII **8** aedeagus in ventral view **9** aedeagus in lateral view. Scale bars: 1.0 mm (**5**); 0.5 mm (**6–9**).

Comparative notes. The new species is very similar to *N. divisus* Hu & Li, 2015 in general appearance, but can be separated by the wider and shallower posterior excision of male sternite VIII (Fig. 12), by the ventral process with acute apex (Fig. 13), and by the wider dorso-lateral apophyses of aedeagus (Fig. 13).

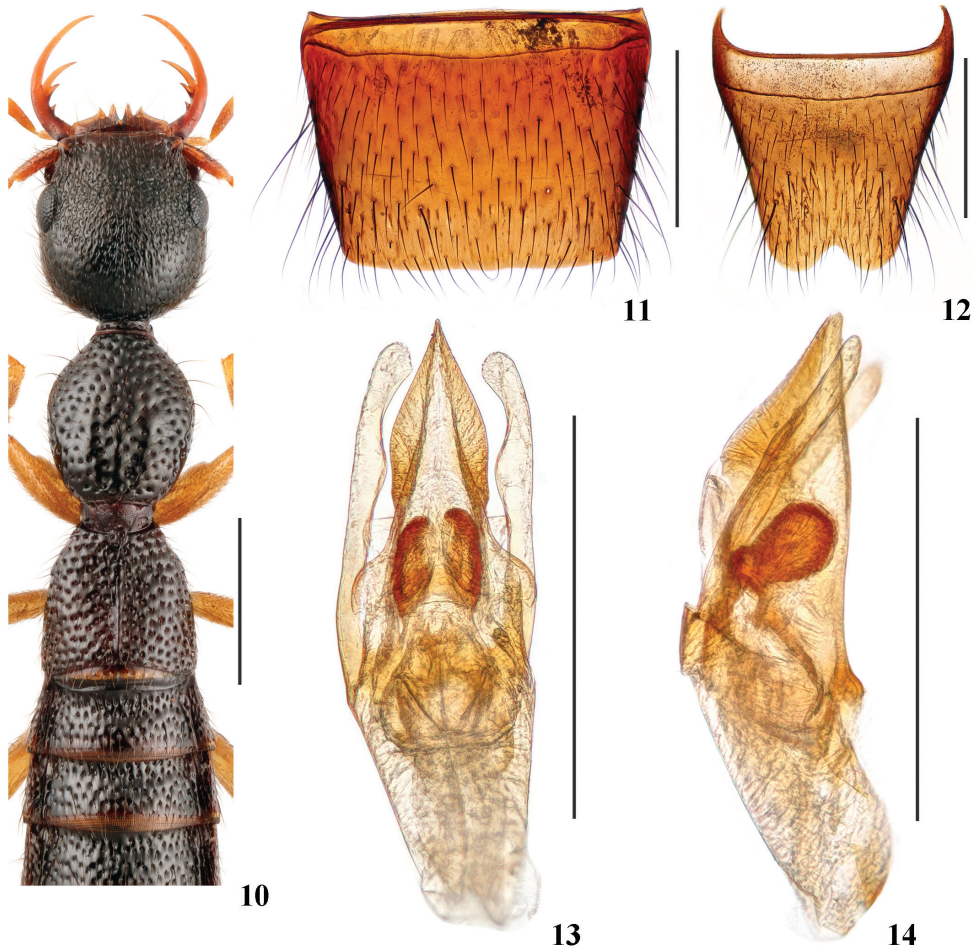
Etymology. The species is named in honor of Huai-Wen Wang (Administration of Nanling National Nature Reserve) who helped a lot during our collection in Nanling.

***Nazeris meihuaae* Lin & Hu, sp. nov.**

<http://zoobank.org/B62BB393-C4B6-41EE-96A7-2B3E49F0C50A>

Figs 3, 15–21, 27

Type material. **Holotype:** CHINA: ♂: “China: Guangdong Prov., Shixing County, Chebaling N. R., 24°40'41.82"N, 114°10'20.42"E, 1067 m, 20.viii.2020, Liang Tang leg.” (SNUC). **Paratypes:** 5 ♂♂, 18 ♀♀, same data as holotype; 3 ♂♂, 8 ♀♀, same data, except “872 m, 20.viii.2020”; 2 ♀♀, “China: Guangdong Prov., Shixing County, Chebaling

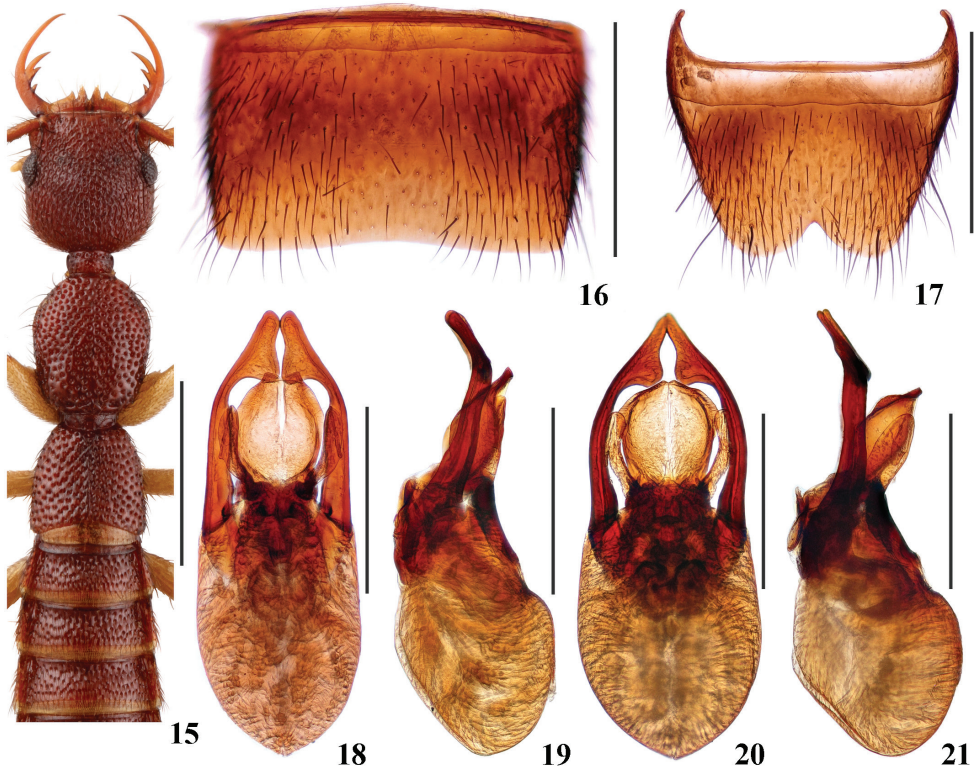


Figures 10–14. *Nazeris huaiweni* **10** forebody **11** male sternite VII **12** male sternite VIII **13** aedeagus in ventral view **14** aedeagus in lateral view. Scale bars: 1.0 mm (**10**); 0.5 mm (**11–14**).

N. R., 24°40'58"N, 114°10'14"E, 468–870 m, 24.vi.2020, Xia, Zhang, Yin and Lin leg.”; 6 ♂♂, 3 ♀♀, “China: Jiangxi Prov., Longnan County, Jiulianshan N. R., 24°30'10"N, 114°26'35"E, 795 m, 18.viii.2020, Liang Tang leg.”; 1 ♂, 2 ♀♀, “China: Jiangxi Prov., Longnan County, Jiulianshan N. R., 24°30'10.43"N, 114°26'35.28"E, leaf litter, sifted, 1253 m, 17.viii.2020, Liang Tang leg.”; 5 ♂♂, 1 ♀, “China: Jiangxi Prov., Longnan County, Jiulianshan, Huangniushi, 24°31'22.7"N, 114°25'3.6"E, 600–1000 m, 10.v.2021, C.-L. Zhou & C. Li leg.”; 3 ♀♀, “China: Jiangxi Prov., Longnan County, Jiulianshan, summit of Huangniushi, 24°30'53"N, 114°26'6.72"E, 1000–1230 m, 12.v.2021, Zhou and Li leg.”; 1 ♂, “China: Jiangxi Prov., Longnan County, Jiulianshan, summit of Huangniushi, 24°30'53"N, 114°26'6.72"E, 1,000–1,230 m, 12.v.2021, Zhou and Li leg.” (SNUC).

Description. Body length 4.1–4.8 mm; forebody length 2.2–2.6 mm.

Body (Fig. 3) reddish brown; antennae and legs yellowish brown.



Figures 15–21. *Nazeris meihuuae* (15–19 specimen from Chebaling 20–21 specimen from Jiulianshan) 15 forebody 16 male sternite VII 17 male sternite VIII 18, 20 aedeagus in ventral view 19, 21 aedeagus in lateral view. Scale bars: 1.0 mm (15); 0.5 mm (16–21).

Head (Fig. 15) 0.97–1.03 times as long as wide; punctuation very dense, moderately coarse, distinctly umbilicate and partly confluent, interstices lacking microsculpture; postocular portion approximately 1.5–2.1 times as long as eye length.

Pronotum (Fig. 15) 1.05–1.23 times as long as wide, 0.91–1.10 times as long and 0.83–0.87 times as broad as head; punctuation non-umbilicate, moderately dense and as coarse as that of head; midline posteriorly with short and very narrow impunctate elevation; interstices lacking microsculpture.

Elytra (Fig. 15) 0.61–0.75 times as long as wide, 0.54–0.66 times as long and 0.97–1.10 times as broad as pronotum; punctuation as dense as, and slightly coarser than that of pronotum; interstices lacking microsculpture.

Abdomen with punctuation dense and rather coarse on tergites III–V, dense and less coarse on tergite VI, moderately dense and fine on tergites VII–VIII; interstices lacking microsculpture.

Male. Sternite VII (Fig. 16) with posterior margin shallowly emarginate in the middle. Sternite VIII (Fig. 17) with wide triangular posterior excision. Aedeagus (Figs 18–21) with ventral process short, widened near middle in ventral view, with pair of

finger-like basal laminae ventrally; dorso-lateral apophyses distinctly curved and widened in apical third in ventral view, extending beyond apex of ventral process.

Distribution and habitat data. The species is known from Chebaling in northern Guangdong and Jiulianshan in southern Jiangxi (Fig. 27). The specimens were collected by sifting leaf litter at altitudes of 468–1253 m.

Comparative notes. This species is very similar in general appearance and aedeagal characters to *N. pengzhongi* Hu & Li, 2015, but can be separated by the finger-like basal laminae of the ventral process and the longer dorso-lateral apophyses of the aedeagus (Figs 18, 20). The new species is also similar in general appearance to *N. rubidus* and *N. nanlingensis*, but can be separated by the distinctly longer laminae of the ventral process and the apically wider dorso-lateral apophyses of the aedeagus (Figs 18, 20). Compared with the holotype from Chebaling, Guangdong (Figs 18, 19), the specimens from Jiulianshan, Jiangxi (Figs 20, 21) display a slightly shorter ventral process and slightly narrower apices of the dorso-lateral apophyses of the aedeagus. Based on the similar general appearance and male sternites, these aedeagal differences are treated as intraspecific variation.

Etymology. The species is named in honor of Mei-Hua Xia, who collected some of the type specimens.

***Nazeris lichongi* Lin & Hu, sp. nov.**

<http://zoobank.org/8DFC4E1C-104B-47C5-9511-5CB6B1C0662D>

Figs 4, 22–27

Type material. Holotype: CHINA: ♂: “China: Hunan Prov., Yongzhou County, Dupangling N. R., 25°26'12.45"N, 111°20'23.29"E, 448 m, 29.viii.2020, sifted, Chong Li leg.” (SNUC).

Description. Body length 4.7 mm; forebody length 2.4 mm.

Body (Fig. 4) reddish brown; antennae and legs yellowish brown.

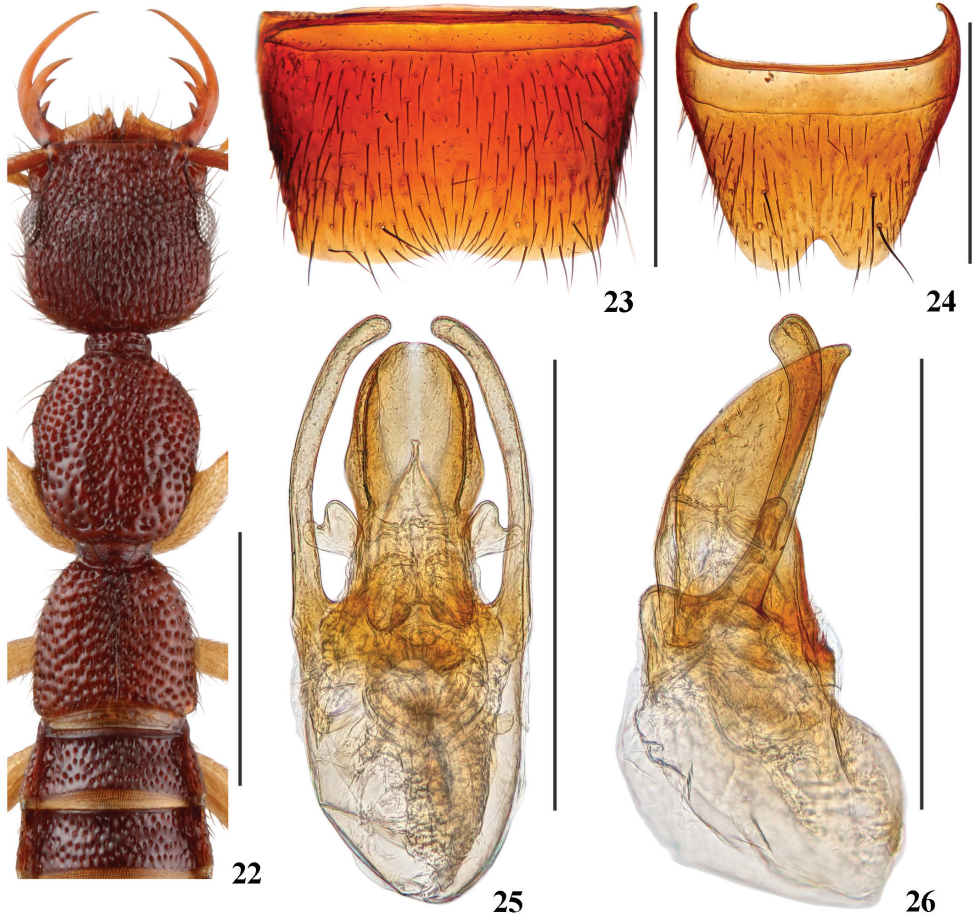
Head (Fig. 22) 0.97 times as long as wide; punctation very dense, moderately coarse, distinctly umbilicate and partly confluent, interstices lacking microsculpture; postocular portion approximately 1.6 times as long as eye length.

Pronotum (Fig. 22) 1.17 times as long as wide, as long as and 0.83 times as broad as head; punctation non-umbilicate, moderately dense and as coarse as that of head; midline posteriorly with short and very narrow impunctate elevation; interstices lacking microsculpture.

Elytra (Fig. 22) 0.77 times as long as wide, 0.66 times as long and as broad as pronotum; punctation as dense as, and slightly coarser than that of pronotum; interstices lacking microsculpture.

Abdomen with punctation dense and rather coarse on tergites III–V, dense and less coarse on tergite VI, moderately dense and fine on tergites VII–VIII; interstices lacking microsculpture.

Male. Sternite VII (Fig. 23) with posterior margin shallowly emarginate in the middle. Sternite VIII (Fig. 24) with triangular posterior excision. Aedeagus (Figs 25,



Figures 22–26. *Nazeris lichongi* **22** forebody **23** male sternite VII **24** male sternite VIII **25** aedeagus in ventral view **26** aedeagus in lateral view. Scale bars: 1.0 mm (**22**); 0.5 mm (**23–26**).

26) with broad ventral process, slightly widened in apical half, with round apex in ventral view, with pair of heart-like basal laminae; dorso-lateral apophyses slender, distinctly curved in ventral view, curved dorsally and slightly widened at apices in lateral view, extending beyond apex of ventral process.

Distribution and habitat data. The species is known only from Dupangling in southern Hunan (Fig. 27). The specimen was collected by sifting leaf litter at an altitude of 448 m.

The new species is similar in general appearance and aedeagal characters to *N. rubidus* and *N. nanlingensis*, but can be separated by the slightly dorsally curved dorso-lateral apophyses of the aedeagus in lateral view (Fig. 26), and by the heart-like basal laminae of the ventral process (Fig. 25).

Etymology. The species is named in honor of Chong Li, who collected some of the type specimens.

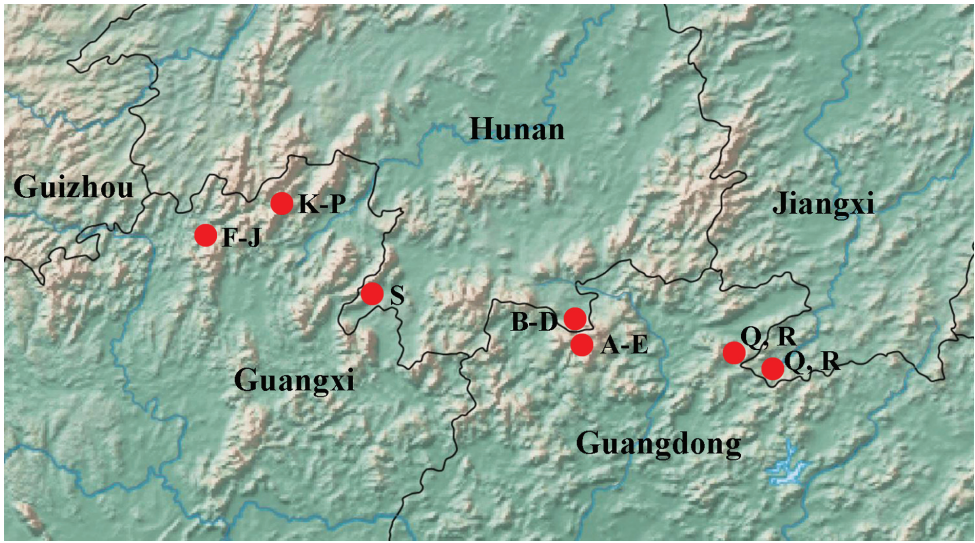


Figure 27. Map showing the distribution of *Nazeris* in Nanling Mountain Range **A** *N. inaequalis* **B** *N. rubidus* **C** *N. nanlingensis* **D** *N. gaoleii* **E** *N. huaiweni* **F** *N. obtortus* **G** *N. huapingensis* **H** *N. alatus* **I** *N. exilis* **J** *N. chenyanae* **K** *N. latilobatus* **L** *N. maoershanus* **M** *N. rugosus* **N** *N. yuyimingi* **O** *N. biacuminatus* **P** *N. yanzhuqii* **Q** *N. xingmini* **R** *N. meihuuae* **S** *N. lichongi*.

Key to *Nazeris* species in Nanling mountain range

- 1 Head with non-umbilicate punctation (Fig. 5).....2
- Head with umbilicate punctation (Fig. 15)6
- 2 Body reddish brown, abdomen with fine microsculpture on all tergites
..... *N. gaoleii* **Hu Luo & Li, 2018**
- Body dark brown, abdomen lacking microsculpture3
- 3 Pronotum with inconspicuous or lacking impunctate elevation in posterior half (Hu and Qiao 2019: 440, fig. 35); forebody length at most 2.9 mm.....
..... *N. yanzhuqii* **Hu & Qiao, 2019**
- Pronotum with narrow impunctate elevation in posterior half (Fig. 5); forebody length at least 3.1 mm.....4
- 4 Ventral process of the aedeagus distinctly asymmetrical, dorso-lateral apophyses not reaching apex of ventral process (Assing, 2014: 26, fig. 58)
..... *N. inaequalis* **Assing, 2014**
- Ventral process of the aedeagus symmetrical, dorso-lateral apophyses extending beyond apex of ventral process5
- 5 Dorso-lateral apophyses of aedeagus moderately strong, with widened apex (Figs 8, 9) *N. xingmini* **sp. nov.**
- Dorso-lateral apophyses of aedeagus slender, with acute apex (Hu and Li 2017: 337, figs 18, 19)..... *N. alatus* **Hu & Li, 2017**

6 Body dark brown (Figs 1, 2), body length at least 6.1 mm, forebody length at least 3.2 mm 7

– Body reddish brown (Figs 3, 4), body length at most 6.0 mm, forebody length at most 3.0 mm 11

7 Apex of ventral process of aedeagus divided into two branches in ventral view (Hu and Li 2017: 338, fig. 23) 8

– Apex of ventral process of aedeagus not divided into two branches in ventral view 9

8 Sternite VII with posterior margin weakly protruding at middle (Hu and Li 2017: 338, fig. 21); ventral process of aedeagus with thin apical branches (Hu and Li 2017: 338, figs 23, 24); dorso-lateral apophyses of aedeagus slightly curved in lateral view (Hu and Li 2017: 338, fig. 24) ***N. exilis* Hu & Li, 2017**

– Sternite VII with posterior margin truncate at middle (Hu and Qiao 2019: 438, fig. 31); ventral process of aedeagus with wide apical branches (Hu and Qiao 2019: 438, figs 33, 34); dorso-lateral apophyses of aedeagus straight in lateral view (Hu and Qiao 2019: 438, fig. 34) ***N. biacuminatus* Hu & Qiao, 2019**

9 Sternite VIII with rounded triangular posterior excision (Fig. 12); dorso-lateral apophyses of aedeagus not reaching apex of ventral process (Fig. 13)..... ***N. huaiweni* sp. nov.**

– Sternite VIII with sharp, V-shaped posterior excision (Hu and Qiao 2019: 437, fig. 27); dorso-lateral apophyses of aedeagus extending slightly beyond apex of ventral process (Hu and Qiao 2019: 437, fig. 28) 10

10 Male sternite VII shallowly emarginate in the middle (Hu and Qiao 2019: 437, fig. 26); dorso-lateral apophyses of aedeagus widened near apex in ventral view (Hu and Qiao 2019: 437, fig. 28) ***N. yuyimingi* Hu & Qiao, 2019**

– Male sternite VII not emarginate in the middle (Hu and Li 2017: 340, fig. 26); dorso-lateral apophyses of aedeagus not widened near apices in ventral view (Hu and Li 2017: 340, fig. 28) ***N. chenyanae* Hu & Li, 2017**

11 Head and pronotum with fine microsculpture (Hu and Qiao 2019: 436, figs 18, 19)..... ***N. rugosus* Hu & Qiao, 2019**

– Head and pronotum lacking microsculpture..... 12

12 Dorso-lateral apophyses of aedeagus extending to same level as apex of ventral process (Hu and Qiao 2019: 434, fig. 10)..... ***N. latilobatus* Assing, 2016**

– Dorso-lateral apophyses of aedeagus extending distinctly beyond apex of ventral process..... 13

13 Ventral process of aedeagus nearly triangular, with narrow apex in ventral view (Assing 2016: 309, fig. 16)..... ***N. obtortus* Assing, 2016**

– Ventral process of aedeagus broad, with wide apex in ventral view 14

14 Basal laminae of ventral process of aedeagus very long, more than half length of ventral process (Figs 18, 20)..... ***N. meihuaae* sp. nov.**

– Basal laminae of ventral process of aedeagus very short, much less than half length of ventral process..... 15

- 15 Ventral process of aedeagus with round apex in ventral view **16**
 – Ventral process of aedeagus with truncate or emarginate apex in ventral view
 **17**
- 16 Dorso-lateral apophyses of aedeagus curved ventrally in lateral view (Hu et al.
 2018a: 176, fig. 13); ventral process with wing-like basal laminae (Hu et al.
 2018a: 176, fig. 12) ***N. rubidus* Hu, Luo & Li, 2018**
 – Dorso-lateral apophyses of aedeagus curved dorsally in lateral view (Fig. 26);
 ventral process with heart-like basal laminae (Fig. 25).....***N. lichongi* sp. nov.**
- 17 Ventral process of aedeagus in ventral view distinctly widened in apical half
 (Hu et al. 2018a: 177, fig. 17) ***N. nanlingensis* Hu, Luo & Li, 2018**
 – Ventral process of aedeagus in ventral view narrowed in apical half (Hu and
 Li 2017: 336, fig. 13)..... **18**
- 18 Apex of ventral process of aedeagus nearly truncate in ventral view (Hu and
 Li 2017: 336, fig. 13); apices of dorso-lateral apophyses roundly widened in
 ventral view (Hu and Li 2017: 336, fig. 13).....
 ***N. huapingensis* Hu & Li, 2017**
 – Apex of ventral process of aedeagus with small semi-circular emargination in
 ventral view (Hu and Qiao 2019: 435, fig. 15); apices of dorso-lateral apo-
 physes not widened in ventral view (Hu and Qiao 2019: 435, fig. 15).....
 ***N. maershanus* Hu & Qiao, 2019**

Acknowledgements

We thank Chong Li, Zhong Peng, Liang Tang, Mei-Hua Xia, Jia-Min Yin, Wen-Xuan Zhang and Cheng-Lin Zhou (Shanghai, China) for collecting specimens, and Xing-Min Wang (South China Agricultural University) and Huai-Wen Wang (Administration of Nanling National Nature Reserve) for assisting us during our trip to Nanling. We are also most grateful to two anonymous reviewers for their helpful comments on an earlier version of the manuscript.

References

- Assing V (2009) A revision of the Western Palaearctic species of *Nazeris* Fauvel, 1873 (Coleoptera: Staphylinidae: Paederinae). Deutsche Entomologische Zeitschrift 56(1): 109–131. <https://doi.org/10.1002/mmnd.200900010>
- Assing V (2014) A revision of *Nazeris*. IV. New species from China, Taiwan, and Thailand, and additional records (Coleoptera: Staphylinidae: Paederinae). Stuttgarter Beiträge zur Naturkunde A Neue Serie 7: 11–32.
- Assing V (2016) A revision of *Nazeris* VIII. Five new species from China and additional records (Coleoptera: Staphylinidae: Paederinae). Linzer Biologische Beiträge 48(1): 301–315.

- Fauvel A (1873) Faune Gallo-Rhénane ou species des insectes qui habitent la France, la Belgique, la Hollande, le Luxembourg, la Prusse Rhénane, la Nassau et la Valais avec tableaux synoptiques et planches gravées. Tome 3. Livraison 4. Le Blanc-Hardel, Caen, 215–390.
- Hu JY, Li LZ, Zhao MJ (2012) Six new species of *Nazeris* Fauvel (Coleoptera, Staphylinidae, Paederinae) from Guangxi, South China. *Zootaxa* 3399: 35–44. <https://doi.org/10.11646/zootaxa.3399.1.3>
- Hu JY, Li LZ (2015) The *Nazeris* fauna of the Luoxiao Mountain Range, China. (Coleoptera, Staphylinidae, Paederinae). *PLoS ONE* 10(7): 1–21. <https://doi.org/10.1371/journal.pone.0131942>
- Hu JY, Li LZ (2017) Four new species of *Nazeris* Fauvel in Guangxi, China (Coleoptera, Staphylinidae, Paederinae). *Zootaxa* 4312(2): 333–342. <https://doi.org/10.11646/zootaxa.4312.2.8>
- Hu JY, Luo YT, Li LZ (2018a) New species and record of *Nazeris* Fauvel in southern China (Coleoptera, Staphylinidae, Paederinae). *Zootaxa* 4429(1): 173–180. <https://doi.org/10.11646/zootaxa.4429.1.10>
- Hu JY, Liu YX, Li LZ (2018b) Two new species of *Nazeris* Fauvel in the Luoxiao Mountain Range, China (Coleoptera, Staphylinidae, Paederinae). *Zootaxa* 4370(2): 180–188. <https://doi.org/10.11646/zootaxa.4370.2.6>
- Hu JY, Qiao YJ (2019) Five new species of *Nazeris* Fauvel in Guangxi, China (Coleoptera, Staphylinidae, Paederinae). *Zootaxa* 4543(3): 431–441. <https://doi.org/10.11646/zootaxa.4543.3.8>

Scenopinus jerei, a new species of window fly (Diptera, Scenopinidae) from Finland

Jaakko Pohjoismäki¹, Antti Haarto²

¹ University of Eastern Finland, Department of Biology, P.O. Box 111, FI-80101 Joensuu, Finland ² Zoological Museum, Biodiversity Unit, University of Turku, FI-20014 Turku, Finland

Corresponding author: Jaakko Pohjoismäki (jaakko.pohjoismaki@uef.fi)

Academic editor: Davide Badano | Received 13 June 2021 | Accepted 10 August 2021 | Published 10 September 2021

<http://zoobank.org/1AC29987-58F7-4FC3-BFC9-1C4C7C90F2A0>

Citation: Pohjoismäki J, Haarto A (2021) *Scenopinus jerei*, a new species of window fly (Diptera, Scenopinidae) from Finland. ZooKeys 1059: 135–156. <https://doi.org/10.3897/zookeys.1059.70085>

Abstract

A new species of window fly (Diptera: Scenopinidae), *Scenopinus jerei* **sp. nov.**, with characteristic bi-coloured legs and completely black halteres, is described from Finland. To exclude potential previously named species, a survey of the relevant type specimens as well as original descriptions of the Palearctic and Nearctic *Scenopinus* species has been conducted, including old *Scenopinus fenestralis* (Linnaeus) synonyms. *Scenopinus jerei* **sp. nov.** is likely to be an overlooked, boreal forest specialist living in the nests of cavity-nesting birds. An identification key to the European species is provided.

Keywords

DNA barcoding, synonyms, taxonomy

Introduction

Window flies (Diptera: Scenopinidae) are a small family of primitive flies belonging to the therevoid clade of the Asiloidea superfamily (Winterton & Ware, 2015). The family has a cosmopolitan distribution, with more than 420 described species in 25 genera. Scenopinidae consists of three subfamilies, Caenotinae (1 genus), Proratinae (6

genera), and Scenopininae (18 genera) (Yeates 1992; Winterton and Gaimari 2017), with only the last one being present in Europe. For a more detailed description of the family and subfamilies, including their biology and classification see Winterton and Gaimari (2017). In total, 18 species have been known to occur in Europe (Kelsey 1969, 1981; Narchuk 1988; Carles-Tolrá 1999; Bystrowski et al. 2021): *Caenoneura nigra* Kelsey, 1969, *Scenopinus albicinctus* (Rossi, 1794), *S. bouvieri* (Seguy, 1921) (not listed in Fauna Europaea – see Kelsey 1969; Narchuk 1988), *S. bulbapennis* Kelsey, 1969, *S. canarius* Kelsey, 1969, *S. efflatouni* Kelsey, 1969, *S. fenestralis* (Linnaeus, 1758), *S. glabrifrons* Meigen, 1824, *S. gobiensis* Kelsey, 1981, *S. griseus* (Kröber, 1913), *S. halteralis* Frey, 1936, *S. lesinensis* Strobl, 1902, *S. niger* (De Geer, 1776), *S. oldenbergi* (Kröber) (not listed in Fauna Europaea – see Kelsey 1969; Narchuk 1988), *S. retuertensis* Carles-Tolra, 2001, *S. unifasciatus* (Krober, 1913), *S. verrucosus* Carles-Tolra, 2001, and *S. vitripennis* Meigen, 1824. In addition, *S. phaidimos* Kelsey, 1969 is present in Turkey and might be expected to occur in the eastern Mediterranean.

The greatest diversity of Scenopinidae is in the arid regions of the world (Winterton and Ware 2015), which is also reflected by the fact that the majority of the European species are present in the Mediterranean countries and Macaronesian islands. Only *Scenopinus fenestralis*, *S. glabrifrons*, *S. niger*, and *S. vitripennis* extend their range to central and northern Europe. Three species are known from Finland (Kahanpää et al. 2014), *Scenopinus fenestralis*, *S. niger*, and a relatively common, but previously unnamed species close to *S. fenestralis*. The unnamed species was originally reported as *S. vitripennis* (Haarto 2000), but a closer examination proved this to be a misidentification (Kahanpää and Winqvist 2005; Kahanpää et al. 2014).

In this paper we finally provide a formal description of the previously undescribed species as well as information about its distribution and biology. We focus on differentiating the species from *Scenopinus fenestralis* and *S. vitripennis*, as these are most likely to be confused with the new species due to the variability of all three species as well as because of the diagnostic characters used in older literature. We also compared it with written descriptions of other known species in the Holarctic and the old synonyms of *Scenopinus fenestralis* to rule out existing names for the candidate species. Finally, a key for the identification of the European *Scenopinus* species is provided.

Materials and methods

Material examined

Apart for the two old museum specimens of *Scenopinus vitripennis*, most of the examined material were collected relatively recently by the authors and their close associates. Except for the reared specimens, majority of the examples have been collected indoors (see notes) directly to vials and killed by freezing, ethyl acetate or potassium cyanide prior to mounting them on entomological pins.

Label data of newly collected specimens are given verbatim using the following symbols: / end of a line and beginning of the next; // end of label and beginning of the next (from top to bottom on the same pin). The specimens are deposited in the following collections and are indicated with the given acronym in the text:

- AHC** Private collection of Antti Haarto, Mynämäki, Finland
JPC Private collection of Jaakko Pohjoismäki, Joensuu, Finland
MIZ Museum and Institute of Zoology, Polish Academy of Sciences, Warszawa, Poland
MZH Finnish Museum of Natural History, Zoological Museum, University of Helsinki, Helsinki, Finland
MZT Zoological Museum of the University of Turku, Turku, Finland
SMNS Staatliches Museum für Naturkunde Stuttgart, Germany

Male terminalia were dissected and prepared for examination essentially as described by O'Hara (2002). The dissected terminalia are preserved in glycerol in a small plastic vial pinned together with the specimen. Location abbreviations refer to the geographical provinces (e.g., Kb = Karelia borealis, explained when mentioned for the first time, see <https://laji.fi/theme/emk> for more details) and coordinates (NNNN:EEEE) on the labels are mostly given in the old national Finnish map grid coordinate system (YKJ; see Ollikainen and Ollikainen 2004), which is still in common use for biological sampling. As the first number of the longitude coordinate is always 3, this is often left out in the collection labels to save space. Sampling coordinates in decimal degrees as well as additional notes or commentaries about the specimen are given in brackets.

Scenopinus fenestralis (Linnaeus, 1758)

Finland. (6♂♂, 8♀♀) 1♂(dissected): FENNIA Kb [Karelia borealis – north Karelia]: Liperi/ Kontkala 6950:3616 [62.6257, 29.3264]/ 19.7.2014/ Ali Karhu leg. [JPC]; 1♀: Same collection data [JPC, DNA barcoded JP01083]; 1♀: FINLAND, Kb: Ilomantsi/ Kelovaara 70008:36825 [63.0638, 30.6144]/ 25.6.2016/ J. Pohjoismäki leg. [JPC]; 1♀: FINLAND, Sa [Savonia australis – south Savo]: Taipalsaari/ Riihilahti 6778:3564 [61.1055, 28.1867]/ 21.7.2015/ J. Pohjoismäki leg. [JPC, DNA barcoded JP01084]; 1♂: FINLAND, Ta [Tavastia australis – south Häme]: Orivesi/ Siitama 6835:3354 [61.5946, 24.2496]/ 11.7.2009/ J. Pohjoismäki leg. [JPC]; 1♀: FINLAND, Ok [Ostrobothnia kajanensis – Kainuu region]: Sotkamo/ Laukkala, 7114:3565 [64.1192, 28.3340]/ 1.7.2005/ J. Pohjoismäki leg. [JPC]; 1♀: FINLAND, Ab [regio Aboensis – Turku region]: Mynämäki/ Perkko 6733:3222 [60.6105, 21.9209]/ 22.7.2011/ A. Haarto leg. [MZH, DNA barcoded, MZH_HP392]. 1♂: FINLAND, Ab: Mynämäki/ Perkko 6733:3222 [60.6105, 21.9209]/ 13.6.2009/ A. Haarto leg.// SCENOPINIDAE/ Scenopinus/ fenestralis (L.)/ det. A. Haarto 2009/ AHa09–000593 [MZT]; 1♀: FINLAND, Ab: Mietoinen/ Perkko

6733:[3]222 [60.6105, 21.9209]/ 17.7.2003/ A. Haarto leg.// SCENOPINIDAE/ Scenopinus/ fenestralis (L.)/ det. A. Haarto 2008/ AHa08–001324 [AHC]; 1♀: FINLAND, Ab: Mietoinen/ Perkko 6733:[3]222 [60.6105, 21.9209]/ 17.7.2003/ A. Haarto leg.// SCENOPINIDAE/ Scenopinus/ fenestralis (L.)/ det. A. Haarto 2008/ AHa08–001324 [AHC]; 1♂: FINLAND, Ab: Mietoinen/ Perkko 6733: [3]222 [60.6105, 21.9209]/ / 16.5.2004/ A. Haarto leg.// SCENOPINIDAE/ Scenopinus/ fenestralis (L.)/ det. A. Haarto 2021/ AHa21–000589 [AHC]; 1♂: FINLAND, Ab: Mietoinen/ Perkko 6733: [3]222 [60.6105, 21.9209]/ 5.6.2004/ A. Haarto leg.// SCENOPINIDAE/ Scenopinus/ fenestralis (L.)/ det. A. Haarto 2021/ AHa21–000590 [MZT]; 1♂: FINLAND, EP [Etelä-Pohjanmaa]: Isokyrö/ Orisberg 6983: [3]265 [62.8744, 22.3795]/ 7.7.1999/ A. Haarto leg.// SCENOPINIDAE/ Scenopinus/ fenestralis (L.)/ det. A. Haarto 1999 [AHC]; 1♀: Same collection and determination data [AHC];

Scenopinus glabrifrons Meigen, 1824

Germany: 2♀♀: Germany/ Hessen, Friedberg/ Ockstadt 50.3319, 8.7208 [Geographic coordinate]/ 13.6.2010/ J. Pohjoismäki leg. [JPC]

Greece: 2♀♀: GR CRETE Chania/ Thymia 35.4106, 24.0440 [Geographic coordinate]/ 5.-6.vi.2019/ J. Pohjoismäki leg. [JPC]

Scenopinus jerei sp. nov.

Finland: 6♂♂, 4♀♀. See the type material below for details.

Scenopinus niger (De Geer, 1776)

Finland: (4♂♂, 7♀♀) 2♀♀: FINLAND, Sa: Kouvola, 674–679:347–350 [60.7686–61.2184, 26.4495–27.0000]/ e.l. 2018 ex *Strix aluco* nest box. / M. Mutanen leg. [JPC]; 1♂: FINLAND, Sa: Taipalsaari/ Riihilahti 6778:3564 [61.1055, 28.1867]/ 21.7.2015/ J. Pohjoismäki leg. [JPC, DNA barcoded, JP01085]; 1♀: FINLAND, Ta: Tampere/ Rantaperkiö 6822:3327 [61.4669, 23.7541] / 26.6.2009/ J. Pohjoismäki leg. [JPC]; 1♀: FINLAND, Ab: Mynämäki/ Perkko 6733:3222 [60.6105, 21.9209]/ 12.6.2011/ A. Haarto leg. [MZH, DNA barcoded, MZH_HP.185]; 1♀: FINLAND, V [Varsinais-Suomi]: Turku Hirvensalo/ Rauhala 6707:[3]233/ 22.5.1996/ A. Haarto leg.// SCENOPINIDAE/ Scenopinus/ niger (DeGeer)/ det. A. Haarto [AHC];]; 1♂: FINLAND, V: Turku Hirvensalo/ Rauhala 6707: [3]233 [60.3854, 22.1559]/ 7.6.1996/ A. Haarto leg.// SCENOPINIDAE/ Scenopinus/ niger (DeGeer)/ det. A. Haarto [AHC]; 1♂1♀: FINLAND, V: Turku Hirvensalo/ Rauhala 6707: [3]233 [60.3854, 22.1559]/ 7.6.1996/ A. Haarto leg.// SCENOPI- NIDAE/ Scenopinus/ niger (DeGeer)/ det. A. Haarto [MZT]; 1♂: FINLAND, Ab: Mynämäki/ Perkko 67333:32223 [60.6105, 21.9209]/ 22.5.2017/ A. Haarto leg.//

SCENOPINIDAE/ *Scenopinus/ niger* (De Geer)/ det. A. Haarto 2017/ AHa17–001063 [AHC]; 1♀: FINLAND, V: Kaarina/ Kuusisto Rövarholm/ 9.7.1998/ A. Haarto leg.// SCENOPINIDAE/ *Scenopinus/ niger* (De Geer)/ det. A. Haarto 2008/ AHa08–001326 [AHC].

***Scenopinus vitripennis* Meigen, 1824**

Germany: 1♂: *Scen. glabrifrons*/ Württbg Meig. ?/ v.Roser 1872 [handwritten]// *Scenopinus/ vitripennis* Meig./ det. L.P. Kelsey 1964 [SMNS]. Examined from high resolution photographs. See the discussion regarding the identity of this specimen.

Poland: 1♀: Warszawa [barely visible]/ 14.vii.1953 r./ leg. R. Trojan// *Omphrale* ♀/ *vitripennis* (Meig)/ P. Trojan det. 1954. [MIZ]. Examined from high resolution photographs.

Classification and terminology

The classification follows Herting and Dely-Draskovits (1993). The morphological terminology used in this study follows Cumming and Wood (2017), except for the features of male terminalia, where Winterton and Gaimari (2017) is used.

Microscopy and imaging

The images were taken with a Leica Z6APO stereomicroscope and a Leica DFC450c (5MPix) camera, MSV266 motorised focus and using the Leica Application Suite 4.6.0 software for Z-axis stacking. Images were cropped, colour- and contrast-enhanced but not manipulated otherwise.

DNA extraction, PCR, and sequencing

Cytochrome oxidase subunit 1 (*COI*) DNA barcoding was performed as a part of the Tachinidae project of Finnish Barcode of Life initiative (FinBoL). The 5'-terminal part of *COI* was amplified using the routine barcoding primers LepF1 and LepR1 (Hebert et al. 2004). The sample identifiers in the barcode of life database (BOLD) are given for each barcoded specimen.

Sequence comparisons and COI tree

Sequence comparisons were performed using MUSCLE alignment (Edgar 2004) and Bayesian inference phylogenetic tree generated using MrBayes 3.2. (Ronquist et al. 2012), applying GTR substitution model with gamma-distributed rate variation across sites and a proportion of invariable sites, and 1,000,000 MCMC generations. The tree was visualised using FigTree 1.4.4. (Rambaut 2009).

Results

We report here a new species of window flies, *Scenopinus jerei* sp. nov. from Finland based on the following material and diagnostic characters.

Scenopinus jerei sp. nov.

<http://zoobank.org/7BBF06EE-AA55-42A8-B2DF-88FC4640AFA0>

Figures 1A, B, 2, 3A, B, 4A, B, 4E, F

Type material. *Holotype* (1♂): FINLAND, Sa: Kouvola, 674–679:347–350 [60.7686–61.2184, 26.4495–27.0000] / e.l. 2018 ex *Strix aluco* nest box. / M. Mutanen leg. // *Scenopinus jerei* sp. nov. Pohjoismäki & Haarto 2021 / (Diptera: Scenopinidae) / J. Pohjoismäki det. // HOLOTYPE [red label] [MZH] **Paratypes:** 1♂ (dissected, DNA barcoded JP2020-S1), 1♀, same collection data; // *Scenopinus jerei* sp. nov. Pohjoismäki & Haarto 2021 / (Diptera: Scenopinidae) / J. Pohjoismäki det. // PARATYPE [yellow label] [MZH]; 1♂: FINLAND, EP: Isokyrö/ Orisberg 6983:3]265 [62.8744, 22.3795]/ 7.7.1999/ A. Haarto leg.// SCENOPINIDAE/ *Scenopinus vitripennis* Meig./ det. A. Haarto 1999// PARATYPE/ Diptera: Scenopinidae/ *Scenopinus jerei*/ Pohjoismäki & Haarto 2021 [red label] [AHC]; 1♂: FINLAND, ES [Etelä-Savo]: Rantasalmi/ Korhola 68720:3]5802 [61.9458, 28.5278] / 27.6.2006/ A. Haarto leg.// SCENOPINIDAE/ *Scenopinus*/ sp./ det. A. Haarto 2006// PARATYPE/ Diptera: Scenopinidae/ *Scenopinus jerei*/ Pohjoismäki & Haarto 2021 [red label] [AHC]; 2♂: FINLAND, Kb: Ilomantsi/ Kelovaara 70008:36826 [63.0638, 30.6144]/ 24.7.2021/ J. Pohjoismäki leg. // PARATYPE/ Diptera: Scenopinidae/ *Scenopinus jerei*/ Pohjoismäki & Haarto 2021 [yellow label] [JPC]; 1♀: FINLAND, ES: Rantasalmi/ Korhola 68720:5802 [61.9458, 28.5278]/ 29.6.2006/ A. Haarto leg.// SCENOPINIDAE/ *Scenopinus*/ sp./ det. A. Haarto 2006// PARATYPE/ Diptera: Scenopinidae/ *Scenopinus jerei*/ Pohjoismäki & Haarto 2021 [red label] [AHC]; 1♀: FINLAND, Kb: Liperi/ Viinijärvi 6951:3615 [62.6451, 29.2425] / e larva 2013/ Ali Karhu leg.// linnunpönttö [nest box]// SCENOPINIDAE/ *Scenopinus*/ sp./ det. A. Haarto 2014/ AHa14–000891// PARATYPE/ Diptera: Scenopinidae/ *Scenopinus jerei*/ Pohjoismäki & Haarto 2021 [red label] [AHC]; 1♀: FINLAND, Kb: Liperi/ Käsämä suo 6950:3619 [62.6349, 29.3197]/ 26.–28.6.2013/ Ali Karhu leg.// SCENOPINIDAE/ *Scenopinus*/ sp./ det. A. Haarto 2020/ AHa20–000473// PARATYPE/ Diptera: Scenopinidae/ *Scenopinus jerei*/ Pohjoismäki & Haarto 2021 [red label] [MZT].

Diagnosis. *Scenopinus jerei* sp. nov. belongs to the *S. fenestralis* group and is easily recognisable from the other species in this group based on the contrasting colour differences between the femora and the yellow to orange tibiae. The coxae as well as the knob of the halteres are always uniformly black or dark brown, similar to the colour of the thorax.

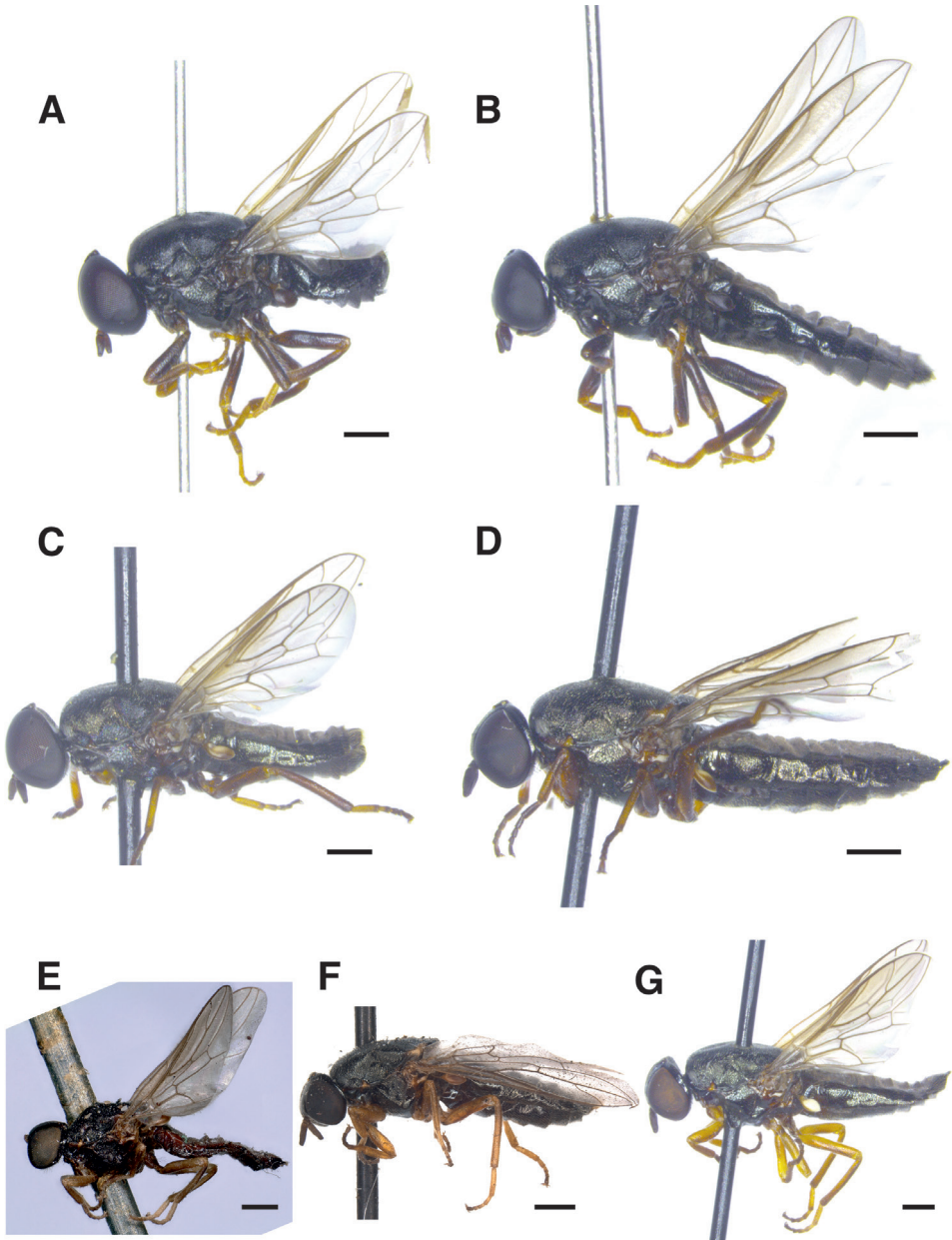


Figure 1. Habitus of northern European *Scenopinus fenestralis* group species of Scenopinidae **A** holotype male of *Scenopinus jerei* sp. nov., Kouvola, Finland **B** paratype female of *Scenopinus jerei* sp. nov., Kouvola, Finland **C** male of *Scenopinus fenestralis*, Liperi, Finland **D** female of *Scenopinus fenestralis*, Liperi, Finland **E** male of *Scenopinus vitripennis*, Württburg, Germany. Photograph by Susanne Leidenroth **F** female of *Scenopinus vitripennis*, Warszawa, Poland. Photograph by D. Schimroszyk **G** female of *Scenopinus glabri-frons*, Ockstadt, Germany. Scale bar: 500 μ m.

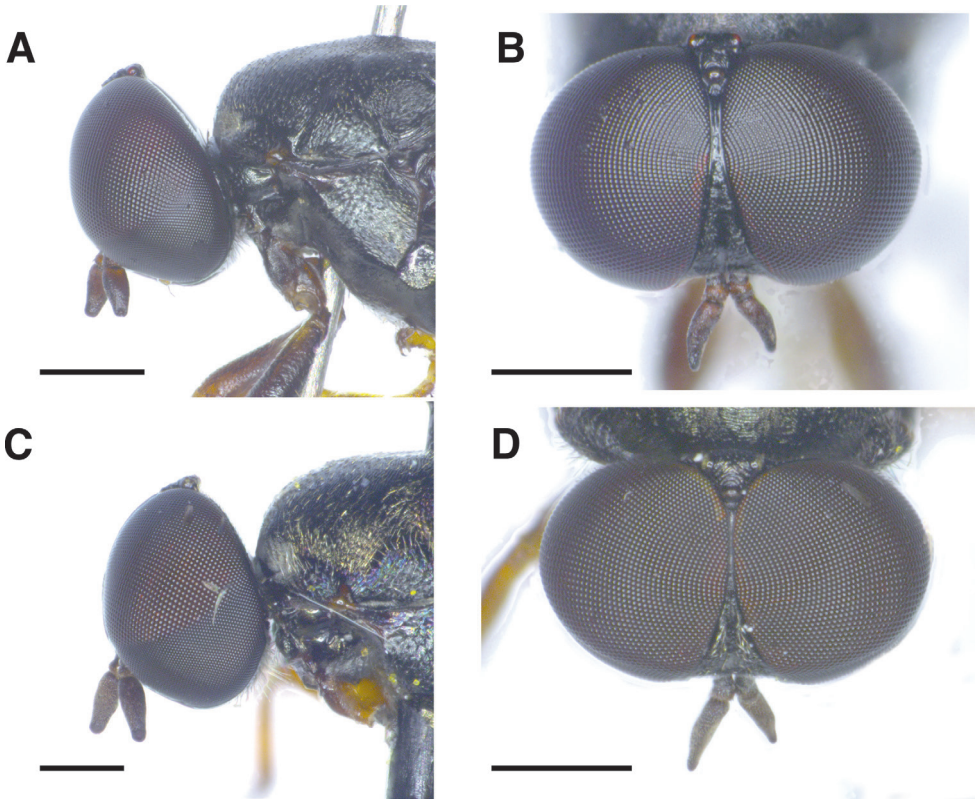


Figure 2. Male heads of *Scenopinus* species **A** lateral view of holotype *Scenopinus jerei* sp. nov., male head **B** frontal view of holotype *Scenopinus jerei* sp. nov., head **C** lateral view of *Scenopinus fenestralis* male head **D** frontal view of *Scenopinus fenestralis* male head. For the illustrations of male heads of *S. vitripennis* and *S. glabrifrons*, see Krivosheina (1981). Scale bar: 500 μ m.

Description. Male (Figs 1A; 2A, B; 4A, B, F, G) (characters in square brackets refer to the holotype). Body length: [4.1]–4.9 mm ($n = 6$) [dried specimens, fresh specimens are longer].

Head (Fig. 2A, B). Black with greasy-looking shine, including oral margin and occiput, apart from weak grey microtomentum around occipital foramen, mouth edge and antennal base; semi-circular, height 1.5–1.7 [1.6] ($n = 6$) \times its maximum width in lateral view. Antennal insertion slightly below mid eye level. Antenna dark brown with pedicel and anterior part of flagellomere paler; scape short and subrectangular; pedicel short and cylindrical, [0.8]–1.0 ($n = 6$) \times as long as wide, flagellomere laterally flattened, 1.8[1.9]–2.0 \times as long as high, subrectangular, narrowing apically and 4.8–[5.4] ($n = 6$) \times as long as pedicel and with subcircular, subapical, sensory pore on outer side. Eyes large and bare; fronto-orbital plates meeting at [0.25]–0.3 ($n = 6$) length of frons; no frontal vitta; gena reduced to narrow strip between lower eye margin and mouth edge. Diameter of ommatidia on upper half of compound eye, above antennal base, 2–3 \times diameter of ommatidia on lower half. Ocellar triangle acute, distance between posterior ocelli distinctly shorter than their distance to anterior ocellus. Frons bare but

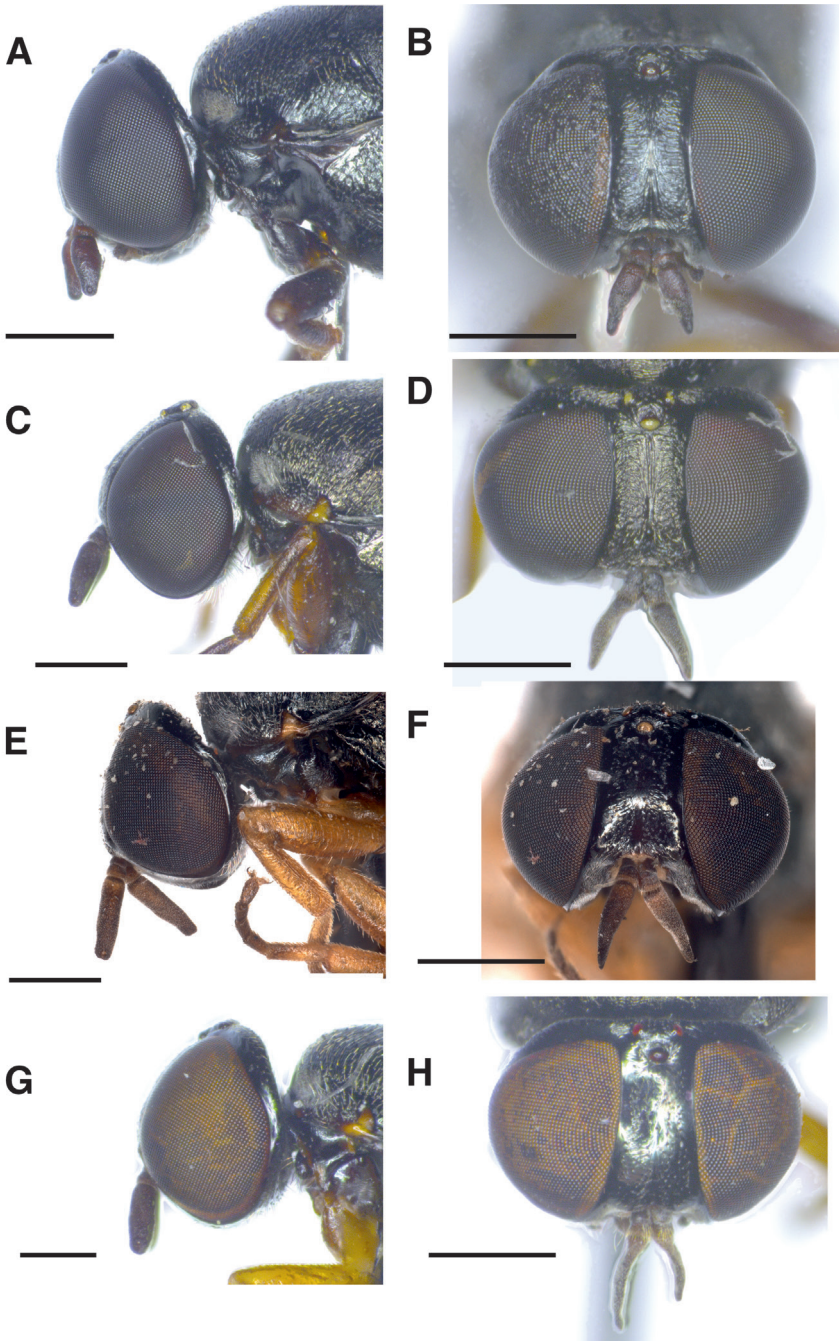


Figure 3. Female heads of *Scenopinus* species **A** lateral view of paratype *Scenopinus jerei* sp. nov., female head **B** frontal view of paratype *Scenopinus jerei* sp. nov., head **C** lateral view of *Scenopinus fenestralis* female head **D** frontal view of *Scenopinus fenestralis* female head **E** lateral view of *Scenopinus vitripennis* female head. Photograph D. Schimroszczyk **F** frontal view of *Scenopinus vitripennis* female head. Photograph D. Schimroszczyk **G** lateral view of *Scenopinus glabrifrons* female head **H** frontal view of *Scenopinus glabrifrons* female head. Scale bar: 500 μ m.

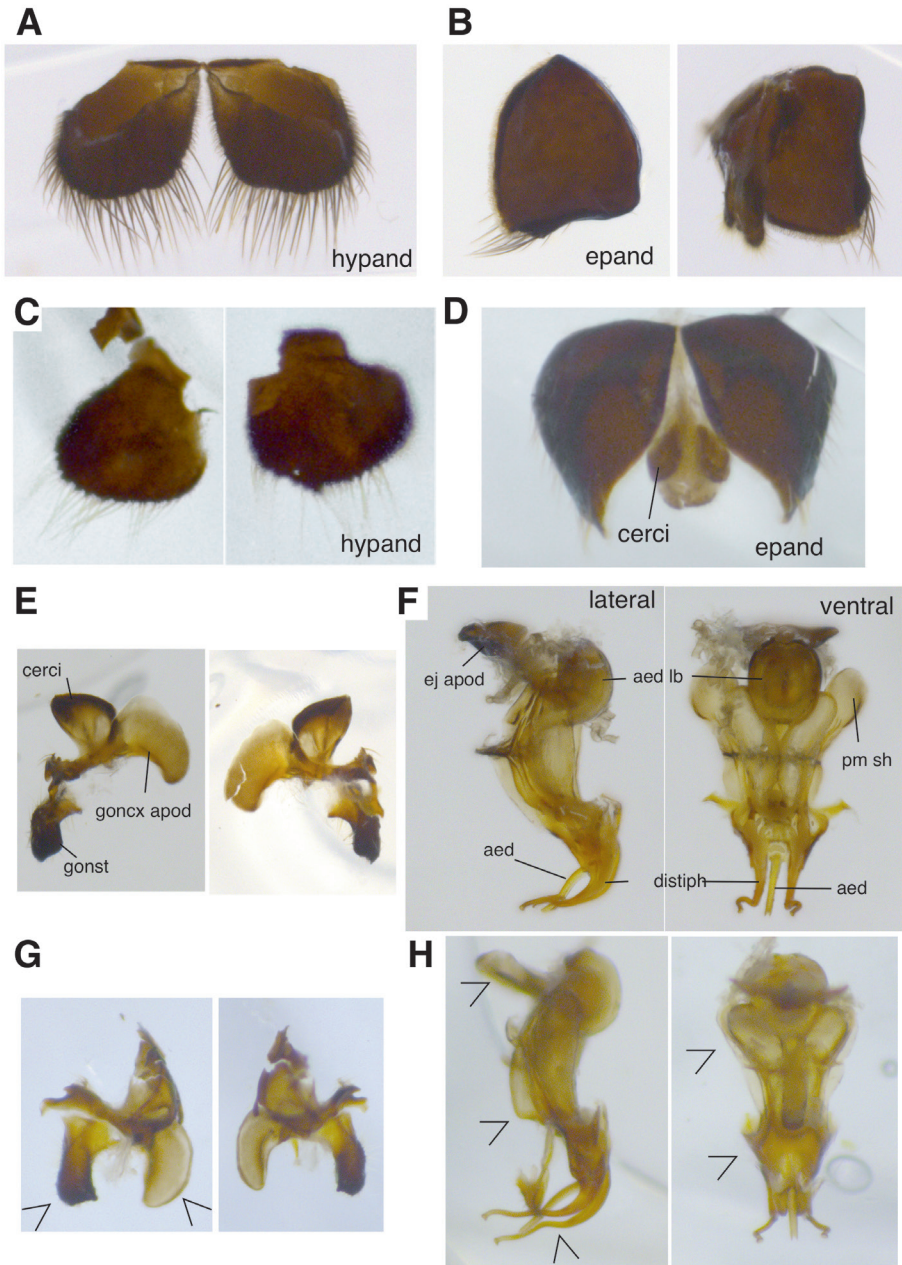


Figure 4. *Scenopinus* male terminalia **A** hypandrium of *Scenopinus jerei* sp. nov. paratype **B** epandrium of *Scenopinus jerei* sp. nov. paratype **C** hypandrium of *Scenopinus fenestralis* **D** epandrium of *Scenopinus fenestralis* **E** terminal segments of *Scenopinus jerei* sp. nov. paratype **F** aedeagus of *Scenopinus jerei* sp. nov. paratype **G** terminal segments of *Scenopinus fenestralis* **H** aedeagus of *Scenopinus fenestralis*. *aed* – aedeagus; *aed lb* – aedeagal lobe; *distiph* – distiphallus; *ej apod* – ejaculatory apodeme; *epand* – epandrium; *goncx apod* – gonocoxal apodeme; *gonst* – gonostylus; *hypand* – hypandrium; *pm sh* – parameral sheath. For the illustrations of male terminalia of *S. vitripennis* and *S. glabrifrons*, see Krivosheina (1981).

patterned with minute pits. No setae or setulae on head, apart for short brown setulae at lower posterior part of gena behind mouth edge. Mouthparts, including palpus, black.

Thorax (Fig. 1A). Dorsally and laterally black with greasy-looking shine. Scutum patterned with small rugae and minute, barely distinguishable setulae. Pleura with similar patterning but with more distinct, short, sparse, greyish to brownish setulae. Hirsuteness most developed on anepisternum, where longest setulae are approximately same length as width of flagellomere.

Legs (Fig. 1A). Coxae black; femora brown and apically paler. Fore and mid tibiae [pale brown] to dirty orange, clearly paler than femora. Hind tibia otherwise of similar colour as femora but paler at base and apex. Hind coxa with thin black posterior setulae, longest setulae as long as width of coxa at its base. Femora with thin posterodorsal setulae, longest being $0.5 \times$ as long as width of femora. Fore tibia preapically with [2]–3 ventral setulae. Mid tibia with two short, ventral, preapical setae and two adjacent setulae. Hind tibia with one ventral preapical setula and thin posteroventral setulae covering proximal half, longest of which are as long as width of tibia. Apart from aforementioned setae and setulae, all legs covered in minute setulae that provide rugous texture.

Wings (Fig. 1A). Hyaline with greyish tinge. Tegula black, basicosta brownish black, wing veins brown. Petiole and knob of haltere uniformly black.

Abdomen (Fig. 1A). Elongated, dorsally flattened except for domed terminal segments, black in colour, with greasy shine and covered by irregular, minute, robust setulae. Tergites 6, 7, and 8 with black marginal setulae, longest of which ca. as long as width of hind femora.

Terminalia (Fig. 4A, B, E, F). Hypandrium divided to two similar subrectangular halves, posterior margin with long dense setulae (Fig. 4A). Epandrium similarly divided into subtriangular halves with long posteroventral marginal setulae (Fig. 4B). Cercus subtriangular (Fig. 4E); gonocoxal apodeme scapula-shaped and curving slightly inwards at its posterior part; gonostylym bluntly subrectangular, posteriorly concave and ending with a ventral apex. Distiphallus with long, narrow, curved apical processes, hooking outwards prior to apex (Fig. 4F). Aedeagus rod-shaped, slightly bent at middle and with a short-forked apex.

Female (Figs 1B, 3A, B). Differs from male as follows:

Body length: 4.3–5.7 mm ($n = 4$). **Head** (Fig. 3A, B). Frons broad, at its narrowest point 0.62 – 0.69 ($n = 4$) \times as wide as an eye in dorsal view. Frons shiny black with minute longitudinal rugae on frontal stripe and transverse rugae on sides. Orbital plates smooth and shiny. Ocellar triangle equilateral. No obvious size difference between ommatidia of upper and lower half of compound eye. **Thorax** (Fig. 1B). Very weak whitish grey microtomentum at anterior parts of postpronotum and proepisternum. **Abdomen** (Fig. 1B). Dorsally flattened along its entire length. **Terminalia**. Last visible tergite 9 bluntly triangular at its posterior edge and not divided into hemitergites.

DNA barcode divergence among *Scenopinus*. *Scenopinus* spp. are poorly covered in the DNA barcode databases, such as Barcode of Life Database (BOLD, www.boldsystems.org) or GenBank. It is noteworthy that all *S. fenestralis* specimens in the databases from Europe to North America have almost identical *COI* sequences and

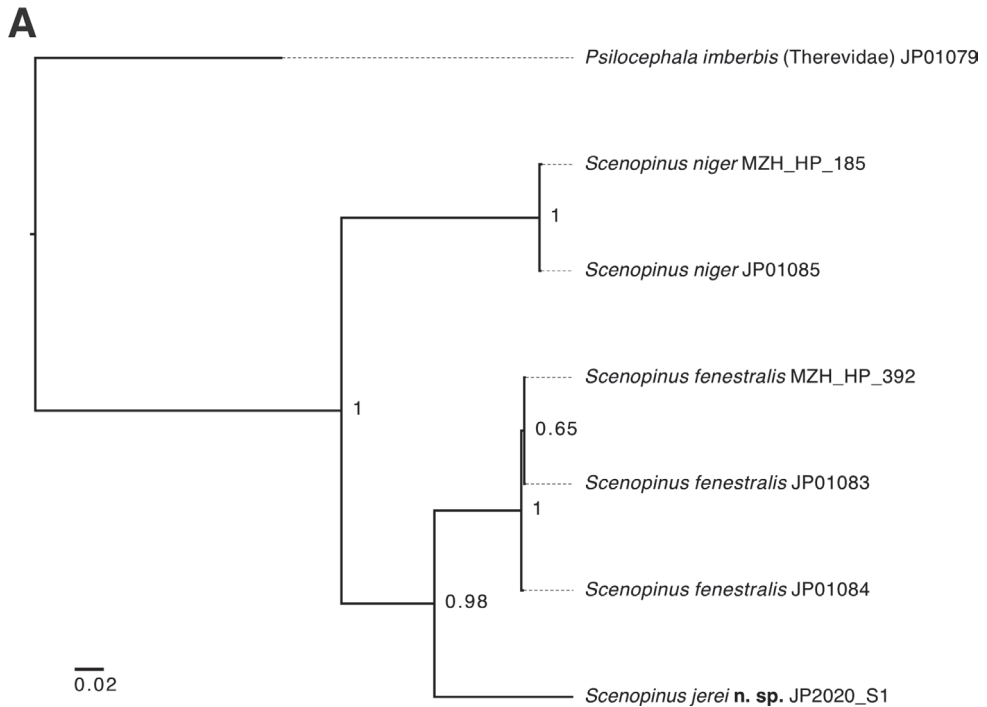


Figure 5. Maximum likelihood tree of *COI* sequence similarities among *Scenopinus* spp. Numbers at nodes indicate posterior probabilities and scale bar the relative sequence divergence. BOLD sample ID number is given after the species name.

represent the same barcode index number (BIN). The DNA barcode of *Scenopinus jerei* sp. nov. differs markedly from the other northern European species, its closest match being *Scenopinus fenestralis* from which it is separated by 12.48% sequence difference (Fig. 5). There are no other closer matches among the barcode sequences in the BOLD or GenBank.

Notes on the biology and distribution of *Scenopinus jerei* sp. nov. The larvae of *Scenopinus* species are predators of other invertebrates living in dry organic substrates, such as in animal nests. In Finland, *Scenopinus jerei* sp. nov. has been collected inside sheds, attics and indoor storages as well as reared from nest boxes of birds. These rearings produced large numbers of tineid moths (Lepidoptera: Tineidea), especially *Monopis laevigella* (Denis & Schiffermüller), but also other *Monopis* spp., *Niditinea striolella* (Matsumura), and *Tinea* spp. Other insects observed from the same nest boxes included *Ceratophyllus* fleas, various beetles (Histeridae, Dermestidae) and flies (Piophilidae, Fanniidae, Heleomyzidae). Apart for two male specimens found dead on a windowsill in an attic of an old house in Kelovaara on July 24 (see type specimens), most observations are from third week of June. According to the observations of Jere Kahanpää (pers. comm.), *Scenopinus jerei* sp. nov. hibernates as full-grown larvae and the adults emerge in a couple of weeks in room temperature rearing conditions. Based on the collection locations, it is likely that *Scenopinus jerei* sp. nov. is a boreal forest specialist.

Like other *Scenopinus* spp., *Scenopinus jerei* sp. nov. is not very active flier, does not visit flowers and therefore is rarely collected by active netting or traps. Judging from the few Finnish observations, the species appears widespread in the southern and central parts of the country. We are certain that *Scenopinus jerei* sp. nov. can also be found in boreal forest biotopes in the other Nordic countries and Russia but has been until now overlooked.

Etymology. This species is named after Mr. Jere Kahanpää, Helsinki, who was to first to discover that the taxon is new to science and kindly agreed with the current arrangement for its formal description.

Provisional key to the identification of European *Scenopinidae* species

Because the existing literature on the European species of Scenopinidae are outdated or difficult to obtain, we felt necessary to provide a key for the known European species of Scenopinidae. We must emphasise that we have been only able to examine the species with specimens listed in this paper, for which the identification key should work well. For the remainder, our approach was to go through the written species descriptions and pick features which we judged, by our collective species identification experience, to be useful for determination. To us this approach was better justified than reproducing the keys given in earlier literature, which are often difficult to follow or focus on limited number of poorly defined features. The diagnostic features for the key have been obtained from the descriptions in Kröber (1925), Trojan (1956), Kelsey (1969), Krivosheina (1981), Narchuk (1988), and Carles-Tolrá (2001). Fortunately, the European species separate into three easily recognisable species groups, each with relatively few species. The species groups appear in the key in alphabetical order, enabling fast navigation when one is familiar with the groups. Although result appears satisfactory, the key might not capture all the variations seen within each species and we strongly encourage DNA barcoding of specimens for future reference. In any case, we hope that this key can form a basis for forthcoming work with this interesting family of flies.

Key to genera

- 1 Cell r_5 closed and petiolate (Fig. 6B)..... *Caenoneura nigra* Kelsey, 1969 (Spain)
- Cell r_5 open (Fig. 6C). Genus *Scenopinus* 2

Genus *Scenopinus*

- 2 Flagellomere short and stout, $\sim 1.5 \times$ as long as wide, pear-shaped by distinctly narrowing towards the tip *brevicornis* group 9
- Flagellomere elongated, if apically narrowing then $> 1.7 \times$ as long as wide 3
- 3 Generally small in size (< 3 mm); R_4 branching from R_5 beyond the middle of cell r_5 (Fig. 6D); aedeagus in males not concealed by the epandrium..... *albicinctus* group 4
- Larger and more robust flies; R_4 branching from R_5 at or before the middle of cell r_5 (Fig. 6C); aedeagus in males concealed by the epandrium..... *fenestralis* group 13

***albicinctus* group**

- 4 Thorax and abdomen shining black; wings hyaline; legs black with orange-brown tarsi..... ***Scenopinus phaidimos* Kelsey, 1969** (Turkey)
 – Other combination of features **5**
- 5 Thorax and legs with moderately long golden setulae; thorax black-brown; humeral callus red-brown with yellow posterior patch; abdomen in males with narrow white bands on the posterior margin of tergites 3 and 4
 ***Scenopinus canarius* Kelsey, 1969** (Canary Islands)
 – No long golden setulae on thorax and legs. **6**
- 6 Tarsal claws as long as the last tarsal segment; single white band on the abdomen; antenna black; halter knob pale.....
 ***Scenopinus bouvieri* (Seguy, 1921)** (central and southern Europe)
 – Tarsal claws shorter than the last tarsal segment. **7**
- 7 Frons white; thorax dark with wide yellow band [spot?] extending from the humeral area to the posterior margin of the scutellum; male abdomen with 3 distinct white bands, female abdomen black with yellow spot on tergite 2.....
 ***Scenopinus albicinctus* (Rossi, 1794)** (southern Europe)
 – Other combinations of features. **8**
- 8 Thorax black with rugous texture and patch of microtomentum above the humeral callus; humeral callus red-brown with yellow posterior patch; wings opaque brown; halteres and legs uniformly brown; abdomen in males with narrow white bands on the posterior margin of tergites 3 and 4, in females uniform dark red-brown ***Scenopinus bulbapennis* Kelsey, 1969** (Spain)
 – Uniformly matt grey-brown species; thorax with two dark longitudinal stripes; tergite margins of the abdomen with diffuse brown-yellow banding; legs dark brown with paler knees and tarsi
 .. ***Scenopinus oldenbergi* (Kröber, 1913)** (African species imported to Europe?)

***brevicornis* group**

- 9 Abdomen with broad white bands on the posterior margins of tergites 2–6, giving it a solid white appearance.
 ***Scenopinus gobiensis* Kelsey, 1981** (Hungary, eastern Palearctic)
 – Not as above **10**
- 10 Wing opaque white; a very small species (1.5 mm)
 ***Scenopinus halteralis* Frey, 1936** [only males known] (Canary Islands)
 – Wing opaque brown; larger species **11**
- 11 Supra-alar callus (anteriorly to wing base) orange with a distinct dark brown, warty protuberance in both sexes
 ***Scenopinus verrucosus* Carles-Tolrá, 2001** (Spain)
 – No warty protuberance on supra-alar callus..... **12**

- 12 Humeral callus red-brown with white posterior border; abdomen in males black-brown with white band on the posterior margin of tergites 3–5, in females uniform red-brown..... *Scenopinus unifasciatus* (Kröber, 1913) (eastern Mediterranean)
- Humeral callus uniform black-brown; male abdomen brown.....
.....*Scenopinus retuertensis* Carles-Tolrá, 2001 (Spain)

fenestralis group

- 13 Thorax and abdomen red brown with short white setulae; posterior margin of humeral callus orange; legs brown except for yellow tarsi
.....*Scenopinus efflatouni* Kelsey, 1969 [only females known] (Andorra)
- Not as above 14
- 14 Cell cu narrow (Fig. 6E); wings opaque brown; male with white-banded abdomen and distinct grey microtomentum on mesonotum.....
..... *Scenopinus griseus* (Kröber, 1913) (south-eastern Europe)
- Cell cu wide (Fig. 6C)..... 15
- 15 Legs bicoloured; coxae and femora black or dark brown, apically paler; fore and mid tibiae orange to pale brown; haltere entirely black.....
..... *Scenopinus jerei* sp. nov. (Finland [northern Europe])
- No colour difference between femora and tibia; haltere variable, from white to black. 16
- 16 Legs unicolourous black or dark brown (in doubtful cases, as dark as ground..... colour of thorax), only tarsi paler than tibiae..... 17
- Legs orange to pale brown (in doubtful cases, paler than ground colour of thorax) 18
- 17 Wings black. Head subrectangular in lateral profile, antennae ~ 1/2 as long as the frons. In males, the apex of the hind tibia wider than the femora. Eyes not touching in either sex *Scenopinus niger* (De Geer, 1776) (northern and central Europe)
- Wings clear with yellow veins. Head hemispherical in profile. Eyes touching in males, widely separated in females.....
..... *Scenopinus lesinensis* Strobl, 1902 (southern Europe)
- 18 Lower part of head with thin white microtomentum, genal setulae mostly dark.. Flagellomere subrectangular and apically narrowing. Female frons with distinct rugae..... *Scenopinus fenestralis* (Linnaeus, 1758) (cosmopolitan)
- Lower part of head around the mouth edge to the antennal insertion with dense white microtomentum, genal setulae pale. Flagellomere cylindrical, not (or scarcely) narrowing apically. Female frons smooth and shiny. 19
- 19 The knob of haltere brown, as dark as its stem
..... *Scenopinus vitripennis* Meigen, 1824 (central and eastern Europe)
- The knob of haltere white, paler than its stem
..... *Scenopinus glabrifrons* Meigen, 1824 (central and southern Europe, cosmopolitan)

Discussion

Survey of candidate species among the *Scenopinus fenestralis* group

Scenopinus jerei sp. nov. was originally confused with *Scenopinus vitripennis* (Haarto 2000; Kahanpää and Winqvist 2005). The mistake occurred because *Scenopinus jerei* sp. nov. easily keys out as *S. vitripennis* using the key in Kelsey (1969), due to the dark halteres and relatively smooth female frons. As pointed out by Kelsey (1969), *S. vitripennis* was treated as a synonym of *S. glabrifrons* by many authors prior to Trojan (1956), who established it as a valid species based on female characters. In retrospect this conclusion is problematic, as the original type specimen of Meigen was a male and is presumed lost. At the time of Kelsey's work (1969), the type was the only reported male specimen of the species. Interestingly, there is one male identified in 1964 by Kelsey as *S. vitripennis* in SMNS. It is unknown to us why Kelsey did not include this specimen in his work on world Scenopinidae. The specimen is only 3.4 mm long, dark, has entirely grey-brown legs and, apart for some dirt and broken antennae, is in good condition (Fig. 1E). The colour of the legs, including the pale coxae, and general appearance of the specimen does not agree with our concept of *Scenopinus jerei* sp. nov. and neither does the examined female specimen in the ZIM collection (Fig. 1F). Notably, the halteres of these specimens are grey or reddish brown, much paler than the thorax, whereas those of *Scenopinus jerei* sp. nov. are black or as dark as the thorax, similar to the situation in *S. niger*.

The original description of *Scenopinus vitripennis* by Meigen (1824:115) is brief but provides sufficient information: “Schwartz; Beine gelbroth [sic]; Schwinger braun; Kopf unten weiß; Flügel glasshelle [sic]. Niger; pedibus rufis; halteribus fuscis; clava subtus alba; alis hyalinis.” [Black; legs yellow-red; halteres brown, underside of the head white; wings hyaline.]

Meigen's description of the colouration of the legs as well as the underside of the head make it clear that *S. vitripennis* is not conspecific with our *Scenopinus jerei* sp. nov. However, these features are also not evident in the small, dark male specimen in the SMNS collection either. It may be that Kelsey disregarded this specimen from his work for the same reason. In fact, the male of *S. vitripennis* was later redescribed and illustrated by Krivosheina (1981). The shape of the antennae, terminal sternites as well as the visible genitalia features in Krivosheina's illustrations differ markedly from those of *Scenopinus jerei* sp. nov. However, the comparison with *S. glabrifrons* is not very detailed in Krivosheina's work. We also note that the female specimen in MIZ, collected and identified by Trojan, is very similar to *S. glabrifrons* in general appearance, including the flagellomere, which is cylindrical and parallel sided, compared to the basally more robust, apically narrowing flagellomere *Scenopinus jerei* sp. nov.

For some reason, the male genitalia of Scenopinidae have been traditionally dissected only partially, the only visible parts being the proximal parts of the aedeagus as well as the terminal segments, which makes the comparison of the published illustrations prone to interpretation errors. When fully dissected, the aedeagus has very

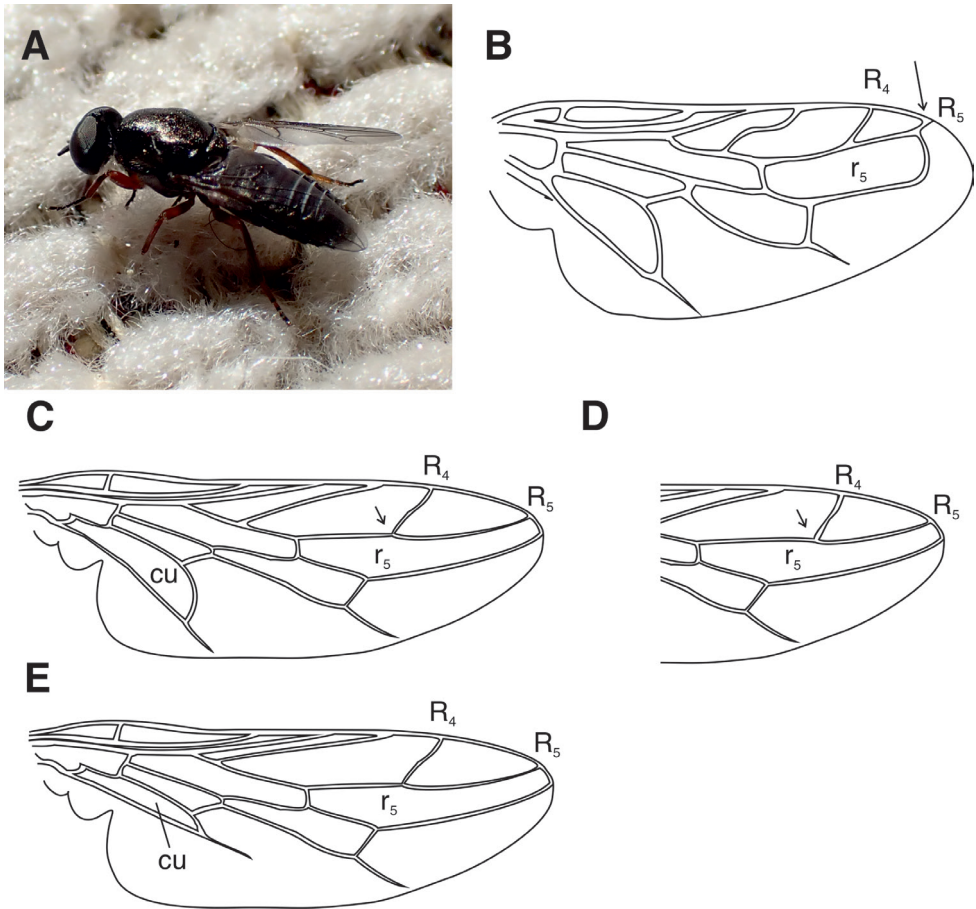


Figure 6. Identification of Scenopinidae **A** male *Scenopinus fenestralis*. Hanko, Finland, June 22, 2021. Note the three stripes on the abdomen caused by the white integument protruding between the tergites. These should not be confused with white bands of microtomentum on tergites of some *Scenopinus* species. Photograph by J. Pohjoismäki **B** illustration of *Caenoneura* wing. Arrow pointing the petiole on r_5 . Drawn after Kelsey (1969) **C** generic *Scenopinus* wing. Modified from Winterton and Gaimari (2017) **D** wing venation in *albicinctus*-group with R_4 branching from R_5 beyond the middle of cell r_5 (arrow; compare with C) **E** Wing of *Scenopinus griseus* (Kröber) with narrow cu cell. Drawn after Narchuk (1988).

distinct, species-specific features (Fig. 4), which could be better utilised for species identification. Unfortunately, *S. vitripennis* is very rare in collections, and clearly more work is needed to fully understand the extent of interspecific variation between it and *S. glabrifrons*. These future efforts should also focus on applying modern sequencing methods that allow the genotyping of old museum specimens (Staats et al. 2013; Prosser et al. 2016; Nakahama 2021).

To further validate our interpretation of the new species status of *Scenopinus jerei* sp. nov., we also checked the potential candidates among the known species of *Scenopinus* outside Europe. Since the revision of the world Scenopinidae by Kelsey (1969),

relatively few *Scenopinus* species have been described (Pape and Thompson 2021), most of which can be excluded by their exotic location. However, as several Eastern Palearctic species in other families extend their range to Finland (e.g., Cannings and Kahanpää 2013; Stuke et al. 2020; Pohjoismäki and Bergström 2021), we wanted to rule out the following species from the Russian Far East:

- *Scenopinus mariensis* Kelsey, 1981. This species is close to *S. lesinensis* but has notable colour patterning on the thorax.
- *Scenopinus sibiricus* Krivosheina, 1982. Wings dark brown, tibiae black. Eyes separated by a frontal stripe in males. The species is morphologically close to the Nearctic *Scenopinus aquelonius* Kelsey, 1969, *S. breviterminus* Kelsey, 1969, and *S. undulafrons* Kelsey, 1969.
- *Scenopinus ussuriensis* Krivosheina, 1981. Illustrations of the antenna shape and male genitalia are dissimilar to those of *Scenopinus jerei* sp. nov.
- *Scenopinus zhelochovtsevi* Krivosheina, 1982. Legs uniform in colour. Illustrations of the antenna shape and male genitalia are dissimilar to those of *Scenopinus jerei* sp. nov.

No potential candidates were found among the known Nearctic species.

Survey of the old *Scenopinus fenestralis* synonyms

Scenopinus fenestralis is a common, variable, and widespread species. It also lacks clear morphological features, such as strong setae that are used as diagnostic characters for many fly groups, making it difficult to devise generalised descriptions or identification keys for both sexes. For example, the colour of the halteres can vary from dark brown to white and the colour of the legs from pale brown to orange. It is probable that developmental factors and possibly age of the fly play a big role in the morphological variation. Among others, it is known that hoverflies (Diptera: Syrphidae) developing in cool and humid conditions are typically darker than the ones developed in warm and dry conditions (e.g., Ottenheim et al. 1996). Similarly, small specimens developed under insufficient nutrition tend to be darker and morphologically more plain than larger specimens, which could also explain the aberrative habitus of the putative *S. vitripennis* male specimen in SMNS, mentioned earlier.

This intraspecies variation has contributed to the wealth of synonyms for *S. fenestralis*, which raised the question if some of the names could correspond to our concept of *Scenopinus jerei* sp. nov. However, checking all the old, synonymised type specimens dispersed over several collections would have been impossible. Fortunately, the colouration of *Scenopinus jerei* sp. nov. legs and halteres are so distinct that we were able to validate these diagnostic characters even from the quite brief old descriptions. Pape and Thompson (2021) list the following synonyms for *S. fenestralis*, whose original descriptions differ from the characters of *Scenopinus jerei* sp. nov. as indicated:

- *Musca tarda* Linnaeus, 1761 – White halteres, yellow legs.
- *Musca saltitans* Scopoli, 1763 – White halteres, red legs.
- *Musca spoliata* Scopoli, 1763 – Male specimen of the latter.
- *Musca senilis* Fabricius, 1794 – Legs yellow-red, head white from below.
- *Atricha fasciatus* Schrank, 1803 – Greyish specimen with milk-white bands on the abdomen. While the abdominal banding sounds like an unusual feature for *S. fenestralis*, we have observed that the soft white integument can be protruding between the tergites in newly hatched *Scenopinus* specimens, giving the abdomen a banded appearance (Fig. 6A). Legs entirely olive brown.
 - *Scenopinus pallipes* Say, 1823 – White halteres, yellow legs.
 - *Scenopinus domesticus* Meigen, 1824 – Legs yellow-red, head white from below.
 - *Scenopinus sulcicollis* Meigen, 1824 – Legs yellow-red, head white from below, halteres white.
 - *Scenopinus scutellatus* Macquart, 1843 – Halteres white, scutellum yellow.
 - *Scenopinus furcinervis* Zetterstedt, 1844 – Legs fully yellow.
 - *Scenopinus fuscinervis* Schiner, 1860 – The name is not mentioned in Schiner (1860).
 - However, Kelsey attributes the synonymy to Schiner (1862), where *S. fuscinervis* Zetterstedt is given as a synonym of *S. fenestralis*. It is obvious that in this context, *S. fuscinervis* is a misspelling of *S. furcinervis*. In fact, the spelling is later corrected in Schiner (1864).
 - *Scenopinus graminicola* Zetterstedt, 1859 – Halteres white.
 - *Scenopinus nigroscutellatus* Frey, 1945 – From Azores, halteres white.

Based on this survey, we are confident that the species presented here as *Scenopinus jerei* sp. nov. is not among the accepted species nor hidden among the synonyms of *S. fenestralis*. We hope that the species discovery reported here, together with the provisional identification key we have provided, will encourage more research towards this exciting but poorly known family of flies.

Acknowledgements

We would like to acknowledge Mr. Jere Kahanpää (Finnish Natural History Museum) for his brilliant insight into Scenopinidae and for giving us the opportunity to describe the species. Dr. Olga G. Ovtshinnikova (The Zoological Institute of Russian Academy of Sciences, St Petersburg, Russia) is thanked for her kind help with obtaining the articles of N. P. Krivosheina. Dr. Daniel Whitmore, Susanne Leidenroth (both SMNS), and D. Schimroszyk (MIZ) are thanked for the images of *Scenopinus vitripennis*. Dr. Marko Mutanen (Oulu, Finland) donated his reared material and provided details about the rearings. He also provided valuable support for the species' barcoding as a part of the Finnish Barcode of Life (FinBoL) project. Mr. Ali Karhu (Liperi Finland) provided additional specimens and Jiri Vihavainen (Joensuu)

suu, Finland) provided valuable laboratory assistance. We are grateful to Dr. Davide Badano (Sapienza Università di Roma) for the excellent editorial process, and Dr Steve Gaimari (CDFA, Sacramento, CA, USA) and Dr Paul Beuk (Natuurhistorisch Museum Maastricht, the Netherlands) for their constructive and highly insightful reviews, which helped to improve our manuscript. Finally, we would like to thank the Finnish Ministry of Environment for supporting our book project on the Asiloidea of Finland and adjacent countries.

References

- Bystrowski C, Richter VA, Beuk P, Pape T, Carles-Tolrá M (2021) Fauna Europaea: Scenopinidae. In: Beuk P, Pape T (Eds) Fauna Europaea: Diptera, Brachycera. Fauna Europaea version 2017.06. <https://fauna-eu.org>
- Cannings RA, Kahanpää J (2013) *Lasiopogon septentrionalis*, a robber fly (Diptera: Asilidae) new to the European Fauna. *Entomologica Fennica* 24: 113–116.
- Carles-Tolrá M (1999) *Scenopinus efflatouni* Kelsey, 1969: new record to Europe (Diptera, Scenopinidae). *Boletín de la Asociación Española de Entomología* 23: e328. <https://doi.org/10.33338/ef.8347>
- Carles-Tolrá M (2001) Two new species of *Scenopinus* Latreille from Spain (Diptera, Scenopinidae). *Boletín de la Asociación Española de Entomología* 25: 35–41.
- Cumming JM, Wood DM (2017) Adult morphology and terminology. In: Kirk-Spriggs A, Sinclair BJ (Eds) *Afrotropical Diptera*. Vol. 1. South African National Biodiversity Institute, Pretoria, 89–133.
- Edgar RC (2004) MUSCLE: multiple sequence alignment with high accuracy and high throughput. *Nucleic Acids Research* 32: 1792–7. <https://doi.org/10.1093/nar/gkh340>
- Fabricius JC (1794) *Entomologia systematica emendata et aucta*. Vol. 4. Copenhagen, 472 pp.
- Frey R (1945) Tiergeographische Studien über die Dipterenfauna der Azoren. I: Verzeichnis der bisher von den Azoren bekannten Dipteren. *Commentationes Biologicae VIII*. 10. Societas Scientiarum Fennica, 114 pp.
- Haarto A (2000) Taxa new to Finland. *Scenopinus vitripennis* Meigen (Scenopinidae). *Entomologica Fennica* 11: e1.
- Hebert PDN, Penton EH, Burns JM, Janzen DH, Hallwachs W (2004) Ten species in one: DNA barcoding reveals cryptic species in the neotropical skipper butterfly *Astraptes fulgerator*. *Proceedings of the National Academy of Sciences of the United States of America* 101: 14812–14817.
- Kahanpää J, Winqvist K (2005) Checklist of Finnish flies: families Xylophagidae – Microphoridae. *Sahlbergia* 10: 10–27.
- Kahanpää J, Winqvist K, Zeegers T (2014) Checklist of the ‘lower Brachycera’ of Finland: Tabanomorpha, Asilomorpha and associated families (Diptera). *ZooKeys* 441: 165–181. <https://doi.org/10.3897/zookeys.441.7198>
- Kelsey LP (1969) A revision of the Scenopinidae (Diptera) of the world. *Bulletin of the United States National Museum* 277: 1–336. <https://doi.org/10.5962/bhl.title.16405>

- Kelsey LP (1981) New Scenopinidae (Diptera) from the Palearctic. *Folia Entomologica Hungarica* 42: 85–93.
- Krivosheina NP (1981) Taxonomy of *fenestralis* group species of the genus *Scenopinus* Latr. (Diptera, Scenopinidae). *Vestnik Zoologii* 4: 24–31. [In Russian, English summary]
- Krivosheina NP (1982) New representatives of the genus *Scenopinus* (Diptera, Scenopinidae) in the fauna of the USSR. *Zoologicheskii Zhurnal* 60: 160–164. [In Russian, English summary]
- Kröber O (1925) 27. Omphralidae (Scenopinidae). In: Lindner E (Ed.) *Die Fliegen der Palaarktischen Region IV* (Lieferung 123): 1–8.
- Linnaeus C (1760) *Fauna Svecica sistens animalia Sveciae regni: Mammalia, Aves, Amphibia, Pisces, Insecta, Vermes. Distributa per classes & ordines, genera & species, cum differentiis specierum, synonymis auctorum, nominibus incolarum, locis natalium, discriptionibus insectorum. Editio altera, auctior. “1761”. Laurentii Salvii. Stockholmiae* [Stockholm], 455 pp. <https://doi.org/10.5962/bhl.title.46380>
- Macquart J (1844) *Diptères exotiques nouveaux ou peu connus. Tome deuxième, 3.e partie. “1843”*, N.E. Roret, Paris, 5–304.
- Meigen JW (1824) CXXXIII. Fensterfliege SCENOPINUS. Systematische Beschreibung der Bekannten Europäischen Zweiflügeligen Insekten, Theil 4, Schulz-Wundermann’schen Buchhandlung, Beaufort Sohn, Aachen, Germany, 111–118.
- Nakahama N (2021) Museum specimens: An overlooked and valuable material for conservation genetics. *Ecological Research* 36: 13–23. <https://doi.org/10.1111/1440-1703.12181>
- Narchuk EP (1988) 42. Family Scenopinidae (Omphralidae). In: Bei-Bienko GI (Ed.) *Keys to the insects of the European USSR. Volume V. Diptera and Siphonaptera. Part I*. Amerind Publishing Co. Pvt. Ltd. New Delhi, 838–842.
- O’Hara JE (2002) Revision of the Polideini (Tachinidae) of America north of Mexico. *Studia Dipterologica, Supplement* 10: 1–170.
- Ollikainen M, Ollikainen M (2004) The Finnish coordinate reference systems. Published by the Finnish Geodetic Institute and National Land Survey. http://www.maanmittauslaitos.fi/sites/default/files/Finnish_Coordinate_Systems.pdf
- Ottenheim MM, Volmer AD, Holloway GJ (1996) The genetics of phenotypic plasticity in adult abdominal colour pattern of *Eristalis arbustorum* (Diptera: Syrphidae). *Heredity* 77: 493–499. <https://doi.org/10.1038/hdy.1996.176>
- Pape T, Thompson FC (2021) *Systema Dipteriorum* (version 2.0, Jan 2011). In: *Catalogue of Life* (2021). Species 2000 & ITIS Catalogue of Life, 2021-05-07. Digital resource at: www.catalogueoflife.org. Species 2000: Naturalis, Leiden. ISSN 2405–8858.
- Pohjoismäki J, Bergström C (2021) Review of the Nordic *Gymnocheeta* Robineau-Desvoidy (Diptera, Tachinidae) with report of two species new to Europe. *ZooKeys* 1053: 145–184. <https://doi.org/10.3897/zookeys.1053.52761>
- Prosser SWJ, deWaard JR, Miller SE, Hebert PDN (2016) DNA barcodes from century-old type specimens using next-generation sequencing. *Molecular Ecology Resources* 16: 487–497. <https://doi.org/10.1111/1755-0998.12474>
- Rambaut A (2009) Computer program distributed by the author. [website:] <http://tree.bio.ed.ac.uk/software/figtree/>

- Ronquist F, Teslenko M, van der Mark P, Ayres D, Darling A, Höhna S, Larget B, Liu L, Suchard MA, Huelsenbeck JP (2012) MrBayes 3.2: Efficient Bayesian phylogenetic inference and model choice across a large model space. *Systematic Biology* 61: 539–542. <https://doi.org/10.1093/sysbio/sys029>
- Say T (1823) Descriptions of dipterous insects of the United States. *Journal of the Academy of Natural Sciences of Philadelphia* 3: 9–54, 73–104.
- Schiner IR (1860) Vorläufiger Commentar zum dipterologischen Theile der Fauna austriaca. II. *Wiener Entomologische Monatschrift*, 4. Bd, Vienna, 208–287.
- Schiner IR (1862) Die Fliegen (Diptera) In: Redtenbacher L, Schiner IR (Eds) *Fauna Austriaca*. Vol. 1, Vienna, 159 pp.
- Schiner IR (1864) *Catalogus Systematicus Dipteriorum Europae*. Impensis Societatis zoologico-botanicae, Vindobonae [Vienna], 30–31. <https://doi.org/10.5962/bhl.title.39977>
- Schrank F von P (1803) *Favna Boica*. Durchgedachte Geschichte der in Baiern einheimischen und zahmen Thiere. Vol. 3, Landshut, 103 pp.
- Scopoli JA (1763) *Entomologia Carniolica exhibens insecta Carnioliae indigene et distributa in ordenes, genera, species varietates Methodo Linneana*. I.T. Trattner, Vindobonae [Vienna], 420 pp. <https://doi.org/10.5962/bhl.title.119976>
- Staats M, Erkens RHJ, van de Vossen B, Wieringa JJ, Kraaijeveld K, Stielow B, Geml J, Richardson JE, Bakker FT (2013) Genomic Treasure Troves: Complete Genome Sequencing of Herbarium and Insect Museum Specimens. *PLoS ONE* 8(7): e69189. <https://doi.org/10.1371/journal.pone.0069189>
- Stuke J-H, Kahanpää J, Haarto A, Kakko I (2020) *Sicus ogumae* (Matsumura, 1916) recorded from Finland, new to Europe (Diptera: Conopidae). *Entomologist's Monthly Magazine* 156: 117–125. <https://doi.org/10.31184/M00138908.1562.4022>
- Trojan P (1956) Notes on the taxonomy of some European species of the genus *Omphrale* Meigen (Diptera, Omphralidae). *Annales Zoologici* 16: 147–156.
- Winterton SL, Ware JL (2015) Phylogeny, divergence times and biogeography of window flies (Scenopinidae) and the therevoid clade (Diptera: Asiloidea). *Systematic Entomology* 40: 491–519. <https://doi.org/10.1111/syen.12117>
- Winterton SL, Gaimari SD (2017) 50. Scenopinidae (window flies). In: Kirk-Spriggs AH, Sinclair BJ (Eds) *Manual of Afrotropical Diptera*. Volume 2. Nematoceros Diptera and lower Brachycera. Suricata 5. SANBI Graphics & Editing, Pretoria, 1209–1218.
- Yeates DK (1992) Towards a monophyletic Bombyliidae (Diptera): the removal of the Proratinae (Diptera: Scenopinidae). *American Museum Novitates* 3051: 1–30.
- Zetterstedt JW (1844) *Diptera Scandinaviae. Disposita et descripta*. Tomus tertius. Lund, Sweden, 895–1280.
- Zetterstedt JW (1859) *Diptera Scandinaviae. Disposita et descripta*. Tomus tridecimus seu supplementum quartum, continens addenda, corrigenda & emendanda tomis duodecim prioribus, una cum conspecta omnium generum. Lund, Sweden, 4943–6190.

The distribution and behavioral characteristics of plateau pikas (*Ochotona curzoniae*)

Jun Qiu^{1,2}, Cang Ma³, Ying-Hui Jia⁴, Jin-Zhao Wang³, Shou-Kai Cao³, Fang-Fang Li^{1,4}

1 State Key Laboratory of Plateau Ecology and Agriculture, Qinghai University, Xining, 810016, China **2** State Key Laboratory of Hydrosience & Engineering, Tsinghua University, Beijing, 100084, China **3** School of Water Resources and Electric Power, Qinghai University, Xining, 810016, China **4** College of Water Resources & Civil Engineering, China Agricultural University, Beijing, 100083, China

Corresponding author: Fang-Fang Li (liff@cau.edu.cn)

Academic editor: Jesus Maldonado | Received 25 January 2021 | Accepted 9 August 2021 | Published 14 September 2021

<http://zoobank.org/3FA17A75-7523-4B95-8AFE-1E518136D1EC>

Citation: Qiu J, Ma C, Jia Y-H, Wang J-Z, Cao S-K, Li F-F (2021) The distribution and behavioral characteristics of plateau pikas (*Ochotona curzoniae*). ZooKeys 1059: 157–171. <https://doi.org/10.3897/zookeys.1059.63581>

Abstract

Plateau pikas (*Ochotona curzoniae*) are regarded as one of the main causes of the degradation of alpine meadows in the Qinghai-Tibet Plateau (QTP). The population density of plateau pikas is directly related to the degree of grassland damage. In this study, field observation was conducted for one week in the south-eastern QTP in August 2019. A random encounter model (REM) was used to estimate the population density of plateau pikas from photographs and videos, and the frequencies of different behaviors were calculated. In addition, the effects of water-source distance and terrain on the distribution of plateau pikas and the frequencies of different pika behaviors under different population densities were explored. The observations and knowledge derived from this study provide a reference for the population control of plateau pikas.

Keywords

Dari County, field observations, population density, Qinghai-Tibet Plateau (QTP), random encounter model (REM)

Introduction

The Qinghai-Tibet Plateau (QTP) is the highest plateau in the world, with an average altitude of 4500 m, and it is known as the roof of the world. Alpine meadows are widespread in the QTP, accounting for more than 50% of the total area of the QTP

(Gao et al. 2013; Chen et al. 2014). Such meadows are especially widespread in the source areas of the Yangtze, Yellow, and Lancang Rivers. Alpine meadows play very important roles in forage production, water conservation, climate regulation, biodiversity maintenance and so on (Chen et al. 2008; Wen et al. 2013; Yao et al. 2019). Due to the special climatic conditions and natural environment of the QTP, the QTP ecosystem is fragile. Once the habitat is destroyed, it is difficult to recover, and recovery takes a long time (Schleuss et al. 2015; Guo et al. 2019). To date, the degraded area of alpine meadows in the QTP has reached 4.67×10^6 hm², accounting for 25% of the total area of the region; moreover, 50% of the total alpine meadow area, 2.13×10^6 hm², comprises black-soil-type degraded grasslands (Dong et al. 2013). This “black soil beach” grassland is the product of severe degradation of alpine meadow grassland and has extremely low production capacity. The appearance of bald patches is a prominent feature of these black soil beaches and drives their formation (Gao and Li 2016).

In recent years, the black soil beach area has continued to expand, and there are few countermeasures for this problem. Degraded alpine meadows seriously affect the sustainable development of the ecological environment and animal husbandry in the QTP (Gao et al. 2019). Previous studies have indicated that overgrazing, rampant rodent damage, climate change and glacier retreat are the main reasons for the degradation of alpine meadows in the QTP (Chen et al. 2017). Rodent damage is mainly caused by the plateau pika, *Ochotona curzoniae* (Hodgson, 1858). This small non-hibernating herbivore belongs to the family Ochotonidae. In the QTP, plateau pikas are mainly distributed in areas with altitudes of 3200–5300 m and live in groups (Smith et al. 2010; Koju et al. 2017). A family of plateau pikas consists of 2–6 adult pikas and their offspring (Pan and Migmar 2016; Wei et al. 2019). Due to their strong survival and reproductive abilities, they are widely distributed in the QTP, and their population density can reach more than 300 individuals/ha. Plateau pikas burrow in and dig soil, gnaw at grass and roots, and destroy the grass layer. In addition, long-term overgrazing creates favorable conditions for plateau pika invasion, thereby accelerating grassland degradation (Bai et al. 2002). According to Fan et al.’s study (Fan 1999), the annual consumption of forage by plateau pikas is approximately 150×10^6 t, equivalent to that of 150×10^6 grazing sheep a year. Therefore, it is important to control the number of pikas to reduce grassland degradation.

Controlling population density is the key to animal management and protection (Qu et al. 2017). The population density of rodents is directly related to the degree of grassland damage; higher numbers of rodents cause more serious damage. Plateau pikas are a key species on the QTP and play an irreplaceable role in maintaining the balance and stability of grassland ecosystems (Smith et al. 2019). Controlling the population of plateau pikas is a fundamental way to implement grassland protection, which is facilitated by understanding the distribution and behavior patterns of plateau pikas. Many studies on this topic have been completed. Qu et al. (2017) found that the population of plateau pikas exhibits almost no interyear changes but exhibits intrayear variation, with population numbers peaking in June. They also

demonstrated that survival of plateau pikas experience seasonal fluctuations, while demographic features and climate together regulate population dynamics. Since the altitude of the QTP ranges from 3000 to 5000 m, the population dynamics and population peaking of plateau pikas may differ between regions with different altitudes and climates.

Some researchers are also concerned with the behavioral characteristics of plateau pikas. Smith et al. (1986) has categorized different pika activities into social behaviors (such as chasing, playing and following) and nonsocial behaviors (such as eating, vigilance and digging). Wang et al. (2005) investigated the varied behavioral patterns with different population densities, and discovered that the behavior change of plateau pika was obviously related to its breeding period and sex. It is also reported that plateau pikas reduce the risk of predation by adjusting behavioral strategies (Wei et al. 2004). Therefore, the behavioral patterns of plateau pikas change with different population densities and external environments to enable better survival.

Wei et al. (2003) indicated that the population size of plateau pikas differed significantly among grasslands with varying degrees of degradation and increased with the aggravation of grassland degradation; in addition, they found that the population size was highest in moderately degraded grasslands and decreased in severely degraded grasslands due to a lack of food. Wangdwei (2019) used Poisson regression to analyze the effects of yaks and land use type on plateau pika behavior. The results indicated that the frequency of foraging behavior was higher than that of warning behavior in winter but lower than that of warning behavior in summer, and that the level of vegetation coverage was inversely proportional to pika foraging frequency. Such knowledge helps us better understand the relationship between plateau pikas and grassland degradation.

In this study, field observation was conducted for one week in the southeastern QTP from August 12 to 18, 2019. The random encounter model (REM) established by Rowcliffe et al. (2008) was used to estimate the population density of plateau pikas from photographs and videos, and the frequencies of different behaviors were calculated. In addition, the effects of water-source distance and terrain on the distribution of plateau pikas and the frequencies of different pika behaviors under different population densities were explored. This study contributes to the ecological knowledge on plateau pikas and provides a reference for the control of plateau pikas.

Methods

Study area

The source area of the Yellow River is located in the southern portion of the Qinghai Province and has a total area of 137.7×10^3 km², of which grassland accounts for 81.2%. Alpine grassland and alpine meadows are typical vegetation types in the

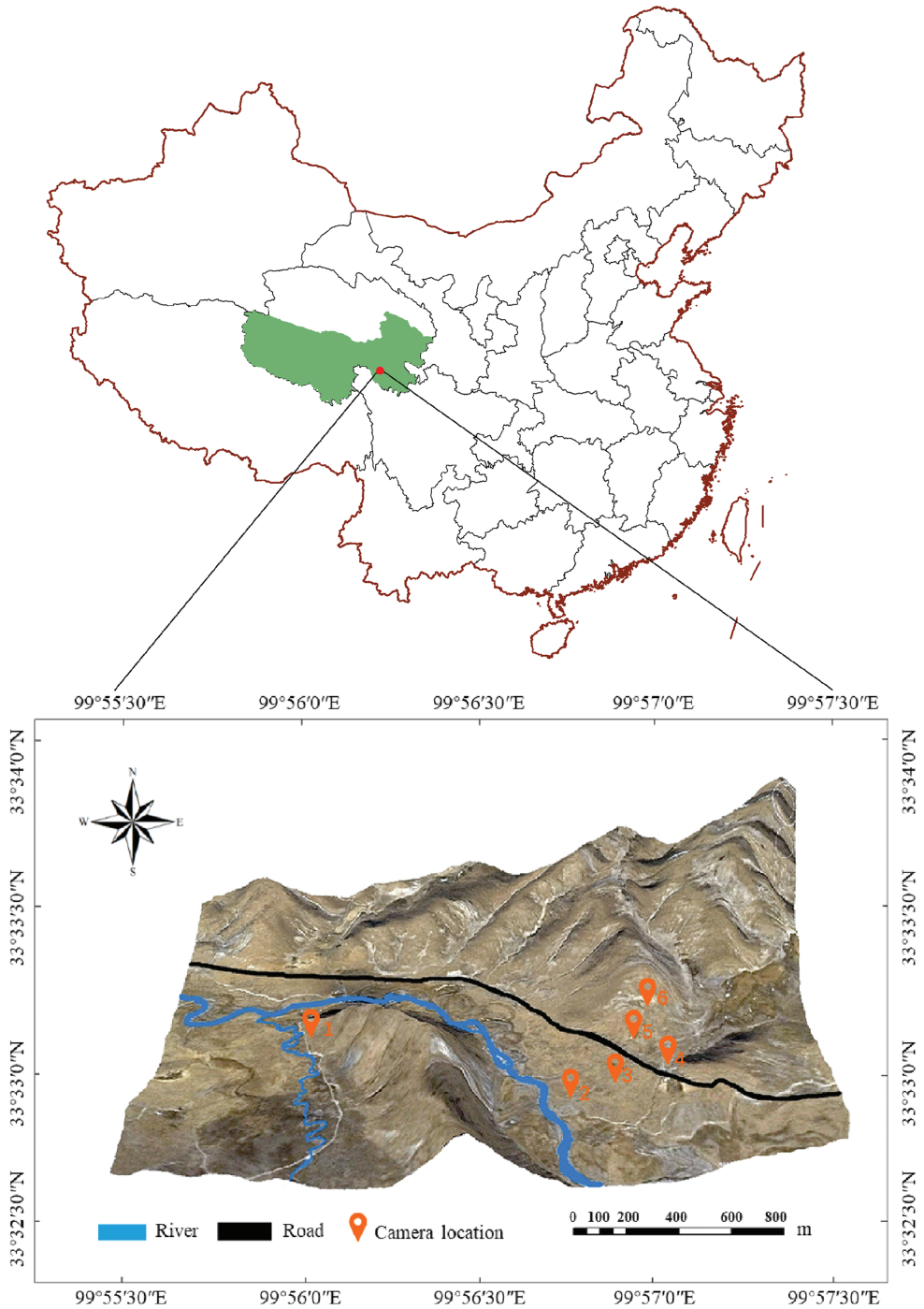
source region of the Yellow River (Li et al. 2016). The source area of the Yellow River has been the habitat of many wild animals and the grazing area of livestock for a long time. However, in recent decades, due to environmental changes driven by rodent and human activities and other adverse factors, the ecological environment of the Yellow River source area has deteriorated, resulting in severe grassland degradation.

Dari County is located in the southern portion of the Yellow River source area (32°36'42"–34°15'20"N, 98°15'29"–100°32'41"E). The county has an average altitude of 4426 m and an alpine semihumid climate. There is no obvious division of the year into four seasons; rather, there are cold and warm seasons. There are cold monsoons and heavy snow in winter, which lasts for up to 7–8 months. The warm season is humid but lasts for only 4–5 months. The average temperature of the county is between -0.1 °C and -3.5 °C. The annual precipitation is approximately 560 mm and mostly occurs from June to September. There are only a few grassland types, with most grasslands being alpine meadow grasslands. The grasslands begin to turn green in mid-May, and the annual growth period is only 120 days.

There are 1,402 million hectares of natural grasslands in Dari County, accounting for 94% of the county's total land area, and 1,117 million hectares of usable grasslands, accounting for 80% of the total natural grassland area. In recent decades, the grasslands in Dari County have undergone continuous degradation, with the area of moderately degraded grasslands reaching 50%–60% of the total usable grassland area (Zhang et al. 2011). The black soil beach area, which has extremely low utilization value, is expanding, rodent infestation is rampant, and vegetation patches are widespread; therefore, Dari County has become the county with the most severe grassland degradation in the source region of the Yellow River (Liu et al. 2008). Due to its significance, Dari County was selected as the study area.

Field observation

Camera trap technology has been widely used for wildlife population density estimation and behavior observation due to its low labor cost, minimal interference with the environment and strong adaptability. The camera used in this study was the Foresafe H885 field infrared camera, as shown in Fig. 1. In the layout, the camera was oriented so that the lens was approximately parallel to the ground to avoid direct sunlight on the lens. The front view of the camera was cleared, without occlusion, and the scene environment restored once the camera was installed. Deployment time and other local information, such as GPS coordinates, were recorded. Six cameras numbered #1 to #6 were arranged at six different locations differing in water-source distance and terrain. Camera #1 was installed in the floodplain; cameras #2, #3 and #4 were placed 100 m, 300 m and 600 m, respectively, from the river channel; and cameras #5 and #6 were placed on a steep slope and gentle slope, respectively. The camera locations are shown in Fig. 1.



The six cameras were installed from August 12 to August 18, 2019. The infrared sensor on each camera could actively detect sudden changes in infrared energy in the field of view, triggering the activation of the camera. Each camera was operational 24 h a day in photo and video modes, and the video recording time was set to 30 s. Once triggered, the camera took a photograph, recorded 30 s of video, and then returned to standby mode. The time, temperature and other information associated with the images and videos were stored on the memory card in chronological order.

With the aim of reducing the autocorrelation of the field observation photographs, two photographs were considered independent if the time interval between them was more than two minutes. The camera trigger time, temperature, frequencies of plateau pika behaviors and other data from the videos were recorded.

Estimation of population density

The REM proposed by Rowcliffe et al. (2008) was adopted in this study to estimate population density from the camera trap data; this approach does not require individual recognition of animals. Since it was proposed, the REM has been applied to estimate the population density of many animal species (Manzo et al. 2012; Anile et al. 2014; Caravaggi et al. 2016) and is shown in the following equation:

$$D = \frac{y}{t} \frac{\pi}{vr(2 + \theta)}$$

where D is population density; y is the number of independent images; t is the number of days the camera was operational; v is the daily movement speed of animals; r is the radius of the camera detection area; and θ is the camera detection angle, as shown in Fig. 2.

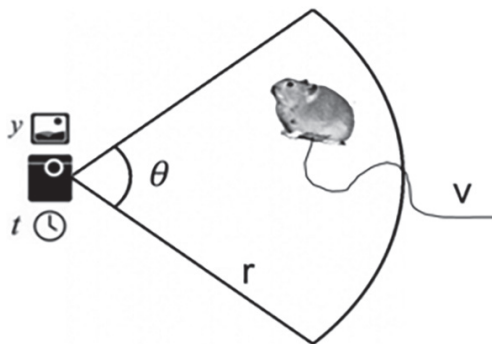


图 2 REM 示意图

Figure 2. Schematic diagram of the REM parameters.

Preliminary experiments revealed that the detection information of each camera was $r = 8$ m and $\theta = 55^\circ$ (0.96 rad). According to Zhang et al. (Zhang et al. 2013), the daily travel distance of plateau pikas is approximately 300 m; thus, v was set to 0.3 km/d. The total number of independent images (y) was obtained by counting the number of images taken by each camera.

Classification of pika behavior

According to the literature and obtained video data, the behavior of plateau pikas was classified into five types: foraging, traveling, being vigilant, grooming and fighting, as described and illustrated in Table 1 and Fig. 3.

Table 1. Classification of plateau pika behavior.

Behavior	Description
Foraging	Consuming food while in place or collecting food while moving
Traveling	Moving quickly from one place to another
Being vigilant	Sitting on the ground with neck extended or standing with the forefeet off the ground
Fighting	Aggressively grabbing and biting another pika
Grooming	Cleaning the body with the paws or mouth

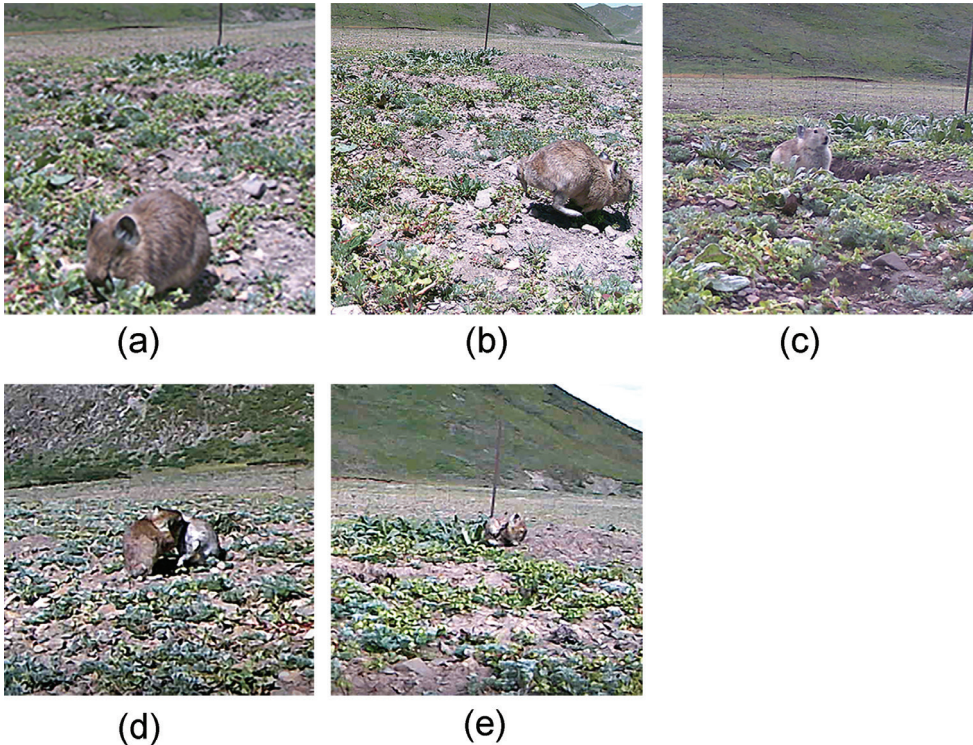


Figure 3. Classification of plateau pika behavior **a** foraging **b** traveling **c** being vigilant **d** fighting; and **e** grooming.

Results

Population density

During the one week of field observation, a few of the cameras did not function properly on some days due to displacement and other reasons. A total of 1138 independent images were obtained. The working days of the camera at each position, the total number of independent images taken, and the population density of plateau pikas estimated by the REM equation are presented in Table 2. The results showed that the average density of plateau pikas in the study area was 144 per hectare, the highest density was 200 individuals/ha, at 100 m along the riverbank, and the lowest density was 77 individuals/ha, on the sunny side of the steep slope.

The distance from the water source had a strong impact on the density of plateau pikas, which was highest at the location 100 m from the riverbank, followed by the locations 300 m from the riverbank, 600 m from the riverbank, and on the riverbank. In addition, the density of plateau pikas was significantly higher on the sunny side of the gentle slope than on that of the steep slope.

Frequencies of different behaviors at different locations

From August 15 to August 18, all six cameras functioned normally. The frequencies of the five behaviors defined in Table 1 and Fig. 3 in the different locations are shown in Fig. 4.

As shown in Fig. 4a, foraging and traveling behaviors accounted for the largest proportions of plateau pika behavior, with percentages of 38.73% and 35.50%, respectively; vigilance behavior accounted for 20.12% of the behavior, and fighting and grooming accounted for only 3.68% and 1.97%, respectively. Figure 4b indicates that the frequency of foraging behavior was highest 100 m from the riverbank and that the frequencies of vigilance behavior and traveling were highest on the riverbank. Compared with that at the riverbank, the frequency of vigilance behavior was significantly lower at the other locations, and the frequencies of all behaviors were lower on the sunny side of the steep slope than on the sunny side of the gentle slope. Foraging and traveling make up a large part of the pika's ground activities, which is consistent with findings of Smith et al. (1986). Thus, it can be inferred that the main purpose for

Table 2. Population density of plateau pikas estimated by REM at different locations.

Location	Number of camera working days	Number of independent images	Number of plateau pikas per ha
Riverbank	5	161	142
100 m from riverbank	6	271	200
300 m from riverbank	7	270	171
600 m from riverbank	4	130	144
Sunny side of gentle slope	7	201	127
Sunny side of steep slope	6	105	77
MEAN population density			144

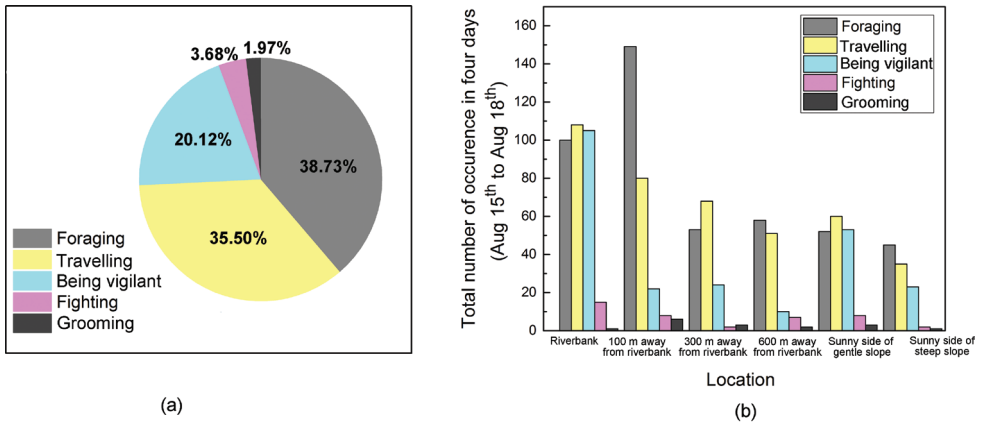


Figure 4. Frequencies of the five behaviors defined in Table 1 and Fig. 3 **a** percentages of occurrence of the different behaviors and **b** total number of occurrences of different behaviors in different locations.

pikas to go out is to seek food, with constant moving to find a better and safer place to eat. To reduce the risk of predation, pikas may increase their running and vigilance frequencies, resulting a relatively large proportion in the two behavioral patterns. It is shown in the camera records that pikas living 100 m away from riverbank exhibit the greatest chance of foraging, which may result from better food supplies and larger population density.

Frequencies of different behaviors during different periods

To investigate behavior differences among different time periods, the frequencies of the different behaviors during the time periods of 6:00–7:00, 7:00–8:00, ..., and 19:00–20:00 were calculated and are shown in Fig. 5. Two peaks of foraging behavior occurred, at 8:00–9:00 and 17:00–18:00. From 6:00 to 9:00, foraging, vigilance and traveling behaviors gradually increased in frequency, and after 18:00, foraging and vigilance behaviors decreased significantly. The Pearson correlation analysis revealed a significant positive correlation between foraging and vigilance behavior ($r = 0.734$, $P = 0.003$).

The highest surface temperature recorded by the infrared cameras was 48 °C, and the surface temperature was above 0 °C throughout the observation period. The frequency of each behavior under different temperature gradients is shown in Fig. 6. With increasing temperature, the frequencies of foraging, vigilance and traveling behaviors of plateau pikas increased gradually until 35 °C, decreasing significantly thereafter.

Observations have shown that the period when plateau pikas are active is mainly influenced by light intensity (Hao et al. 1987). It is reported that pikas start their ground activities after daybreak and almost disappear on the ground at night. This may explain the results of Fig. 5, and the preferable temperature for pikas may be around 31–35 °C according to Fig. 6.

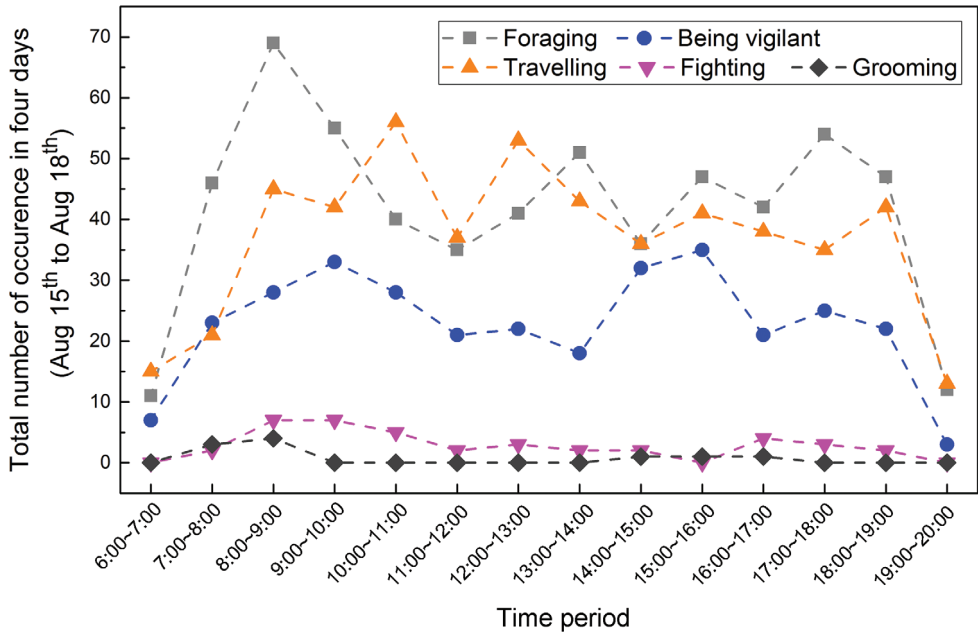


Figure 5. Total number of occurrences of different behaviors during different time periods.

Correlation between density of plateau pikas and area of barren patches

According to Ma's study (Ma 2006), plateau pikas tend to occupy open habitats with low vegetation coverage. Moderately degraded grassland with sparse vegetation is conducive to pika survival. Studies have shown that among grassland types, moderately degraded grasslands have the highest population densities of pikas. As the pika population increases, the vegetation in the habitat gradually decreases, and the proportion of bare land area increases, which leads to more severe grassland degradation.

To verify this conclusion, ArcGIS software (2018) was used to classify barren land and grassland and calculate the area of barren land in the study area. The results are shown in Fig. 7, with both the original picture and the processed image by ArcGIS software. The percentage area of barren land was 18.2%–30.1%, with an average of 23.3%. According to these percentages and the classification criteria proposed by Ma (2006), the grassland in the study area has reached a moderate level of degradation.

Discussion and conclusion

Distribution of plateau pikas

The breeding peak of plateau pikas occurs in May and June, with no breeding occurring in middle and late August. In July and August, because of the slow reproduction rate of pikas, interspecies competition, increased precipitation and other

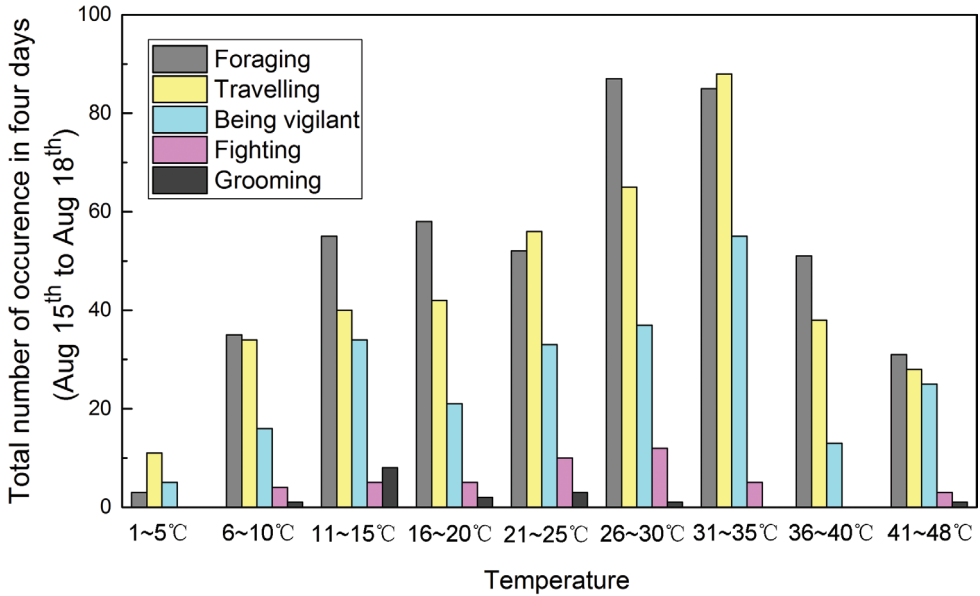


Figure 6. Total number of occurrences of different behaviors under different temperature gradients.

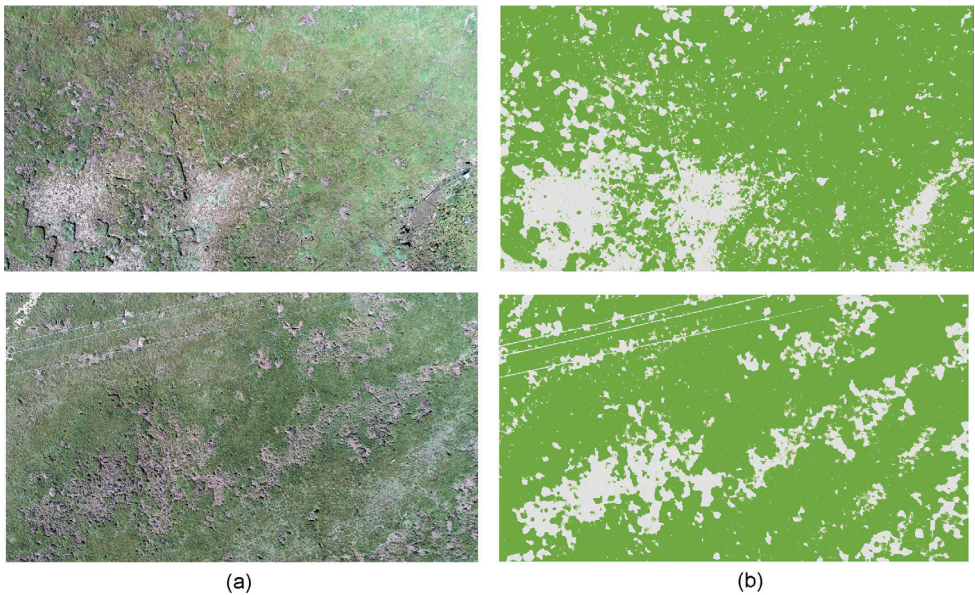


Figure 7. The area of barren land in the study area **a** original remote sensing images of the study area, and **b** images processed to identify the area of barren land.

factors, the mortality of pikas increased, and the population decreased. The field observations in this study were completed in mid-August, and the average population density of pikas in the study area was estimated to be 144/ha. During the breeding peak of pikas, the average density of pikas in the area could have been much higher than 144/ha.

Plateau pikas were more densely distributed in the environments near the water source and in the gentle terrain. This pattern may have been due to the following reasons: (1) greater vegetation growth near the water source, (2) a shorter distance to the source of drinking water, and (3) the reduced energy consumption and risk of predation associated with drinking water. However, the highest density did not appear at the riverbank, which was the site nearest the water source. This finding may have been due to river flooding in the summer rainy season, which increases the risk of submergence of rodent burrows; in addition, water consumption by predators occurs frequently at this time. The highest population density of pikas occurred at the site 100 m from the riverbank, followed by that 300 m from the riverbank. The growth of vegetation on sunny, steep slopes is poor, and such slopes are not conducive to pika escape from natural enemies. These observations might explain why the density of pikas on the sunny gentle slope was significantly higher than that on the sunny steep slope.

Behavioral characteristics of plateau pikas

In the areas with higher population densities of pikas (100 m and 300 m from the riverbank), the plateau pikas had low vigilance times, whereas in the area with low densities (the sunny gentle and sunny steep slopes), they alerted each other more frequently. This difference may have been due to the higher individual safety in the areas with higher population density. The numbers of traveling and vigilance activities were highest at the riverbank, where predators frequently drink water; thus, pikas increased their vigilance and traveling behaviors to avoid the risk of predation.

The plateau pika is a diurnal animal, and its foraging behavior exhibited two peaks: 8:00–9:00 and 17:00–18:00. Plateau pikas forage frequently in the early morning and at dusk to reduce energy consumption and the risk of predation. In Dari County, there is abundant sunshine. When the ground temperature is high, the activity of pikas is reduced to reduce energy consumption.

References

- Anile S, Ragni B, Randi E, Mattucci F, Rovero F (2014) Wildcat population density on the Etna volcano, Italy: a comparison of density estimation methods. *Journal of Zoology* 293: 252–261. <https://doi.org/10.1111/jzo.12141>
- ArcGIS software (2018) ArcGIS 10.6. January 2018. Environmental Systems Research Institute, California, US.
- Bai W, Zhang Y, Xie G, Shen Z (2002) Analysis of formation causes of grassland degradation in Maduo County in the source region of Yellow River. *The Journal of Applied Ecology* 13: 823–826.
- Caravaggi A, Zaccaroni M, Riga F, Schai-Braun SC, Dick JT, Montgomery WI, Reid N (2016) An invasive-native mammalian species replacement process captured by camera trap sur-

- vey random encounter models. *Remote Sensing in Ecology and Conservation* 2: 45–58. <https://doi.org/10.1002/rse2.11>
- Chen B, Zhang X, Tao J, Wu J, Wang J, Shi P, Zhang Y, Yu C (2014) The impact of climate change and anthropogenic activities on alpine grassland over the Qinghai-Tibet Plateau. *Agricultural and Forest Meteorology* 189: 11–18. <https://doi.org/10.1016/j.agrformet.2014.01.002>
- Chen J, Yamamura Y, Hori Y, Shiyomi M, Yasuda T, Zhou H-k, Li Y-n, Tang Y-h (2008) Small-scale species richness and its spatial variation in an alpine meadow on the Qinghai-Tibet Plateau. *Ecological Research* 23: 657–663. <https://doi.org/10.1007/s11284-007-0423-7>
- Chen J, Yi S, Qin Y (2017) The contribution of plateau pika disturbance and erosion on patchy alpine grassland soil on the Qinghai-Tibetan Plateau: Implications for grassland restoration. *Geoderma* 297: 1–9. <https://doi.org/10.1016/j.geoderma.2017.03.001>
- Dong Q-M, Zhao X-Q, Wu G-L, Shi J-J, Ren G-H (2013) A review of formation mechanism and restoration measures of “black-soil-type” degraded grassland in the Qinghai-Tibetan Plateau. *Environmental Earth Sciences* 70: 2359–2370. <https://doi.org/10.1007/s12665-013-2338-7>
- Fan N (1999) Rodent pest management in the Qinghai-Tibet alpine meadow ecosystem. Ecologically-based management of rodent pests.
- Gao J, Li X (2016) Degradation of frigid swampy meadows on the Qinghai–Tibet Plateau: Current status and future directions of research. *Progress in Physical Geography* 40(6): 794–810. <https://doi.org/10.1177/0309133316659283>
- Gao X, Dong S, Xu Y, Wu S, Wu X, Zhang X, Zhi Y, Li S, Liu S, Li Y, Shang Z, Dong Q, Zhou H, Stufkens P (2019) Resilience of revegetated grassland for restoring severely degraded alpine meadows is driven by plant and soil quality along recovery time: A case study from the Three-river Headwater Area of Qinghai-Tibetan Plateau. *Agriculture, Ecosystems & Environment* 279: 169–177. <https://doi.org/10.1016/j.agee.2019.01.010>
- Gao Y, Zhou X, Wang Q, Wang C, Zhan Z, Chen L, Yan J, Qu R (2013) Vegetation net primary productivity and its response to climate change during 2001–2008 in the Tibetan Plateau. *Science of the Total Environment* 444: 356–362. <https://doi.org/10.1016/j.scitotenv.2012.12.014>
- Guo N, Degen AA, Deng B, Shi F, Bai Y, Zhang T, Long R, Shang Z (2019) Changes in vegetation parameters and soil nutrients along degradation and recovery successions on alpine grasslands of the Tibetan plateau. *Agriculture, Ecosystems & Environment* 284: 106593. <https://doi.org/10.1016/j.agee.2019.106593>
- Hao Z, Xia WP (1987) Circadian activity rhythms of plateau pikas *Ochotona curzoniae*. *Acta Theriologica Sinica* 03: 211–223. [in Chinese]
- Koju NP, He K, Chalise MK, Ray C, Chen Z, Zhang B, Wan T, Chen S, Jiang X (2017) Multilocus approaches reveal underestimated species diversity and inter-specific gene flow in pikas (*Ochotona*) from southwestern China. *Molecular phylogenetics and evolution* 107: 239–245. <https://doi.org/10.1016/j.ympev.2016.11.005>
- Li X, Perry G, Brierley GJ (2016) Grassland Ecosystems of the Yellow River Source Zone: Degradation and Restoration. In: Brierley G, Li X, Cullum C, Gao J (Eds) *Landscape*

- and Ecosystem Diversity, Dynamics and Management in the Yellow River Source Zone. Springer Geography. Springer, Cham, 137–165. https://doi.org/10.1007/978-3-319-30475-5_7
- Liu J, Xu X, Shao Q (2008) Grassland degradation in the “three-river headwaters” region, Qinghai province. *Journal of Geographical Sciences* 18: 259–273. <https://doi.org/10.1007/s11442-008-0259-2>
- Ma Y (2006) Studies on formation mechanism of ‘black soil type’ degraded grassland and restoring pattern in the source region of Yangtze, Yellow and Lantsang Rivers. PhD Thesis, Gansu Agricultural University, China.
- Manzo E, Bartolommei P, Rowcliffe JM, Cozzolino R (2012) Estimation of population density of European pine marten in central Italy using camera trapping. *Acta Theriologica* 57: 165–172. <https://doi.org/10.1007/s13364-011-0055-8>
- Pan X, Mi MWD (2016) Plateau pika ecology: A review. *Chinese Journal of Ecology* 35: 2537.
- Qu J, Russell JC, Ji W, Yang M, Chen Q, Li W, Zhang Y (2017) Five-year population dynamics of plateau pikas (*Ochotona curzoniae*) on the east of Tibetan Plateau. *European Journal of Wildlife Research* 63: e51. <https://doi.org/10.1007/s10344-017-1109-2>
- Rowcliffe JM, Field J, Turvey ST, Carbone C (2008) Estimating animal density using camera traps without the need for individual recognition. *Journal of Applied Ecology* 45: 1228–1236. <https://doi.org/10.1111/j.1365-2664.2008.01473.x>
- Schleuss P-M, Heitkamp F, Sun Y, Miehe G, Xu X, Kuzyakov Y (2015) Nitrogen uptake in an alpine Kobresia pasture on the Tibetan Plateau: Localization by 15 N labeling and implications for a vulnerable ecosystem. *Ecosystems* 18: 946–957. <https://doi.org/10.1007/s10021-015-9874-9>
- Smith AT, Wilson MC, Hogan BW (2019) Functional-trait ecology of the plateau pika *Ochotona curzoniae* in the Qinghai–Tibetan Plateau ecosystem. *Integrative Zoology* 14(1): 87–103. <https://doi.org/10.1111/1749-4877.12300>
- Smith AT, Smith HJ, Wang XG, Gao X, Xiangchu XY, Junxiun JL (1986) Social behaviour of the steppe-dwelling black-lipped pika. [J]. *National Geographic Research* 2(1): 57–74.
- Smith AT, Xie Y, Hoffmann RS, Lunde D, MacKinnon J, Wilson DE, Wozencraft WC, Gemma F (2010) A guide to the mammals of China. Princeton University Press, 576 pp. <https://doi.org/10.1515/9781400834112>
- Wang JL, Wei WH, Zhang YM, Yin BF (2005) Behavior patterns of plateau pika *Ochotona curzoniae* at different population densities. *Current Zoology* 04: 598–607. [in Chinese]
- Wangdwei M (2019) Effects of vegetation cover and pastoral land-use types on the foraging and vigilance behaviors of the plateau pika. *Acta Theriologica Sinica* 39: 000–000.
- Wei L, Xi W, Li Z, Huakun Z (2003) Studies on destruction, prevention and control of Plateau Pikas in *Kobresia pygmaea* meadow. *Acta Theriologica Sinica* 23: 214–219.
- Wen L, Dong S, Li Y, Wang X, Li X, Shi J, Dong Q (2013) The impact of land degradation on the C pools in alpine grasslands of the Qinghai-Tibet Plateau. *Plant and Soil* 368: 329–340. <https://doi.org/10.1007/s11104-012-1500-4>
- Wei WH, Cao YF, Zhang YM, Wang JL (2004) Influence of the predation risk on the behavior of the plateau pika [J]. *Acta Zoologica Sinica* (03): 319–325. [in Chinese]

- Wei W, Knops JM, Zhang W (2019) The impact of plateau pikas (*Ochotona curzoniae*) on alpine grassland vegetation and soil is not uniform within the home range of pika families. *Plant Ecology & Diversity* 12(5): 417–426. <https://doi.org/10.1080/17550874.2019.1628113>
- Yao T, Wu G, Xu B, Wang W, Gao J, An B (2019) Asian water tower change and its impacts. *Bulletin of the Chinese Academy of Sciences* 34: 1203–1209.
- Zhang Q, Bai W, Zhang Y, Liu L (2011) Herdsmen's perception of grassland degradation in the source region of the Yellow River: A case study in Dalag County. *Resources Science* 33: 942–949.
- Zhang S, Bao Y, Wang Y, Fang P, Ye B (2013) Estimating rodent density using infrared-triggered camera technology. *Acta Ecologica Sinica* 33: 3241–3247. <https://doi.org/10.5846/stxb201202290272>

Two new species of the genus *Pseudidonauton* Hering, 1931 from China (Lepidoptera, Limacodidae)

Jun Wu¹, Alexey V. Solovyev², Hui-Lin Han^{1,3}

1 School of Forestry, Northeast Forestry University, Harbin, 150040, China **2** Department of Biology and Chemistry, Ulyanovsk State Pedagogical University, Ulyanovsk, 432071, Russia **3** Key Laboratory of Sustainable Forest Ecosystem Management, Ministry of Education, Northeast Forestry University, Harbin, 150040, China

Corresponding author: Hui-Lin Han (hanhuilin@aliyun.com)

Academic editor: Erik J. van Nieuwerkerken | Received 10 May 2021 | Accepted 16 August 2021 | Published 14 September 2021

<http://zoobank.org/41E786F9-E7A9-42BF-9C7E-6BCDB44D27F3>

Citation: Wu J, Solovyev AV, Han H-L (2021) Two new species of the genus *Pseudidonauton* Hering, 1931 from China (Lepidoptera, Limacodidae). ZooKeys 1059: 173–181. <https://doi.org/10.3897/zookeys.1059.68512>

Abstract

Two new species of the genus *Pseudidonauton* Hering (Lepidoptera, Limacodidae), *P. sinensis* **sp. nov.** and *P. puera* **sp. nov.**, are described from China. The new species are illustrated with images of the adults and male genitalia, and compared with similar species. Distribution maps of these species and a key to all known species of the genus are provided.

Keywords

Limacodidae, new species, slug caterpillar moths, South-East Asia, taxonomy

Introduction

The genus *Pseudidonauton* was erected by Hering (1931), with *P. admirabile* Hering, 1931 as its type species. While erecting this genus, Hering proposed that *Idonauton nigribasis* Hampson, 1905 should also belong to this genus (Hering 1931). Later, Holloway (1986) revised the genus and transferred to it *Thosea bhaga* Swinhoe, 1901 and *Idonauton nigribasis* Hampson, 1905. In 2009, three additional species were described, *P. siamica* Solovyev, 2009, *P. chihpyh* Solovyev, 2009 and *P. vexa* Solovyev, 2009, two of

which were subsequently recorded from Vietnam (Solovyev 2009; Solovyev and Witt 2009). The type species *P. admirabile* was the first species to be recorded from China (Cai 1981), but we think this record was based on a misidentification. Currently, the genus consists of six described species ranging from India to Sundaland, including *P. admirabile* Hering, 1931, *P. bhaga* (Swinhoe, 1901), *P. nigribasis* (Hampson, 1905), *P. siamica* Solovyev, 2009, *P. chihpyh* Solovyev, 2009 and *P. vexa* Solovyev, 2009. The moths belonging to this genus are small-sized. The antennae in both sexes are filiform, those of the male slightly thickened. The labial palpus is up-curved, with the third segment conspicuous. The proboscis is reduced. The hind tibia has two pairs of spurs. The forewing has R_{2-5} stalked and R_2 separated behind R_3 ; the hindwing has R_s and M_1 arising from the same place at the upper angle of the cell. The ground colour of forewing is pale brown, and their unique feature is that the basal third of the forewing and the apical area are usually brown. The male genitalia are strongly modified and highly diagnostic for the genus: the uncus is usually broad, flattened, single or bifid; the gnathos is reduced to a small band; the transtilla is well developed and strongly sclerotized, having a large, strongly sclerotized, medial plate that is bifid apically; the valva is generically divided into an upper and a lower part, the lower part having a long spine.

Holloway (1986) recorded the morphology of the larva, pupa and cocoon of *P. nigribasis*, but we have not yet found immature stages of this genus. In this study, we describe two new species, *P. sinensis* sp. nov. and *P. puera* sp. nov., from China, one of which also occurs in Vietnam.

Material and methods

The specimens were collected with a 220V/450W mercury vapour lamp and a DC black light in southern China and Vietnam. Standard methods for dissection and preparation of the genitalia slides were used (Kononenko and Han 2007). The specimens were photographed using a Nikon D700 camera, whereas the genitalia slides were photographed with an Olympus photo microscope aided by the Helicon Focus software and further processed in Adobe Photoshop CS6. Almost all the type material of the new species is deposited in the collection of Northeast Forestry University (NEFU), Harbin, China, except for one male paratype deposited in the collection of Alexey V. Solovyev, Ulyanovsk, Russia (CASU). Material from Museum Witt München / Zoologische Staatssammlung München, Munich, Germany (MWM/ZSM) was also examined in this study.

Taxonomic account

Genus *Pseudidonauton* Hering, 1931

Pseudidonauton Hering, 1931, 670, 705. Type species (original designation): *Pseudidonauton admirabile* Hering, 1931 [Malay Peninsula: Padang Rengas].

***Pseudidonauton sinensis* sp. nov.**

<http://zoobank.org/47290A63-4817-4513-BC9E-F158A18D3445>

Figures 1, 2, 3, 10, 11, 18

Holotype. ♂, China, Chongqing Municipality, Mt. Simian, 29.VII–2.VIII.2020, leg. HL. Han and J. Wu, genit. prep. WuJ-388–1 (NEFU).

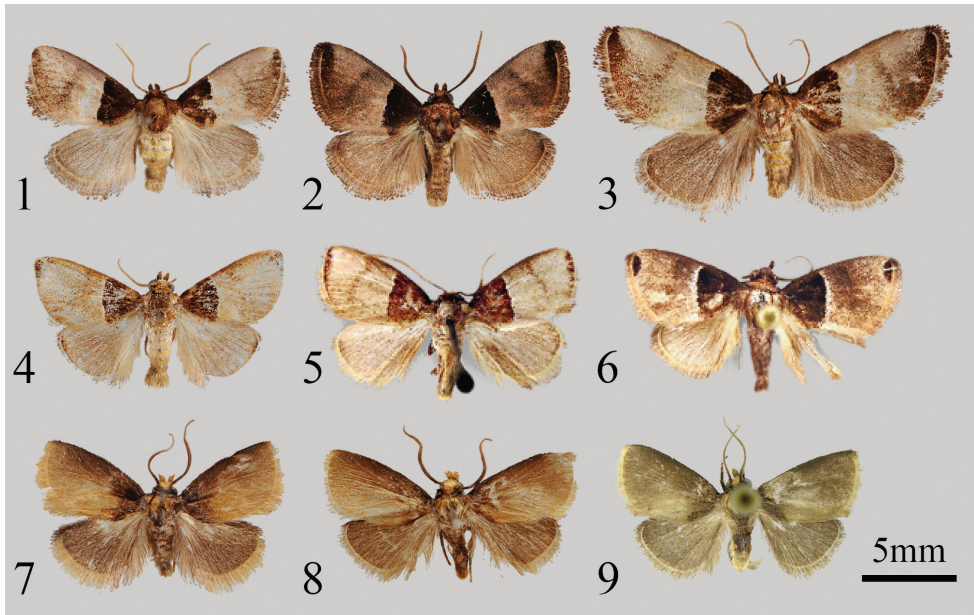
Paratypes. 15♂, 1♀, same data as for holotype, genit. prep. for four dissected paratypes WuJ-288–1, 289–1, 387–1 and 389–2 (NEFU); 3♂, 1♀, China, Prov. Guizhou, Zunyi City, Shierbeihou scenic spots, Shuanghe village, 3–5.VIII.2020, leg. HL. Han and J. Wu, genit. prep. for three dissected paratypes WuJ-382–1, 383–1 and 384–2 (NEFU); 4♂, China, Prov. Guizhou, Zunyi City, Xishui County, Sanchahe Town, 1.VII.2019, leg. MR. Xing, BX. Zhao, and H. Sun (NEFU); 4♂, China, Prov. Jiangxi, Guanshan Nature Reserve, 21–27.VIII.2017, leg. GX. Wang and WJ. Li, genit. prep. for two dissected paratypes WuJ-342–1, 343–1 (NEFU); 1♂, China, Prov. Jiangxi, Guanshan Nature Reserve, 21–23.VIII.2017, leg. HL. Han, genit. prep. WuJ-379–1 (NEFU); 41♂, China, Prov. Zhejiang, Pan'an County, Mt. Dapan, 25.VI–6.VII.2019, leg. J. Wu and JJ. Fan, genit. prep. for four dissected paratypes WuJ-390–1, 440–1, 441–1, 442–1 (NEFU); 3♂, China, Prov. Zhejiang, Jiangshan City, Laofoyan Village, 3.VII.2017, leg. ZG. Zhang, YY. Jia and J. Li (NEFU); 1♂, China, Prov. Zhejiang, Jiangshan City, Xiayangping Village, 4.VII.2017, leg. ZG. Zhang, YY. Jia and J. Li (NEFU); 2♂, China, Prov. Fujian, Mt. Wuyi, Taohuayu, 6.VIII.2020, leg. MJ. Qi and XY. Jin (NEFU); 3♂, China, Aut. Reg. Xizang, Linzhi City, Lulang station, 15.VII.2017, leg. HL. Han, genit. prep. for three dissected paratypes WuJ-379–1, 380–1, 381–1 (NEFU).

Diagnosis. The new species is very similar to its congeners in appearance, especially to *P. bhaga* (Fig. 4), *P. chihpyh* (Fig. 5) and *P. vexa* (Fig. 6), but it can be distinguished from these species by having no distinct borderline between the apical patch and the ground colour in the forewing. Moreover, the whole outer margin area in the new species is covered by a conspicuous dark brown smudge.

The male genitalia are clearly different from those of the other congeners: in *P. sinensis* sp. nov. (Figs 10, 11), the uncus is shallowly divided into two parts; the transtilla is narrow apically and bearing a pair of long slender spine-like process at the base; the sacculus process is straight. The vesica lacks cornuti. However, in *P. bhaga* (Fig. 12), *P. chihpyh* (Fig. 16) and *P. vexa* (Fig. 17), the uncus is deeply divided into two parts; the apical plate of the transtilla is broad, without a slender spine-like process at the base; the sacculus process is strongly curved. The vesica bears a row of small cornuti.

In the female genitalia, the diagnostic difference between *P. sinensis* sp. nov. (Fig. 18) and *P. vexa* (Fig. 19) is that the former has a thick ductus bursae, and the surface of the 1/2 near the ostium bursae is rough; a leaf-shaped signum is located at the upper part of the corpus bursae.

Description. Adult (Figs 1, 2, 3). Wingspan 14–16 mm in male, 18–20 mm in female. Head brown; labial palpus up-curved; antenna filiform in both sexes, brown. Thorax and tegula brown. Scales on legs brown mixed with a little yellow. Forewing



Figures 1–9. Adults of *Pseudidonauton* spp. **1** *P. sinensis* sp. nov., male, holotype **2** ditto, male, paratype **3** ditto, female, paratype **4** *P. bhaga* Swinhoe, 1901, male, Borneo, Malaysia (in NEFU) **5** *P. chibpyh* Solovyev, 2009, male, holotype (in MWM/ZSM) **6** *P. vexa* Solovyev, 2009, male, holotype (in MWM/ZSM) **7** *P. puera* sp. nov., male, holotype **8** ditto, male, paratype **9** ditto, male, paratype (in CASU). Scale bar: 5 mm.

ground colour pale brown to reddish brown, basal 1/3 with unique dark brown area. Apical patch dark brown, no visible borderline with the ground colour. Whole outer margin area covered by a conspicuous dark brown smudge. Median line slightly visible, arched, dark brown, runs from costal at ca. 3/5 distance from wing base to tornus. In some individuals, median line barely visible. Fringe long, brown. Hindwing ground colour slightly darker than forewing, reddish brown; apex dark brown; fringe long, brown. On abdomen, hair covering each abdominal segment golden yellow mixed with pale brown, with long pale brown hairs in terminal area.

Male genitalia (Figs 10, 11). Uncus broad, flattened, weakly divided into two parts, each covered with dense hairs on surface. Gnathos reduced. Tegumen broad, slightly trapezoidal. Transtilla well developed and strongly sclerotized, with small, apically bifid medial plate; basal part of transtilla bearing pair of long, slender, spine-like process slightly enlarged at base. Valva strongly modified and clearly divided into upper and lower parts: upper part finger-shaped, with ear-like process at base and nearly membranous triangular structure behind it; in lower part, sacculus slightly inflated, with swollen base and straight spine-like sacculus process ca. 1/2 length of phallus. Juxta flattened, slightly concave in middle of apex. Saccus not obvious. Phallus slender, tube-shaped, slightly sclerotized terminally; vesica without cornuti.

Female genitalia (Fig. 18). Ovipositor lobes ear-shaped, covered with dense hairs on surface. Postvaginal plate strongly sclerotized. Apophysis anterioris very short, with

only a small spine; apophysis posterioris long, ca. 2/3 length of ovipositor lobes, inflated at base and blunt at apex. There is a distinct, nearly square incision on the ostium bursae. Ductus bursae thick, not spiral-shaped, with rough sclerotized surface on upper half, membranous on lower half. Corpus bursae pear-shaped, with tiny hairs on surface and a strongly sclerotized, leaf-shaped signum on upper 1/3.

Distribution. China (Chongqing, Zhejiang, Guizhou, Fujian, Jiangxi, Xizang) (Fig. 20).

Etymology. The species is named *sinensis* because of its wide distribution in China.

Bionomics. The specimens were collected from June to August at altitudes of 560–2,800 m.

***Pseudidonauton puera* sp. nov.**

<http://zoobank.org/31B3CA5B-866B-4240-A92A-F7CEA1EC4B1C>

Figures 7, 8, 9, 13, 14, 15

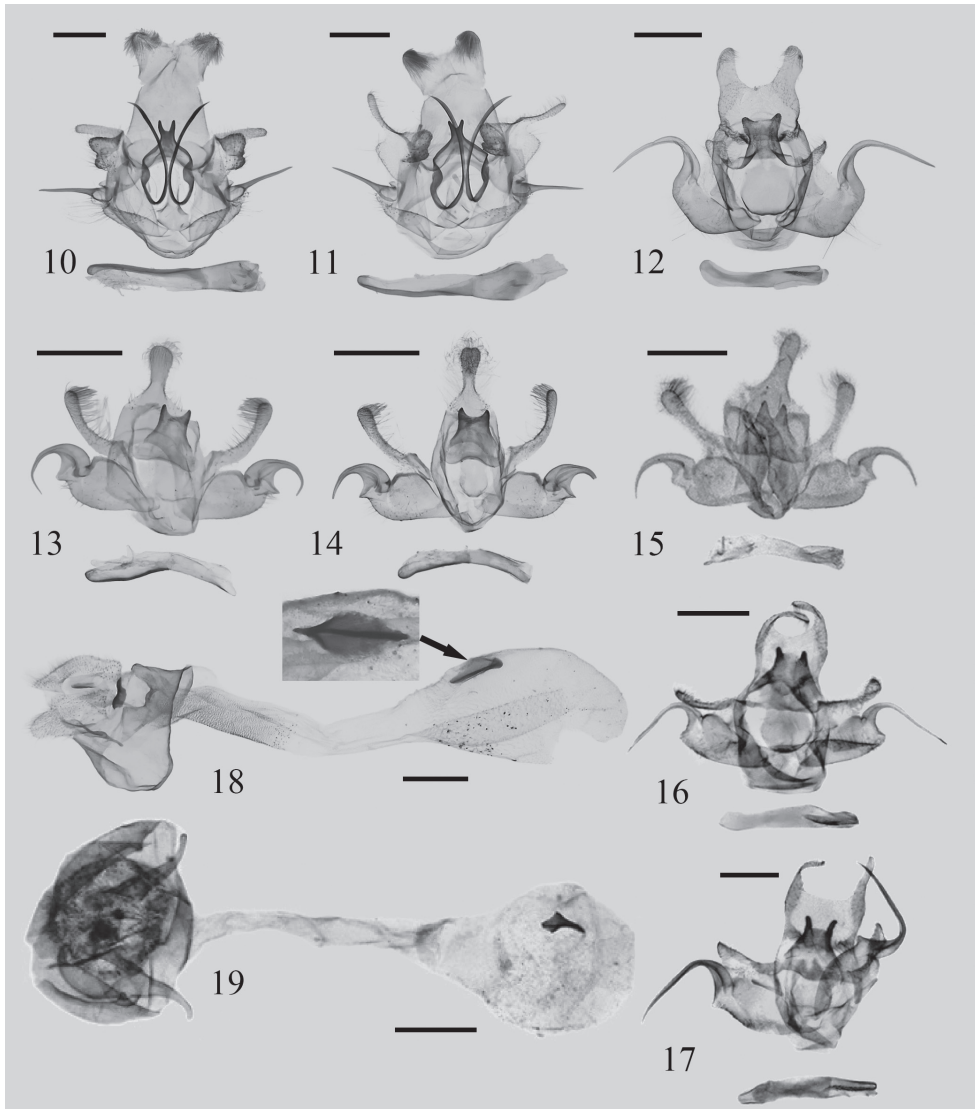
Holotype. ♂, China, Prov. Yunnan, Puer City, Manxieba, 3.VIII.2018, leg. HL. Han, J. Wu, MR. Li, genit. prep. WuJ-237–1 (NEFU).

Paratypes. 1♂, same data as for holotype, genit. prep. WuJ-236–1 (NEFU); 1♂, Vietnam, Dong Nai, Vinh Cuu Nat. Res., Phu Ly, Dakinde, 11.41203°N, 107.10508°E, 106 m a.s.l., 27.VI.2011, leg. A. Solovyev, S. Pugaev, S. Nedoshivina, genit. prep. 0234 (CASU).

Diagnosis. The new species can be clearly distinguished from the known species in its appearance: the dark brown area at the base of the forewing has no obvious borderline with the ground colour and has no apical patch. In the male genitalia, the new species is similar to *P. chihpyh* (Fig. 16), but uncus rod-shaped and not divided into two parts apically is the main combination that distinguishes the new species from *P. chihpyh* and from all other known species in this genus.

Description. Adult (Figs 7, 8, 9). Wingspan 14 mm in male. Head brown, with golden scales on the frons; labial palpus up-curved, golden; antenna filiform in male, brown. Thorax golden, mixed brown scales; tegula brown. Scales on legs dark brown to golden. Forewing ground colour yellowish brown, dark brown at ca. 1/3 from wing base and costal margin area and no clear borderline with the ground colour; fringe long, especially in the tornus area, yellow; forewing without other lines. Hindwing ground colour reddish brown; fringe long, yellow to light brown, but dark brown in costal area. Abdomen dark brown, with light brown and golden hairs between each abdominal segment.

Male genitalia (Figs 13, 14, 15). Uncus short, rod-shaped, slightly enlarged and rounded apically, covered with dense hairs. Gnathos reduced to a small plate. Tegumen broad. Transtilla very developed and strongly sclerotized, wide at base, slightly narrower in apical part and with semicircular depression in middle of apex. Valva strongly modified, clearly divided into two parts: upper part finger-shaped, slightly thin at middle and covered with dense hairs on apex; in basal part, sacculus visibly enlarged, bearing swollen base and eagle-claw-shaped sacculus process; small triangular structure



Figures 10–19. Genitalia of *Pseudidonauton* spp. **10** *P. sinensis* sp. nov., male, holotype **11** ditto, male, paratype **12** *P. bhaga* Swinhoe, 1901, male, Borneo, Malaysia, genitalia No. WuJ-392–1 (in NEFU) **13** *P. puera* sp. nov., male, holotype **14** ditto, male, paratype **15** ditto, male, paratype (in CASU) **16** *P. chihpyh* Solovyev, 2009, male, holotype (in MWM/ZSM) **17** *P. vexa* Solovyev, 2009, male, holotype (in MWM/ZSM) **18** *P. sinensis* sp. nov., female, paratype; **19** *P. vexa* Solovyev, 2009, female, paratype (in MWM/ZSM). Scale bars: 0.5 mm.

located at base of sacculus process. Juxta shield-shaped. Saccus not obvious. Phallus slender, tube-shaped, slightly curved at middle.

Female genitalia. Unknown.

Distribution. China (Yunnan), Vietnam (Dong Nai) (Fig. 20).

Etymology. The species is named *puera* (a noun in apposition) after its type locality in Puer City, Prov. Yunnan, China, which is famous for Puer tea.



Figure 20. Distribution map of two new species of *Pseudidonauton*: circle: *P. sinensis* sp. nov. (China: Chongqing, Zhejiang, Guizhou, Fujian, Jiangxi, Xizang); triangle: *P. puera* sp. nov. (China: Yunnan; Vietnam: Dong Nai).

Bionomics. The moths fly in late June and August. The Chinese specimens were collected with a light trap close to a coniferous forest; the main vegetation around the collecting site consists of *Pinus yunnanensis* Franch. (Pinaceae).

Key to the species of *Pseudidonauton* based on male genitalia, with distributions

- 1 Uncus not bifid..... **2**
- Uncus divided into two parts (bifid) **3**
- 2 Uncus not rod-shaped; medial process of transtilla fish-tail-like; basal part of valva with large pads; saccular spine long ***P. siamica* Solovjev (northern Thailand, central Vietnam)**
- Uncus rod-shaped; medial process of transtilla broad and not fish-tail-like; basal part of valva without pads; saccular spine short ***P. puera* sp. nov. (south-western China, south-eastern Vietnam)**
- 3 Uncus with a V-shaped cleft..... ***P. admirabile* Hering (Peninsular Malaysia, ? southern China)**
- Uncus with a U-shaped cleft **4**
- 4 Uncus bearing long, strong spurs; upper part of valva longer than lower part ***P. nigribasis* (Hampson) (India)**
- Uncus without spurs; upper part of valva shorter than lower part **5**

- 5 Medial notch of uncus narrow, lateral parts of uncus as wide as 1/3 of uncus width **6**
- Medial notch of uncus broad, lateral parts of uncus as wide as 1/4 of uncus width **7**
- 6 Medial notch of uncus shallow, basal part of transtilla bearing pair of long, slender, spine-like processes..... ***P. sinensis* sp. nov. (southern China)**
- Medial notch of uncus deep, basal part of transtilla without processes ***P. bhaga* (Swinhoe) (Borneo, Peninsular Malaysia, Sumatra)**
- 7 Small papula-shaped acute process present near saccular spine ***P. vexa* Solovyev (northern and central Vietnam, south-eastern Thailand)**
- Papula-shaped process absent near saccular spine ***P. chibpyh* Solovyev (China: Taiwan)**

Discussion

The genus *Pseudidonauton* comprises eight species in total to date, but the presence of *P. admirabile* in China is still unclear. It is possible that the record from southern China of this species by Cai (1981) is based on a misidentification. Cai described the uncus of two male specimens to have a U-shaped cleft, but the same structure is V-shaped in the holotype of *P. admirabile* (Solovyev 2009). In the paper of Cai, only a blurred picture of an adult was given, but no images of the genitalia were provided. As we did not examine these two old specimens (collected in 1956), we cannot make a final decision on whether this is a misidentification of *P. sinensis* sp. nov., and more specimens are needed for comparison.

In addition, two unidentified females of *Pseudidonauton* were collected from southern China (Guangdong and Hainan Province) in 2017 and 2019, respectively; the female from Hainan may belong to a species known from Vietnam. However, due to the lack of male specimens at present, we cannot accurately identify which species they belong to.

Acknowledgements

The present study was supported by the National Nature Science Foundation of China (No. 31872261) and the Fundamental Research Funds for the Central Universities (No. 2572019CP11). We sincerely thank Mr. Weiwei Zhang and Mr. Yuansheng Li for their help during collecting in Chongqing and Guizhou; Mr. Mujie Qi and his team from Nankai University for providing some material; and the colleagues from our laboratory for collecting a part of the material of the new species.

The second author's research was supported financially by the Thomas-Witt-Stiftung in 2005–2014, and the field expedition by special RFBI-grant № 11–04–93001-Viet a.

References

- Cai RQ (1981) Limacodidae. In: Wang PY (Ed.) *Iconographia Heterocerorum Sinicorum* 1. Science Press, Beijing, 97–104. [In Chinese]
- Hering M (1931) Limacodidae. In: Seitz A (Ed.) *Die Gross-Schmetterlinge der Erde*, 10. Alfred Kernen Verlag, Stuttgart, 665–728.
- Holloway JD (1986) The moths of Borneo: Part I. Key to families; families Cossidae, Metarbelidae, Ratardidae, Dudgeoneidae, Epipyropidae and Limacodidae. *Malayan Nature Journal* 40(1–2): 1–165.
- Kononenko VS, Han HL (2007) Atlas Genitalia of Noctuidae in Korea (Lepidoptera). In: Park K-T (Ed.) *Insects of Korea (Series 11)*. Junhaeng-Sa, Seoul, 464 pp.
- Solovyev AV (2009) Notes on South-East Asian Limacodidae (Lepidoptera, Zygaenoidea) with one new genus and eleven new species. *Tijdschrift voor Entomologie* 152(1): 167–183. <https://doi.org/10.1163/22119434-900000273>
- Solovyev AV, Witt ThJ (2009) The Limacodidae of Vietnam. *Entomofauna, Supplement No.* 16: 33–229.

